Experimental study of the transitional behaviour of the silty soils from the Venice Lagoon

By Agnese Marcosanti

Thesis submitted to the Università di Bologna in partial fulfilment of the requirements for the degree of Doctor of Philosophy in the Faculty of Engineering

Supervisors:

Guido Gottardi

Co-supervisors:

Matthew Richard Coop

Daniele Costanzo

15th June 2011

TABLE OF CONTENTS

INTRODUCTION

In this work of thesis the mechanical behaviour of granular soils consisting of mixtures of different percentages of sand and fines is shown. The soils come from the Venice lagoon, particularly from Treporti, a site in the north east of the lagoon. A summary of some important contributions to research on Venice soils is presented in Chapter 1.

The main aim of the research was to investigate the response of reconstituted samples in normal compression and shearing in order to identify a possible transitional behaviour (Martins et al., 2002; Nocilla et al., 2006). Moreover, it was studied whether a link between the properties at the macro-scale and micro-structural features occurred. A Scanning Electron Microscopy analysis was performed and its main objective was to identify, if possible, some patterns or mode of orientation that could explain at a micro-scale level the reason for transitional behaviour. In other terms, an investigation of microstructure, particularly microfabric and particle orientations, was undertaken.

CHAPTER 1

The soils from the Venice lagoon

The soils from the Venice lagoon have long been object of studies, given the historical and cultural importance of the city and the need to protect its delicate environment.

These soils consist of a highly chaotic interbedding of different sediments (Cola and Simonini, 2002), whose main characteristic is the presence of a silt fraction, always combined with sand and/ or clay. Although the soils profiles vary from site to site, the unique geological origin and common depositional environment lead to quite uniform mineralogical properties. Several different factors, both natural and man-origined, influenced the soils distribution within the lagoon. Among the others, there are marine transgression and regression, the diversion of river mouths, the tidal movements, the waves action, the wind direction, all the different kind of constructions built in the harbour areas.

Different researches pointed out the high heterogeneity of the Venetian soils, as their most peculiar feature.

1.1. Morphology of the lagoon

The Venice lagoon surrounds the city of Venice in the north-west of Italy. It is located on an area of around 550 km2, between the Brenta river on the south side and the Sile river, also known as the foce di Piave vecchia (literally Piave river old mouth) , on the north side. On the west side its borders mainly consist in industrial and reclaimed areas.

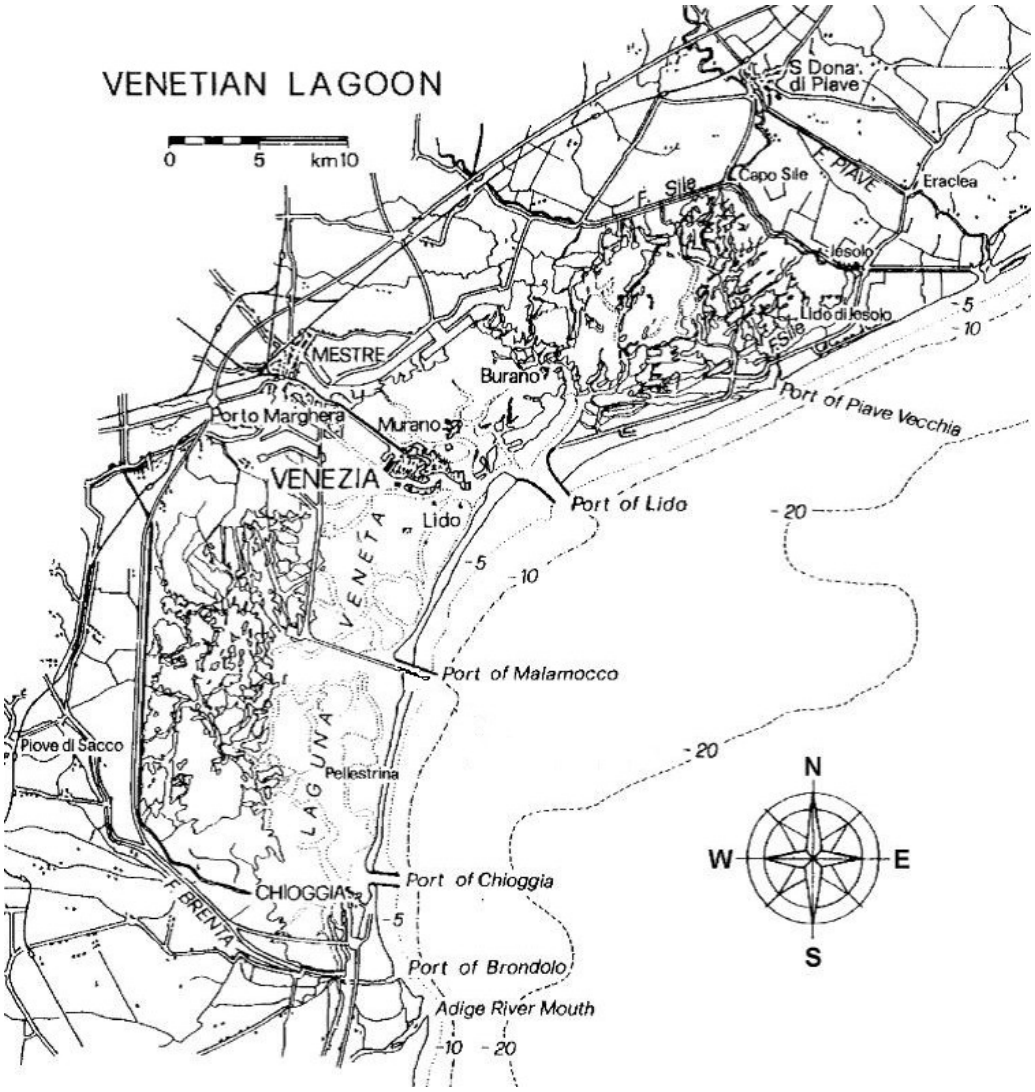

Fig. 1. 1: general view of the Venice lagoon at present (modified from Ricceri *et al*., 2002).

On the east side, the area is limited by the coast line defined by, going from south to north, Sottomarina, Pellestrina, Lido del Cavallino and Lido di Jesolo. The area is around 13 km wide and 55 km long. The lagoon has three inlets to the open sea, Lido, Malamocco and Chioggia.

The present configuration and morphology of the Venice lagoon, represented in the figure above, are the result of natural modifications but also of several human actions that have altered the spontaneous equilibrium of the lacustrine environment.

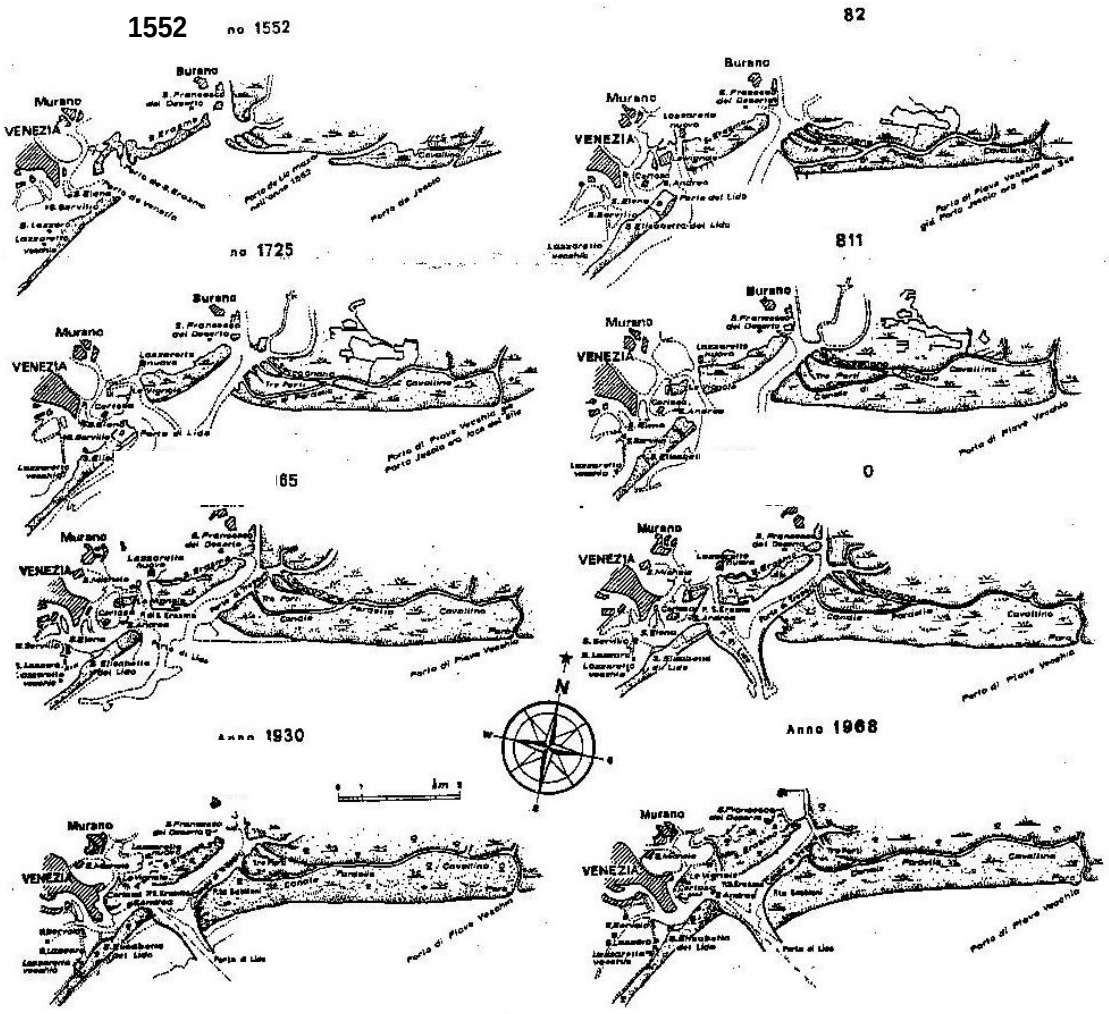

Fig. 1. 2: Evolution of the Lido inlet morphology (Ricceri, 2007)

Those intervents had mainly the aim of protecting the historic city of Venice and of maintaining its typical insularity (Ricceri, 2007).

The most important actions involved:

- the deviation of the Brenta, Sile and Piave rivers into canals on the outside of the lagoon, whereas their mouths were previously located inside the lagoon;
- the modifications of the inlets morphology aiming at reducing the effects of the solid transport of sediments on the navigation;

the reinforcing of the coastline.

In figure 1.2 the evolution of the morphology of the Lido inlet area through the centuries is reported. It can be noted that the first modifications date back to the early 1300s when the river diversions started in order to prevent excessive amount of fluvial sediments deposit in the lagoon.

1.2. Brief geological background

In order to study the characteristics of the Venetian subsoil an overview of the geological history of the area has been attempted. According to the geological and paleontological history, the soils within the Venice lagoon are characterised by a common mineralogical origin and depositional environment.

The Quaternary basin of the Venice lagoon is around 900 m deep. During this period, there was an alternation of ingression and regression of the sea in the lagoon area, therefore both fluvial and marine sediments can be found. The geological history of the area explains the chaotic distribution of the soil sediments in layers with different thickness considering even sites close to each other. The actual origin of the Venice lagoon is traced around 6000 years ago, during a marine transgression called flandrian in the Holocene epoch, with the sea water diffusing into the lacustrine basin (Simonini et al., 2006).

According to Ricceri (2007), the sediments deposited during the Quaternary can be divided into four groups with respect to the depth below mean sea level:

- until 5-10 m below mean sea level: the depositional environment of these shallowest deposits is lacustrine and it can be referred to the Holocene epoch;
- from 5-10 m until 50-60 m below mean sea level: the depositional environment is the result of the last Wurmian glaciations that characterised the superior Pleistocene epoch;
- from 50-60 m until 300 m below sea mean level: the depositional environment is the result of alternating lacustrine, continental and marine sediments from superior Pleistocene epoch;
- from 300 m until 900-950 m below mean sea level: the depositional environment is mainly marine from inferior Pleistocene and Pliocene

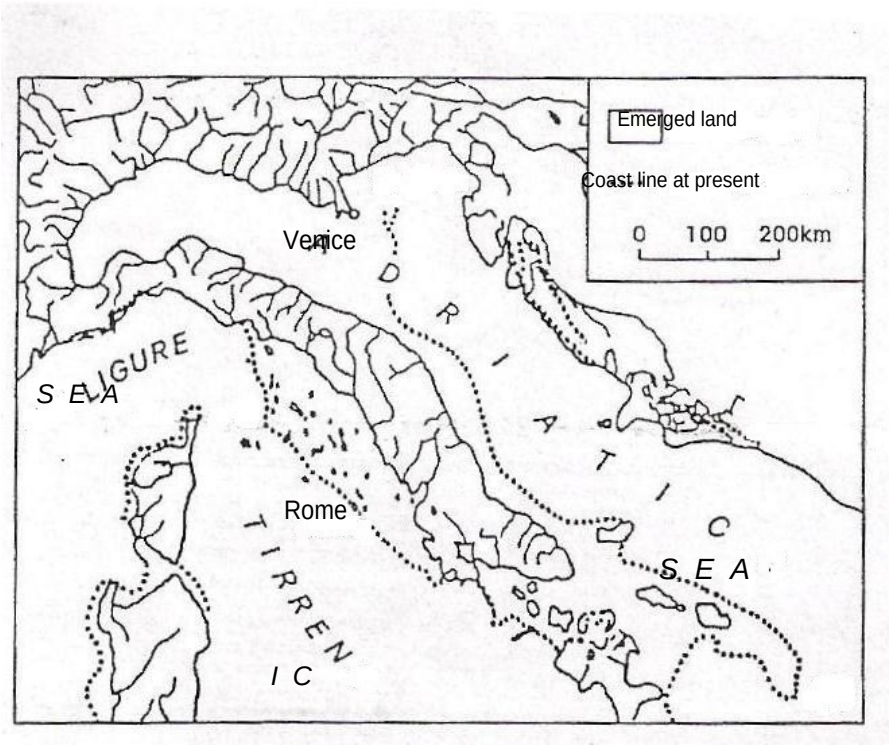

Fig. 1. 3: reconstruction of the emerged land during Pliocene epoch in the moment of the largest marine ingression (modified from Ricceri, 2007).

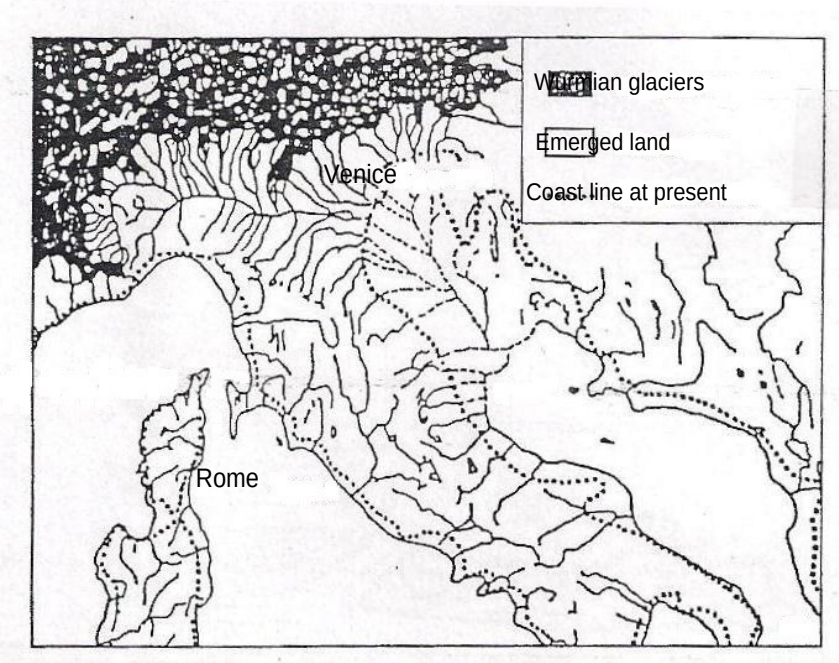

Fig. 1. 4: reconstruction of the emerged land in the moment of the largest marine transgression, during the last Wurmian glaciation (modified from Ricceri, 2007).

Sedimentological studies pointed out that, because of the intrinsic discontinuous nature of the lacustrine environment, it was possible to distinguish between the

Holocene and the superior Pleistocene deposits only using a combination of sedimentological, paleontological, geotechnical and mineralogical investigations among the others (Belloni et al. 2007).

Particularly interesting for the research carried out in this thesis is the analysis of the upper hundred metres below sea level, that consist in a chaotic alternation of sand, silt and clay layers deposited apparently without any pattern during the superior Pleistocene, especially during Wurmian glaciations (Favero et al, 1973). The shallowest 10-15 metres were deposited during Holocene epoch.

The upper Wurmian deposit is a layer 5-12 m deep known as caranto. This consists of a crust of highly overconsolidated very silty clay, originated by essiccation phenomena during the last Pleistocenic glaciation (Simonini et al., 2002). This is where the historical venetian buildings were founded because of its good mechanical properties. The caranto is considered as a benchmark between the Holocenic lacustrine deposits and the continental Pleistocenic sands, silts and clay.

In figure 1.5 a reconstruction of the most recent passages in the evolution of the Venice lagoon geology is shown through sections of the modelled subsoil.

In particular, the continental deposits from the Pleistocene epoch and the lacustrine and coastal deposits from the Holocene epoch can be distinguished. The Pleistocenic continental sediments are characterised by an intrinsic heterogeneous nature which is the most peculiar feature of the Venetian soils, as it will be seen in the following paragraphs.

The depositional patterns of the Venetian sediments are therefore quite difficult to describe because different soil types correspond to the same depth in different areas of the lagoon.

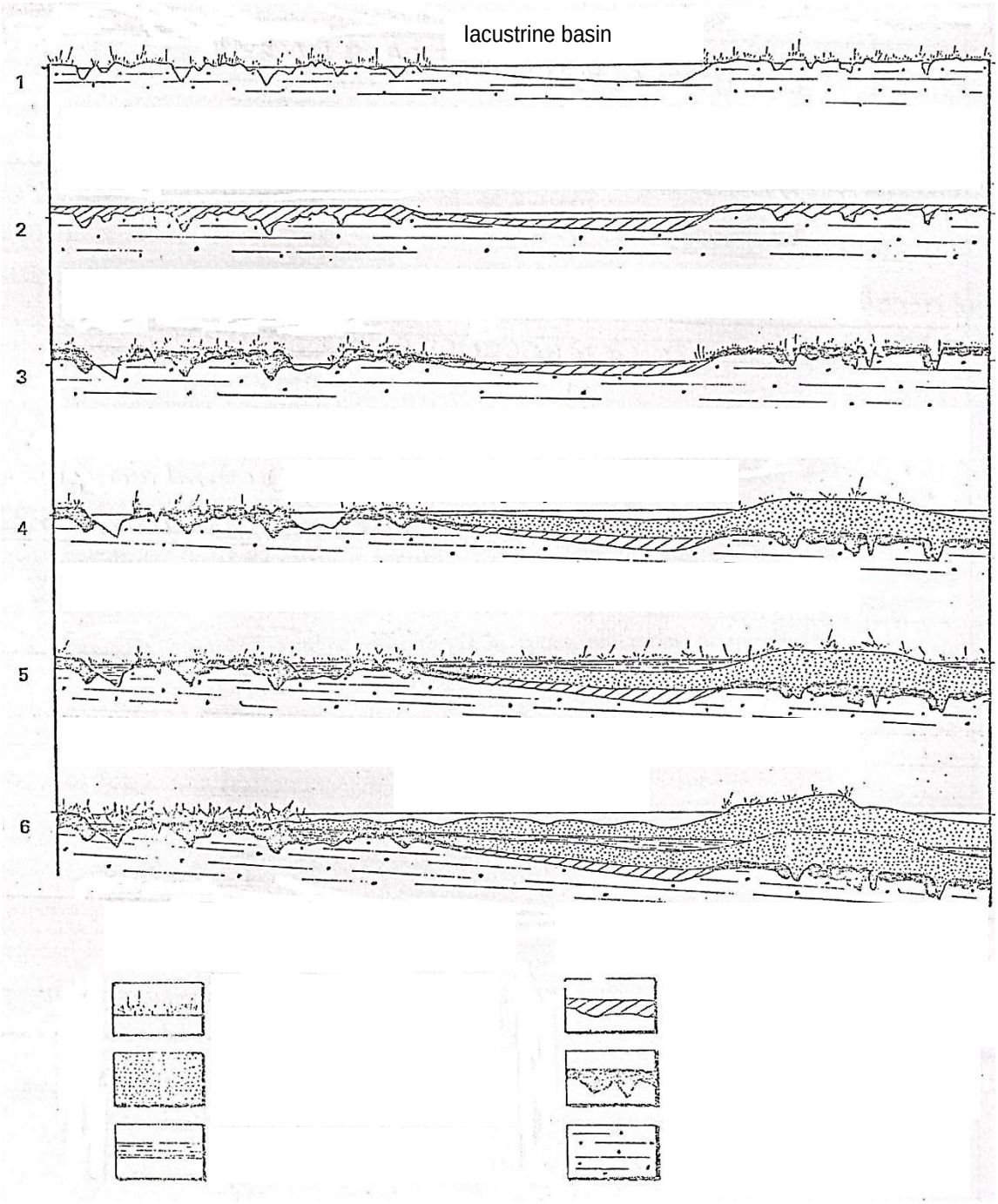

Fig. 1. 5: Overview of the most recent geological phases with particular respect to the superior Pleistocene and the Holocene (modified from Gatto and Previatello, 1974).

In figure 1.6 below, typical soil profiles of the Venice lagoon are reported. These data are representative of a collection of the most important comprehensive geotechnical and geological studies carried out on Venice soils.

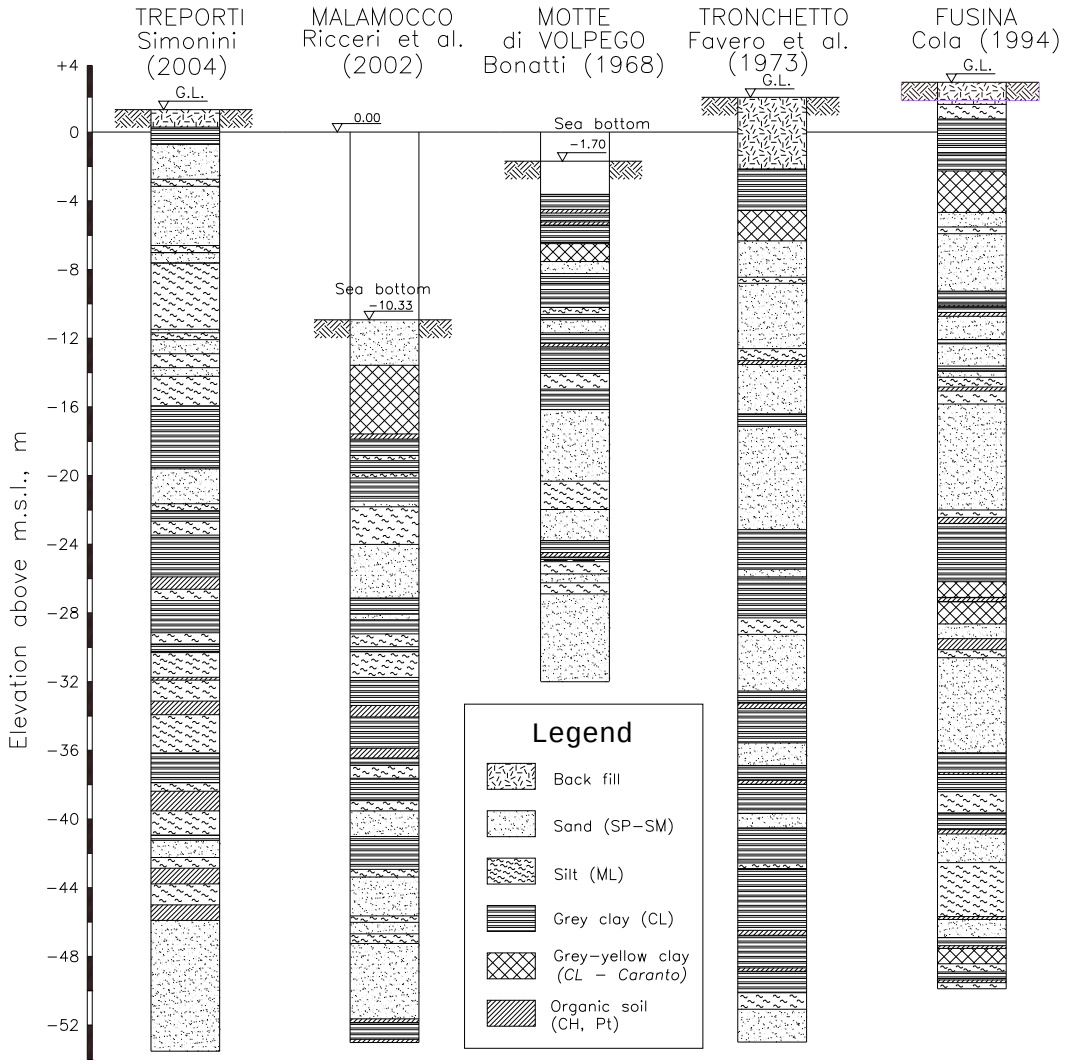

Fig. 1. 6: Typical soil profiles of the Venice lagoon (from Simonini *et al.*, 2006).

1.3. Literature review of the Venice lagoon soils

The soils of the Venice lagoon have long been the object of study, due to several different issues that have developed in the area in the last sixty years and contributed to its precarious equilibrium (Colombo, 1970). The first researches aiming at characterising the geology and the geotechnical properties of the lagoon soils have been undertaken between 1965 and 1975, particularly Bonatti in 1968 carried out mineralogical and paleontological studies on the sediments at a site called Motte di Volpego.

The Venice lagoon has long been subjected to subsidence, both natural and man-induced, the latter increased by the indiscriminate use of the water sources in the subsoil. Particularly during the 70s, great attention has been given to the issues of

the Venice lagoon, especially because of the subsidence effects on the frequency of flooding of the historic city, phenomenon known as acqua alta,.

The Italian Government through the Consiglio Nazionale delle Ricerche (CNR), under the advice of UNESCO, commissioned a 1000 m deep borehole, located at Tronchetto, with the aim of getting an insight of the geotechnical properties and of the aquifer and aquitard system, in order to prevent the increase of this issue (Favero et al. 1973; Rowe 1973; Ricceri & Butterfield 1974). Studies necessary for the design of the foundations of new large industrial settlements on the mainland lead to a thorough knowledge of the shallowest ground of the lagoon, between 70s and 80s, especially with respect to the geotechnical properties obtained through standard tests.

In the following years several commissioned were set up by the Italian Government with the aim of protecting the historic city of Venice and in 1989 a project involving the construction of movable gates at the three lagoon inlets was outlined (Gentilomo 1997; Harleman et al., 2000; Sanzeni, 2006). These gates control the tidal flow and when particularly high tides occur, they have to temporarily separate the lagoon from the sea (Harleman et al. 2000).

Therefore, preliminary geotechnical investigations were necessarily carried out to draw relevant soil profiles and cross-sections at the inlets, thus to achieve a suitable design of the movable gates foundations. The results of these analyses showed that, although the stratigraphy is very heterogeneous, there is a predominance of a silt fraction, combined with clay and/ or sand diffused in the subsoil of the lagoon. Moreover the sediments present similar mineralogical features.

Given the relevant heterogeneity of soil layering, a few test sites were selected as representative of the Venetian lagoon soils.

The tests carried out at the Malamocco Test Site aimed essentially at investigating the soil properties by means of in-situ investigations, which included boreholes, piezocone and dilatometer tests (Cola & Simonini 1999, 2002). Some researchers tried to use the data coming from these tests to evaluate the reliability of the most widely used charts or correlative equations for the piezocone and dilatometer interpretation on the basis of the comparison with the results of the laboratory tests (Simonini & Cola 2000; Ricceri et al. 2002). The heterogeneous layering however, prevented from obtaining certain correlations. A comprehensive laboratory test program was completed on samples coming from at Malamocco Test Site (Cola & Simonini 2002; Simonini et al., 2006; Biscontin et al. 2001, 2006). The results highlighted the sensitiveness of samples to stress relief and sampling disturbance. Moreover the heterogeneity of the Venice sediments resulted in the need of a quite large number of tests in order to define accurately the basic soil properties.

Another site was chosen, the Treporti Test Site located close to the Lido inlet. This site was dedicated to the study of in-situ the stress-strain-time properties of the heterogeneous Venetian soils (Simonini, 2004, 2006). With this aim, a circular embankment was constructed, applying a load of 100 kPa, and the t measurements of the ground displacements and of pore pressure evolution were collected.

Boreholes with undisturbed sampling, traditional CPTU (Gottardi & Tonni 2004) and DMT (Marchetti et al. 2004), seismic SCPTU and SDMT (Mayne & McGillivray 2004) were employed to characterize soil profile and estimate the soil properties for comparison with those directly measured in situ.

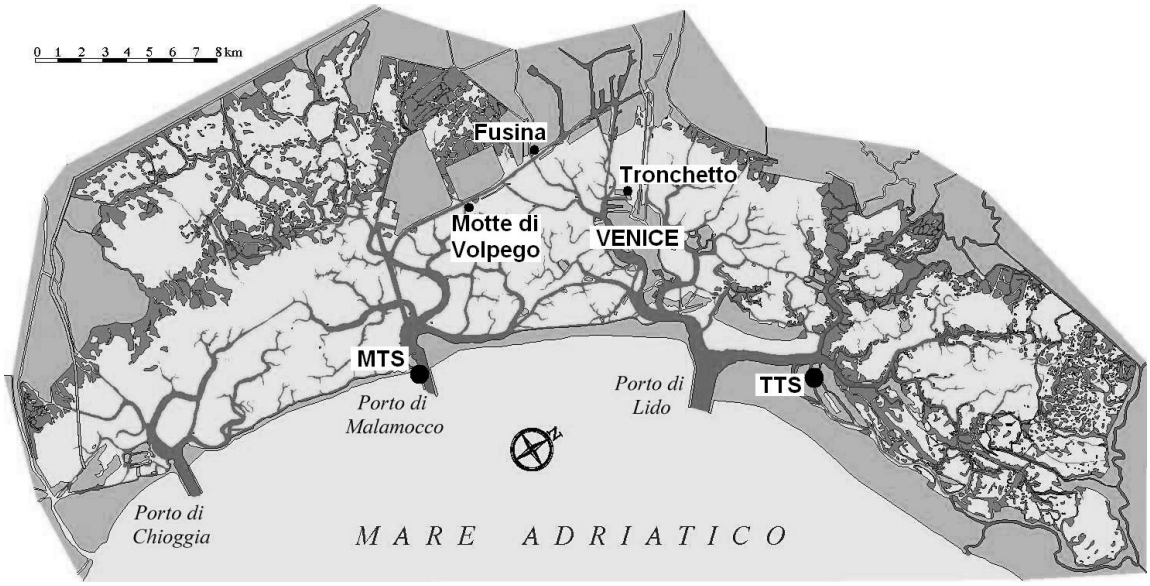

Fig. 1. 7: View of the Venice lagoon with the locations of some test sites (from Simonini *et al.*, 2006).

Other studies carried out on the Venice lagoon soils comprise the work by Cola (1994), who collected data regarding the mechanical properties of clayey and silty soils at Fusina.

Moreover, Biscontin et al. (2006) assessed the compressibility of Venetian soils, as natural silty clayey soils, in order to present a number of constitutive laws, relating the influence on the normal compression behaviour of a particle distributions with varying coarse-grained and fines fraction.

1.4. Basic material properties

Although the soil layers distribution varies greatly from site to site of the lagoon and it is difficult to indicate a soil profile , the same cannot be said for the basic soil features.

The soil profiles at the Malamocco inlet have been widely studied (Simonini et al., 2002). and the Malamocco test site can be considered typical and representative of the entire lagoon area. Several geotechnical investigations have been undertaken at Malamocco, within the project aimed at the construction of the movable gates at the inlets of the lagoon. According to the results of these analyses data are available regarding the grain size distributions, shape of the particles and basic soil properties.

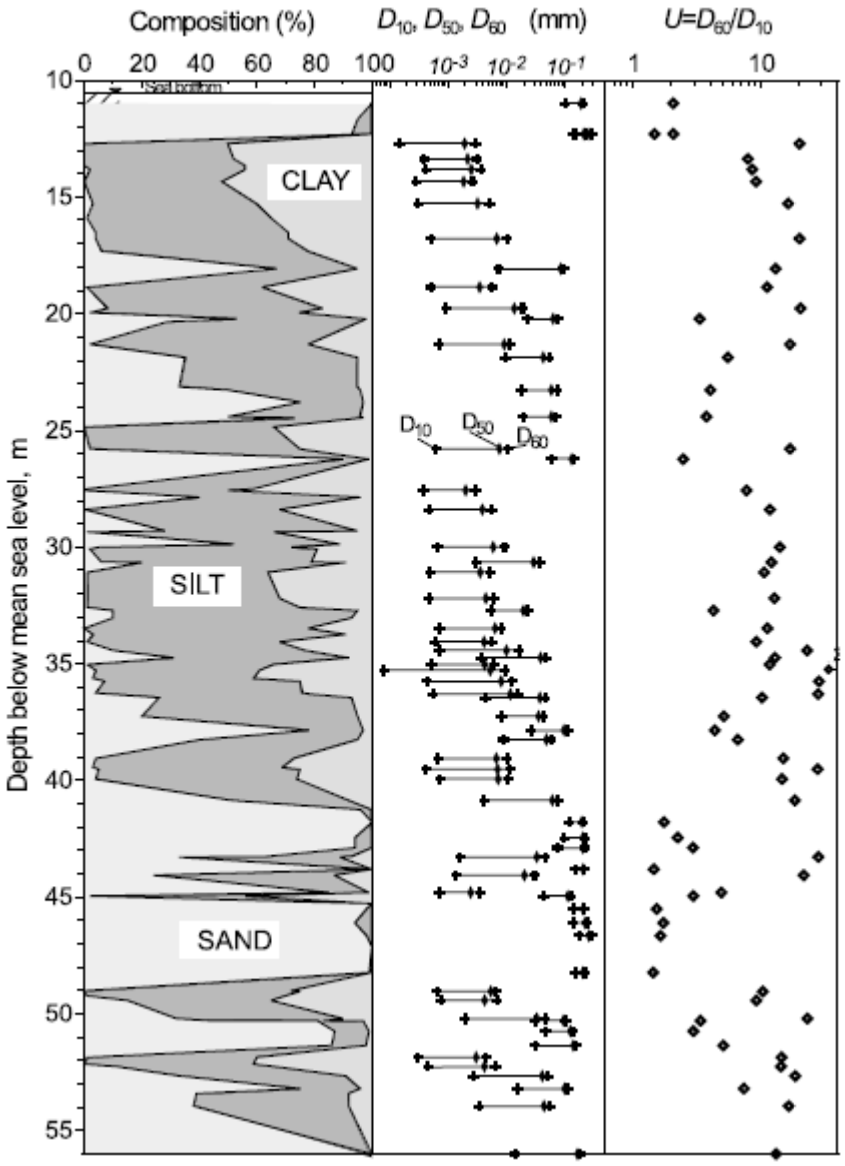

Fig. 1. 8: soil profile at Malamocco test site. It can be noted that the ground level is at 10.5 m below mean sea level (modified from Simonini *et al.*, 2006).

Three main soil types have been identified in the irregular alternation of sediments: sand, silt and very silty clay with a few thin layers of compacted peat (Ricceri et al., 2002; Simonini et al., 2006). According to the Unified Soil Classification System these groups were described as:

- medium to fine sand (SP-SM);
- silt (ML);
- very silty clay (CL).

In figure 1.8, it can be noted that the sand fraction is quite uniform, but moving towards finer materials the grain size curves display a larger range of particle diameters and the soil becomes more graded (Cola and Simonini, 2002).

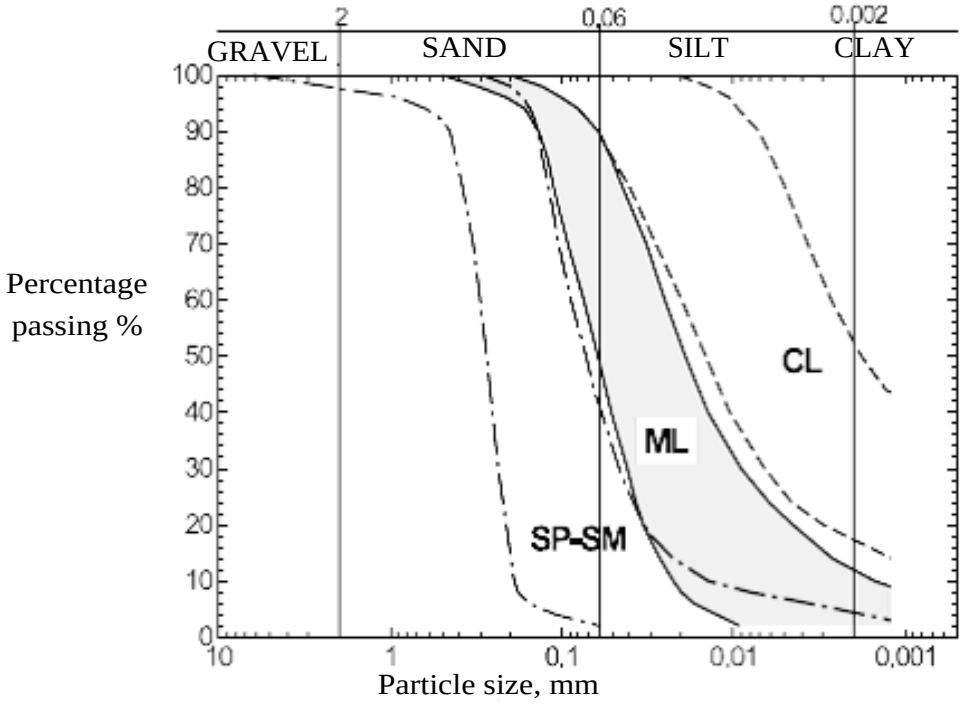

Fig. 1. 9: Typical grain-size distributions of the groups SM-SP, ML and CL at Malamocco test site (from Simonini et al., 2002).

From particle size analysis, the three classes of soils occur, at Malamocco, in proportions of 35% sand (SM-SP), 20% silts (ML), 40% very silty clays (CL) and 5% medium plasticity clays and peat (CH, OH and Pt). Percentages of silts higher than 50% are present in the 65% of the analysed samples.

With respect to the whole soil profile at Malamocco (see figure 1.6) the diameter corresponding to the 60% of passing particles, D_{60} varies from around 0.005 mm to

0.1 mm; whereas the D_{10} varies within the range 0.0001 mm and 0.1 mm. Therefore it can be noticed that both parameters have an oscillation of around two orders of magnitude.

In order to take into consideration the fact that with decreasing diameter, the soil samples are more graded , thus the non- uniformity coefficient U decreases, Cola and Simonini (2002) introduced a new grain size index I_{GS}, coupling the opposite variation of D_{50} and U with depth. This parameter is defined as:

$$I_{GS} = \frac{D_{50} / D_0}{U}$$

where D_0 is a reference diameter equal to 1 mm.

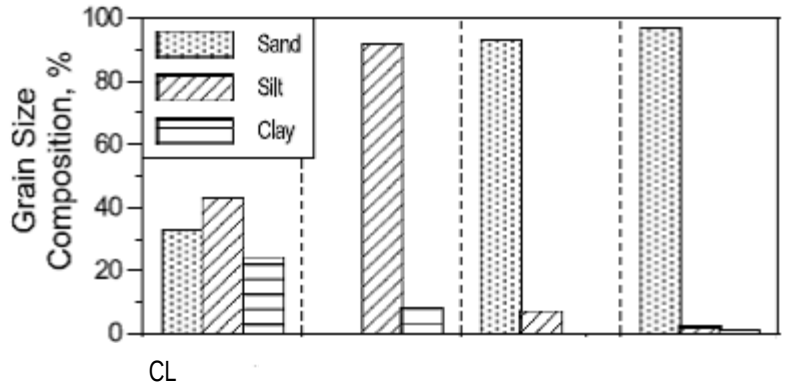

Fig. 1. 10: percentages of the three classes of soils at Malamocco test site (from Simonini *et al.*, 2002).

The average specific gravity G_S is around 2.77±0.03. The liquid limit of the cohesive fraction is on average 36.9% and the plasticity index is on average 14.7%.

In figure 1.10 typical grain size compositions of the three fractions are shown. For the sand fraction (SP-SM) two compositions are represented, each referring to one of the two different mineralogical composition, the carbonatic (a) and the siliceous (b), as it will be seen in details in the following paragraph.

1.5. Mineralogical analysis

One of the most important process that originated the soils from the Venice lagoon is the fluvial deposition of sediments. Within these deposits, two distinct types of

petrographic sources were found: one consisting in the granitic province and one consisting in the limestone-dolomite province. The Po and Adige rivers contribute to the first petrographic source, sometimes called Padana province, that has a mainly siliceous-clastic composition, whereas the Brenta, Piave, Livenza and Tagliamento rivers contribute to the second one, often called Veneta province, which consists mainly of carbonate sediments, with a predominance of dolomite over calcite (Favero, 1973).

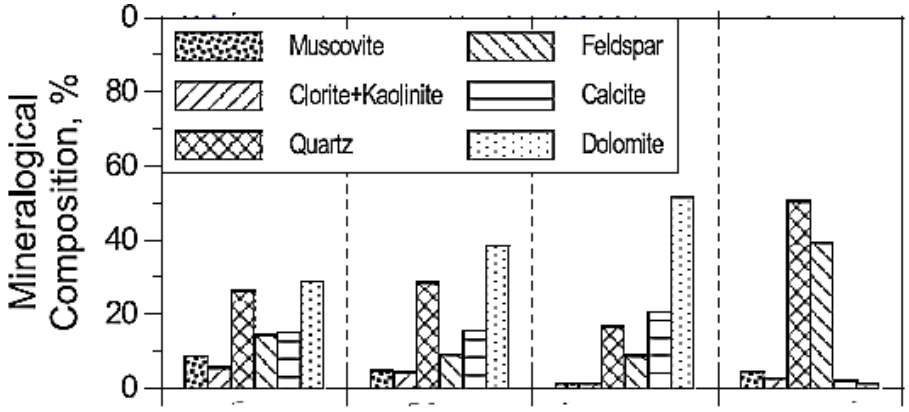

Fig. 1. 11: mineralogical compositions with respect to the grain size distributions of the three fractions. It can be noted that for the sand fraction two mineralogical composition are displayed. (modified from Cola and Simonini, 2002).

One of the most recent study carried out to determine the mineralogical composition of the soils from the Venice lagoon was performed on samples coming from Malamocco test site through X-ray diffractometric technique by Curzi in 1995. The analysis was undertaken on three different kinds of samples coming from a borehole 60 m-deep. The results are summarised in the graph below. The mineralogical composition of the bulk samples, of the sand and of the clay fraction are reported.

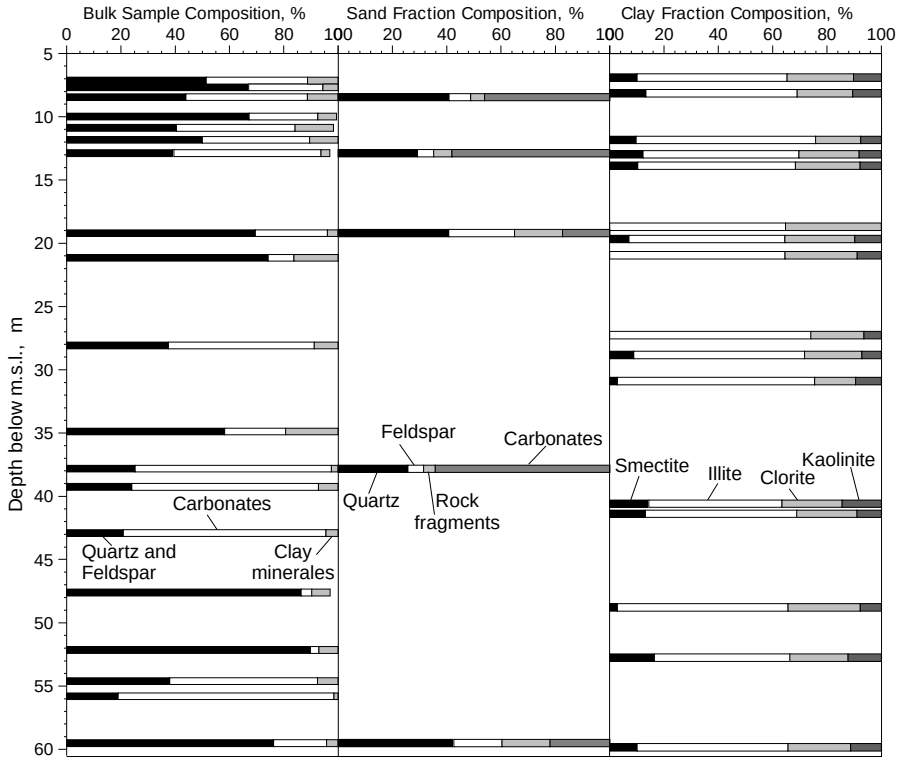

Fig. 1. 12: mineralogical composition obtained from X Ray-diffractometric analysis referring to bulk samples, sand and clay fraction from Malamocco test site (from Simonini et al., 2006)

Considering the overall composition of the sediments (bulk samples), carbonates, consisting mainly in a mixture of calcite and dolomite, are the most significant component, but quartz, feldspar, muscovite and chlorite are quite abundant as well. It can be noted that the percentage of quartz and feldspar increases with increasing depths. The clay minerals fraction is on average lower or equal to 20%, mainly composed of illite (50-60%), with chlorite, kaolinite and smectites as secondary minerals.

In the sand fraction, carbonates and quartz are the main mineralogical components, with feldspar and rock fragments. Within the sand fraction the minerals distribution at different depths is less uniform than the clay fraction

It can be shown that with decreasing particle diameter from sand to clay, the percentage of clay minerals (illite, chlorite, kaolinite and smectite) increases whereas the carbonate and quartz-feldspar content decreases.

In the table below, the mineralogical components of bulk samples representative of different depths at Malamocco test site are shown. It can be seen that even for samples coming from depth values very close to each other the mineralogy can be very different, as it is the case of the sample coming from 34.88 m, which has carbonates as the dominant fraction and the sample coming from 37.82 m, which has quartz as the major component.

Sample depth (m)	Calcite and Dolomite (%)	Quartz (%)	Feldspar (%)	Muscovite (%)	Chlorite and Kaolinite (%)	Chlorite/ Smectite (%)	Illite/ Smectite (%)
8.45	44.7	40.5	3.4	5.7	3.7	2.0	-
34.88	22.4	33.6	24.6	14.0	5.4	-	-
59.51	19.5	66.3	9.9	1.1	2.2	-	1.0
37.82	72.2	16.5	8.7	1.3	1.3		

Table 1. 1. Major components of some samples from MTS (selection of data from Simonini et al. 2006)

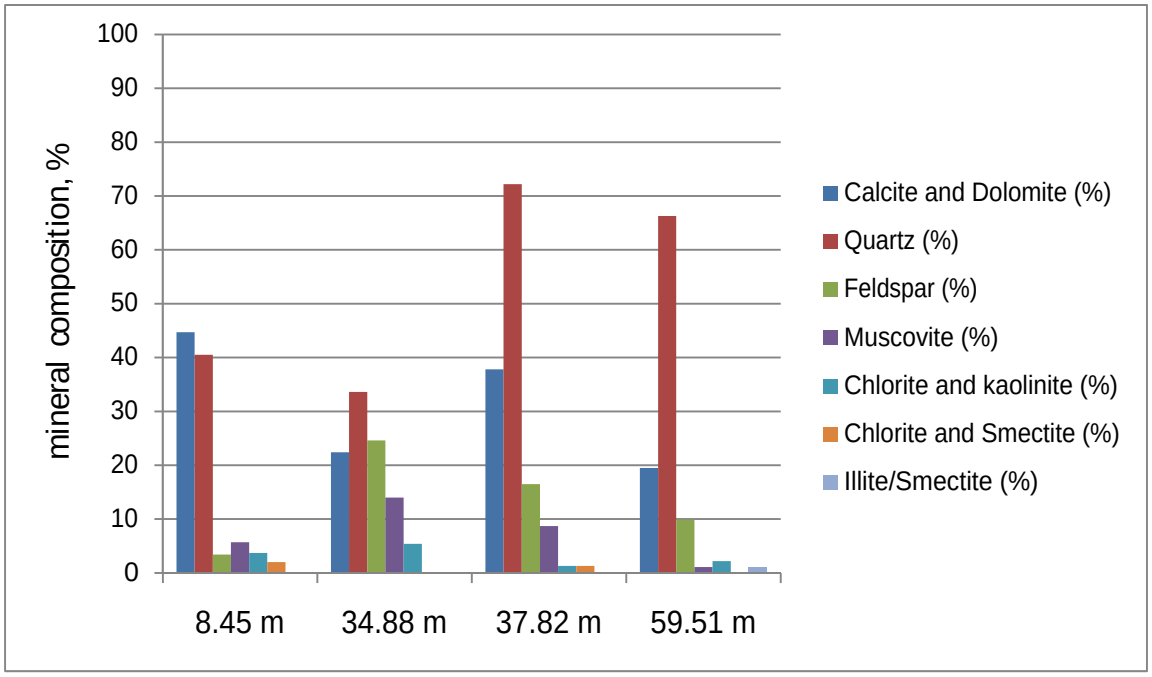

Fig. 1. 13: mineralogical composition of bulk samples at different depths from Malamocco test site (data from Curzi, 1995 and Simonini et al., 2006)

A comparison between the different mineralogical compositions found in the soil profiles at four different sites (Motte di Volpego, Tronchetto, Fusina, Malamocco and Treporti) was carried out by Simonini et al. (2006). According to this study, the

carbonate minerals, Calcite and Dolomite, are the major component with percentages higher than 50-70%. Only a thick layer of around 3-5 m with a low carbonate content was identified at depth varying between 20 and 27 m below mean sea level. A few other deposits with low carbonate content are found at higher and lower depths in the lagoon area, especially at Malamocco test site. It is generally acknowledged that soil layers poor in carbonates, but characterised by peat and organic matter, can be attributed to lacustrine sedimentation episodes (Simonini et al., 2006).

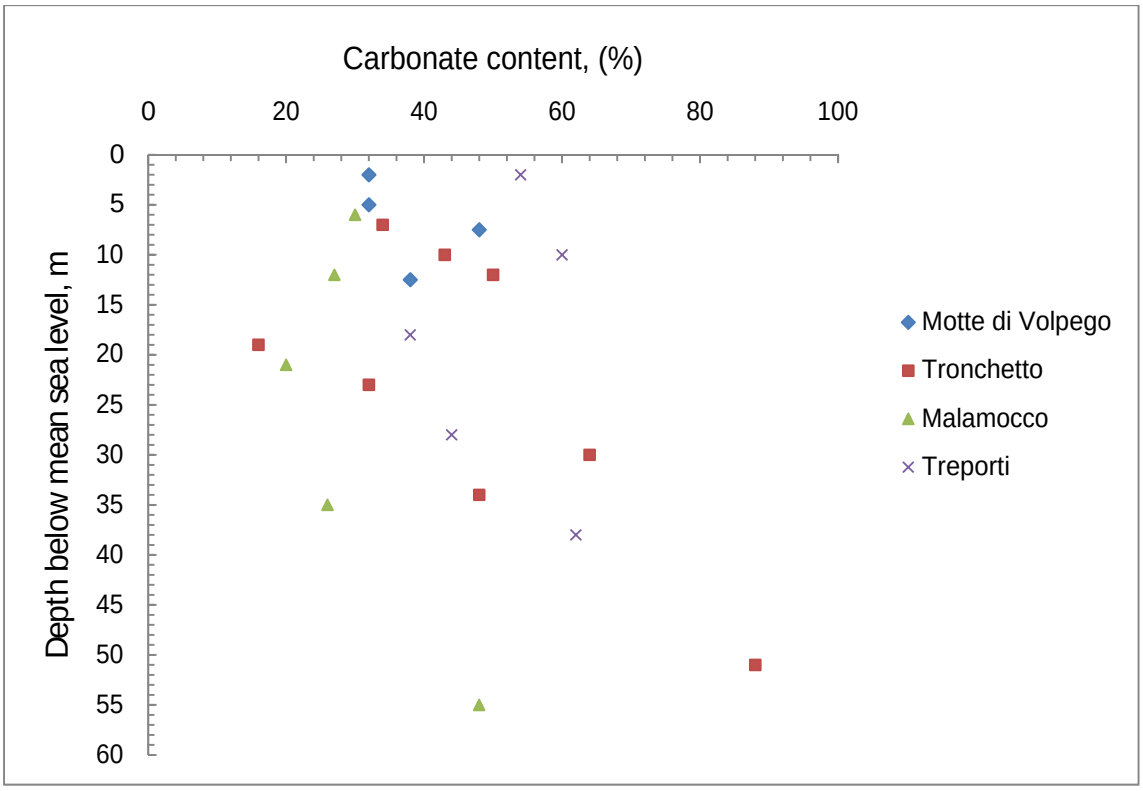

Fig. 1. 14: carbonate content values at four different sites (see also figure 1.6), Motte di Volpego, Tronchetto, MTS and TTS (modified from Simonini et al., 2006).

The shapes of the particles within the two fractions were analysed by means of scanning electron microscopy. In figure 1.12 and 1.13 below, an overview of their shapes can be appreciated. The mean rounding index of the grains of both the sand and the silt fractions ranges between 0.23 and 0.34. The particle size does not seem to affect this parameter. Among the different minerals, quartz and feldspar grains are generally angular.

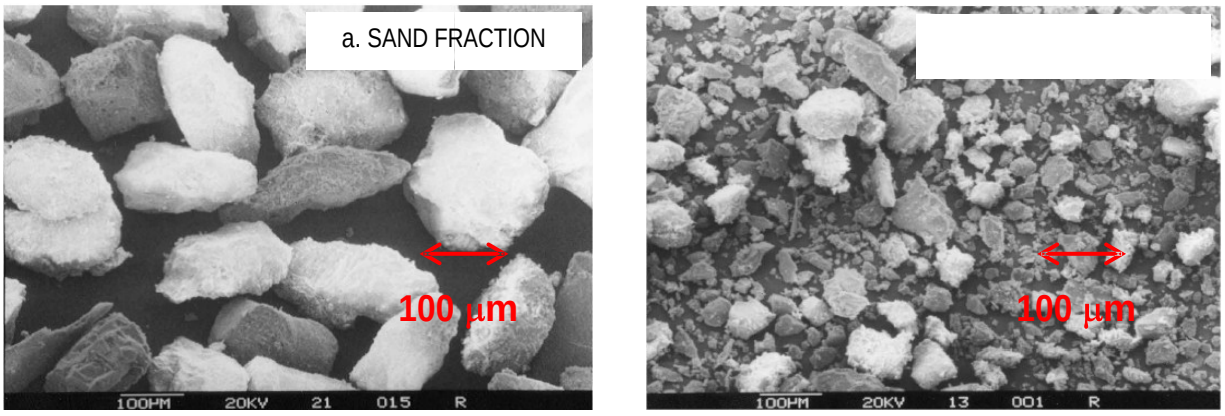

Fig. 1. 15: scanning electron micrographs of the sand and clay fraction obtained from the bulk samples at Malamocco test site (modified from Cola and Simonini, 2002).

CHAPTER 2

The mechanical behaviour of soils

Introduction

In this chapter the main theorical framework of reference for mechanical behavior (drained and undrained) of soils is presented, paying particular attention to granular soils.

The critical state framework theory, established thanks to the work of Rendulic, Skempton and Casagrande among the others, is reviewed for clays and sands.

Several factors influence the mechanical behaviour of soils: the influence of the initial density, for granular soils, and of the stress history, for cohesive soils, on their shear strength and strain are described.

2.1. The Critical state framework

The Critical State framework was developed thanks to the works of Roscoe, Schofield, Wroth and other researchers from Cambridge University. This theory allows to define a comprehensive view of the mechanics of soils, because it takes into account the stress history, the stress paths and the initial characteristics of the material. This theory is powerful also with respect to its applicability to both cohesive and granular soils, for drained and undrained conditions. Within this framework a particular state, called Critical State is described and to this condition soils subjected to shear stresses aim, irrespectively of their initial conditions.

The studies that lead to the development of this theory were first carried out on reconstituted clays. According to Burland, (1990) a reconstituted clay can be defined as one that has been thoroughly mixed at a water content equal or greater than the liquid limit w_L.

Roscoe et al., (1958) identified a unique Normal Compression line (NCL) for reconstituted clays. that separates normally consolidated and over-consolidated states. Moreover, considering shearing behaviour, a Critical State Line (CSL) was identified at high strains. and it represents the locus of the stress-strain states reached eventually in drained and undrained shearing. It can be considered the locus of points that separate contractive and dilative behaviour.

Following this research carried out on clays, the mechanics of sands, was investigated. The Critical State framework (Stationary State theory) was found to be applicable even to granular materials. Loose and dense samples within a wide range of different initial void ratios converge to a unique normal compression line, that runs parallel to the critical state line determined from shearing behaviour at high stress levels.

It has to be pointed out that although the Critical State framework is applicable to both sands and clays, the compression mechanisms involved are different. In clays the compression mode of behaviour relies on superficial, electro-static forces, whereas in sands it is due to particle breakage (Coop and Lee, 1993).

A first hint of the experimental findings is reported below. In figure 2.1, the behaviour of a sand at different initial densities is reported, particularly the shear strength τ , the volumetric strain ε_v and the void ratio as functions of the axial strain, for dense and loose sands under shear stresses. It can be seen that the mechanical behaviour of loose and dense sands shows a great dependence on the initial void ratio: a dense sand shows first a peak strength, then with increasing stresses a critical state is reached at high strains (strain softening behaviour). For loose sands a monotonic increase of shear strength is observed until the critical state condition is reached without any peak resistance (strain hardening behaviour). To the peak condition corresponds a peak shear strength angle φ'_p, whereas at the critical state this parameter is equal to φ'_c. Loose sands only have the critical shear strength angle.

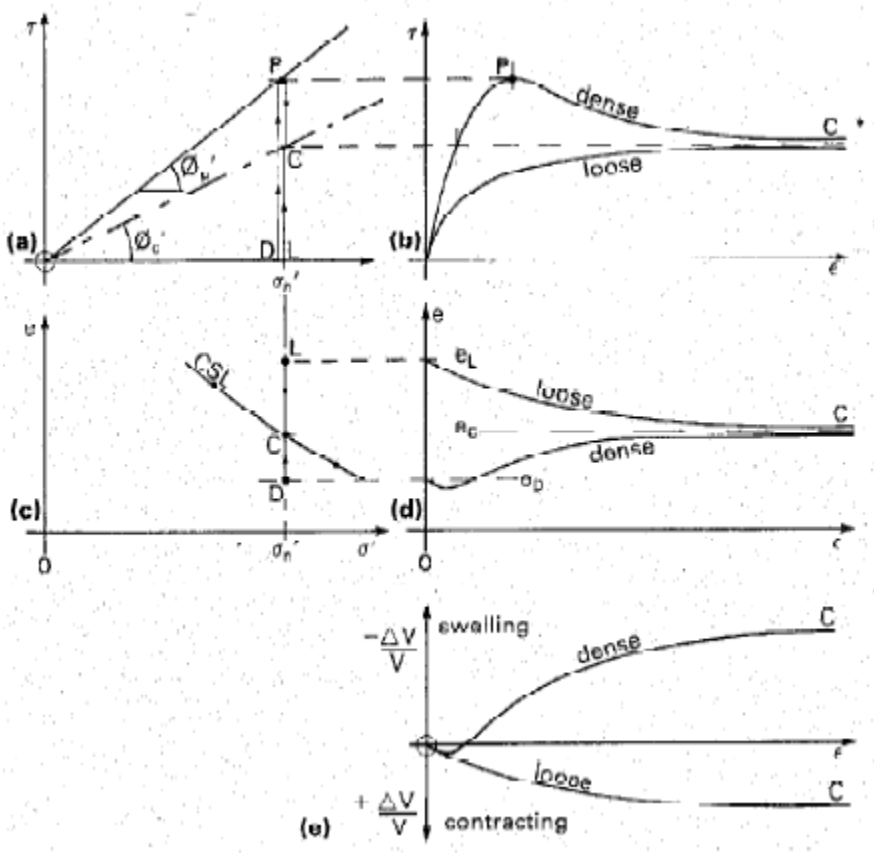

Figure 2. 1 overall view of the shearing response of loose and dense sands (from Head, 2004).

Both sands reaches the critical state condition C, characterised by strains at constant volume and constant shear stresses.

Thus the Critical state and a critical void ratio e_c is reached by both loose and dense sands, thus it does not depend on the initial density. Moreover, nevertheless the different response in shearing (dilating for dense samples, $e_c > e_0$, and contractive for loose samples, $e_c < e_0$), as soon as they both finally reach the critical state, they show a constant volume.

It can be concluded that the critical state is an intrinsic property of the material and does not depend on the initial density, but only on the principal effective stress, whereas the peak shear strength depends on the dilatancy, thus on the initial void ratio. Clays tend to a critical state as well, but for these soils the mechanical response in shearing is linked to the stress history and not to the initial density, as seen for granular soils.

As a matter of fact, the studies by the Cambridge group focused on the mechanics of reconstituted clays and these studies lead to deep interest on the critical state of cohesive and granular soils (see paragraph 2.2).

As it will be described in the following paragraphs, the stress-strain behaviour of normally consolidated clays can be compared to the one of loose sands and the over-consolidated clays one can be compared to the dense sands behaviour.

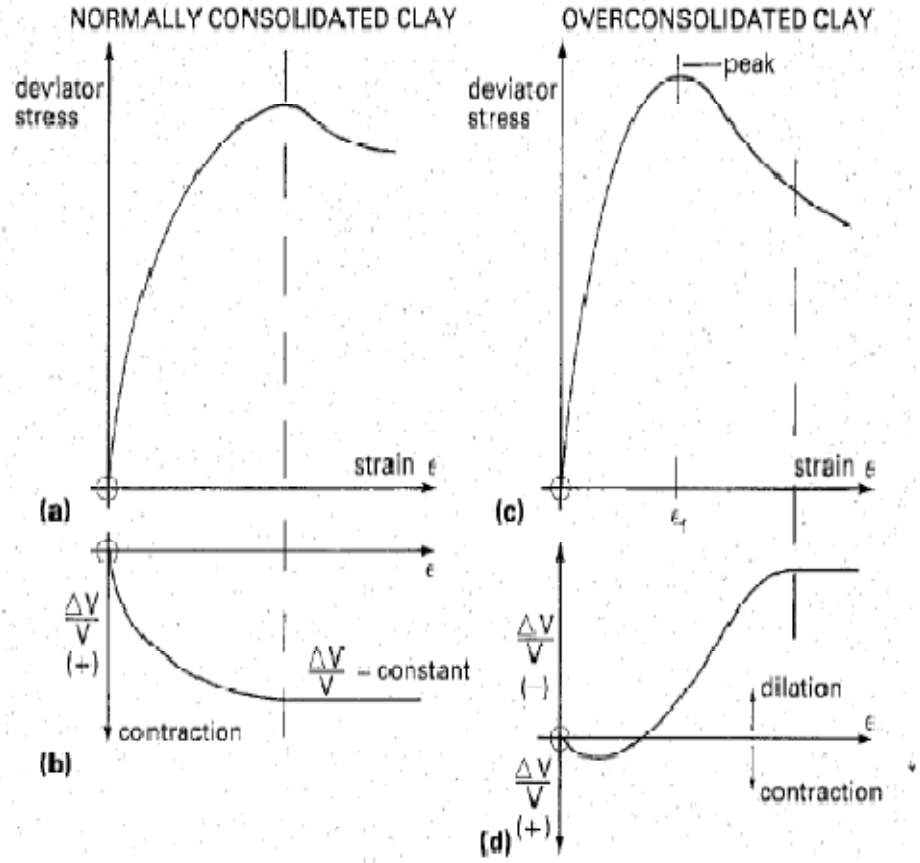

Figure 2. 2: Stress-strain behaviour in shearing of normally consolidated clays and over-consolidated clays in drained triaxial tests (from Head, 2004).

In order to characterize the mechanics of cohesive and granular soils, triaxial tests are performed in drained and undrained conditions. If the shearing phase is drained, the effective stresses coincides with the total stresses. For granular soils, this is usually the case: given their high permeability the induced excess pore pressures are quickly dissipated, whereas if the test is carried out on a cohesive soil, the load should be applied slowly enough for the generated excess pore pressures to dissipate.

If the shearing phase is undrained, the drainage is closed and the shearing phase is performed without any volume change. Thus it is necessary to measure the excess pore pressures in order to determine the effective stress variation.

2.2. Mechanical behaviour of clays

In this paragraph, a review of the different researches that contributed to the development of the Critical State framework is presented. Particularly, the results of drained and undrained triaxial tests on reconstituted, and subsequently natural, clay lead to the identification of a unique state surface.

2.2. 1 Reconstituted clays

The need of a theoretical framework able to describe the mechanical behaviour of clays and to be a reference for both samples in their reconstituted/ remoulded and in their natural states, was one of the first challenge for soil mechanics researchers.

Modern soil mechanics is based on the studies by Rendulic and Hvorslev carried out in the 1930s on the properties of reconstituted natural soils or artificial materials such as illite or kaolinite. These works were the starting point for the development of the critical state framework by the Cambridge soil mechanics school.

In 1936 Rendulic performed the first laboratory studies on the compressibility and shear strength properties of reconstituted normally consolidated clays, Wiener Tegel clay among the others. He focused on the relationship between the void ratio and the stress states during drained and undrained shearing paths, both in compression and in extension.

From the results of tests in undrained and drained shearing conditions, he observed a unique failure line, which in the following years would have been described as Critical State line.

Following Rendulic′s approach, Henkel (1956, 1960) carried out a comprehensive laboratory program consisting of triaxial tests on reconstituted samples of Weald clay. His findings essentially confirmed Rendulic′s results. He hypothesised that, if the stress paths from drained and undrained tests crosses each other on the q-p′ plane, they belong to the surface referring to a constant void ratio (specific volume).

He obtained contours of constant water content for both drained and undrained tests. During drained shearing, the drainage is allowed and thus the void index (or the water content) varies with the volumetric strain. For the several drained stress paths the water content contours (curves corresponding to equal water contents) were drawn.

A unique surface of constant void ratio could be determined, given the fact that the water content contours were found to coincide with the undrained tests stress paths.

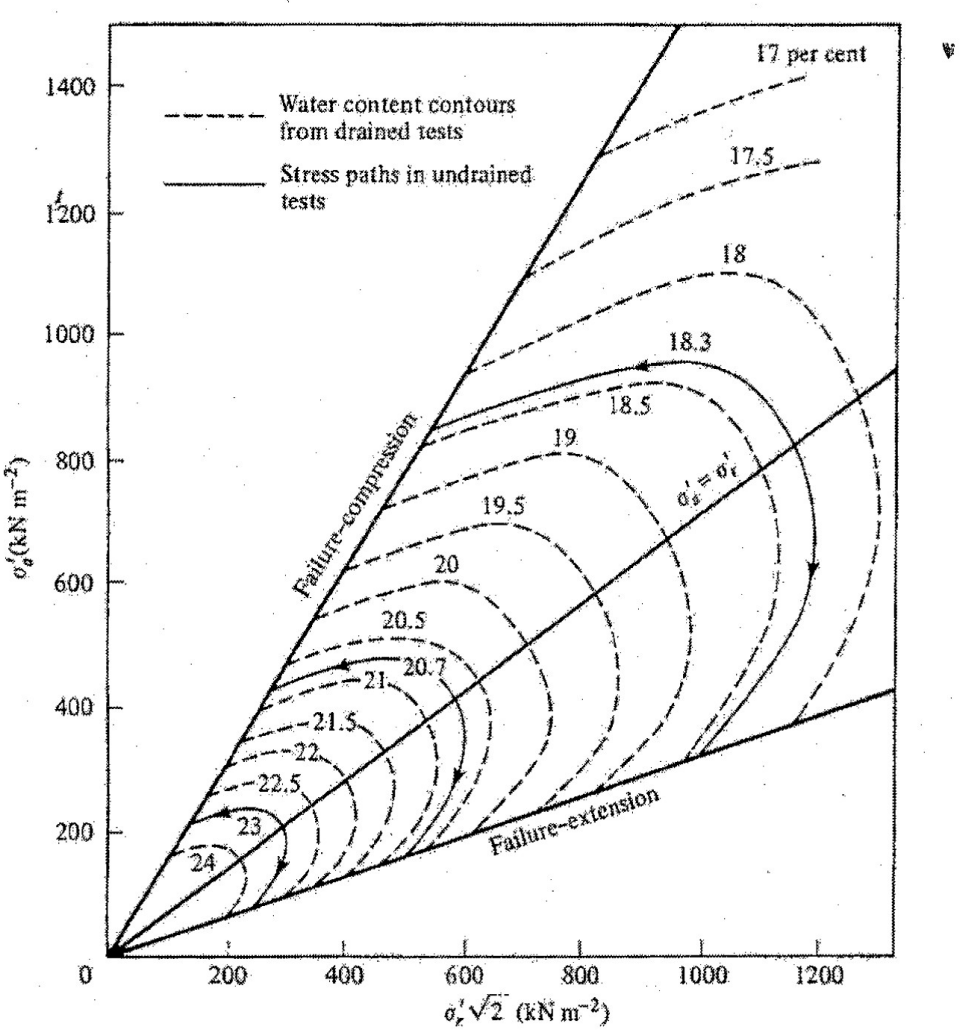

Figure 2. 3: contours of constant water content for drained and undrained tests on Weald clay, observed by Henkel in 1960 (from Atkinson and Bransby, 1978).

With respect to the compression behaviour, one of the first laboratory evidences of the convergence of curves referring to samples with different initial void ratios is presented by Skempton in 1943, studying normally consolidated reconstituted samples of estuarine clay from Gosport. A convergence was found for stresses higher than 100 kPa, as it can be seen in figure 2.3.

These results were also confirmed in 1959 by Leonards and Ramiah, who carried out compression tests on the same material. The normal compression lines were found to converge for stress values of around 100 kPa.

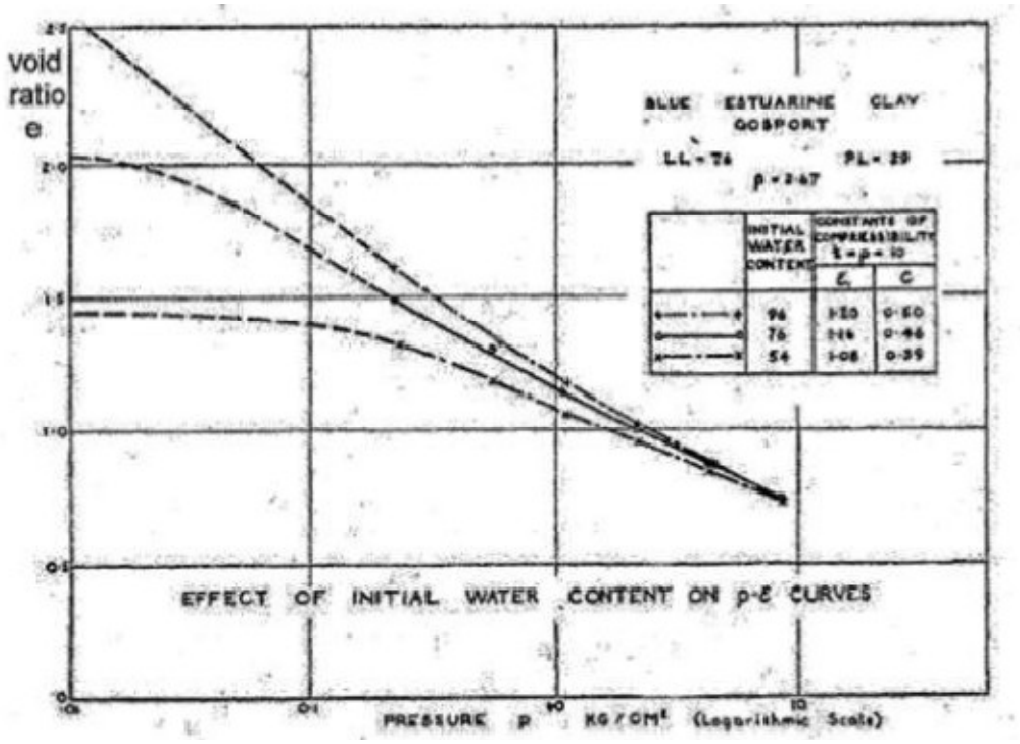

Figure 2. 4: compression tests on reconstituted Gosport clay samples (Skempton, 1943).

Roscoe et al. in 1958 presented the first comprehensive analysis of compressibility and strength of reconstituted clay samples.

With respect to the normal compression behaviour, they reported the results on the $e - \log\sigma'$ (or $v - \log\sigma'$) chart and drew the normal compression line (NCL). The normal compression line represents the boundary of the possible states in the e (w)-logp′ chart. The points on this line represents stress-strain states of normally consolidated clays, whereas the points below represents over-consolidated clays. Soils whose behaviour follow the normal compression line have mainly plastic volumetric strain, whereas on the unloading curve overconsolidated soils are subject to elastic deformation.

Given these experimental evidences from the stress paths in drained and undrained compression and shearing, they hypothesised and demonstrated the existence of a state boundary surface on the $v - p' - q$, which coincides with the Roscoe/ Rendulic surface (or the Hvorslev surface in the case of over-consolidated clays, as will be discussed further).

The stress paths reach this state boundary surface when the soil continues to shear without any change in volume under constant effective stress. This surface defines the so-called Critical State of the soil.

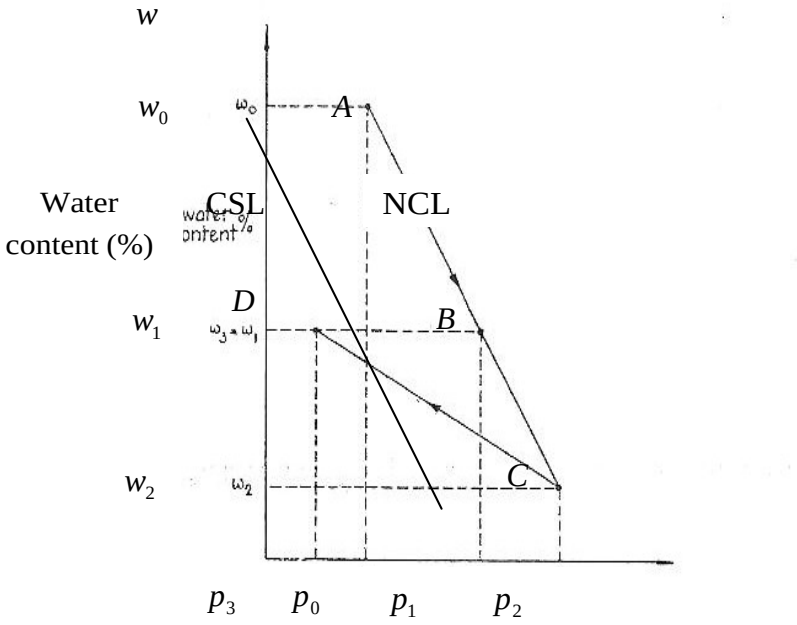

Figure 2. 5: relationship between water content and consolidation pressure for a clay (modified from Roscoe *et al.*, 1958).

The intercept of this surface with the $q = 0$ plane identifies the normal compression line.

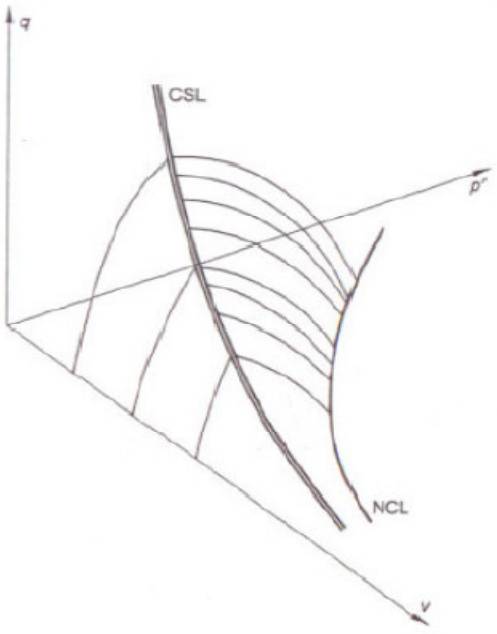

Figure 2. 6: Limit state surface in the v-p′-q plane (modified from Lancellotta, 2004).

The Critical state curve represents the failure points at high strains. In the $p'-q$ chart this curve becomes the Critical State Line. The Critical State can also be represented in the $\tau - \sigma' - e$ t-s′-e chart, as in the figure below.

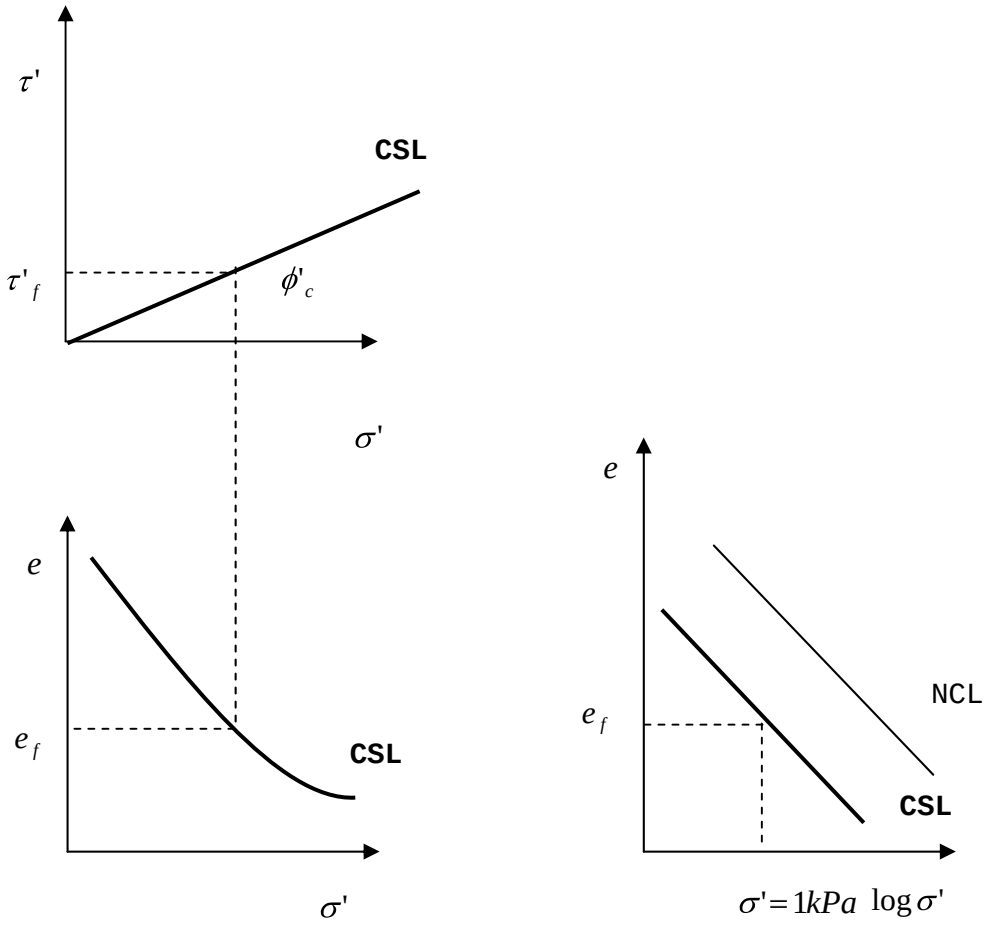

Figure 2. 7: critical state line and normal compression lines in different planes (modified from Atkinson and Bransby, 1978).

When considering drained triaxial shearing of a normally consolidated clay, the stress paths coincide with curves that link the NCL with the CSL and lie on the plane parallel to the v (or e) axis and its intercept with the $p'-q$ plane has a steepness of 3:1. If undrained shearing is analysed, the stress paths link the NCL and the CSL, but in this case they belong to a plane perpendicular to the v axis, being the specific volume constant in drained conditions (see figure 2.8).

The mechanical behaviour of over-consolidated clays is quite different from the one above described for normally consolidated clays. First of all, their state on the $v-p'$ chart needs not only the stress value, but also the v value to be univocally described, given that it lies on the left of the NCL.

When considering drained and undrained compression and shearing of over-consolidated clays, a state boundary surface on the $v-p'-q$, is reached at failure,

defined as Hvorslev surface. In fact, over-consolidated clays first show a peak resistance at low strains, then it decreases to a constant value.

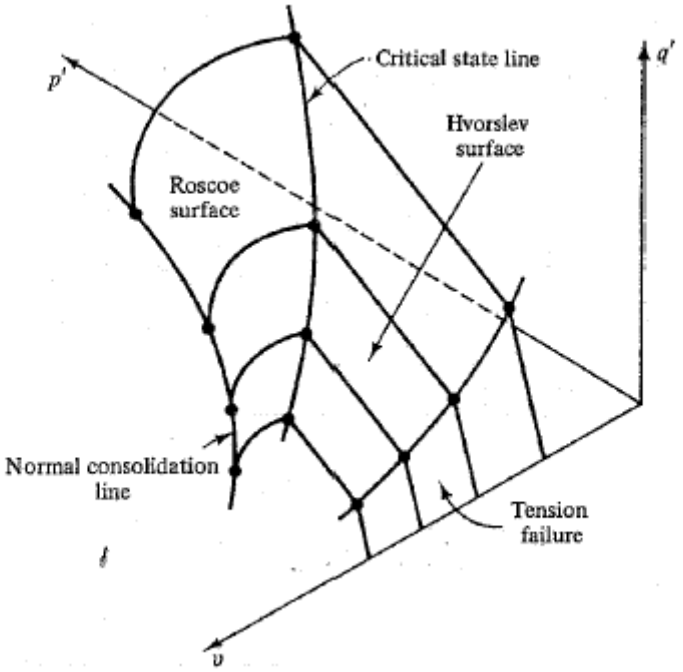

Figure 2. 8: the three dimensional state boundary or yield surface in the $v - p' - q$ space (from Atkinson and Bransby, 1978) with detail of the Hvorslev surface for undrained paths and of the Roscoe surface for drained paths.

In figure 2.9, undrained boundary surfaces and stress paths are represented with increasing overconsolidatio ratio $R_p = OCR$.

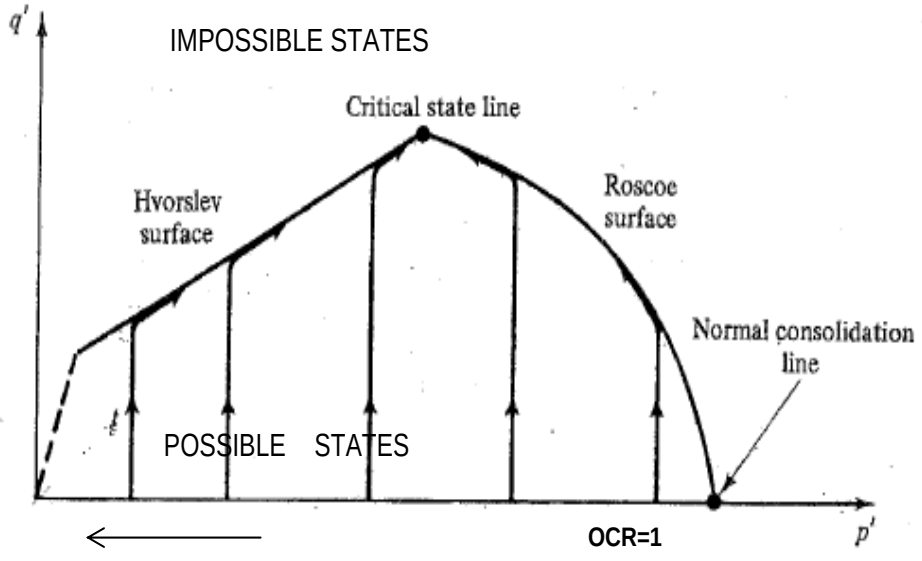

Figure 2. 9: possible undrained stress paths and critical state line for overconsolidated clays.

Another important step in the development of the critical state framework was presented in 1963 by Roscoe and Poorooshasb; they demonstrated that the undrained and the drained stress paths, once normalized with respect to an equivalent pressure p_e' resulted in the same curves. The equivalent pressure p_e' is defined as the pressure, for a given stress-strain state, corresponding to the same void ratio but on the normal compression line.

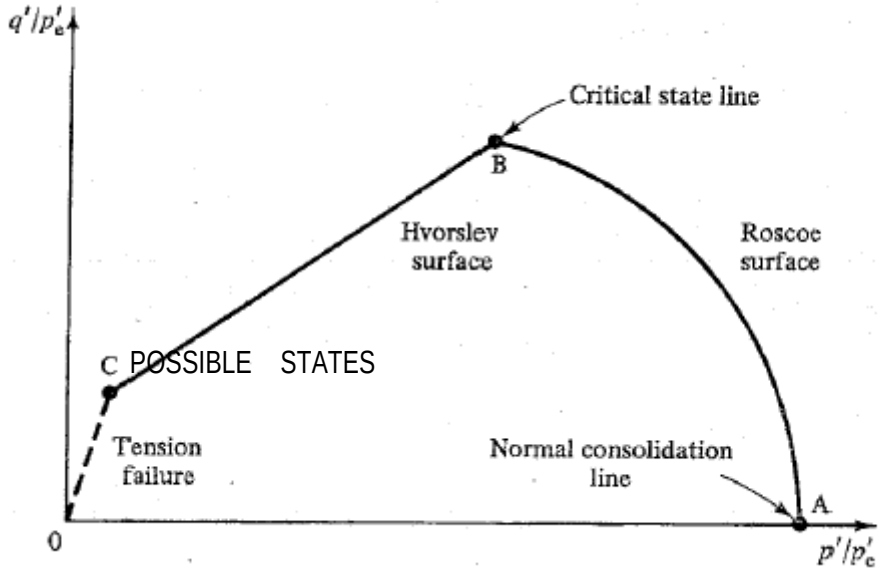

Fig.2. 1: normalized critical state line and state boundary surface (modified from Atkinson and Bransby, 1978)

The Critical state framework resulted therefore in a very powerful means to model the behaviour of clays (Schofield and Wroth, 1968). However, some limitations of the equations were found when applying the model to medium to high plasticity clays in overconsolidated conditions, limitations probably due to microfabric.

2.1.1. Note for Natural clays

The behaviour in normal compression and in shearing of natural clay samples was defined in more recent thanks to the contributions of several authors, but Burland in 1990 presented a comprehensive and exhaustive review of the subject.

It can be stated that the theorical framework found for reconstituted clays can be applied also to natural clays. However, the structure of the material and its intrinsic properties were found to lead a fundamental role in the mechanics of natural clays. Structure is defined as the combination of ‘fabric’ (arrangement of particles) and interparticle bonding (Mitchell, 1976).

Burland related the mechanical properties of consolidated reconstituted clays with the ones of natural clays, whose geological origin greatly influence the behaviour, because particle arrangements and bonds are created, defining structure.

2.3. Mechanical behaviour of sands

In this paragraph, a review of the mechanics of granular soil is shown, particularly with reference to the experimental results, from drained and undrained shearing, that lead to the application of the Critical State Theory to sands, also defined as Stationary State theory (Casagrande, 1936; Castro, 1967).

A comprehensive analysis that lead to the demonstration of the applicability of the framework to both clays and sands was showed by Roscoe et al. (1958).

However, some features are still object of discussion. The stress-strain behaviour of sands depends on its density and not on the stress history, as seen for cohesive soils. Therefore, the behaviour of loose and dense soils will be compared and the concepts of dilatancy, stationary state of strain and instability line will be introduced. Moreover, whereas for reconstituted and natural clays the initial differences in structure, such as density, are erased quickly, for sands it is the density that influence the behaviour, so that, for example, the onset of particle breakage causes the yielding point of the curves to be located at much higher stresses.

2.3.1. Behaviour of loose and dense sands

The first researches on the different mechanics exhibited by loose and dense sand specimens were carried out by Casagrande in 1936. The sand samples were sheared at the same effective confining pressure p'_C in drained strain controlled triaxial tests. His results showed that loose sand samples contracted and dense samples tended to dilate, but they both reached the same value of void ratio (or specific volume) at large strains (see further for details).

Loose sands

The mechanical response of a sand in a loose state was found to be strongly non-linear and irreversible. As the stresses increased, the strain increased until an asymptotic value of the deviatoric stress at failure is reached at high strains (strain

hardening). The stress paths in terms of total stresses coincide with the ones in terms of effective stresses.

When considering drained triaxial tests on two samples having the same initial density, but at different confining pressures, it could be observed that, with increasing cell pressure, the deviatoric stress reached at failure proportionally increased.At failure the single sand grains moved in order to reach the most stable new spatial configuration and this determined a progressive reduction of the void ratio until a critical void ratio ec was reached (contractive behaviour): As soon as the material reached this state, subsequently defined as critical, as seen for clays, the soil continued to deform at constant stresses and volume.

Dense sands

Sand dense samples showed a mechanical response in shearing characterised by a peak of strength, associated with the maximum value of dilatancy (see section 2.3.2). It can be stated that the resistance offered by this material is higher than the one offered by loose sands.

Moreover, at higher strains the stresses that the soil can sustain decrease until a constant value is reached at constant volumetric strain (critical state): due to dilatancy, the particles points of contacts decrease. This corresponds to a dilating behaviour. The stress-strain curve is the one typical of strain softening.

A sample with a medium density behave in a similar way as the dense sample, but with a less evident dilatancy effect. The volumetric strain in both cases, after a small contraction, becomes negative, thus the sample dilate.

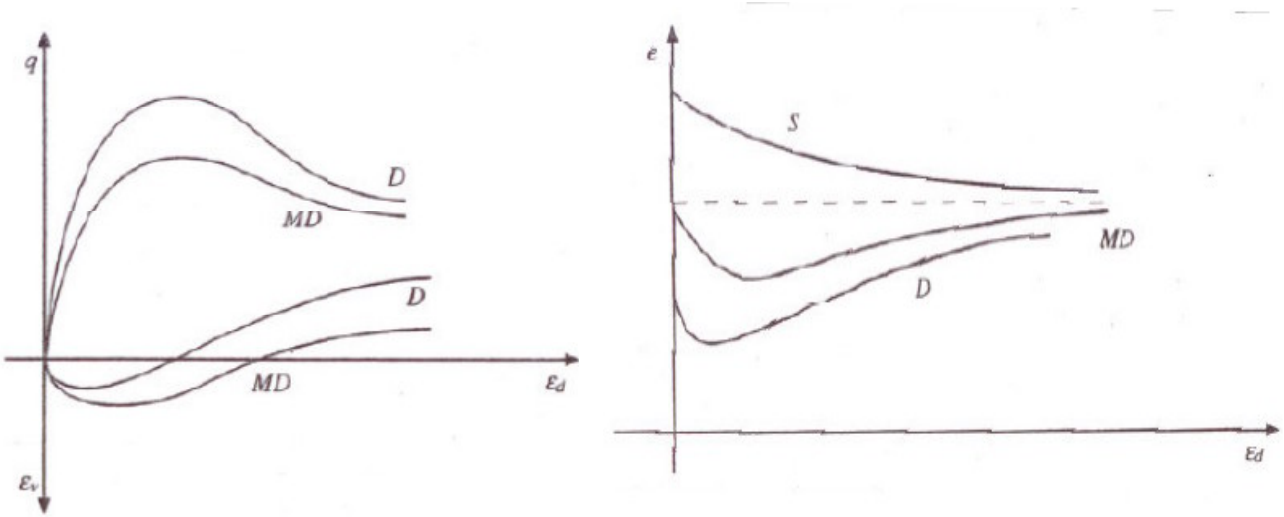

Figure 2. 10: Mechanical response in drained shearing of a dense and a medium-dense sand (from Atkinson and Bransby, 1978)

At the critical state sand samples should present the same shear stress and the same volume, no matter their initial density at the beginning of shearing.

As seen for normally consolidated and overconsolidated clays, a peak friction angle $\varphi_p^{'}$ and a 'final' or critical friction angle at constant volume $\varphi_c^{'}$ can be identified. The $\varphi_p^{'}$ usually belongs to the range of values comprises between 30° and 45°, whereas the critical friction angle, which is more linked to the mineralogical properties, is comprised between 30° and 35°.

Thus, as seen for cohesive soils, the peak shear strength of a sand depends on its initial density, while the critical friction angle is an intrinsic property of the material.

In the figure below, Kramer (1996) reported an overall view of the stress-strain behaviour with respect to the stress-void ratio curve based of dense and loose sand samples, sheared at the same confining pressure.

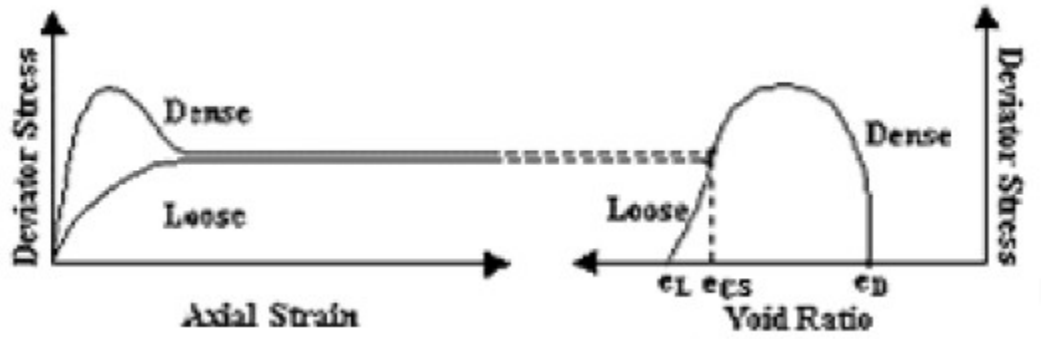

Figure 2. 11: Mechanical behaviour of a dense and a loose sand confined at the same pressure, with particular highlight on the same critical state reached (Kramer, 1996)

If shearing is carried out on samples at the same density, the mechanical behaviour is directly linked to the confining pressure: particularly with decreasing p′c, a loose sand tend to a more dilating behaviour, whereas with increasing confining pressures a dense sand shows a less dilating effect. In figure 2.12, the effect of different confining pressures on a dense sample of Hokksund sand is reported.

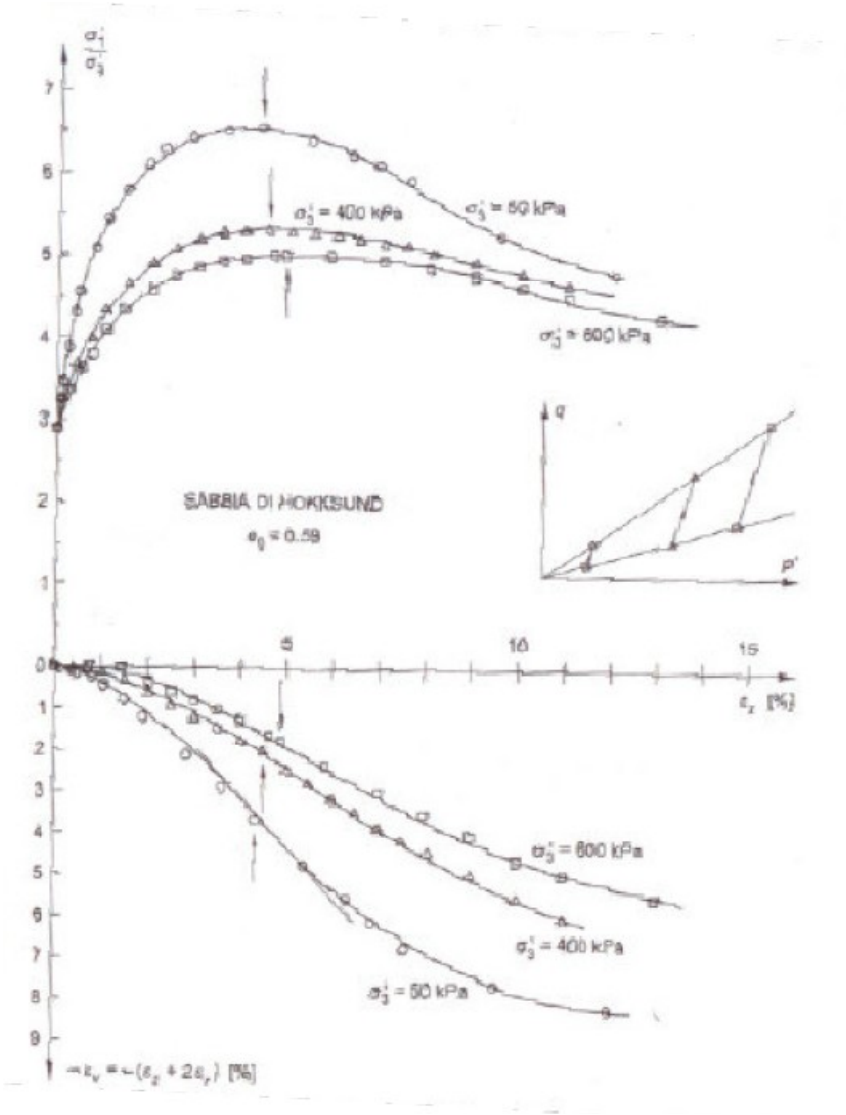

Figure 2. 12 Influence of confining pressure on Hokksund sand samples, tested in drained shearing at the same initial density.

It can be concluded that a granular soil exhibits a dilative or contractive behaviour depending on its initial density and confining pressure.

Undrained behaviour

Castro in 1967 carried out undrained stress-controlled triaxial tests on sandy samples and identified the development of positive pore pressures and negative pore pressures, respectively for loose and dense soils.

On one hand, he identified a correspondence between the contractive behaviour in drained conditions and the development of positive pore pressures in undrained conditions for loose samples, on the other a correspondence between the dilative response and the development of negative pore pressures for dense samples.

Medium-dense samples were found to contract initially, then, with increasing level of strain, they start to dilate.

Castro identified a steady state for high levels of strain where a unique relationship between final void ratios and final stresses could be established. The correlation was called Steady State Line (SSL) and it is similar to Casagrande's Critical State Line.

In the figure below, three different stress paths referring to the same confining pressure are represented in order to draw the Steady State Line (SSL) for the analysed sand.

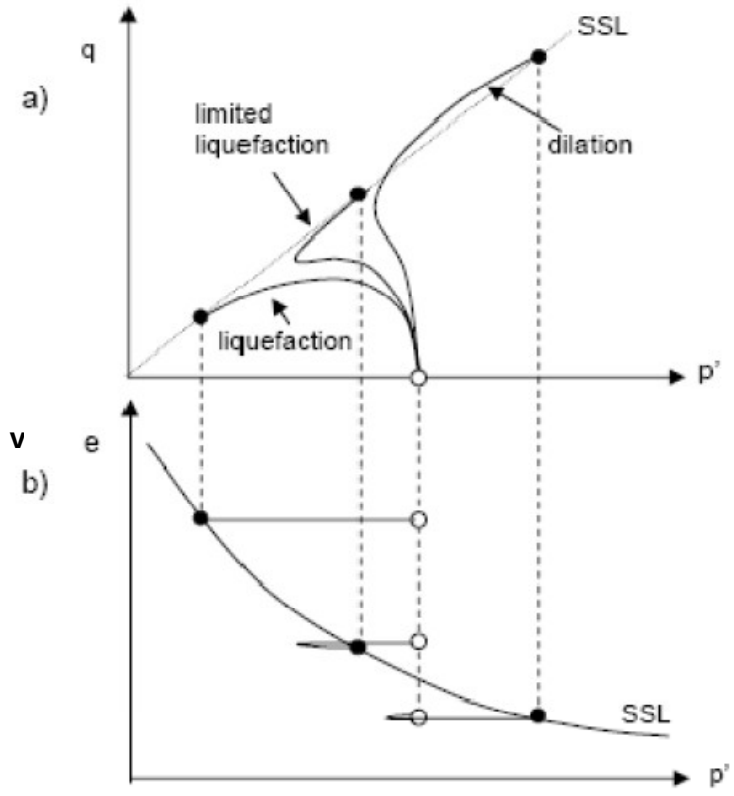

Figure 2. 13 Comparison of the stress paths of three samples with different initial densities but with the same confining pressure. Particularly, the initial and the Steady states in the two planes are highlighted (modified from Carrera, 2008)

In the figure below, the undrained stress paths of loose and a dense sand are reported, given that they have the same initial density but with varying confining pressures.

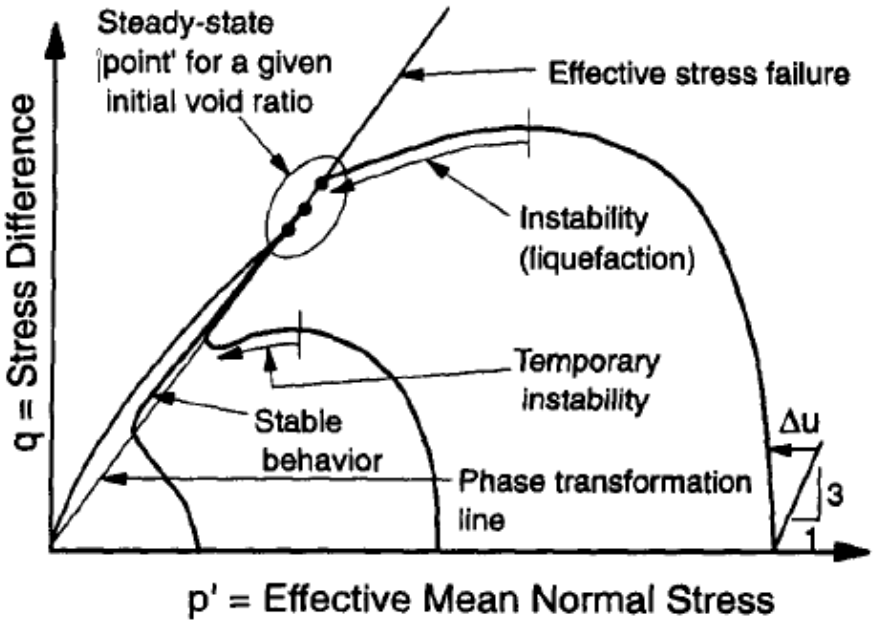

Figure 2. 14 Stress paths for three identical sand samples sheared from three different confining pressures

The main contribution of Castro′s work can be identified in the study of the mechanics of very loose sand. Very loose sands at high confining pressures presented a strongly contracting behaviour and in parallel a monotonic increase in excess pore pressure. However, once overcome the peak point, an instability condition occurred. The steady state was reached instantly, because the shearing is performed in stress-controlled tests. Thus the peak point represents a border and with increasing stresses, the soil deforms in order to pursue a more stable configuration.

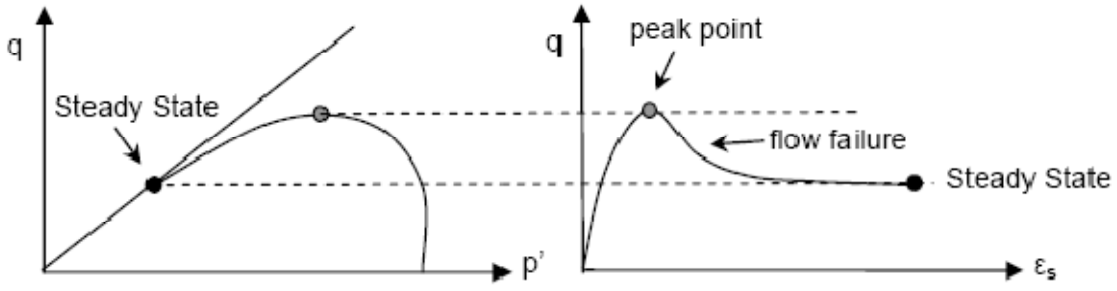

Figure 2. 15: behaviour of a loose sand and of a sand at very high confining pressures (from Carrera, 2008)

At low confining pressures very dense samples initially contracted, but this phenomenon is soon followed by a strong dilation, in parallel with high increase in negative excess pore pressures.

Ishihara et al. (1975) studied the behaviour of Toyoura sand samples and described this behaviour initially contractive and subsequently dilative as phase transformation. The strain state that corresponds to this inversion of behaviour was called quasi-steady state (QSS) (Alarcon-Guzman, 1988).

Yao et al. (2004) tried to model the behaviour of Toyoura sand within a critical state framework and focused on the influence of initial density on the undrained stress paths. As it can be observed in the figure below, loose samples liquefy, whereas medium to dense and dense soils contract but, once reached a minimum mean effective stress, invert their behaviour and tend to dilate.

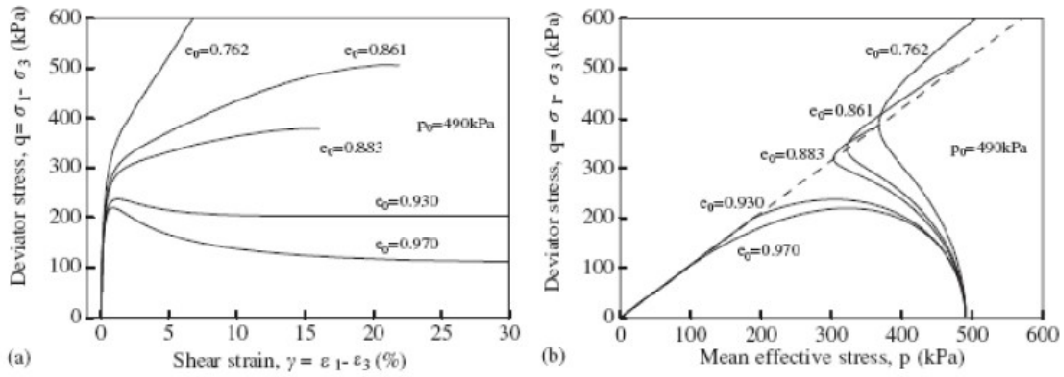

Figure 2. 16: Influence of different initial void ratios on Toyoura sand samples confined at the same confining pressure in undrained tests (from Yao et al. 2004)

When analysing the influence of increasing confining pressures on similar samples having the same initial density, it can be seen that a ultimate steady state is reached at very high strains (USSL).

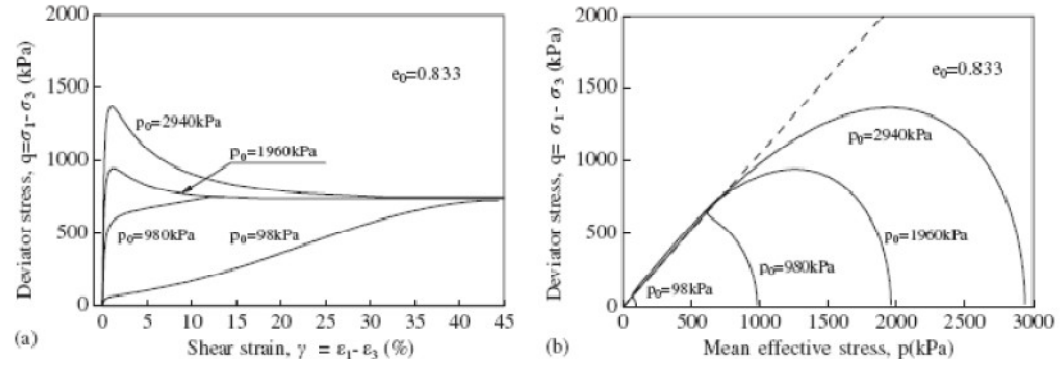

Figure 2. 17: effect of different confining pressures on identical samples of Toyoura sand (Yao et al., 2004)

If the initial void ratio is decreased or the mean effective stress increased, the comparison allows to state that all the transformation phase lines converge to the

USSL, until they reach a totally contractive behaviour defiend as Critical Steady State (CSS).

In the figure below a summary of the states previously introduced can be found: the ultimate steady state (USSL), the quasy-steady state (QSSL) and the phase transformation line (PTL) define the undrained behaviour of sands.

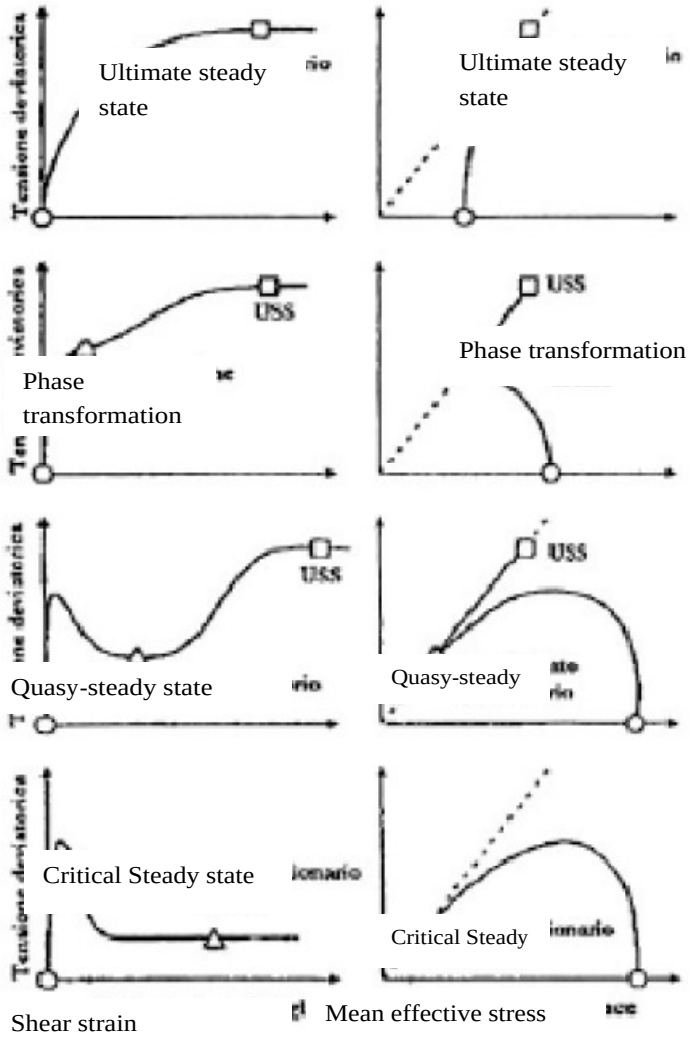

Figure 2. 18: Summary of different undrained behaviour of sands (modified from Carrera, 2008).

The steady state line was also used as a valid means of identification of tendency to liquefaction of sand samples in undrained behaviour.

A formal definition of the Steady State was proposed by Poulos in 1981, who defined it as the state in which the soil mass is continuously deforming at constant volume, constant effective normal stress, constant shear stress and constant velocity.

Been et al. in 1991 demonstrated that the Critical state derived from drained tests and the Steady State derived from undrained tests referred fundamentally to the same condition, irrespectively of the condition of load or strain- control.

The Critical State can be considered as a reference state in order to analyse the mechanics of sands, because it is a stress-strain condition that is not influenced by testing procedures.

Been and Jefferies in 1985 introduced the so-called state-parameter Ψ as:

$$\Psi = e - e_{CS}$$

for that part of the CSL corresponding to medium-low critical confining stress p'_{CS} and high void ratios.

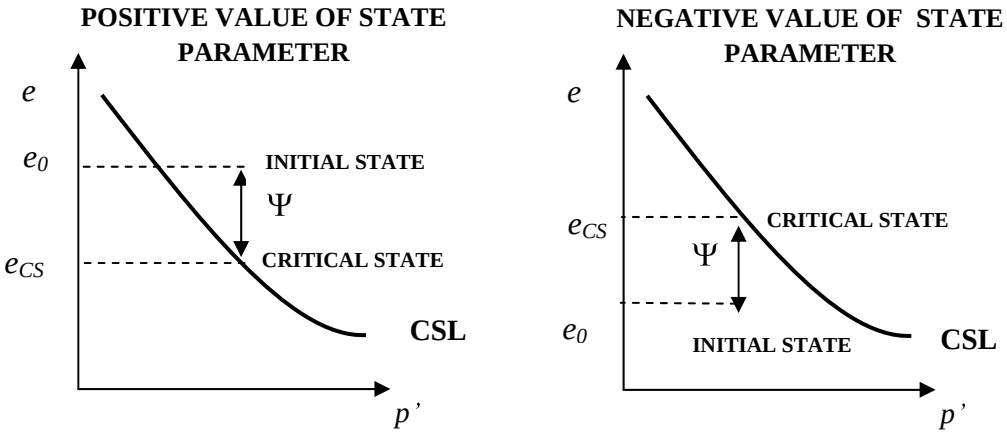

Figure 2. 19: definition of the state parameter: a contractive behavior corresponds to a positive Ψ, while a dilatant behavior corresponds to a negative Ψ. (modified from Atkinson, 1997).

If the state of the sample at the start of the shearing phase is located below the CSL, the specimen dilates upon shearing, whereas if the state of the specimen at the beginning of shearing is above the CSL, the sample contracts.

This parameter allows to identify soils that exhibits the same mechanical behaviour, because the same value of Ψ means that they have the same distance from the Critical state line.

CHAPTER 3

The transitional soils framework

Introduction

The mechanical behaviour of clays and sands has been the object of a great number of studies that can be found the literature. However, clean sands and pure clays are quite rare and usually can be found in well-graded soils.

Given the applicability of the Critical State framework to clays and sands, it had always been assumed that this would have been effective even for those soils with a grading in between. Research carried out in the last decades pointed out that this is not necessarily true, therefore the mechanical behaviour of silts and of soils with an intermediate grading has started to be investigated.

The range of soil composition include silts, silty sands, clayey sands and both gap graded and well-graded soils.

Although the available data on the mechanics of this type of soils is nowadays significant, since the interest began in the 60s, clear conclusions cannot be stated as the results are often contradictory.

In the following paragraphs a review of these researches and a summary of the main evidences is presented, with respect to the mechanics of granular soils mixed with fines. Particularly, a specific mode of behaviour has been identified and defined 'transitional behaviour', whose properties will be described.

From these studies the hint to the research on the Venice soils analysed in this thesis occurred.

Future research needs to focus on the identification of other soils that might show this transitional behaviour in order to see how widespread the phenomenon is.

3.1. Influence of fines content on the mechanics of sands

It is well known that the behaviour of clays is governed by electrostatic forces, whereas for sands grain crushing is the main mechanism involved in the mechanical response.

For a natural granular soil, the behaviour is a function of specific characteristics such as mineralogy, particle dimensions and shape, and other features such as inter-particle contacts.

Very little data are available on the behaviour of pure silts. It had always been assumed that the mechanics of these intermediate soils should be ascribed to electrostatic forces, whereas the first laboratory evidences on silts and silty clayey mixtures seemed to suggest that their behaviour is not that of a plastic material.

Researches have been carried out on the behaviour of mixtures of sand and fines in the last decades, whereas only in recent years studies began to focus on well-graded and gap-graded natural soils.

In this paragraph a review of the most important findings are reported. It can be noted that it is usually acknowledged to indicate with the term fines the soil particles passing through the sieve n° 200 according to ASTM standards, thus to consider the particles whose diameter is lower than 74□□m.

3.1.1. Void index and microstructure in granular soils

A soil matrix is the spatial distribution of voids and grains. From this configuration depends the local shear strength offered under different loading conditions. The microstructure of a granular soil is particularly complex.

The void ratio e (or the specific volume v, $v = 1 + e$) is the parameter that describes how close the particles are, thus resulting in fewer voids and therefore denser soils.

It is defined by the following expression:

$$e = \frac{V_v}{V_s}$$

Where:

V_v is the volume of the voids and V_s is the volume of the particles.

When a granular soil is subjected to a load, the active contacts that develop between the grains try to sustain it.

Recent research pointed out the need to study granular soils containing quantities of fines.

The main difficulty lies in the description of the active contacts between soils with different particle dimensions. It is usually accepted to separate the whole microstructure into two sub-matrixes, a fine and a coarse-grained, and to analyse the internal forces acting between particles.

Thevanayagam (2002) identified three main limit micro-structural conditions, presented in the figure below. In figure 3.1.a the coarse grains prevail and the fines, depending on their quantity, can fill the intergranular spaces without contributing to the support of external forces, can partially sustain the load or even separate the coarse grains. Figure 3.1.b describes the case where the amount of fines particles is high enough to separate all the coarse particles. Finally, in the last configuration the two kinds of soils form separated mono-granular layers.

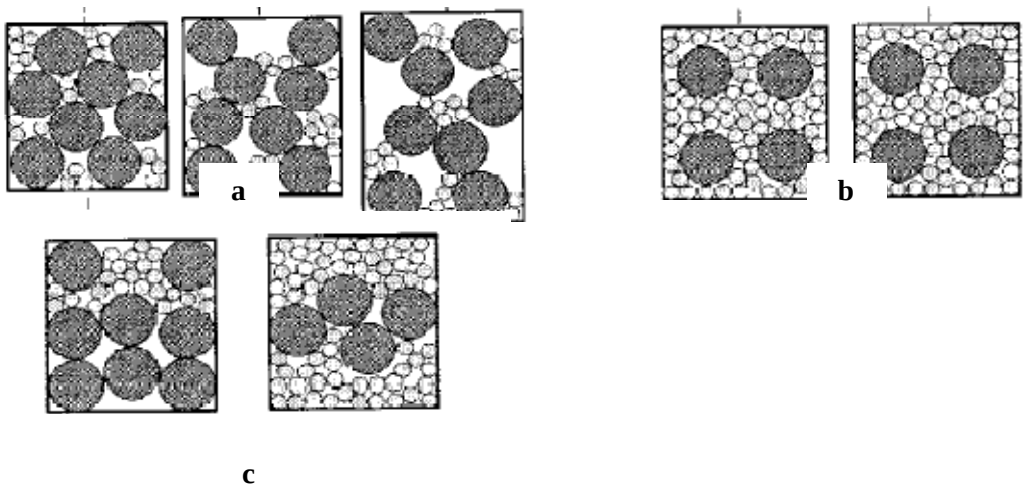

Figure 3. 1: Different microstructures as classified by Thevanayagam (2002)

Once overcome a specific fines percentage, which according to the author usually lies around 15%, the fines particles become to have a role in sustaining the load, but also the intrinsic properties of the two fractions and the void index are determinant.

In soils where the coarser particles are dispersed in a matrix of fines, the whole behaviour is determined by the fines.

The most important consequence of the scheme shown by Thevanayagam is that to the same void index, depending on the fines content, the forces transmitted to the coarse grained material vary within a great range.

Several parameters have been introduced in the last decades in order to take this phenomenon into account.

Mitchell (1976) introduced the 'intergranular' or 'skeleton' void ratio e_{sk} defined as:

$$e_{sk} = \frac{V_v + V_f}{V_s}$$

where V_f is the volume of fines.

If it is assumed that the specific gravity G_S of the sand and of the fines is the same, then the intergranular void ratio can be defined as a function of the fines content f_c (%):

$$e_{sk} = \frac{e + (f_c/100)}{1 - (f_c/100)}$$

Considering a volume of soil formed by grains, coarse and fine, and the voids in between, the volume occupied by fines is $f_c/100$ and the volume occupied by coarse particles is $1 - f_c/100$.According to the scheme introduced by Thevanayagam (1998), the intergranular void ratio is also known as es.

In this framework, the threshold after which the behaviour becomes influenced by fines is determined by a value of f_c because the fines start to lie between the grain contacts, influencing the overall behaviour of the soil.

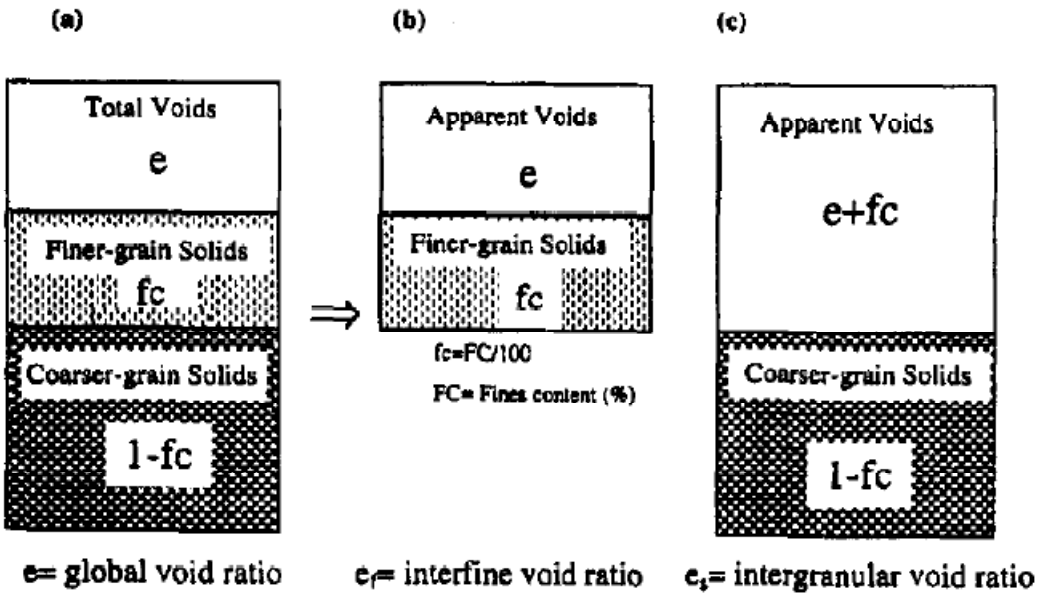

Figure 3. 2: Analysis of the scheme introduced by Thevanayagam (1998), with particular reference to sands containing fines and fines containing sands

The use of this e_{sk} might allow to model the mechanics of these mixtures within the CS framework, because it represents an index of the active grain contacts that sustain the loads.

According to Thevanayagam and Mohan (2000), at high pressures the Critical State lines of different mixtures of sand with increasing fines content were found to converge in the $e_{sk} - \log p'$ chart.

Polito (1999) defined as 'limiting fines content' the value of f_c that separates the domain of sand and the domain of fines.

Within this framework, Yang et al. (2004) define the 'transitional fines content' as the maximum amount of fines that, added to the sand matrix, only fill the voids without giving any contribute to the overall mechanics of the sand.

The influence of grading on the mechanical behaviour of soils was also highlighted in studies on uncemented Dog's Bay sand (Coop, 1990) and on mixture of Dog's Bay sand with uncemented gypsum plaster (Coop and Atkinson, 1993).

In Thevanayagam's framework, the relative density parameter is also adapted to the use of the newly introduced intergranular void ratio.

$$D_R = \frac{e_{\max} - e_s}{e_{\max} - e_{\min}}$$

Where the maximum and minimum void ratio refer only to the clean sand.

The determination of the maximum and minimum void ratio achievable by a clean sand is usually carried out following the procedure described in the standards ASTM D 4253 e D 4254. Those recommendations, however, limit the use of the procedure to a certain grading, particularly for fines content lower than 15%. Measuring $e_{\max}$ and $e_{\min}$ when considering fines contents higher than 15% might be misleading for the well-known effect of formation of 'honey-comb' structures. Within this sample structure, the fines tend to form aggregates and this might lead to inaccurate values of $e_{\max}$ and $e_{\min}$.

Several researches (Pitman et al., 1994; Lade and Yamamuro, 1997; Yang, 2004) pointed out the influence on $e_{\max}$ and $e_{\min}$ of increasing fines content. Lade and Yamamuro (1997) analysed the trend of these parameters referring to Ottawa sand, as it can be seen in figure 3.3.

When fines are added to sands the achievable maximum and minimum void ratios decrease. A fines content known as f_C defines the percentage at which the trend of both parameters change. This value of fines content was found to be between 15% and 40%. It is usually acknowledged that a fines content of 30% allows to separate the behaviour influenced by sand and the one determined by fines.

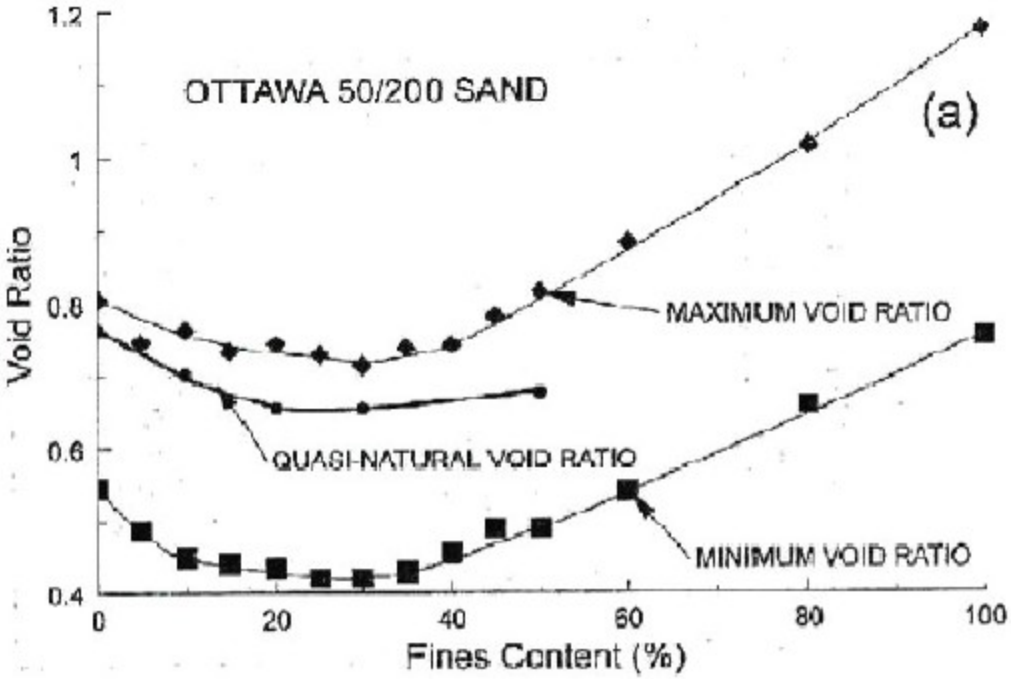

Figure 3. 3: Maximum and minimum void ratio of Ottawa sand mixed with fines, as fines content varies (Lade and Yamamuro, 1997)

One of the most recent study on silty sand from Chlef (Algeria) performed by Arab in 2009 focused on the influence of fines presence on the sand behaviour. The results showed in general a more contractive behaviour.

3.1.2. Influence of fines on the mechanical behaviour of sands

The studies on the mechanics of cohesive soils, performed by Rendulic and Skempton among the others, allowed to define the Critical State for clays. However, it is only thanks to Casagrande's work that this framework was applied to model the behaviour of clean sands.

In the figure below, the 1D- normal compression line (NCL) and the critical state line (CSL) on the v-logp′ are shown.

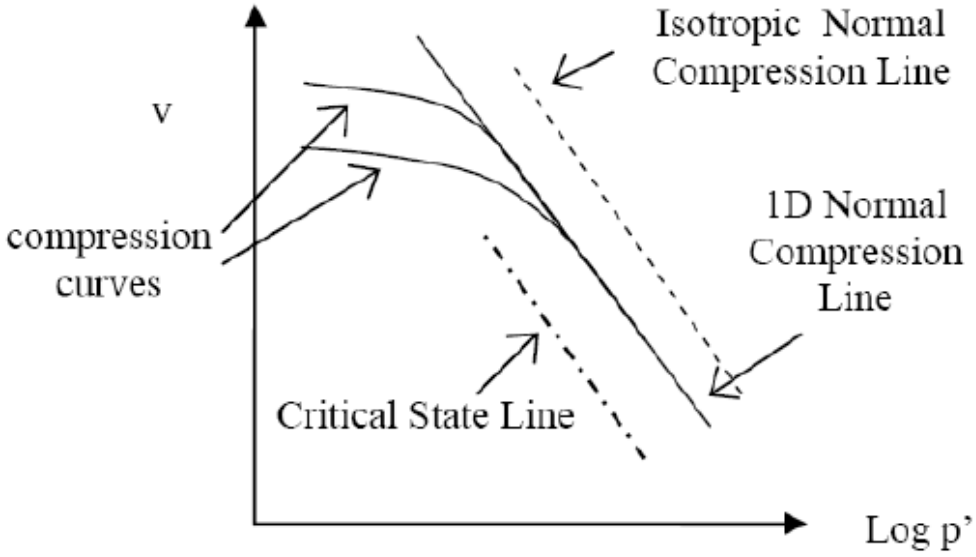

Figure 3. 4: Compression curves of sand at different initial densities converge to a unique Normal Compression Line at high stresses (from Carrera, 2008)

When normally compressed at high stresses, samples with different initial densities reach a unique NCL, that separates possible and impossible soil states, while the Critical State Line (CSL) represents the state reached by soils at high strains in both drained and undrained shearing.

As introduced in Chapter 2, these studies derive from tests on clays and clean sands, but several researches had started to show changes in the mechanics induced by the fines presence.

Kenney (1967,1977) carried out a research on the influence of mineral composition on the residual strength of natural soils. He reported that mineralogy and thus the particle shape strongly influence the residual friction angle. In following years he linked the friction angle variation to the presence of platy particles and thus to mineralogy.

Recent seismic events pointed to researchers how important a significant amount of fines become in the behaviour of natural sands or artificial soil mixtures (Seed and Harder, 1990).

Influence of fines on the friction angle

Lupini et al. in 1981 studied the mechanics of sand-bentonite mixtures and observed that the friction angle values at the Critical State φ'_{CS} decrease with increasing clay content. According to them, three different modes of shearing response at high stresses could be identified, depending on particle shape. Soils

with spherical particles and low fines content the fiction angles are higher and the main mode of behaviour introduced was ‘rolling’.

For higher percentages of fines, particles are platy and strongly orientated, thus the shearing resistance angle is lower and shearing depends on a ‘sliding’ mechanism. An intermediate case was defined as ‘transitional’, comprising both turbulent and sliding mechanisms.

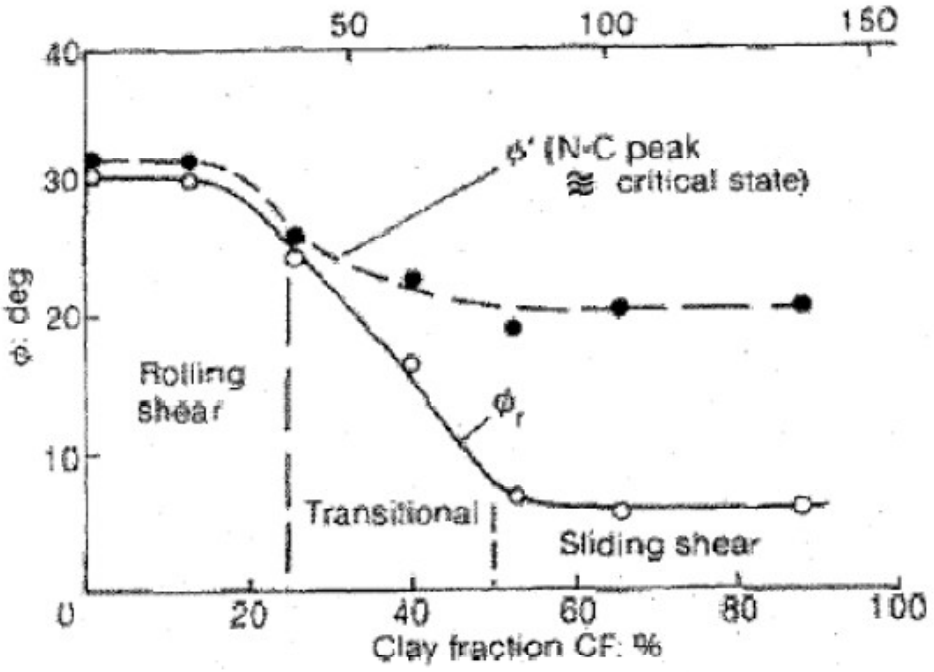

Figure 3. 5: Friction angle values with increasing clay fraction, derived from annular shearing tests on mixture of sand and bentonite (Lupini *et al*., 1981; Skempton, 1985)

In a study by Been and Jefferies (1985) on the mechanics of Kogyuk silty sand, the influence of increasing non-plastic fines content was investigated. The authors observed that the addition of fines itself resulted in looser structures, thus steeper Steady State Lines and higher values of void ratio at low levels of stress were found.

Coop and Atkinson (1993), while investigating the behaviour of mixtures Dog′s Bay sand with different kind of fines, concluded that the addition of gypsum or calcium carbonate fines to a carbonate sand do not influence sensitively φ'_{CS}.

Pitman et al. (1994) performed triaxial tests on quartzitic sand with kaolin (plastic) or silica (non plastic) fines. At low fines percentages, no significant differences were appreciated, but with increasing fines content, at high strains mineralogy was found to influence the post-peak stress in softening.

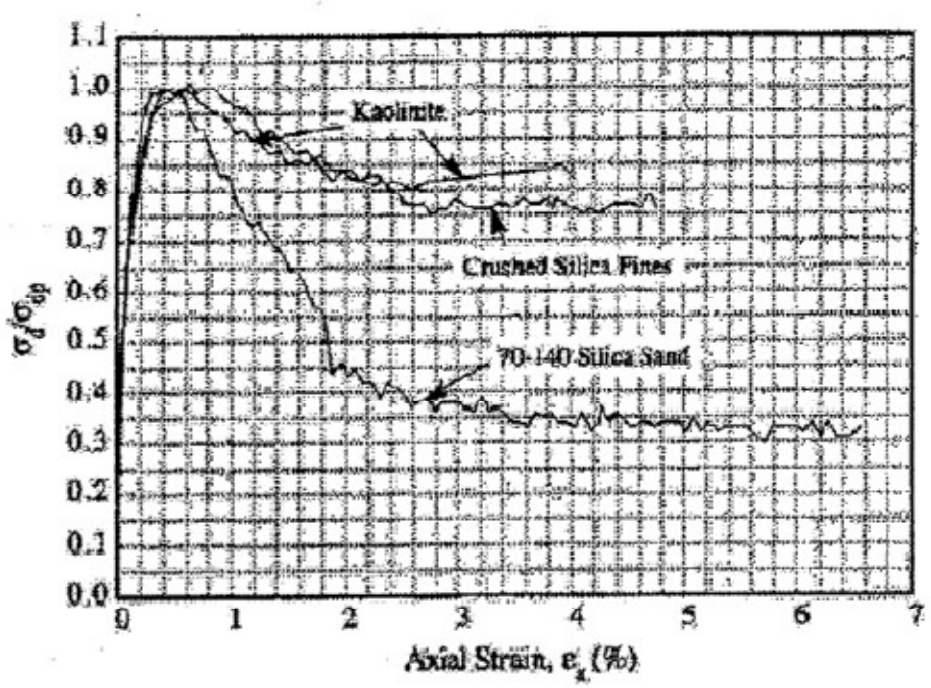

Figure 3. 6: influence of mineralogy on the stress-strain behaviour (Pitman *et al*., 1994)

Fourie and Papageorgiou (2001) studied the mechanics of tailings from Marriespruit. For confining pressure values higher than 200 kPa, with increasing percentage of fines content, they observed a downward shift of the Critical state lines.

Thevanayagam et al. (2002) did not find a difference in the steepness of whereas the Critical State lines, corresponding to different amount of non-plastic fines within the mixtures of cleans sand and fines, were shifted: the higher the amount of fines, the lower the position on the e-logp′ chart. Thus with increasing fines content the samples shear strength decrease, given that their intergranular void ratio decreases.

The authors, however, also observed that for fines content of 40% there was an inversion of this trend. The position of the CSL of the mixtures started to raise again. This threshold fines content was defined as 'transitional fines content'.

Murthy et al. (2007) focused on the behaviour of Ottawa sand and observed an increase of the shearing resistance angle at the critical state with increasing amount of non plastic clay particles. Particularly, at a fines content of 15% the value of φ'_{CS} increased from 30.2 ° to 34.4 °. They hypothesised that the angular silty particles prevented the rounded sandy particles from rolling movements .

Adrianopoulos et al. in 2001 observed for several sand-fines mixtures that with increasing fines content the steepness of the CSL and the intercept at 1 kPa increase.

This result confirms the conclusion given by Been and Jefferies (1985) that the addition of fines itself implies a looser structure, thus higher compressibility and e_{max}.

A result that was presented by Salgado in 2000 seems to contrast with most of the findings described above. Ottawa silty sand samples mixed with non plastic fines were prepared at fines content between 5 and 20% and confined at 100 kPa and 400 kPa. In drained triaxial tests with increasing fines content the shear strength angle increased. This result was related to the natural trend of the particles to reach a more stable configuration, but this behaviour seemed to be applicable only to the specific mixture, if compared with previous researches.

Effects induced by fines content on the compression behaviour of sands

In more recent years the knowledge of the effects induced by fines on the normal compression behaviour of sands started to be investigated.

Coop and Atkinson (1993) studied the mechanics of mixtures of Dog′s bay sand and gypsum/ calcium carbonate. They found that the presence of fines resulted in a lower steepness of the NCL for the mixtures in comparison with the NCL of the clean sand. No significant differences were found between the addition of gypsum or calcium carbonate, therefore it was hypothesised that mineralogy did not have a predominant role in the behaviour of these soil mixtures. Flatter isotropic compression lines and lower e_{max} were also found for samples containing Dog′s bay sand and fines.

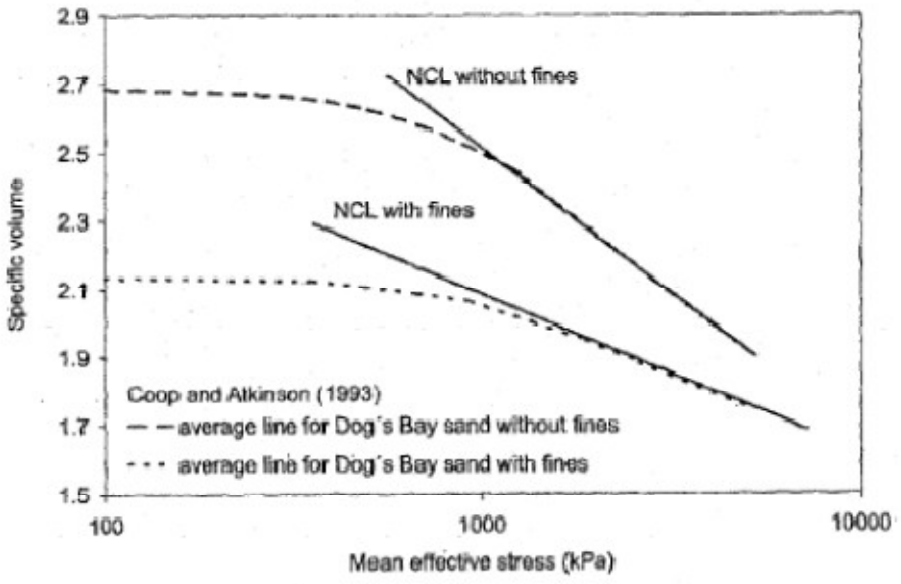

Figure 3. 7 : influence of fines on the steepness of the NCL of Dog′s Bay sand samples (Coop and Atkinson, 1993)

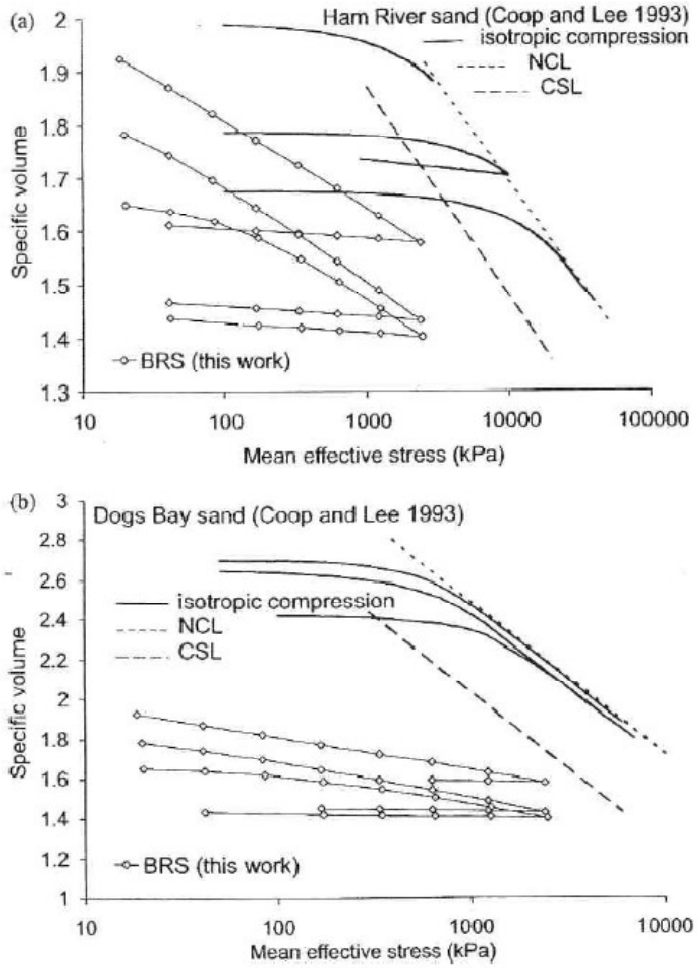

Figure 3. 8: Comparisons of the results by Martins et al. with the NCLs and CSLs determined by Coop and Lee (1993)

Coop and Atkinson (1993) note that the reduction in the steepness of the NCL of mixtures of Dog′s Bay sand and fines in comparison with the NCL of the clean sand has to be related to the smaller amount of particle breakage. The fines act as a cushion between the bigger sandy particles.

They report that the same reduction in steepness is found also for the CSL of the same mixtures in comparison with the clean sand behaviour, moreover the CSL and the NCL found for the mixtures run parallel. Thus only the part of the CSL after the curvature has been observed.

For Dog′s Bay sand the curvature of the CSL is found for level of confining pressure of around 300 kPa.

As it will be shown in section 3.2, these studies were soon followed by an interest in soils with peculiar grading such as gap-graded and well graded.

Yin et al. (1999) studied the influence of fines presence on marine deposits from Hong Kong mainly composed of siliceous silts and sands mixed with clay, in

percentages varying from 5% to 70%. In the figure below, it can be seen that, with increasing clay content, thus with increasing plasticity index, the compression parameters tend to increase.

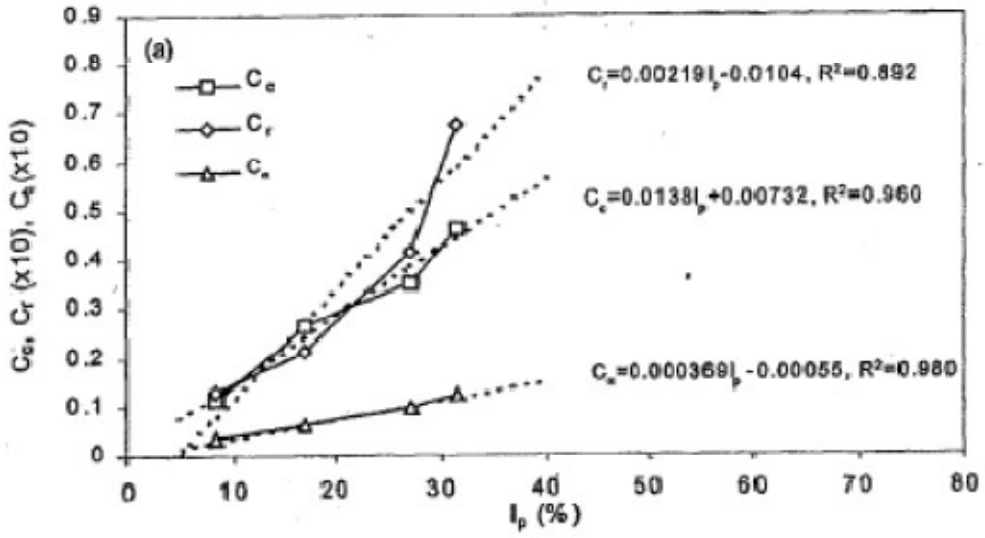

Figure 3. 9: Influence of clay content on the compressibility parameters of the Hong Kong marine deposits (Yin *et al.*, 1999).

3.2. Transitional soils

In the following paragraphs a summary of the most important contributions that lead to the definition of a transitional mode of behaviour for soils non-ascribable to clean sands or pure clays is reported.

3.2.1. Definition of a transitional mode of behaviour

Mechanics of well-graded and gap-graded soils

Natural soils usually consists of a mixture of particles of different dimensions, therefore, given that a comprehensive theorical framework able to describe the mechanics of both sands and clays had already been defined, researchers in recent years became interested in defining with a more accurate degree of detail the behaviour of well-graded and gap-graded soils.

One of the first contributions to this field has to be ascribed to the work by Menkiti (1994) on Ham river soils, particularly triaxial tests on artificial mixtures of sand and kaolin were carried out. Samples with different compositions and at varying initial densities were prepared. Firstly, for low clay contents, it was observed that

the mechanics of the soils was strongly related to the inter-granular void ratio es (esk) introduced by Mitchell (1976); Thevanayagam (2000).

At a clay content of 24% the mixtures behaviour tended to the one of a clay. This experimental study lead Menkiti to carry out oedometer tests on mixture at varying initial void ratios, containing 25% sand, 25% silts and 50% kaolin.

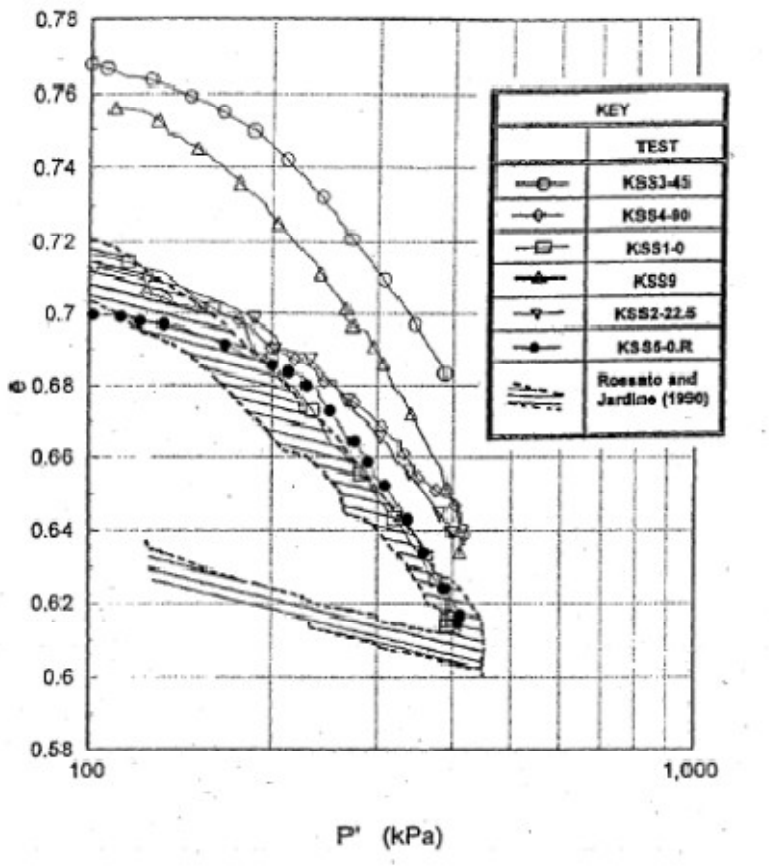

Figure 3. 10: normal compression curves of mixtures of Ham river sand and silt with kaolin (KSS) compared to the behaviour in compression on the same soil shown in the study by Rossato and Jardine (1996).

As it can be noted in figure 3.9, some compression curves maintained parallel to each other, even at the maximum stresses in loading, although with increasing pressures an increase in the steepness of the compression lines can be noted.

However, the first identification and definition of this mode of behaviour non ascribable to sands or clays is due to Martins et al., (2001).

In particular, they carried out compression tests on reconstituted specimens of gap-graded clayey sand. The material consists in residual soil derived from Bocutacu sandstone.

The results showed normal compression lines that ran parallel even to level of stresses of 6 MPa and it was not possible to identify a yield point.

The steepness of the curves was lower than the value tipically found for sands. This behaviour was defined as transitional. Moreover, the influence of the presence of different percentages of plastic fines on the position and shape of the normal compression lines in the e: lnp′ plane was studied. As it can be seen from the figures below referring to two preparation procedures (slurry and air- dried), the samples were created with different initial void ratios.

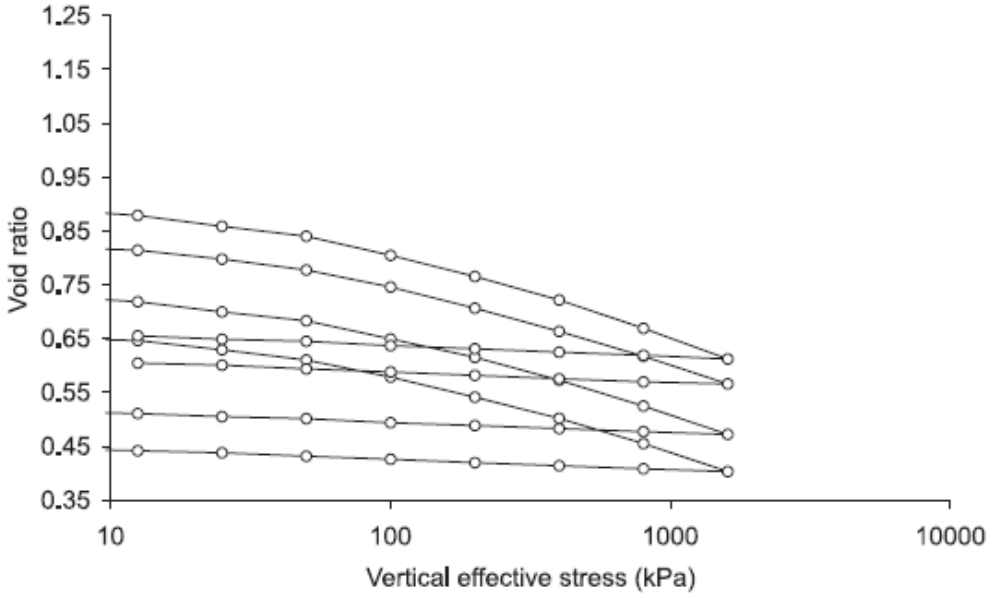

Fig. 3. 1: one-dimensional compression tests on reconstituted slurry samples of residual soil derived from Botucatu sandstone (modified from Martins *et al*., 2002).

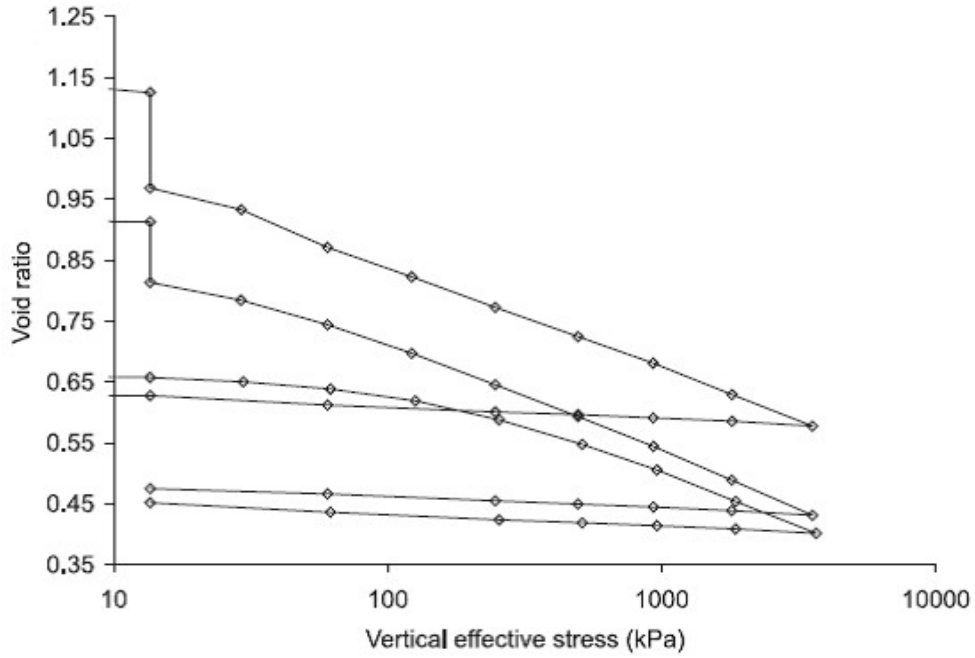

Fig. 3. 2: one-dimensional compression tests on samples, reconstituted in air dried conditions, of residual soil derived from Botucatu sandstone (modified from Martins *et al*., 2002).

The results of this study were quite surprising. In fact, it was not possible to identify a unique normal compression line for neither the slurry or the air-dried samples, even considering pressures up to 6 MPa.

Moreover, considering the sample preparation technique, it could be observed that the steepness of the normal compression lines, referring to different initial void ratios, were quite similar and the curves did not converge even at very high stresses.

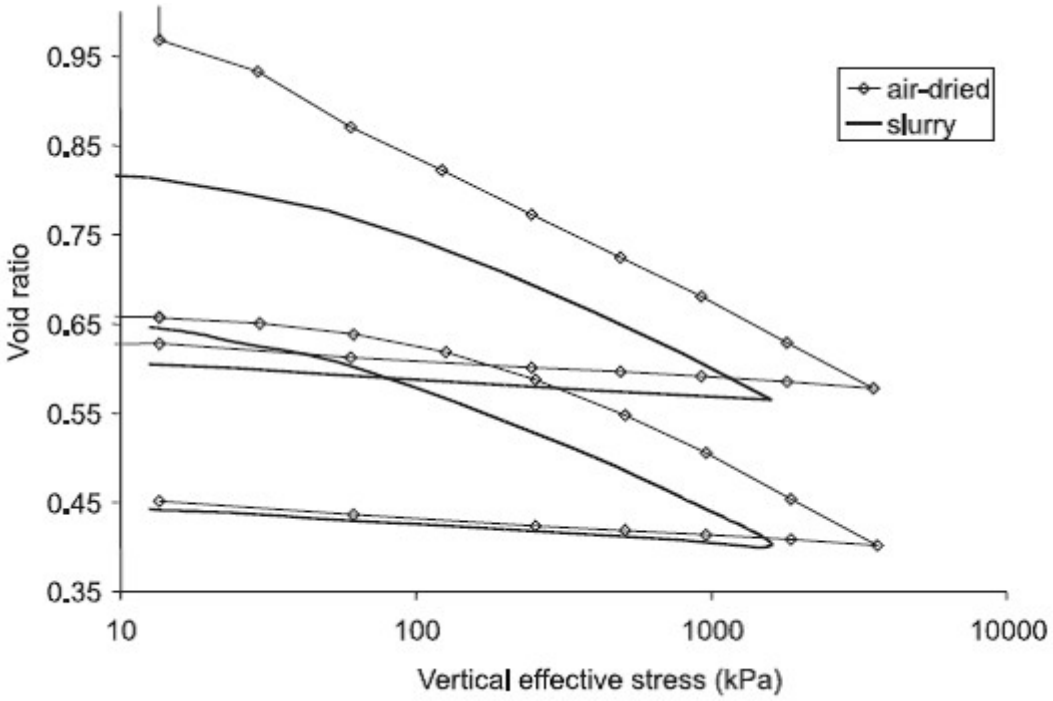

Fig. 3. 3: one-dimensional compression lines for slurry and air-dried reconstituted samples of Botucatu residual sandstone (from Martins *et al.*, 2002).

The authors compared these results with the one-dimensional compression curves obtained on a model clay-sand mixture having similar grading (quartzitic medium sand of fluvial origin mixed with 25% of commercial kaolinite) and again no convergence was found.

The authors identified that this mode of behaviour is one not consistent with the critical state soil mechanics and they ascribed it to the category of non-uniform sandy soils with plastic fines.

Moreover, they pointed out the need for a new theorical framework and vocabulary powerful enough to describe the behaviour of natural soils with a non-uniform grading.

Subsequently, Ferreira and Bica in 2006, following the work by Martins et al. (2001) investigated the behaviour of Botucatu residual gap-graded samples within a triaxial tests programme. They could identify a family of Critical State Lines, thus a

non-convergence was identified even in shearing as it is presented in the figure below.

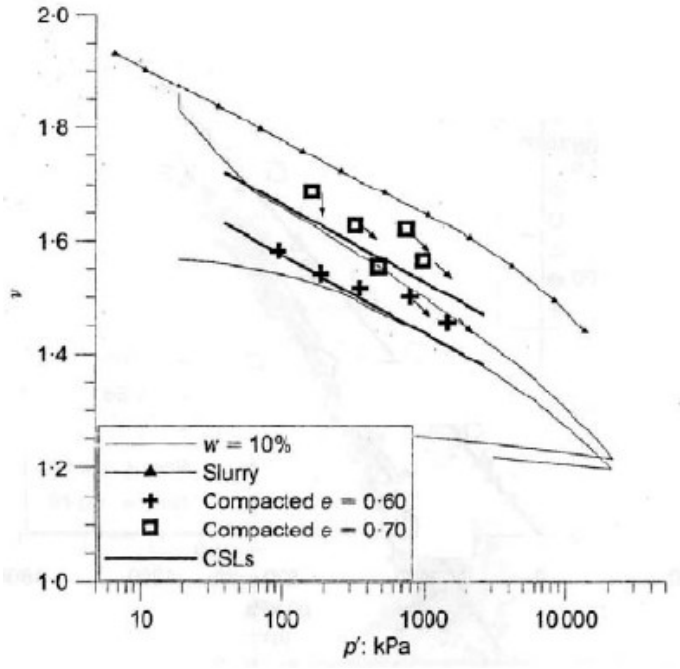

Figure 3. 11: Presence of non-unique Critical State Lines for Botucatu residual stone reconstituted samples (Ferreira and Bica, 2006).

Nocilla et al. (2006) performed oedometer and triaxial tests on reconstituted samples of well graded silty soils from the Po river embankment. The aim was to investigate the influence of different amounts of clay on the mechanical behaviour.

The results showed that for samples with a clay content between 8% and 45%, with decreasing clay content, the slope of the compression lines progressively decrease until a transitional mode of behaviour, similar to the one defined for gap-graded soil, is reached (clay content of 8% and 3.5%). Moreover no unique Critical State line could be identified. They concluded that one of the main question to be answered with following work was to investigate if this behaviour is connected to the presence of fines or to the mineralogy, thus the intrinsic properties of the material, because no evidences of particle breakage were found at these fines content.

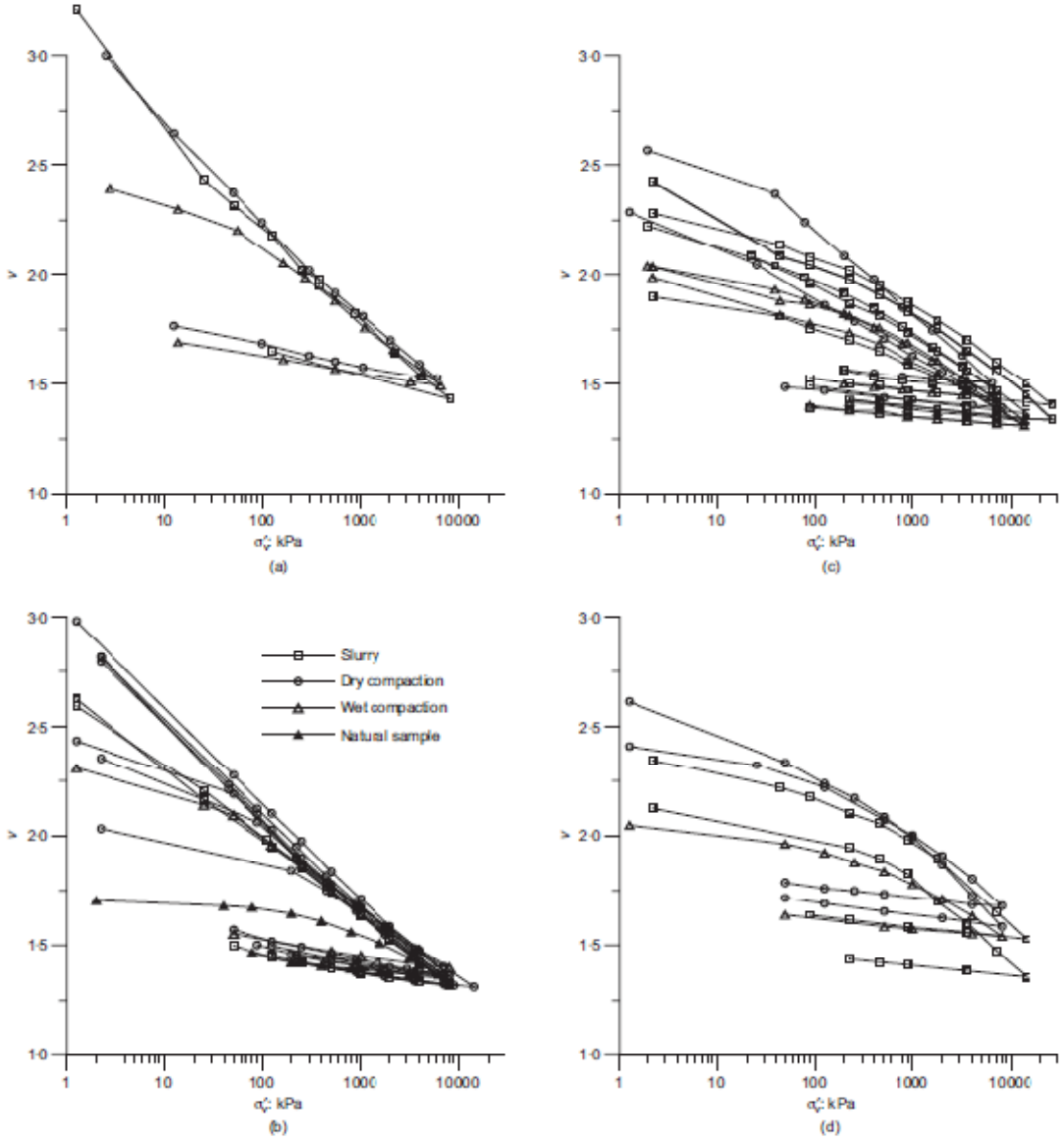

Figure 3. 12: oedometer compression curves on silty soils from the Po river embankment: (a) 45% clay content; (b) 25% clay content; (c) 8% clay content; (d) 3.5% clay content (from Nocilla *et al.*, 2006).

These studies allowed to hypothesize a new mode of behaviour for compression of well-graded soils, together with gap-graded and in general non-uniform grading, that can be summarised in the figure 3.13.

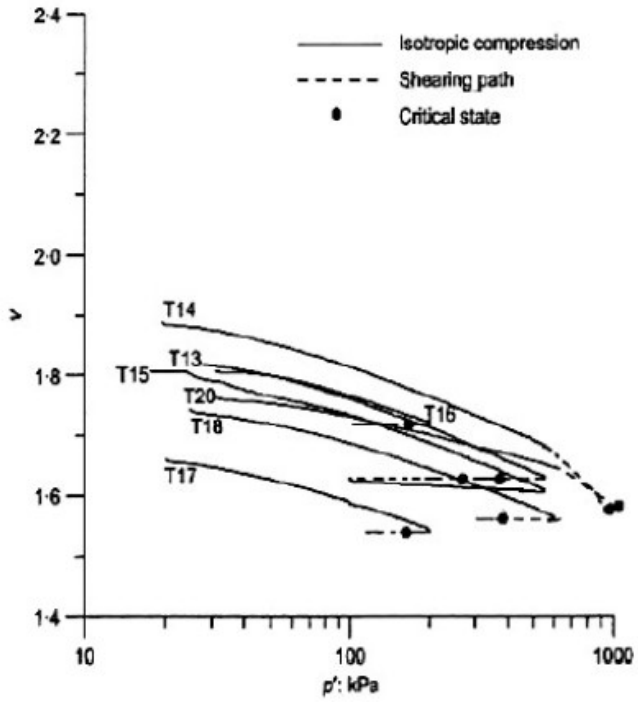

Figure 3. 13: Non-uniqueness of the isotropic compression and of the critical state lines for soils from the Po river embankment (particularly clay content of 8%) (from Nocilla *et al.*, 2006).

The authors agree that further researches were necessary in order to define with a better degree of accuracy how widespread this behaviour is among natural soils (see section 3.2.2 for further details).

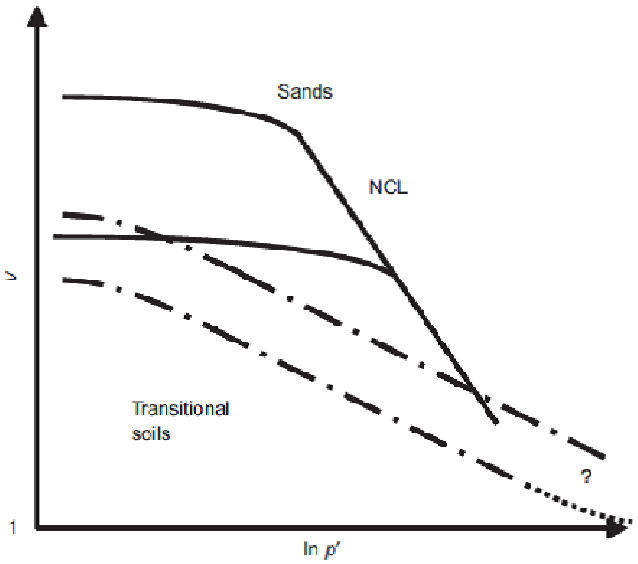

Figure 3. 14: Scheme for the definition of transitional soils, if compared to the normal compression behavior of sands(from Nocilla *et al.*, 2006).

Silts behaviour

However, the identification of this new mode of behaviour allowed to obtain a better understanding of previous results on the mechanics of silts. Silts and clayey silts often showed a behaviour differing from the one of clays.

Atherton (1994) studied the behaviour of a quartzitic clean silt and found that particle contacts between grains seemed to be the main mechanism involved, and not electrostatic forces, nevertheless the presence of fines.

Zdravkovic (1996) carried out oedometer tests on a pure silicatic silt obtained from crushing of quartz. She obtained parallel curves, but, because the reached stresses were low, no conclusions could be stated on the presence of a unique normal compression line.

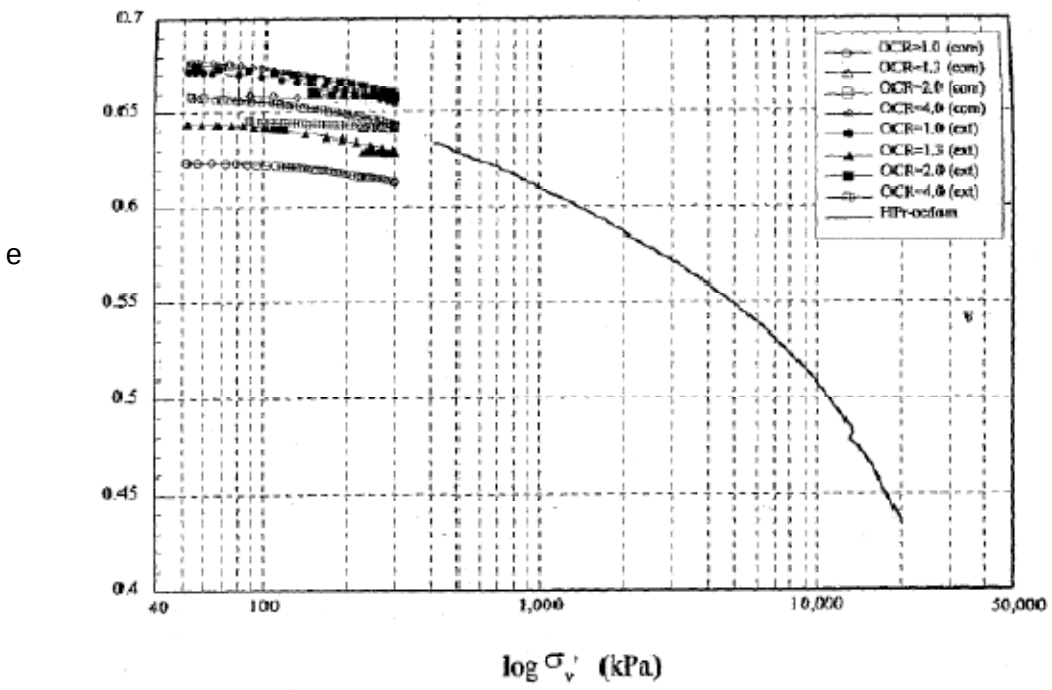

Figure 3. 15: 1D-normal compression curves of a quartzitic silt (from Zdravkovic, 1996)

3.2.2. Review of transitional soils

At present, the group of soils that can be defined as transitional comprises soils whose grading varies between reasonably well graded to gap graded and their behaviour is characterised by parallel NCLs and CSLs, in other terms the position of these lines depends on the initial density.

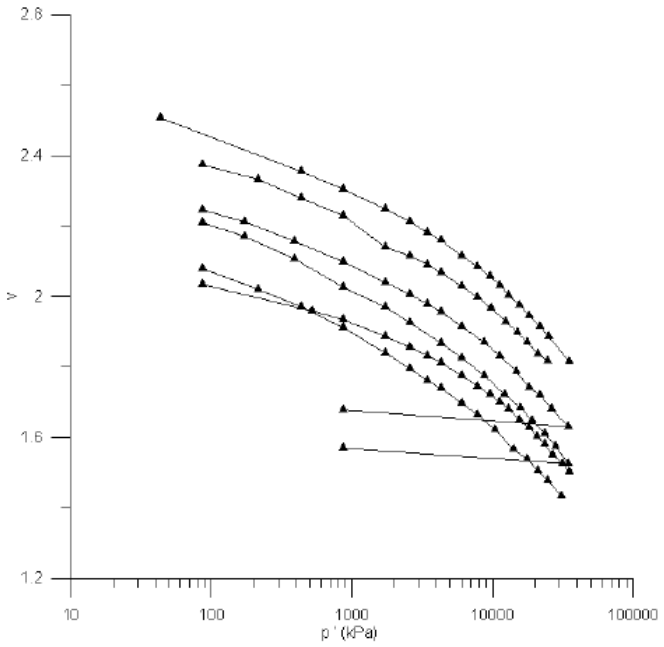

Figure 3. 16 : oedometer tests on high silty reconstituted Thanet sand samples (from Ventouras, 2005).

Shipton et al. (2006) carried out oedometer tests on mixtures constituted by 40% of Dog′s Bay sand and 60% crushed quartzitic silt (mixture 1) and 60% of kaolin (mixture 2). The compression behaviour is reported in the figure below. No convergence could be found.

Carrera (2008) analysed the behaviour of soils constituted by Stava talings, sand and fines fractions at different percentages. However, in this case a unique normal compression line could be identified for the majority of the mixtures as it is shown in the figure below. Only for the mixture composed of 50% sand and 50% fines the curves were more scattered and no clear conclusion could be drawn. Although the soils studied by Carrera and the mixtures tested by Nocilla had very similar gradings and mineralogy, their behaviour is very different in terms of transitional soils framework. Further research is required in order to gain a deeper understanding of these soils.

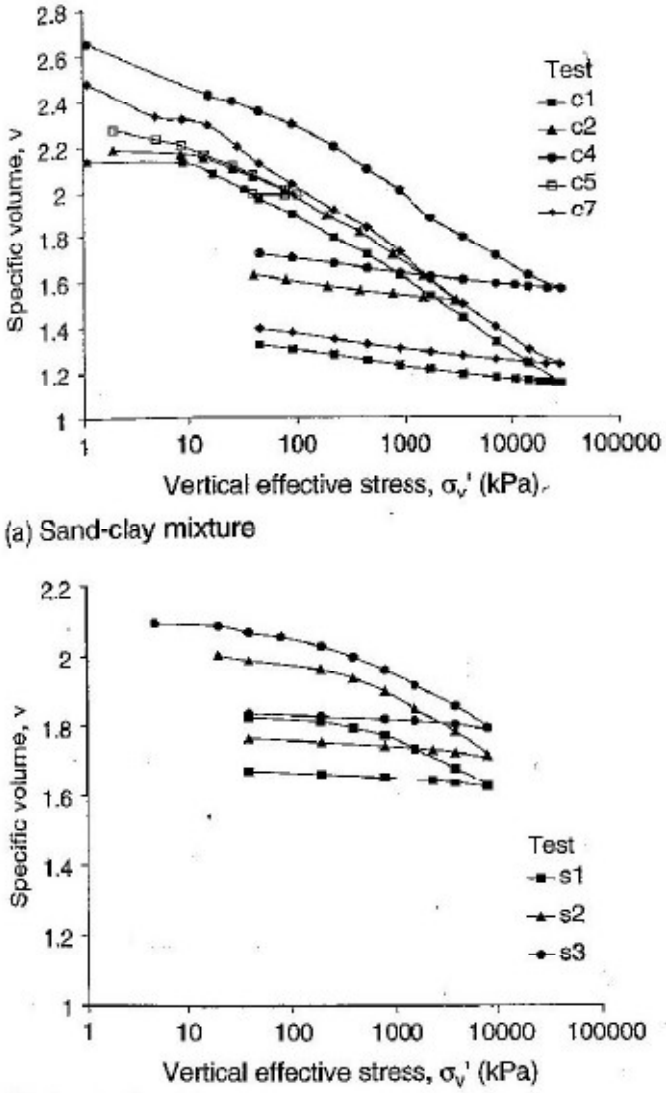

Figure 3. 17: 1D-normal compression curves for 40% Dog′s Bay sand mixed with 60% quartzitic silt (mixture a) and with 60% kaolin (mixture b) (Shipton *et al.*, 2006)

Vilhar (2009), studying the behaviour of Bostanj silty sand samples, did not identify a transitional behaviour.

Long et al. (2010) presented a detailed characterization of glaciomarine silty soils from Os, Norway. Although the main aim of their work was related to the influence of sampling, thus the maximum stress applied in oedometer tests was 1.8 MPa, they state that it is unlikely that Os silt samples reach a unique NCL.

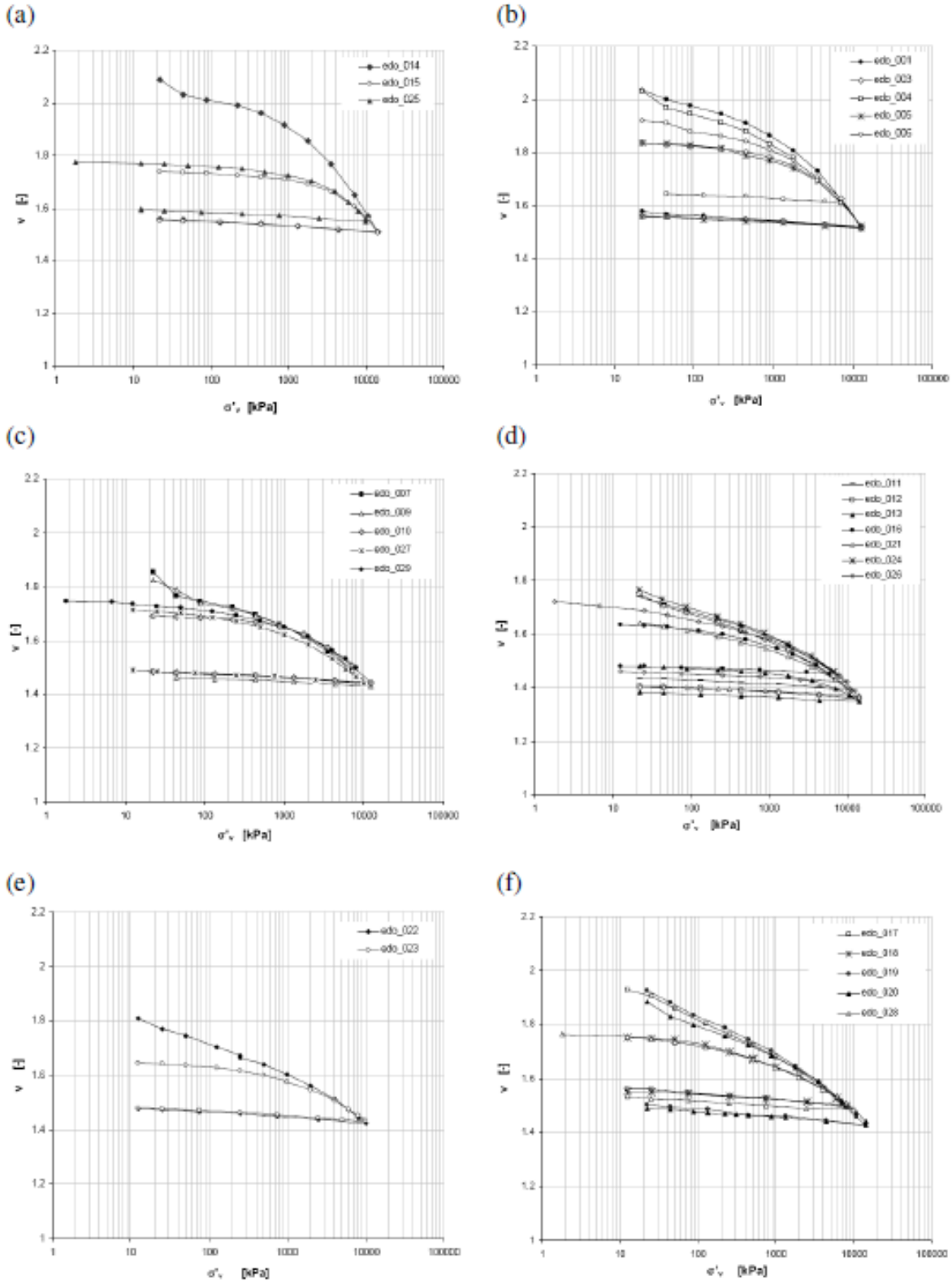

Figure 3. 18: 1D-normal compression curves for Stava tailings: sand mixed with fines at different percentages (from Carrera, 2008)

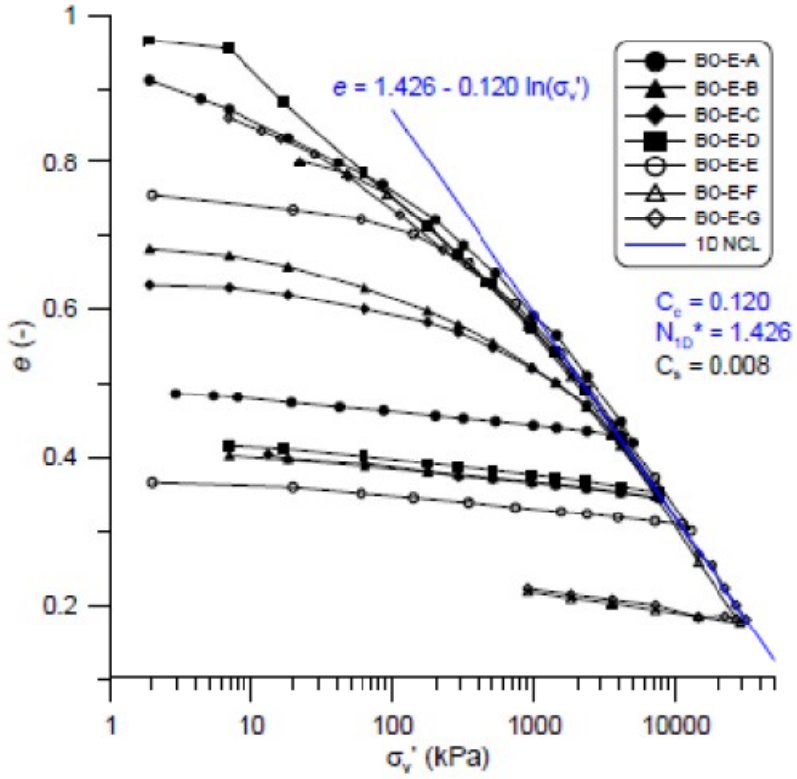

Figure 3. 19: 1D- compression curves and unique NCL from oedometer tests on Bostanj silty sand (from Vilhar, 2010)

In the figure below, the results are reported and can also be compared to the curves obtained from oedometer tests on silty clay from a nearby site Jektevik–Sandvikvåg site. Although Os soils and this material had very similar water content, a convergence can be identified to a unique NCL and this is probably due to the 38% clay and the 5% sand content.

The authors compared their results to the behaviour of other similar soils, particularly with Venice soils, in order to assess if it fitted into theorical published framework.

As pointed out by Biscontin et al. (2007) and Cola and Simonini (2002), no unique NCL could be found for the highly heterogeneous silty soils from the Venice lagoon (see Chapter 1). However, Long et al. stated that the 'transitional behaviour' of these soils was most probably linked more to their complex interbedding of different layers and complex nature of the situ conditions.

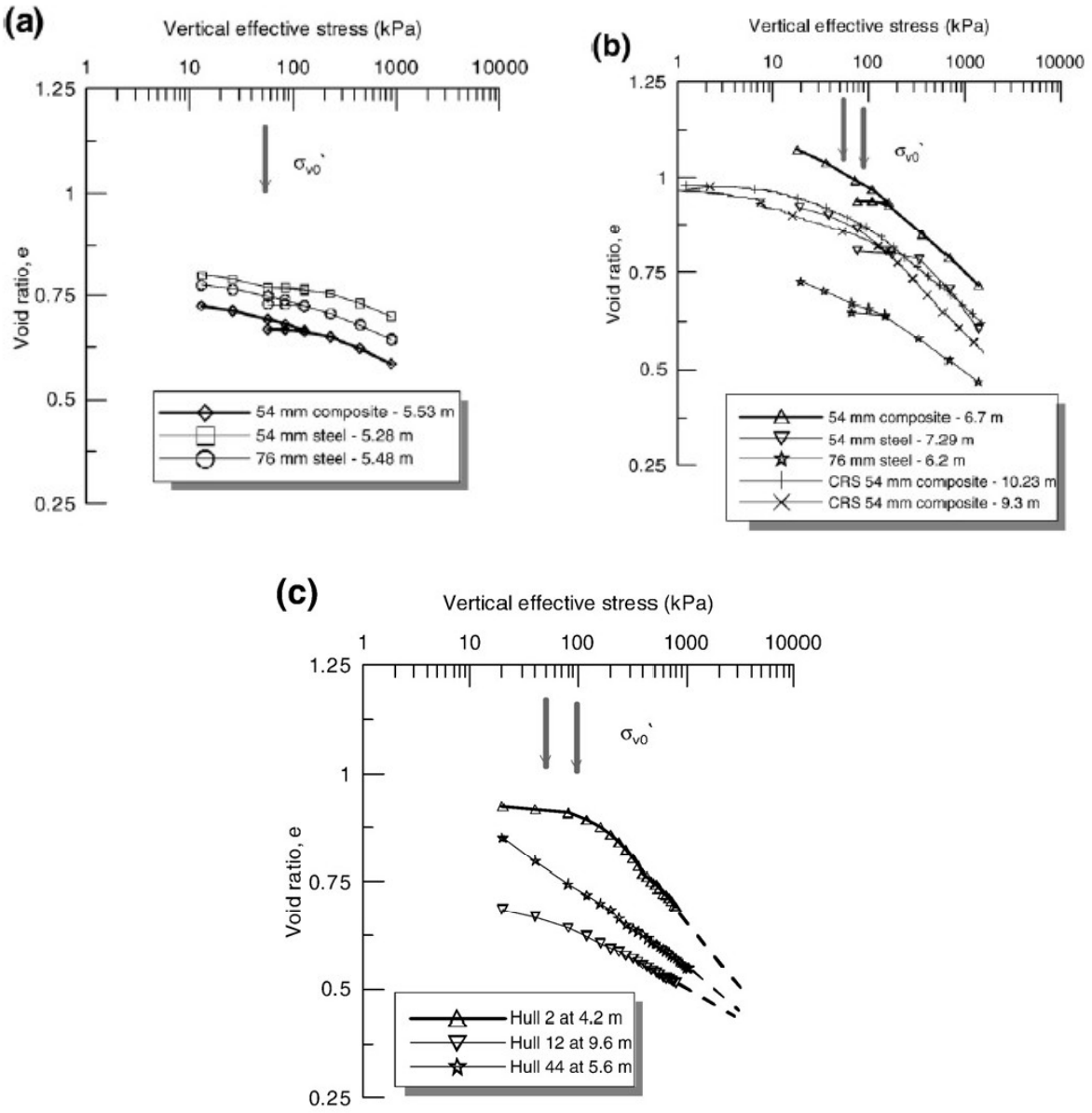

Figure 3. 20: results of oedometer tests perfomed on undisturbed samples of upper Os silts (a), lower Os clayey silts (b) and silty clay samples from the nearby Jektevik–Sandvikvåg site (c) (modified from Long *et al.*, 2009)

As a final example, the work by Altuhafi et al. (2010) is reported.

The authors performed an experimental programme on subglacial sediment from the Icelandic site known as Langjökull, consisting mainly of pure basalt. They found non convergence of the normal compression lines.

Also compression and triaxial tests were performed. In the figure below, the isotropic compression curves are reported and they lie parallel to each other, thus this soil presents a feature of transitional behaviour. However, as it will be showed, these soils present a unique critical state line. The authors tribute this to its peculiar strain history .

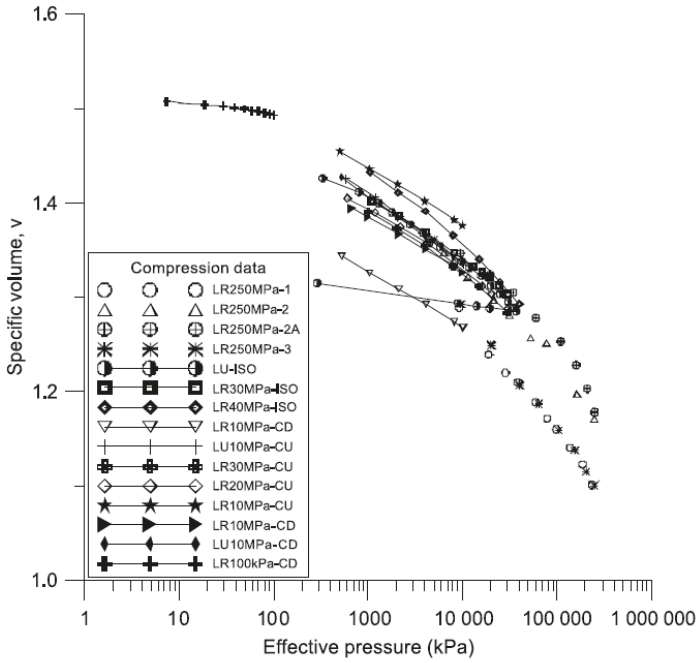

Figure 3. 21: isotropic compression curves from tests on undisturbed and remoulded samples of icelandic Langjökull sediment (from Altuhafi *et al*., 2010)

The well-graded nature of the sediments seems to hinder its capacity to reach a unique normal compression line (Altuhafi et al., 2010) and no clear yielding point could be identified.

When isotropically compressed, this soil presented multiple parallel normal compression lines. The same soil, however, during drained and undrained triaxial tests, reached a unique critical state line, see figure below. All the samples seem to reach a stress ratio of around 1.4, irrespective of the intact or remoulded state. The peculiar strain history of this subglacial soil was related to this behaviour with respect to the material peculiar grading reached after constant shearing.

Altuhafi et al. (2010), when testing Langjökull sediment, proved the existence of an ultimate grading, reached after evolution of the grading due to high stresses and strains.

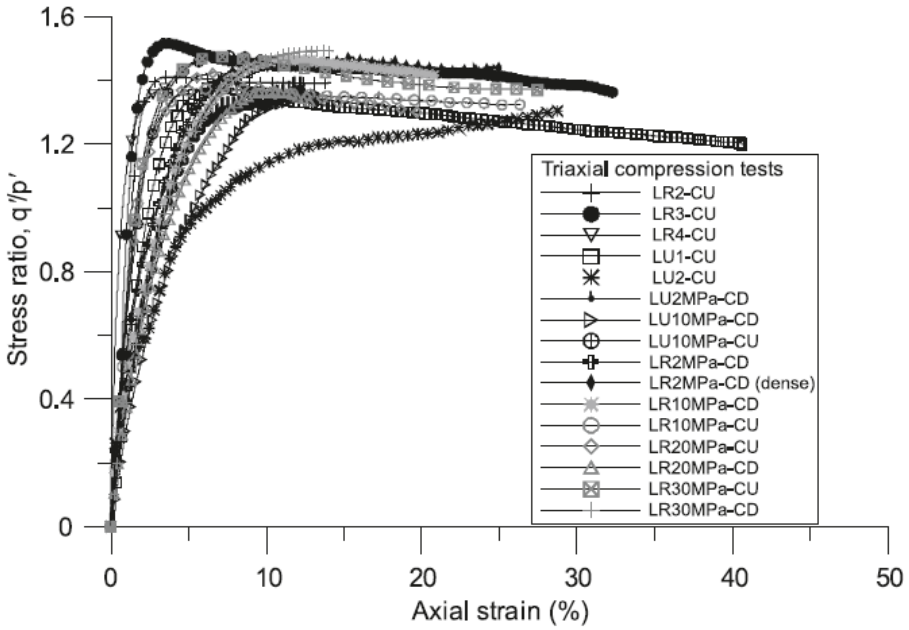

Figure 3. 22: shearing behaviour of Langjökull sediment plotted in the stress ratio vs. axial strain graph (from Altuhafi *et al.* 2010).

In the table below a review of the most important contributions to the definition of a framework for transitional behavior is reported.

Year	Authors	Soil composition	Grading	Results
1981	Lupini et al.	Mixture sand and bentonite	0-88% bentonite 12-100% sand	Decrease of ϕ' with decreasing fines
1985	Been and Jefferies	Kogyuk sand	0-10% silt 100-90% sand	Decrease of ϕ' with increasing clay content; increase in steepness of SSL in the e-p′ plane with increasing silty content
1993	Coop and Atkinson	Dog′s Bay sand with fines	100% sand and sand with varying content of	NCL steepness for sand decrease with

			carbonate/gypsum	decreasing fines content. No influence of mineralogy of fines
1994	Atherton	quartzitic clean silt		particle contacts between grains identified as the main mechanism involved in compression
1994	Menkiti	Mixture of kaolin/ and Ham river sand	25% sand 25% silt 50% kaolin	Parallel compression curves at high pressures
1994	Pitman *et al*.	Mixture of quartzitic sand and fines	0%-40% fines 60-100% sand	CSL steepness variation with increasing fines content
1996	Connolly	Pentre silts	60-90% silts 15% sand with increasing clay content 0-27%	Parallel compression curves without convergence even at high stresses
1996	Zdravkovic	Silicatic silts with quartz	100% clean silicatic sand	Too low pressures to identify a unique NCL
1998	Thevanayagam	Silty sand with different %	Sand with 10% silicatic fines, 10%	Decrease in shear strength for fines

		of fines	and 25% of kaolin	content between 7-15-25%. Increase of shear strength for 40% fines content
1998	Lade and Yamamuro	Nevada sand	Sand with 6% non plastic fines	Parallel CSLs and reverse behaviour: pressure increase provide more stability
1999-2002	Yin	Hong Kong marine deposits sand	15-60% silt 15-80% sand 5-25% clay	Decrease in the steepness of the NCLs with increasing fines
1999	Huang *et al.*	Silty fine sand from Mai-Liao (Taiwan)	Sand with non plastic fines between 10-90%	Mai-Liao sand compressibility 5 times higher than compressibility of quartzitic sand
2000	Salgado *et al.*	Ottawa sand with non plastic fines	Silty sand with fines between 5-20%	Increase of the shear strength angle with increasing fines content in drained triaxial tests.
2001	Adrianopoulos	Mixture of	100%-70% sand	increase in the

		sand with fines	with 0-30% fines	steepness of the CSL and of the intercept at 1 kPa with increasing fines content
2001	Fourie and Papageorgiou	tailings from Marriespruit	0-60% fines content	With increasing percentage of fines content, downward shift of the Critical state lines.
2002	Martins *et al.*	Botucatu residual sandstone	Clayey sand poorly graded, fines mainly kaolin	First identification of transitional behaviour in oedometer tests : no unique NCL
2002	Thevanayagam *et al.*	Silty sand with different % of silicatic fines	Sand with silicatic non plastic fines from 7-15-25-40-60%	Decreasing shear strength for fines content of 7-15-25% Increase for f_c higher than 40%
2005	Ferreira and Bica	Botucatu residual sandstone	Clayey sand poorly graded, fines mainly kaolin	No unique CSL
2006	Yang *et al.*	Mixture of Hokksund sand and	Sand with fines content between 0-94%	Steady state lines coincidental

		Chengbei non plastic silt		for drained and undrained tests only for fines content equal or lower than 30%
2006	Nocilla *et al.*	Clayey silt from the Po river	Varying clay content: 45%; 25%; 8% and 3,5%	Non uniqueness of NCL and CSL for fines content of 3,5 and 8%
2006	Shipton *et al.*	Dog's Bay sand with crushed quartzitic silt or with kaolin	40% sand 60% fines (quartzitic silt in mixture 1) (kaolin in mixture 2)	No convergence of the NCLs
2007	Murthy; Salgado *et al.*	Ottawa sand with different fines content	15% clay content	Increase in ϕ' with increasing fines
2008	Carrera	Stava tailings	Mixtures of sand and fines: 100-90-70-50-30 -10 sand and fines respectively	No transitional behaviour: unique NCL and CSL; decrease in steepness of the NCL at high pressures
2008	Cubrinovki *et al.*	Christchurch (New Zealand) sand with fines	Sand with 1-10-30% of non plastic fines	The SSL tends to move downwards in the e-logp' plane
2009	Ahmed Arab	Chief silty	Sand with fines	Increase in the contractive

		sand	between 0-50%	tendency with increasing fines
2009	Vilhar	Bostanj silty sand		
2010	Altuhafi *et al.*	subglacial basaltic sediment from the Icelandic site known as Langjökull		Non convergence of the normal and isotropic compression lines, but unique critical state line
2010	Long *et al.*	glaciomarine silty soils from Os, Norway	Natural samples with an average water content between 33 and 38%	Probable non convergence to unique NCL, although there is a slight trend

Table 3. 1: review of the most important studies that contributed to the definition of the transitional soils framework

According to the results obtained so far regarding the transitional soils, it is usually acknowledged that, whereas the behaviour in compression is quite straight-forward, the determination of a unique pattern of behaviour is more difficult to single-out.

In conclusion, the Critical State theory does not seem to be applicable to soils with intermediate grading between sands and clays, because the main features of these transitional soils derived from experimental evidences are:

Non uniqueness of the normal compression line NCL;

Non uniqueness of the critical state line CSL.

However, this behaviour can nowadays be referred both to well graded and to gap graded materials, for non plastic and plastic fines and different mineralogies.

Nocilla et al. (2006) found little evidence of particle breakage in the reconstituted samples coming from triaxial tests, whereas Shipton et al. could identify distinct signs of grain crushing with increasing level of stress.

Given the fact that in both cases a transitional mode of behaviour could be identified, it can be concluded that the absence of particle breakage is unlikely to be responsible for this behaviour which is in between that of sands and clays.

More research is necessary in order to identify new characteristics of these soils and to investigate how widespread these soils are in their natural conditions.

One of the main objective of this work of thesis lies in the investigation of the mechanics of the silty sand from Treporti test site (Venice) and to interpret the results within the transitional soils or the critical state framework.

In the following paragraphs, oedometer and triaxial tests were performed on samples made of different percentages of sandy and fines fractions. The results will be shown in the following chapters.

CHAPTER 4

Laboratory equipment, testing procedure and experimental programme

The laboratory work carried out within this research consists mainly of oedometer and triaxial tests. In this chapter, the experimental procedures are presented and all the equipment used is described, with particular reference to the instruments accuracy.

Moreover, the data evaluation methods are described. Finally, a list of all the performed oedometer and triaxial tests and their main characteristics is shown.

4.1. *Instrumentation*

Oedometer tests were carried out at Politecnico di Torino and Imperial College.

The majority of oedometer tests were carried out at Imperial College, but the compression parameters of the two fractions were preliminarly investigated at Politecnico di Torino.

In the following paragraphs the apparatuses that have been used are described in details.

4.1.1. Oedometers

Within an oedometer test a soil sample is vertically loaded in mono-dimensional compression, as it is confined in a steel ring. The ring height is half the ring diameter so that the D/H ratio is kept at 2 and the effect of lateral friction is minimised. The most frequently used ring diameters are of 50 mm, 38 and 36,8 mm.

The load is applied geometrically, each load applied follows the proportion:

$$\frac{(\Delta\sigma_v)_{i+1}}{(\sigma_v)_i} = 1$$

The maximum stress applied when using a 50 mm ring was 8 MPa, around 28 MPa in case of 38 mm diameter ring and 14 MPa in case of 36,8 mm diameter ring.

Two porous stones are placed to confine the sample and to allow drainage when the load is applied. Often the porous stone on top is part of a steel top cap, which has a

seating for the loading ram to be connected to in order to apply the vertical stress. Each load is amplified by 11 or 11.05 times, thanks to a lever arm connected to the ram. As soon as the first load is applied, the water bath is filled with distilled water. The cell has to be always full of water in order to ensure the sample saturation and to avoid its drying, plus during unloading to allow swelling to occur.

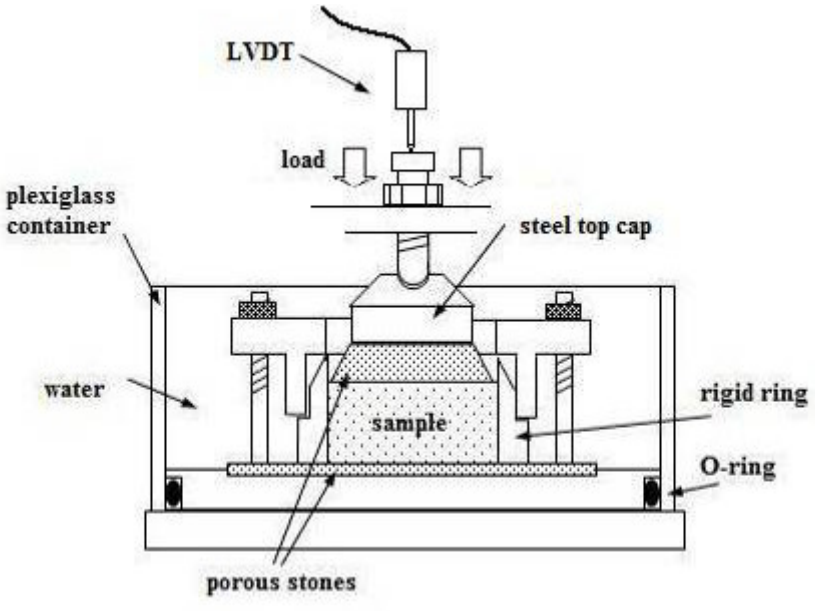

Figure 4. 1: schematic view of an oedometer cell at Imperial College: alternatively to the LVDT a dial gauge was used to collect the axial displacement (from Carrera, 2008).

The soil sample cannot expand laterally, thus each axial strain results in a volumetric strain. The reduction in sample's height during each loading step is measured with a dial gauge or an LVDT. In case of the latter, it is a resistive displacement transducer with a response of 25 mm. It is usually acknowledged that the electrical noise is higher than each eventual error of measurement.

$$\frac{\Delta V}{V_0} = \frac{\Delta H}{H_0} \Rightarrow \varepsilon_v = \varepsilon_a$$

Oedometers at Politecnico di Torino

The silty and sandy fractions of Venice soil were analysed separately in order to obtain some compression parameters to be used as a reference.

Sand samples were prepared directly in a standard cell manufactured by Tecnotest, Italy. This apparatus, having a lever arm ratio of 10, allows to reach a maximum vertical stress σ'_v of 3138 kPa on samples with a diameter of around 50 mm.

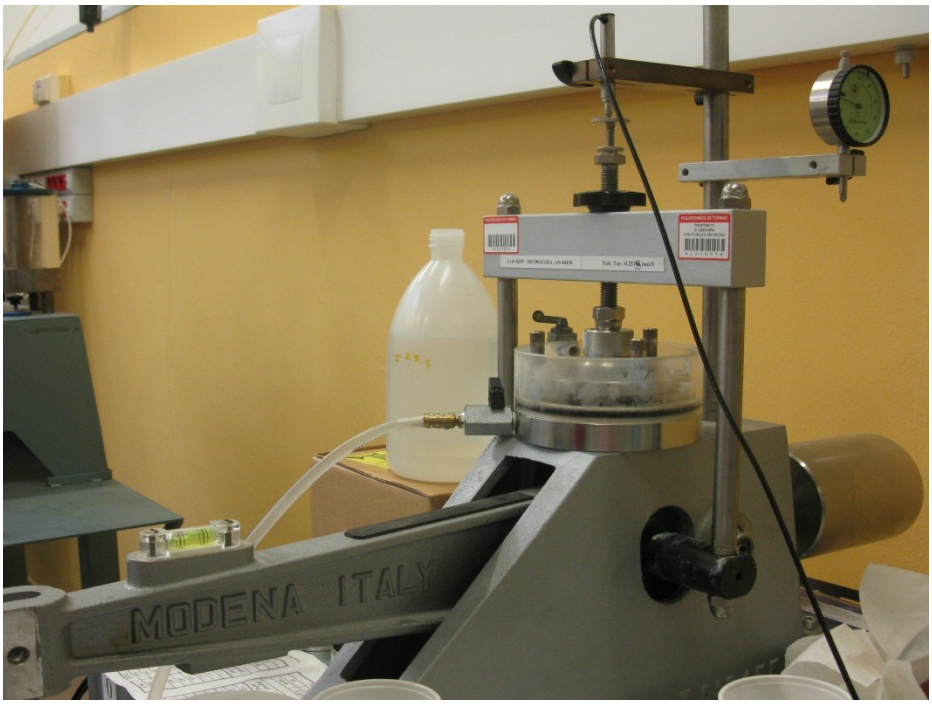

Figure 4. 2 oedometer used to test samples consisting of 100% sandy fraction at Politecnico di Torino

In order to create samples 100% fines, a consolidometer was used to obtain from slurries samples with an apparent cohesion, thus applying a pre-consolidation pressure of around 150-200 kPa. The samples were subsequently extruded and placed in an oedometer manufactured by Wykeham Farrance. The lever arm ratio was 11, thus on samples with a 50 mm diameter the maximum load applied was 3138 kPa.

Oedometers at Imperial College

Different type of oedometers were used at Imperial College. They were all manufactured by Wykeham Farrance, but often modified by the internal laboratory technical staff in order to adapt to research interests, such as reaching higher pressures.

Figure 4. 3: picture of some oedometers at Imperial College, London

Floating ring oedometer

Moreover a special cell was designed for 20 mm diameter samples, called floating ring oedometer, in order to reach very high stresses up to around 100 MPa. This apparatus is one to be used only for granular soil samples. Given the small ring dimensions, the effect of the boundary friction on the vertical stress is minimised thanks to the use of the floating ring.

4.1.2. Triaxial cells

Triaxial cell at Imperial college

The triaxial cells at Imperial College are Bishop-Wesley stress path apparatuses . They were all manufactured at Imperial College according to the design by Bishop and Wesley (1975).

Figure 4. 4: Bishop-Wesley triaxial apparatus at Imperial College, London.

The apparatus allows to test samples with a diameter of 38 mm and a height of around 70 mm. The sample is prepared directly or mounted on a pedestal. A top cap is placed on the sample and its peculiar shape will allow the submersible load cell to attach to it before the shearing phase is started. The plexiglass cell is filled with water.

The apparatus consists of several different equipments:

- the triaxial cell itself;
- a system for regulation and control of the cell and pore pressure;
- a loading ram for the axial compression of the sample;
- different instruments, such as dial gauges and volume gauges, for the measurement of the external axial displacement and of the sample volume changes;
- local transducers for a direct measure of the sample dimensions changes.

The back, cell and axial pressures are regulated via a pressurized water system. Their input values are inserted from a PC, running a program called Triax. The digital signal is connected through an AD converter that transforms the digital signal into an analogue. The signals reach three different electromanostats, that are connected to an air supply at approximately 800 kPa. According to the input values, this pressure is lowered and transmitted to water via air-water interfaces system (cell pressure interface, ram pressure interface and a volume gauge as a back pressure interface).

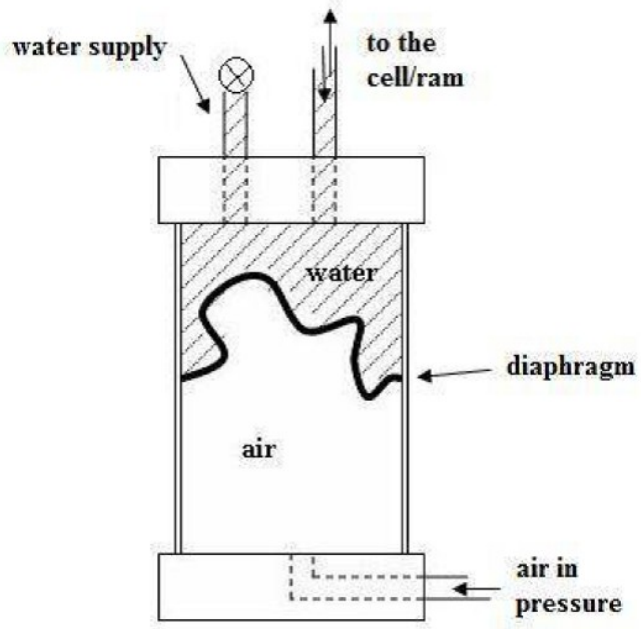

Figure 4. 5: schematic view of an air-water interface in the Bishop- Wesley apparatus at Imperial College, London (from Carrera, 2008)

In the figure below a general layout of the whole triaxial apparatus and its pressures control system is presented. As a summary it can be stated that the computer controls stresses and strains by means of air pressure controllers, each fed with the standard laboratory air supply. Air water interfaces pass the air pressures to the triaxial apparatus.

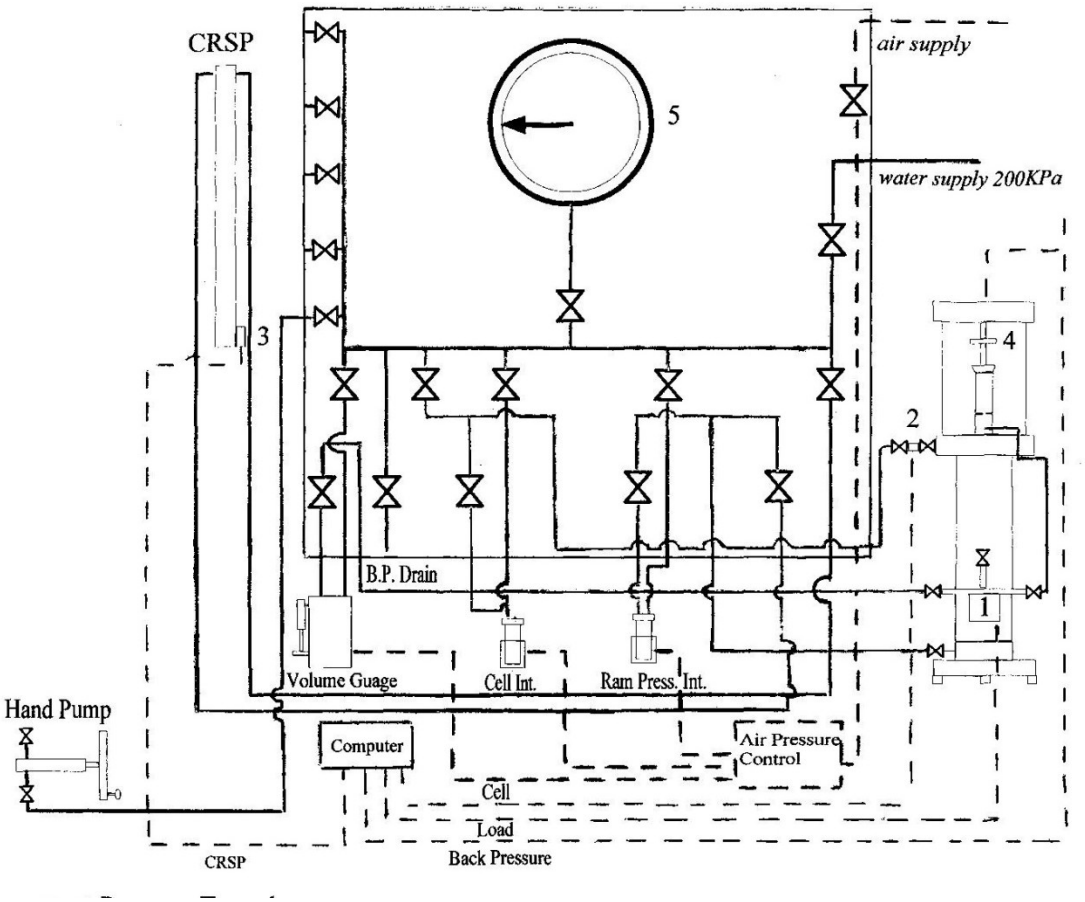

Figure 4. 6: General lay-out of the stress paths Bishop-Wesley triaxial cell at Imperial College

The volume gauge allows to measure the amount of water coming out of the sample during consolidation, thus to estimate the sample volume changes.

The axial stress is applied through a loading ram connected to an air chamber located under the sample pedestal, pushed by the pressurized water. During the shearing phase a constant rate of strain pump (CRSP) allows to apply the axial stress. All the shearing phases were carried out in strain control. This pump is governed by a stepping motor that drives a screw piston up and down: when the screw goes up, water is pumped into the ram. The constant rate of the sample strain is secured by the incompressibility of water. riformulare

In order to measure the sample height variations, an external axial strain transducer is used, although local transducers such as inclinometers and LVDTS, which are all inductive transducers.

4.1.3. Qicpic apparatus

The grain size distribution of the sandy fraction was also measured with an image analysis sensor called Qicpic, manufactured by Sympatech for Imperial college. A schematic layout of the apparatus is shown in the figure below.

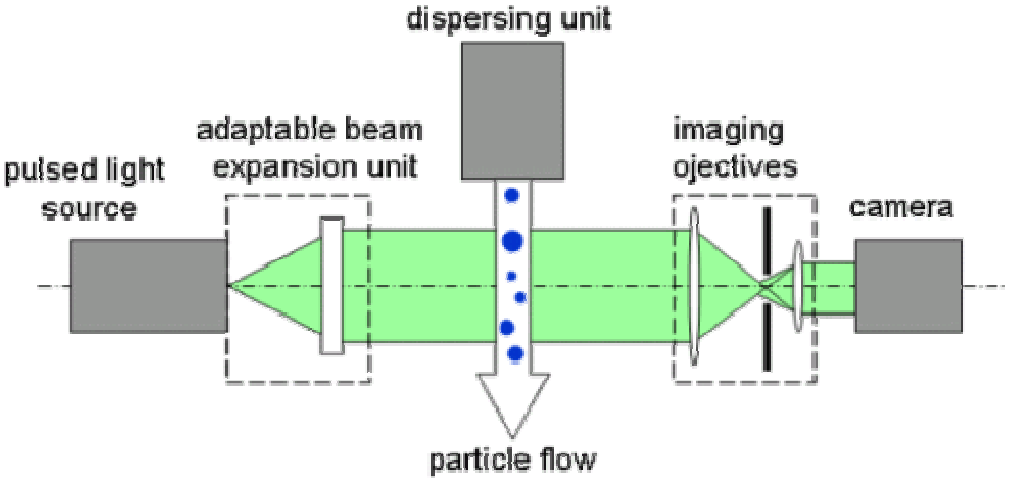

Figure 5. 1: Schematic layout of the Qicpic apparatus developed by Sympatech.

This instrument provides information about the grain size and shape of particles between 2 μm and 20 mm. A particle flow is created and enlightened. A camera captures image frames.

The light rays are nearly parallel to the camera axis so that even transparent particles appear black. The camera and the light source can operate at speed between 0 and 500 frames per second and thus a large amount of particles can be acquired in a short time and stored in the PC. Afterwards it allows to make a statistical analysis of the dimensions and shape of those particles. A picture of the instrumentation is reported in the figure below.

Two adapters are provided, one for dry analysis, called GRADIS, and one for wet analysis called LIXELL.

Data processing

The first information provided on each particle is its contour. Several algorithms allows to obtain the diameter of each particle, whereas the shape is described by means of shape factor. All the curves obtained with Qicpic are highly repeatable.

The most common diameters used to describe the dimensions of the soil particle are:

-the EQPC, which stands for the diameter of a circle of equal projection area: this is the diameter of a circle that has the same area as the projection of the particle;

-the FERET MAXIMUM, which is the maximum distance between two parallel tangent to the particle outline;

- the FERET MINIMUM, which is the minimum distance between two parallel tangents to the particle outline.

Moreover, the most used shape parameters are sphericity, aspect ratio and convexity. The sphericity is:

$$S = \frac{P_{EQPC}}{P_{REAL}} = 2 * \sqrt{(\pi * A) / P_{REAL}}$$

Where P_{REAL} is the real perimeter and P_{EQPC} is the perimeter of the equivalent circle. The sphericity range is between 0 and 1; this means the smaller the value, the more irregular is the shape of the particle because an irregular shape causes an increase of the perimeter. It can be noted that the perimeter of the equivalent circle is the smallest possible perimeter at a given projection area.

The aspect ratio is defined as:

$$\frac{Fe_{MIN}}{Fe_{MAX}}$$

Where:

Fe_{MIN} is the Feret minimum diameter

Fe_{MAX} is the Feret maximum diameter.

Convexity is another important shape parameter describing the compactness of a particle. Convexity can be defined as the measure of the surface roughness of a particle and is calculated by dividing the "convex hull perimeter" by the actual particle perimeter.

4.2. *Laboratory procedures*

4.2.1. Sample preparation techniques

The soils behaviour in compression and shearing is sensibly related to the sample preparation technique, therefore variables such as the compaction energy and the initial water content influence the initial microstructure. Thus, the sample preparation is very important, because it allows to obtain the wanted initial density and void ratio.

Different techniques were used in order to obtain samples within a consistent procedure:

- Slurry (oedometer tests);
- Dry compaction (oedometer tests);
- Moist tamping (triaxial tests);
- Undercompaction.

4.2.2. Experimental procedure for oedometer tests

Slurry

For the 100% fines samples, an alternative technique to the dry compaction was used with the aim of obtaining the widest possible range of initial void ratios.

A small amount of distilled water is added to the dry soil in order to prepare samples with different initial void ratios. According to Burland′s recommendations, the water content w added to these mixtures should be equal to $1 \div 1 - 1.5 \cdot w_L$. The soil and water is thoroughly mixed and is left overnight to uniformly deposit and with an adequate lid in order to prevent evaporation. The slurry is then carefully place inside the oedometer ring, trying to avoid to trap air bubbles. Then a small amount of the leftover is weighed, placed in the oven at 105°C for 24 hours and the dry weight is collected: the initial water content of the sample is calculated. This is one of the methods to estimate the initial specific volume v0 of the samples. (see section 4.2.3 for details) Preparing a slurry sample allows to calculate the initial void ratio using different measures such as: the initial water content, the final dry weight and the final wet weight.

Dry compaction

Knowing the oedometer ring dimensions, an estimate of the theorical wanted volume of the sample is calculated. Thus, thanks to the relative density for the

sandy fraction, a rough amount of dry material can be weighed. Again this procedure should be applied only to the sandy fraction, but it was used also for the mixtures of sand and fines. Ladd′s undercompaction technique was applied in the majority of the samples: three layers containing different quantitities of dry material are prepared. The amount of soil for each layer is calculated according to Ladd′s proportion (see further for details).

Testing procedure

The sample is carefully prepared inside the oedometer ring, two porous stones allows the drainage, both at the top and at the bottom of the sample. Filter paper discs can be placed between the sample and the porous stone in order to prevent the stone pores to be occluded by soil particles. The first load is the upper porous stone itself together with the oedometer load frame.

Several samples were prepared with different initial diameters, in order to apply different high pressures. The applied pressure depends on the force itself but also the sample area. The load weight is multiplied for the lever arm ratio which in general is equal to 10 or 11.

At the end of the loading phase the sample is unloaded and the number of unloading steps is halved. The sample at the end of the test is assumed to be saturated. This assumption is reasonable enough to allow the calculation of the final void ratio $e_f = G_S \cdot w_f$. The initial void ratio is then back calculated.

For each mixture of Venice soil fractions the time needed to the samples to dissipate the increase of neutral pressures caused by the application of the loads was empirically measured: the higher the percentage of fines, the higher the time required to the loading step to stabilize. At the end of the test the loading apparatus is dismantelled, the water bath is emptied and the sample weight is measured. This measurement has to be performed quite carefully, because the initial void ratio is back calculated from that value..

Calculation of the initial void ratio e_0 (specific volume v_0)

Different calculations using different direct measurements can be used to determine the initial void ratio or specific volume of the sample at the beginning of the test. All these methods were attempted, depending on each test conditions, although in the final presentation of the results only the values calculated from the final water content were taken into account. This choice was due to the aim of

presenting results consistent among all the samples mixtures. In the table below, the methods are summarised.

	Specific volume	Assumptions	Notes
Final dry unit weight	$v_f = \frac{G_s V}{P_s}$		
Final water content w_f	$v_f = G_S \cdot w_f + 1$	Sample fully saturated ($S_r = 1$) at the end of the test. From v_f, the initial specific volume for each loading step can be back calculated from the expression: $v_i = v_{i+1} + \left(\frac{\varepsilon_v / 100}{(1 - \varepsilon_v / 100)} \right)$	
Initial water content w_0	$v_0 = G_s \cdot w_0 + 1$	Sample fully saturated at the beginning of the test: not frequently applicable. $v_f = v_i - \left(\frac{\varepsilon_v / 100}{(1 + \varepsilon_v / 100)} \right)$	Slurry samples
Final bulk unit weight γ_f	$v_f = \frac{G_s \cdot \gamma_w - \gamma_f}{\gamma_f - \gamma_w} + 1$		
Initial dry unit weight γ_{d0}	$v_0 = G_s \frac{\gamma_w}{\gamma_{d0}}$		

Table 4. 1:Different calculations derived, from different measured parameters, that can be applied in order to determine the initial specific volume of the oedometer samples.

4.2.3. Experimental procedure for triaxial tests

Each triaxial tests carried out so far involved the following phases:

- Sample preparation;
- Measurement of sample dimensions;
- Mounting of local transducers if applicable (inclinometers or LVDTs);
- Mounting of the cell:
- Flushing of distilled de-aired water;
- Saturation with distilled de-aired water;
- Connection of the suction cap;
- Consolidation;
- Shearing;
- Dismantelling.

Sample preparation techniques

Moist tamping

The sample preparation technique used for the triaxial tests performed within this research is the so-called 'moist tamping' technique or wet compaction.

A rough estimate of the dry weight of the needed material is required, in order to obtain the wanted values of initial void ratio. This estimate can be calculated for the samples consisting of 100% sand, because the values of emax and emin are known. However, given that the ASTM recommendations suggest to avoid the measure of these parameters for soils whose fines component exceeds 15 %, for all the other mixtures of Venice soils emin and emax found in the oedometers tests were used as a reference for e0.

Moist tamping is a static compaction technique that allows to obtain loose specimens. A certain number of layers is prepared (10 is usually the choice) with constant height and density. Once chosen the required initial density and

knowing the initial sample dimensions, the weight of the necessary material is calculated and divided in 10 parts. Each quantity will occupy one tenth of the available volume in order to guarantee a uniform density. It is compulsory to add 5% of distilled water to the dry material in order to create artificially the voids in the sample's structure and to provide an apparent cohesion. Moreover, the so-called 'honeycomb' structure reached with this optimum water content is the loosest achievable (bulking phenomenon).

The best feature of this method is that it allows a good repeatability for sample preparation and to obtain an initial density with a reasonable degree of accuracy.

Figure 4. 7: moist tamping technique for sample preparation: layer compaction by means of a tamper (from Carrera, 2008)

However, the main disadvantage of this technique is that the granular soil sample is macroscopically layered and may not be representative of a natural deposition. Thus the compacting energy applied to the upper layer causes also the layers below to compact, resulting in a non uniform density. In order to prevent this disuniformity, several modifications were proposed (see further for Ladd' undercompaction method).

After compacting each layer, some furrows should be traced on the surface in order to obtain a better connection between layers.

Undercompaction

This technique can be seen as an improvement of the moist tamping technique. It consists of the static compaction of several layers having constant height containing a certain amount of material depending on the wanted initial density. The compaction energy has a fundamental role. The main difficulty is reaching the most uniform sample density as possible.

This technique allows to take into account the fact that inevitably the compaction of the upper layers will compact also the layers below, therefore Ladd suggested to control the compacting effort which should be the same for each layer, but varying the amount of soil.

'Each layer is compacted to a selected percentage of the required dry unit weight of the specimen; this procedure differs from the application of a constant compactive effort to each layer required by ASTM...Each layer is tipically compacted to a lower density than the final desired value by a predetermined amount which is defined as percent undercompaction U_n ' (Ladd, 1978).

In the figure below the linear variation of this parameter with the sample's height is shown: from a maximum value at the base to a minimum at the top.

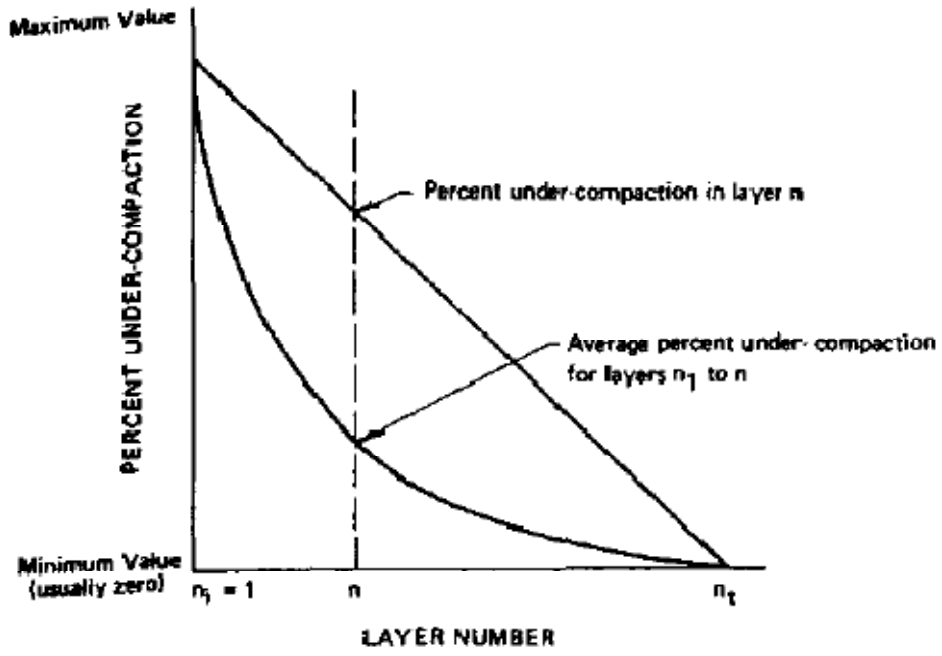

Figure 4. 8: Definition of percent undercompaction (from Ladd, 1978)

If the undercompaction percentage chosen is appropriate, as a final results a uniform density within the sample's height is obtained. The percentage to consider for each layer is calculated from the following equation:

$$U_n = U_{ni} - \left[\frac{U_{ni} \cdot U_{nt}}{n_t - 1} \cdot (n-1) \right]$$

Where:

U_{ni} is the percent undercompaction selected for the first layer;

U_{nt} is the percent undercompaction selected for the final layer, which is usually zero;

n is the number of the layer being considered;

n_t is the total number of layer (final layer).

Measurement of sample dimensions

In order to analyse and interpret the data obtained from triaxial tests it is necessary to know the sample dimensions and shape variation that occur during the test itself. This estimate allows to correct the data processing equations.

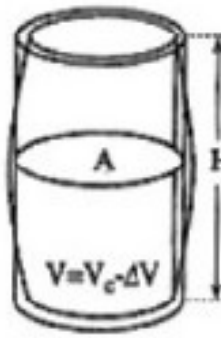

Particularly, the main variation during a triaxial test involve:

- The sample′s area, which usually increases;
- The sample′s height which usually decreases;
- The volume;
- The void index.

Figure 4. 9: Sample′s dimensions and shape variation during the shearing phase. Hc and Vc are the value at the end of the consolidation phase

As a general assumption in geotechnics, the decrease in sample′s dimensions are considered to be positive, whereas the increase is considered negative.

Initial dimensions

In order to evaluate the initial sample′s characteristics the following hypothesis are assumed. Given a cylindrical shape for the sample, the initial area of the cross section A_0 is:

$$A_0 = \frac{\pi \cdot D_0^2}{4} cm^2$$

Where D_0 is the initial diameter measured with the calliper;

The corresponding volume is :

$$V_0 = A_0 \cdot H_0 cm^3$$

Where H_0 is the initial height of the sample. All the samples prepared at Imperial College and the majority of those tested at University of Bologna have:

$D_0 = 38mm$

$H_0 = 76mm$

Thus, $A_0 = 11{,}34cm^2$ and $V_0 = 86{,}18cm^3$

Once known the initial dry weight of the soil W_s the initial density is defined as:

$$\gamma_d = \frac{W_s}{V_0}\frac{g}{cm^3}$$

Thus, the initial void ratio e_0 (or specific volume v_0) can be calculated from the expression:

$$e_0 = \frac{\gamma_s}{\gamma_d} - 1$$

Where γ_s is the specific grain weight, whereas the relative density D_R is determined with:

$$D_R = \frac{e_{\max} - e_0}{e_{\max} - e_{\min}}$$

In order to obtain samples with very different initial densities and thus from the wanted density the corresponding dry amount of material is determined.

Sample's dimensions after saturation

Bishop-Wesley cell

The calculation of the sample dimensions after the saturation phase when working with the Wille Geotechnik apparatus were obtained according to the following procedure. The total water volume entering the sample from the back pressure line is measured from the air-water interface readings at the beginning and at the end of the phase. The volume strain of the sample does not correspond to the inlet water because the pores that were filled with air are then substituted with water.

It is generally acknowledged to assume that during saturation no volume changes can be appreciated.

4.2.1. Analysis of the data from triaxial tests

Calculation of the initial void ratio e_0 (specific volume v_0): the Verdugo and Ishihara procedure (1996)

An accurate estimate of the initial void ratio of granular soil samples in triaxial tests can be difficult to achieve, especially when testing loose specimens. As pointed out by Sladen et al. (1987) during the saturation phase a partial collapse of the structure often happens and the volume changes cannot usually be measured referring to the standard laboratory procedure.

Therefore, in order to calculate the initial void ratio at the end of the saturation phase, the changes in diameter and in height have to be directly measured with calipers or calibrated metal tapes. This option however comprises the dismantelling of the triaxial cell.

Verdugo and Ishihara (1996) suggest a new procedure based on the direct relationship between void ratio and water content in saturated samples.

The measurement of the final water content at the end of a triaxial test needs to be handled with care, especially in the case of sandy samples. Freezing the sample is one option, but is not cost-effective, in terms of energy consume. The authors introduce a method, particularly recommended if the triaxial cell is equipped with volume gauges connected to an air-water interface pressure system, the method is based on the following steps:

1. As soon as the shearing phase is completed, the drainage line is closed in order to create undrained conditions. The back pressure control is released and the present volume gauge value V_i is established as the new reference point for volume changes. The drainage line is then opened, in order to the pore water to be collected and the volume changes to be measured during the subsequent loading-unloading cycle.

2. The cell pressure is increased to the maximum value allowed to the equipment in use, then decreased again, usually to 200 kPa. The back pressure valve is closed and the registered volume gauge value coincides with the final value V_f.

3. The cell pressure is then released and the triaxial cell dismantelled.

4. Given that the sample is in undrained conditions, it develops a negative pore pressure. When the top cap is removed, air enters the sample and it is now possible to dismantle it.

5. All the granular material is collected by means of a spatula and weighed. The remaining water content of the sample is determined. The final void ratio (at the end of the shearing phase) e_f can be calculated with the following equation:

$$e = \frac{(V_f - V_i + \omega_r \cdot W_d)}{W_d} \cdot G_s$$

where ω_r is the sample remaining water content, W_d is the sample final dry weight and G_s is the specific gravity.

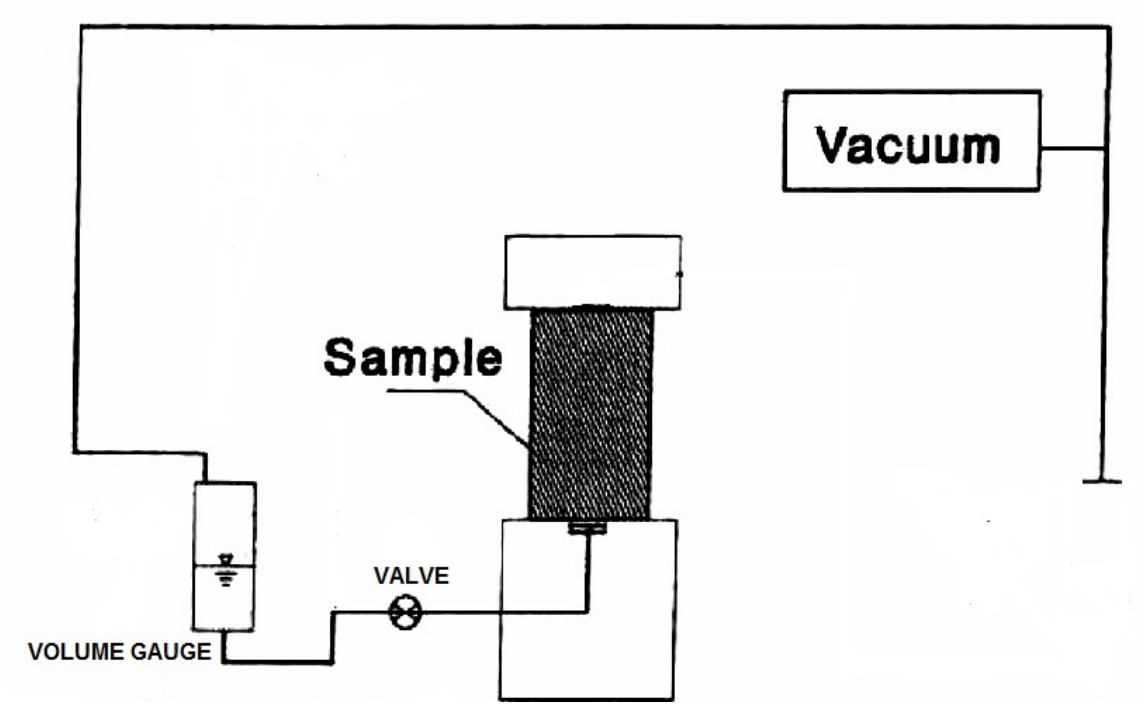

Figure 4. 10: water circulation system (modified from Verdugo and Ishihara, 1996).

The contribution provided by this method to the accuracy in terms of sample e_0 was highlighted. The authors carried out tests on three series of samples, repeating as similar as possible the steps described above. They pointed out the scatter in e_0 values calculated with this procedure is much smaller than the

scatter between the ones obtained from the sample dimensions. However, this difference is particularly high for loose samples , whereas is negligible in case of dense samples.

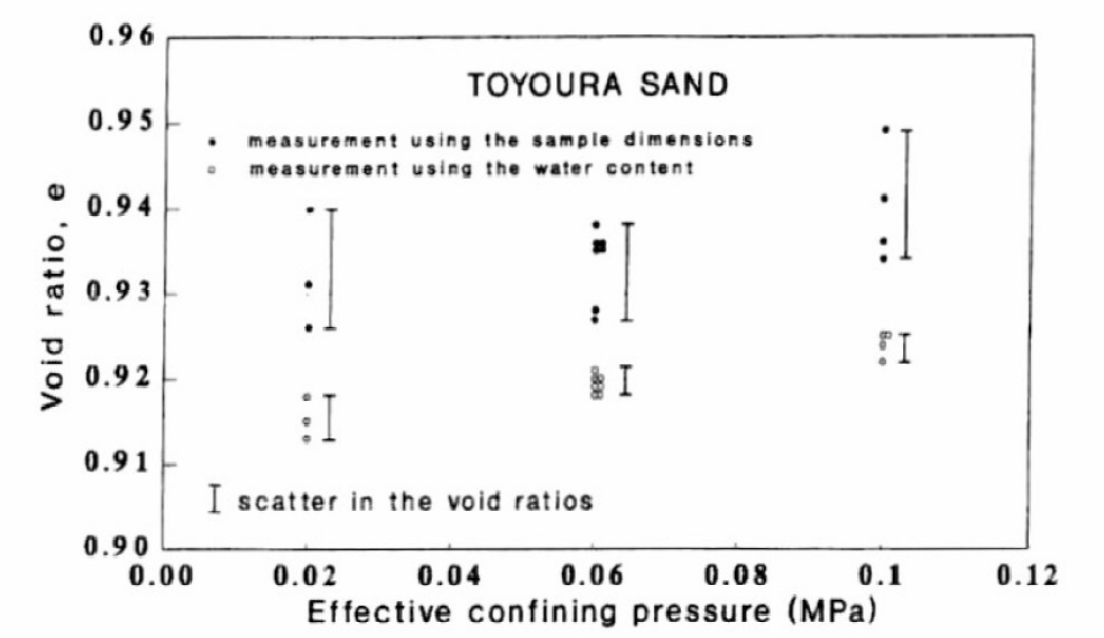

Figure 4. 11 : Comparison between e_0 based on sample dimensions and e_0 based on Verdugo and Ishihara method based on the water content

Calculation of the stresses

The load cell measures a force F_a, not a pressure. Therefore the deviatoric stress q needs to be calculated:

$$q = \frac{F_a}{A_c}$$

Where A_c is the current cross-sectional area of the sample.

Assuming that the sample during shearing deforms in a cylindrical way, the current cross-sectional area during shearing is calculated by means of the following equation:

$$A_c = A_0\left(\frac{1-\varepsilon_v}{1+\varepsilon_a}\right)$$

Where:

A_0 is the cross sectional area before shearing

ε_a is axial strain

ε_v is the volumetric strain

The axial stress is calculated through:

$$\sigma_a = \sigma_r + q$$

The mean effective stress is calculated from the following equation:

$$p' = \frac{(\sigma_a + 2\sigma_r)}{3} - u$$

The stress ratio is : q / p'

Calculation of volumetric strain and axial strain and shear strain

$\varepsilon_a = \frac{\Delta H}{H_c}$ measured from external transducers

$$\varepsilon_v = \frac{\Delta V}{V_c}$$

Where H_c and V_c are values referred to the end of the consolidation before the shearing phase.

$\varepsilon_s = \frac{(3\varepsilon_a - \varepsilon_v)}{3}$ SHEAR STRAIN

During the shearing phase the local transducers can measure the strains with more precision than the external transducer, but only for small strains. The measurements are not realistical anymore when the sample does not deform in a cylindrical way.

Sources of errors and inaccuracies

Axial strain

In order to measure the axial strain in shearing several factors have to be taken into account because they can lead to inaccuracies.

In a Bishop-Wesley triaxial apparatus (1975), several movements that develop during the shearing itself can lead to inaccuracies, particularly overestimates of

the axial strain. All these movements can be ascribed to the compliance of the system. Jardine et al. (1984) stated that the particular design features of this cell are such that the lower reference point for the vertical displacement trasducer is attached to the ram while the upper reference point is located on top of the cell , so that small, but significant deflezions accumulate from the straining of the rolling Bellofram diaphragms.

These observations were at the basis of the implementation of more satisfactory instrumentations, such as local transducers. The authors present the inclinometers, devices that can determine axial strains within a range of 0.002% in triaxial stress path cells designed for 38 mm samples.

4.3. *Introduction to the experimental work: experimental programme and interpretation procedure*

The laboratory work carried out within this research consists of three parts:

- material characterisation;
- oedometer tests;
- triaxial tests.

4.3.1. Material characterization

First of all, natural samples from the Venice lagoon, which had been object of previous studies, were chosen in order to be analysed within the transitional soils framework, as reconstituted samples. As pointed out in Chapter 1, these soils are mainly silts, naturally mixed at various depths with sand and clay and this feature made them highly interesting for a study on the transitional behaviour. However, the chaotic distribution of the different gradings within depth and from site to site makes it difficult to compare natural samples. Thus the material coming from a borehole at Treporti test site was reconstituted and two gradings, a sandy fraction and a fines fraction, were identified and geotechnically characterised. Grain size tests, Atterberg limits tests, carbonate content test, specific gravity tests, maximum and minimum void ratio test for the sandy fraction, particle size and shape analysis were performed. With respect to the mineralogy, results from other studies on Venice soils were used as a

completion of the experimental data, given the assumption of unique geological origin and depositional environment for the Venice silts (see section 1.5)

4.3.2. Oedometer tests

Subsequently, samples consisting of different percentages of the two fractions were prepared with the aim of investigating mixtures of soils that could represent a good candidate of transitional behaviour.

According to Nocilla et al., 2006, one of the key features of the so-called 'transitional soils' is that there are no unique normal compression line and samples having different initial specific volumes show parallel curves.

The first aspect to be investigated was therefore to study the one-dimensional compression behaviour of specimen of different mixtures having different initial void ratios, in order to see if they exhibited a unique normal compression line (NCL). Oedometer tests on sandy samples with varying percentages of fines were performed and in both cases of unique or non-unique NCL, the effect of the presence of different amount of fines on the steepness and on the position of the compression curves was studied.

The analysed mixtures had the following compositions:

- 100% sand;
- 70% sand-30% fines;
- 50% sand-50% fines;
- 100% fines.

In the table below a resume of the tests and of their most important features is presented. The initial void ratio e0 is calculated from the measure of the final dry weight and refers to the stage when the water bath is filled ; □v is the maximum pressure applied to the specific sample. Some problems occurred causing the non-complete reliability of some tests, these problems being mainly related to the measure of the initial sample height.

In the following table the dry compaction technique is indicated as DC and the slurry technique as S. Both values of e0 and ef were calculated from the final water content.

Test	**% sand**	**% fines**	**Preparation technique**	**σ_{vmax} [kPa]**	**e_0**	**e_f**	**comments**
Edo_02_IC	100	0	DC	22501,574	1,08	0,65	Floating ring oedometer
Edo_04_IC	100	0	DC	27694,245	0,97	0,43	
Edo_013_IC	100	0	DC	5516,328	**0,89**	0,66	
Edo_014_IC	100	0	DC	27694,245	0,94	0,65	
Edo_017_IC	100	0	DC	8023,750	0,99	0,63	
Edo_041_IC	100	0	DC	99751,689	1,05	0,26	
Edo_051_IC	100	0	DC	90400,197	**1,23**	0,42	Floating ring oedometer
Edo_056_IC	100	0	DC	49877,066	1,09		Floating ring oedometer
Edo_043_IC	70	30	S	7986,782	0,67	0,22	
Edo_044_IC	70	30	S	15972,578	0,64	0,25	
Edo_045_IC	70	30	S	11963,742	**0,63**	0,23	
Test	**% sand**	**% fines**	**Preparation technique**	**σ_{vmax} [kPa]**	**e_0**	**e_f**	**comments**
Edo_046_IC	70	30	S	11465,299	0,70	0,27	
Edo_049_IC	70	30	DC	15456,990	**1,03**	0,38	
Edo_055_IC	70	30	DC		0,77	0,27	
Edo_057_IC	70	30	DC	16006,719	1,02	0,40	
Edo_058_IC	70	30	DC	15974,709	0,87	0,30	
Edo_030_IC	50	50	S	7978,304	0,72	0,27	
Edo_031_IC	50	50	S	14706,219	0,83	0,28	
Edo_034_IC	50	50	S	7978,265	0,77	0,36	

Edo_036_IC	50	50	S	7981,486	0,76	0,22	
Edo_038_IC	50	50	DC	7981,457	1,10	0,28	
Edo_039_IC	50	50	DC	7482,724	1,14	0,37	
Edo_040_IC	50	50	DC	7497,038	**1,25**	0,36	
Edo_042_IC	50	50	S	7976,138	**0,67**	0,22	
Edo_047_IC	50	50	DC	15453,894	1,01	0,34	
Edo_052_IC	50	50	DC	15955,565	0,79	0,22	
Edo_054_IC	50	50	DC	15955,598	1,05	0,49	
Edo_059_IC	50	50	S	12990,032	0,85	0,36	
Edo_060_IC	50	50	DC	20319,874	0,84	0,25	
Edo_05_IC	0	100	S	28614,831	1,00	0,30	
Edo_08_IC	0	100	S	4985,800	0,98	0,42	
Edo_09_IC	0	100	S	8671,161	0,97	0,33	
Edo_010_IC				27747,715	1,10	0,45	
Edo_012_IC	0	100	S	12815,931	0,96	0,33	
Edo_015_IC	0	100	S	7993,506	1,17	0,42	
Edo_016_IC	0	100	S	14750,979	1,19	0,49	
Edo_020_IC	0	100	S	14754,256	**1,29**	0,54	
Edo_033_IC	0	100	DC	7978,315	**0,95**	0,42	
Edo_048_IC	0	100	S	15951,319	0,99	0,25	

Table 4. 2: list of the performed oedometer tests

4.3.3. Triaxial tests

The laboratory work at the beginning of this research was focused on the implementation of different techniques of sample preparation in order to reach a trustful repeatability in obtaining different initial void ratios.

The performed triaxial tests had the aim of investigating the mechanical behaviour of different mixtures of Venice soils (same percentages of sandy and fines fractions as in the oedometer tests), in order to analyse the existence of a critical state line (CSL) and compare with the monodimensional compression behaviour (NCL). Moreover another aspect that needed further attention was related to the influence of changes in grading on the location and properties of the CSLs.

The experimental work at the end of this PhD was finally addressed to the implementation of the new equipment of the triaxial cell in Bologna.

Six triaxial tests were carried out at Imperial College (London), most of them were undrained. Ten tests were performed at Università di Bologna. Particularly, the tests in details are:

- 3 tests on clean sand (2 on pure sand)
- 9 on mixtures of 50% sand 50% fines (3 drained and 6 undrained)
- 4 on 100% fines
- 3 on mixtures of 70% sand 30% fines.

The description of the tests parameters is reported in the table below. The symbols e_C, p'_C and q_C refer respectively to the void ratio, the mean effective stress and the deviator stress at the end of the consolidation phase.

Moreover, e_{CS}, p'_{CS} and q_{CS} are the void ratio, the mean effective stress and the deviatoric stress at the hypothetical Critical State, supposing that it had been reached at the end of each shearing phase.

As shown in the table below, all the samples were moist tamped indicated as MT.

Nr.	**Test name**	**Type of test**	**Sample composition**	p'_c **[kPa]**	q_c **[kPa]**
3	Tx_50%50%_01_icu	CIU	50%sand-50%fines	300	0
4	Tx_50%50%_02_icd	CID	50%sand-50%fines	300	0

5	Tx_50%50%_03_icu	CIU	50%sand-50%fines	200	0
6	Tx_50%50%_04_icu	CIU	50%sand-50%fines	190	0
7	Tx_100%fines_01_icu	CIU	100% fines	300	0
8	Tx_100%fines_02_icu	CIU	100% fines	200	0
9	Tx_100%fines_03_icu	CIU	100% fines	200	0
10	Tx_50%50%_05_icd	CID	50%sand-50%fines	290	0
11	Tx_50%50%_06_icd	CID	50%sand-50%fines	190	0
12	Tx_50%50%_07_icu	CIU	50%sand-50%fines	400	0
13	Tx_50%50%_08_icu	CIU	50%sand-50%fines	400	0
14	Tx_50%50%_09_icu	CIU	50%sand-50%fines	300 ?	0
15	Tx_100%fines_04_icu	CIU	100% fines	100	0
16	Tx_70%30%_01_icu	CIU	70%sand-30%fines	200	0
17	Tx_70%30%_02_icu	CIU	70%sand-30%fines	200	0
18	Tx_70%30%_03_icu	CIU	70%sand-30%fines	300	0
19	Tx_100%sand_01_icu	CIU	100%sand	100	0
20	Tx_100%sand_02_icu	CIU	100%sand	200	0
21	Tx_100%sand_03_icu	CIU	100%sand	300	0

Table 4. 3 (a): List of the performed triaxial tests and of their most important features

Nr.	e_C	p'_{CS} **[kPa]**	q_{CS} **[kPa]**	e_{CS}	**Preparation technique**	**comments**
1					MT	
2	1,346				MT	Not accepted
3	0,938	108	135	0,938	MT	
4	0,658	700	1212	0,578	MT	
5	0,879	48	56	0,879	MT	
6	0,883	55	106	0,883	MT	
7	1,355	106	138	1,355	MT	Too high measure of e
8	0,823	115	86	0,823	MT	Measure of e from initial dry weight
9	1,274	80,4	140,6	1,274	MT	
10	0,78	730	1294	0,70	MT	Measure of e from initial dry weight
11	0,896	372,1	545,2	0,785	MT	
12					MT	Measure of e from initial dry weight and Shear band
13	0,893			0,893	MT	Measure of e from initial dry weight

14	0,68			0,68	MT	
15	0,98	91,24		0,98	MT	
16					MT	
17					MT	
18					MT	
19	0,91	480,8	543,6	0,939	MT	
20		448,88	513,76		MT	
21		300			MT	

Table 4. 2 (b): List of the performed triaxial tests and of their most important features

CHAPTER 5

Analysis of the results

5.1. *Origin of the material: Treporti case study*

An ambitious research programme was launched in 2000, by the University of Padova and in collaboration with University of Bologna and L′Aquila, in order to get a better understanding of the highly heterogeneous and stratified silty sediments of the Venice lagoon and to compare data from several in situ testing apparatus, such as the piezocone and the dilatometer. Treporti is the name of the test site where the research was carried out. In particular, this is where the soil used to prepare the mixtures comes from. In the figure below, a view of the Venice lagoon is presented. Treporti is located on the Cavallino coast line.

Figure 5. 2: The Venice lagoon.

5.1.1. Sampling at the Treporti test site: soil profile and stress history

The soil which is the object of this study comes from a survey campaign carried out at a site located just outside Treporti, an old fishing village on the Cavallino

coastline, facing the North-Eastern lagoon. In particular, the soil comes from a 10-cm-diameter and 25-m-deep borehole. At the time, soil classification tests and geotechnical characterisation, including oedometer tests, had been carried out on the undisturbed sample. For classification purposes seven main stratigraphic groups had been identified:

- Sand - Silty sand;
- Silty sand - Sandy silt with occasional lenses of silty clay;
- Silty sand interbedded with sandy silt and clayey silt;
- Silty clay;
- Silty clay interbedded with clayey silt;
- Alternance of fine sand and clayey silt;
- Sandy silt.

5.2. *Material characterisation*

After the laboratory characterization, the various fractions coming from this borehole were stored in the Soil Mechanics Laboratory of the University of Bologna, but for around half of them the information of the depth is unfortunately now lost. It was therefore decided to use this disturbed soil in order to study the influence of different percentages of fines on the behaviour of the sand.

5.2.1. Separation into two fractions

The material was split into two main gradings, a fine fraction and a sandy fraction, through wet sieving to the N° 200 sieve.

Sandy fraction	Fines fraction
14.4 kg	10.1 kg

Table 5. 1: Amount of available material for the two fractions coming from the borehole at the Treporti test site

5.2.2. Grain size distribution

In order to study the grain size distribution of the two fractions, the sandy fraction, which consists in the soil not passing through the 74 □m sieve was analysed by sieving whereas the grain size distribution of the fines was obtained

through a sedimentation test, according to the recommendations in the ASTM 422 standards. The sandy fraction can be defined as a poorly graded fine sand. The D_{10} and D_{60} for the sandy fraction are respectively 0.08 mm and 0.14 mm. The grain size curves are reported in the figure below.

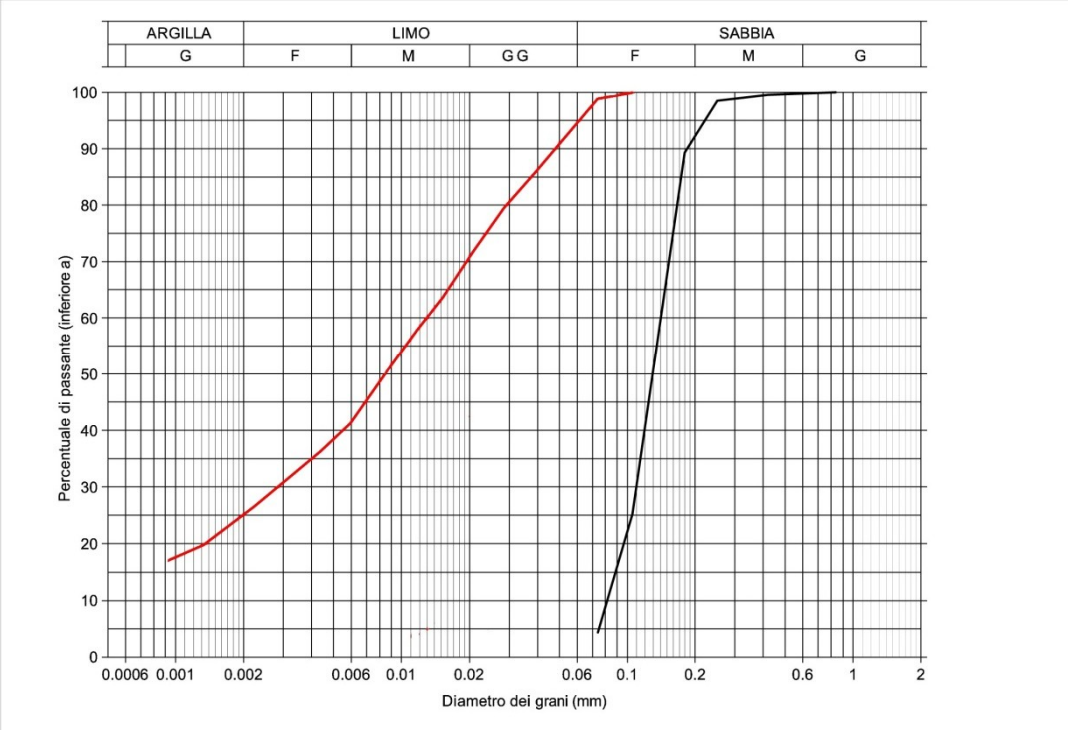

Figure 5. 3: Grain size distributions of the two fractions.

5.2.3. Specific gravity Gs

The specific gravity Gs of the sandy fraction and of the fines was determined according to the recommendations in the ASTM D 854 standard. The two values were found to be very similar as can be noted from the table below:

	Sandy fraction	**Fines fraction**
G_s	2.786	2.784

Table 5. 2: Values of specific gravity Gs determined for the two fractions

These values are very high, due to the mineralogy of the material and they agree with other published data such as in Cola and Simonini (2002) where the Gs values for the Malamocco test site were equal to 2.77±0,03. The values are very similar both for the sandy and the fines fraction; this could be related to the fact

that the fines originated from the crushing of the sandy particles during geological events.

5.2.4. Atterberg limits

The Atterberg limits of the fines fraction were performed following ASTM D 4318. They gave the results summarised in the table below:

w_L **[%]**	29.8
w_P **[%]**	22.7
I_P **[%]**	7.1

Table 5. 3: Atterberg limits and plasticity index for the fines fraction.

According to these values and the Casagrande plasticity chart, the material can be classified as low plasticity clayey silt (ML), although, as shown in the graph below, the point could also describe a low plasticity silty clay (CL). As is common practice in the geotechnical laboratory, the liquid limit w_L was determined with the Casagrande spoon and the plastic limit w_P was chosen when a thread of soil started to fissure. Some values determined from natural samples at different depths from the Treporti test site are also reported.

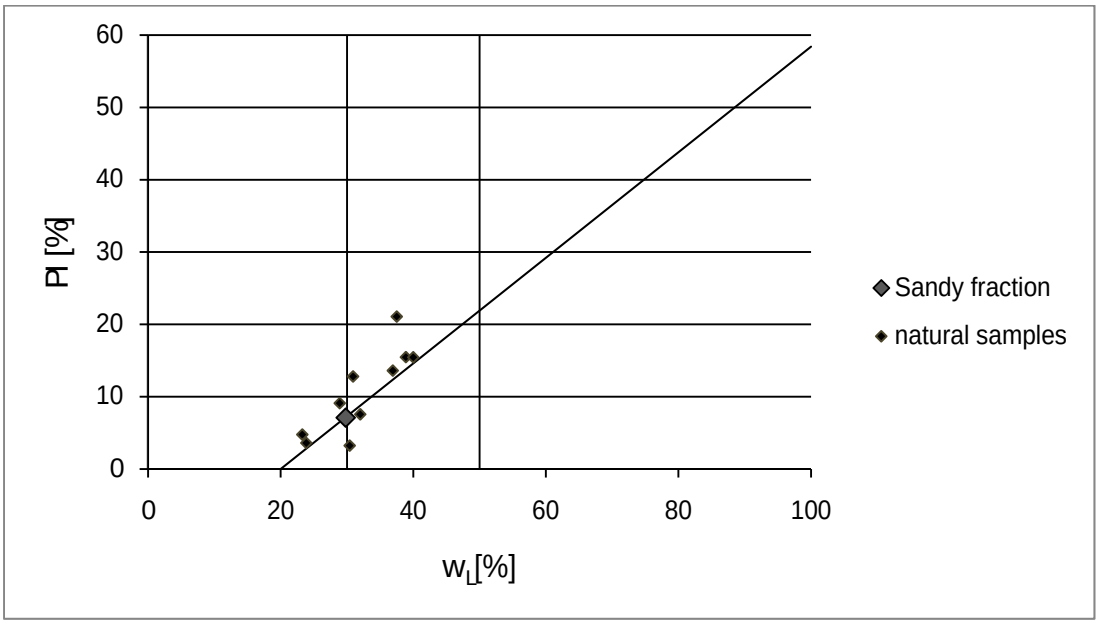

Figure 5. 4: Casagrande plasticity chart; the black points refer to the natural samples at Treporti and the grey one represents the sandy fraction.

5.2.5. Maximum and minimum void ratio of the sandy fraction

The maximum and minimum void ratio for the sandy fraction were measured according to the procedure of ASTM D 4253 and D 4254. The values are summarised in the table below:

e_{min} (estimated)	0.931
e_{max}	1.162

Table 5. 4: Minimum and maximum void ratio for the sandy fraction.

These e_{max} and e_{min} are relatively high, a reason for this feature might lie in the angularity of the grains (see section 5.2.3) or in the uniformity of the grain size distribution curve.

5.2.6. Mineralogy and carbonate content

With respect to the mineralogy of these soils, results of previous investigations were reported, given the same geological origin and depositional environment throughout within the Venice lagoon materials.

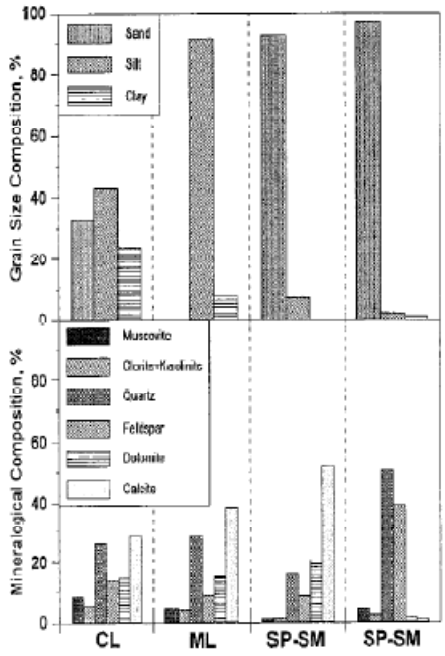

	Sandy fraction	Fines fraction
Muscovite	0-5%	0-10%
Clorite+Kaolinite	0-5%	5%
Quartz	10-50%	25-30%
Feldspar	10-40%	5-15%
Dolomite	0-20%	15%
Calcite	0-50%	30-40%

Figure 5. 5: Mineralogical composition of undisturbed samples from Malamocco test site (modified from Cola and Simonini, 2002).

The carbonate content of both fractions was analysed according to ASTM D 4373. The results can be seen in the table below:

	$CaCO_3$ content(%)
SANDY FRACTION	65.0
FINE FRACTION	33.5

Table 5. 5: Carbonate content of both fractions.

These values are quite high, thus it is quite safe to state that the soil belongs to the limestone-dolomite or Veneta province, as seen in section 1.5. These carbonate contents should result from the contribution of both calcite and dolomite.

These data can be compared to the carbonate content values measured at the Malamocco test site, as reported in Simonini et al., (2006). The authors point out two different mineralogies for the sand (SP-SM) specimens, one mainly quartzitic-siliceous and one mainly carbonate (higher depths). The 70% of carbonates in the latter is composed of approximately 20% of dolomite and 50% of calcite. This value is of the same order of magnitude of carbonate content as the sandy fraction from Treporti. In contrast, in the silty (ML) sample at Malamocco the carbonate content is approximately 50%, which is considerably higher than the value of 35% in the fines fraction at Treporti.

However, as shown in figure 1.11, the bulk samples at different depths from the Malamocco test site have a carbonate content between 20 and 40 %. Thus, the value of 33,5% for the fines fraction from Treporti falls within this range.

Summary

	Sandy fraction	**Fines fraction**
USCS Classification	PS: poorly graded fine sand	ML: low plasticity clayey silt
Grain size parameters	$D_{60} = 0.141$ $D_{10} = 0.081$ $C_U = 1.7$ $C_C = 1.32$	$D_{60} = 0.013$
Atterberg limits	[-]	$w_L = 29.8$ $w_P = 22.7$ $I_P = 7.1$
G_s	2.786	2.784
Carbonate content $CaCO_3$	65.0	33.5
e_{max}	1.162	[-]
e_{min}	0.931	[-]

Table 5. 6: Summary of the characterization of the two fractions

5.2.7. Qicpic analysis of the grain size distribution

The sandy fraction was analysed with an image analysis sensor, called Qicpic, manufactured by Sympatec GmbH (see section 4.1.3). This apparatus creates a particle flow, that is scanned by a laser to give images of each particle. The images are then analysed in order to obtain a statistical distribution of the particle dimensions and shapes. It has to be highlighted that, if the rate of supply of the

particles is too large, the number of images with overlapping particles will be very high and they should be discarded.

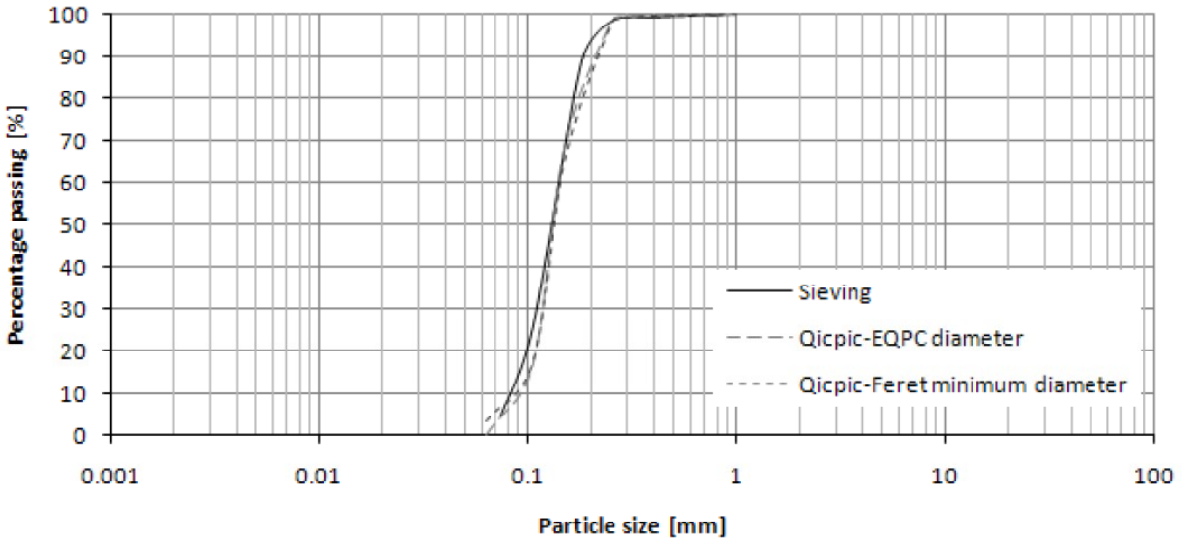

Figure 5. 6: Grain size distribution of the sandy fraction from sieving and curves obtained from the Qicpic apparatus.

Unfortunately, for the fines fraction, the silty and clayey particles tend to form clusters not allowing an efficient dispersed flow. This resulted in incorrect gradings and complex morphologies, as can be seen from the figure below, which shows a comparison between the grain size distribution from sedimentation and a curve obtained from the Qicpic apparatus.

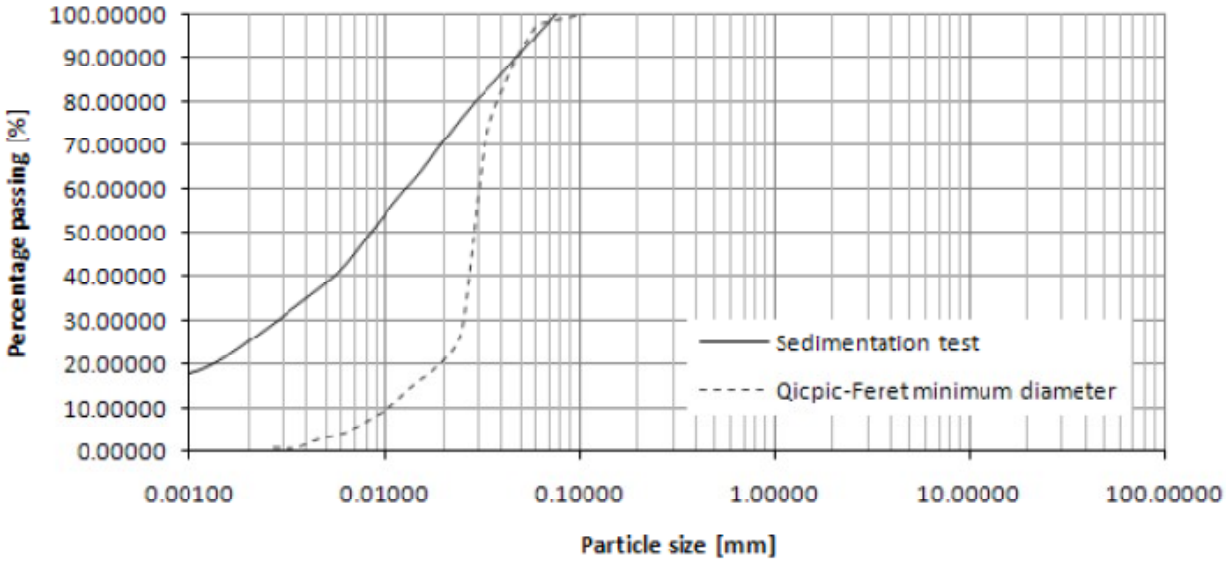

Figure 5. 7: Fines fraction grain size distribution from sieving and curves obtained from the Qicpic apparatus.

As can be seen from the charts above, the grain size distribution curves obtained from the EQPC and Feret minimum diameters both lie on the right side of the sieved curve (for the definition of these parameters, see section 4.1.3). This might be ascribed to the fact that the sieving itself is less repeatable (the strength used and the time spent sieving can heavily influence the results), whereas the other curves are obtained from mathematical modelling.

Both for the sandy and for the fines fraction the best fitting curve was that obtained from the Feret minimum diameter.

5.3. *Oedometer tests*

The oedometer tests were carried out on different type of mixtures: 100% sand, 70% sand and 30% fines, 50% fines-50% sand, 100% fines. In the following paragraphs the samples will be defined with the names 100% sand, 70-30, 50-50 and 100% fines. The main objective of using these mixtures was to study the influence of the presence of fines on the mechanical behaviour of the Venice sand fraction.

All the tests were aimed at obtaining normal compression curves to see if they converge or not, and therefore at investigating the existence of a unique normal compression curve for mixtures with different percentages of fines. All the samples were prepared either as slurries or with the dry compaction technique. The initial void ratio was calculated from the final dry weight. It was tried to prepare samples with different initial void ratios in order to plot the stress-strain behaviour. A floating ring oedometer (see section 4.1.1) was also used and higher pressures up to 100 MPa were applied to the 100% sand samples. The convergence of the normal compression curves was studied in order to define a possible transitional behaviour for these different kinds of soils. The compressibility parameters and their variation with increasing fines content were analysed.

5.3.1. Results of the oedometer tests: convergence and non-convergence of NCLs

In the figure below the normal compression curves obtained from oedometer tests on 100% sand samples are reported. Eight tests have been performed on 100% sand samples and three of them have been carried out with the floating ring oedometer. All the samples have been prepared with dry compaction.

100% Sand samples

As can be seen in the graph below showing tests on 100% sand samples, the normal compression curves from tests carried out with the high pressure oedometer have a different trend if compared to those carried out in the fixed ring oedometers. The majority of the curves seem to converge to a unique 1-dimensional normal compression line (1D-NCL), with the exception of the results from floating ring oedometer tests and test Edo_02_IC. This convergence is highlighted in figure 5.8. The compressibility parameters will be analysed in the following paragraphs.

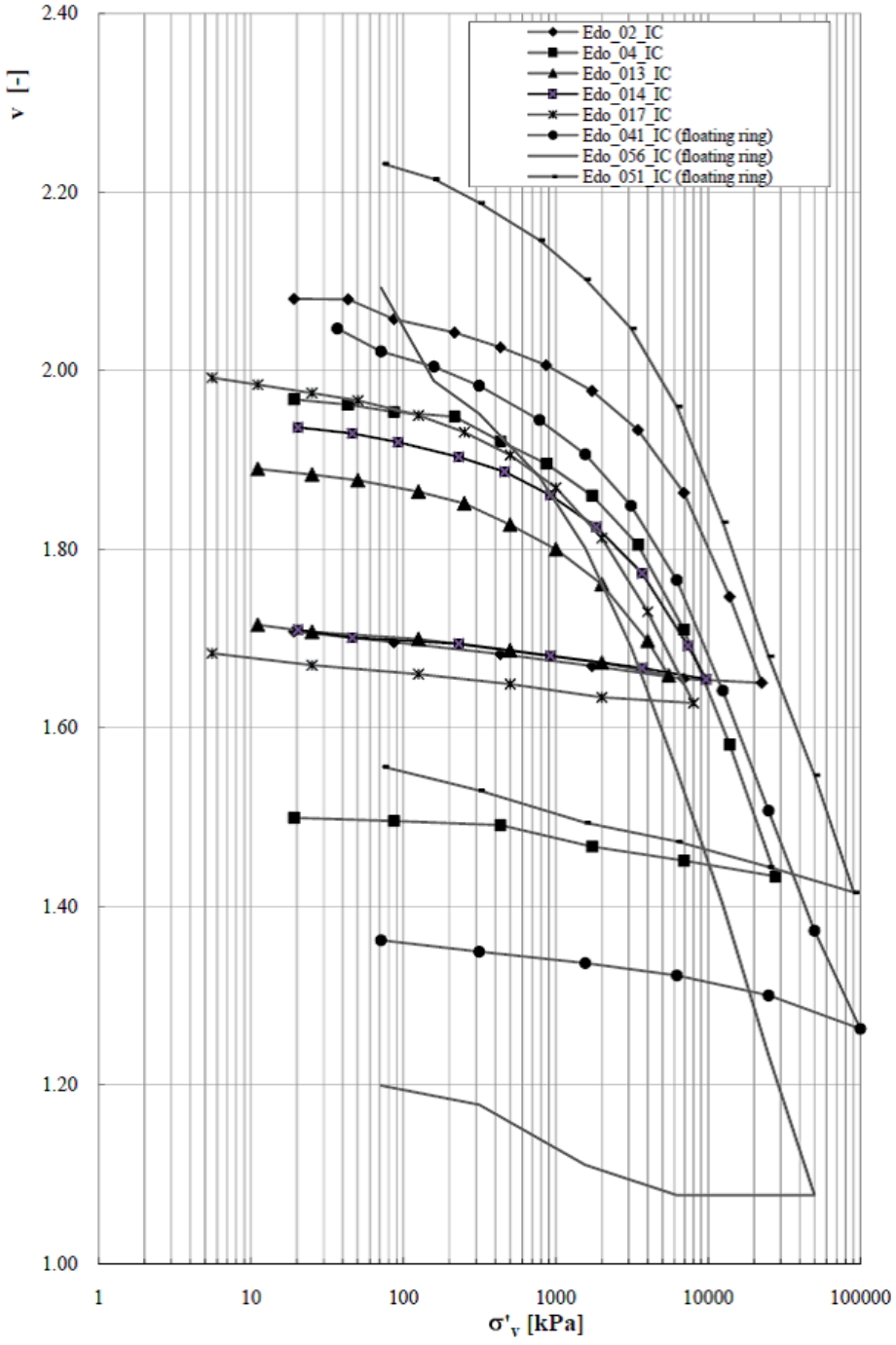

Figure 5. 8: Compression curves from oedometer tests on 100% sand fraction samples.

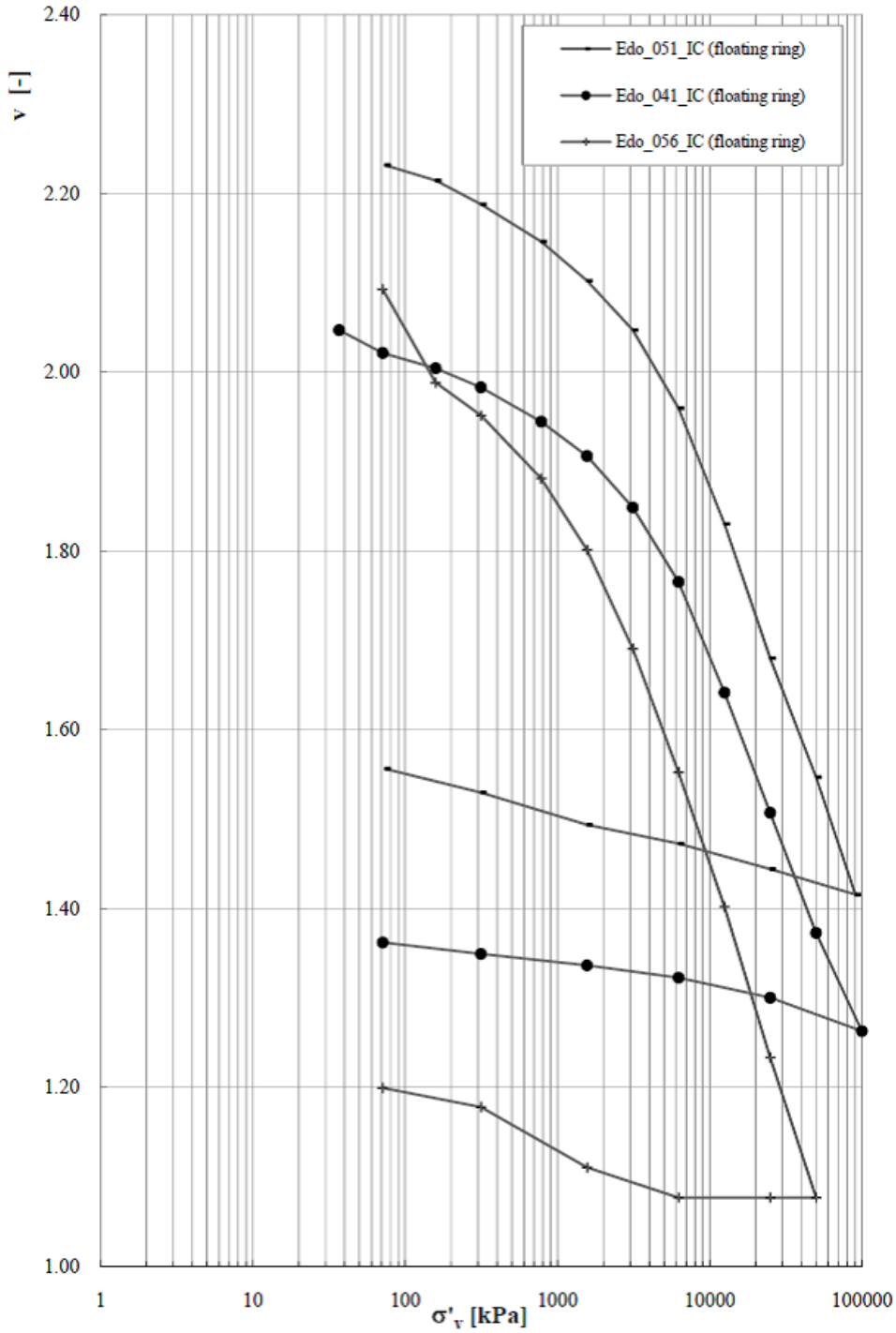

Figure 5. 9: Compression curves from floating ring oedometer tests on 100% sand samples.

70%Sand-30%fines

Several oedometer tests were performed on samples made of 70% sand and 30% fines. The study of mixtures of different compositions allows an investigation of the influence of the presence of fines on the compression behaviour of the sand.

Compared to the soil consisting of 100% sand, this mixture seems to behave differently if the samples were dry compacted or prepared as a slurry.

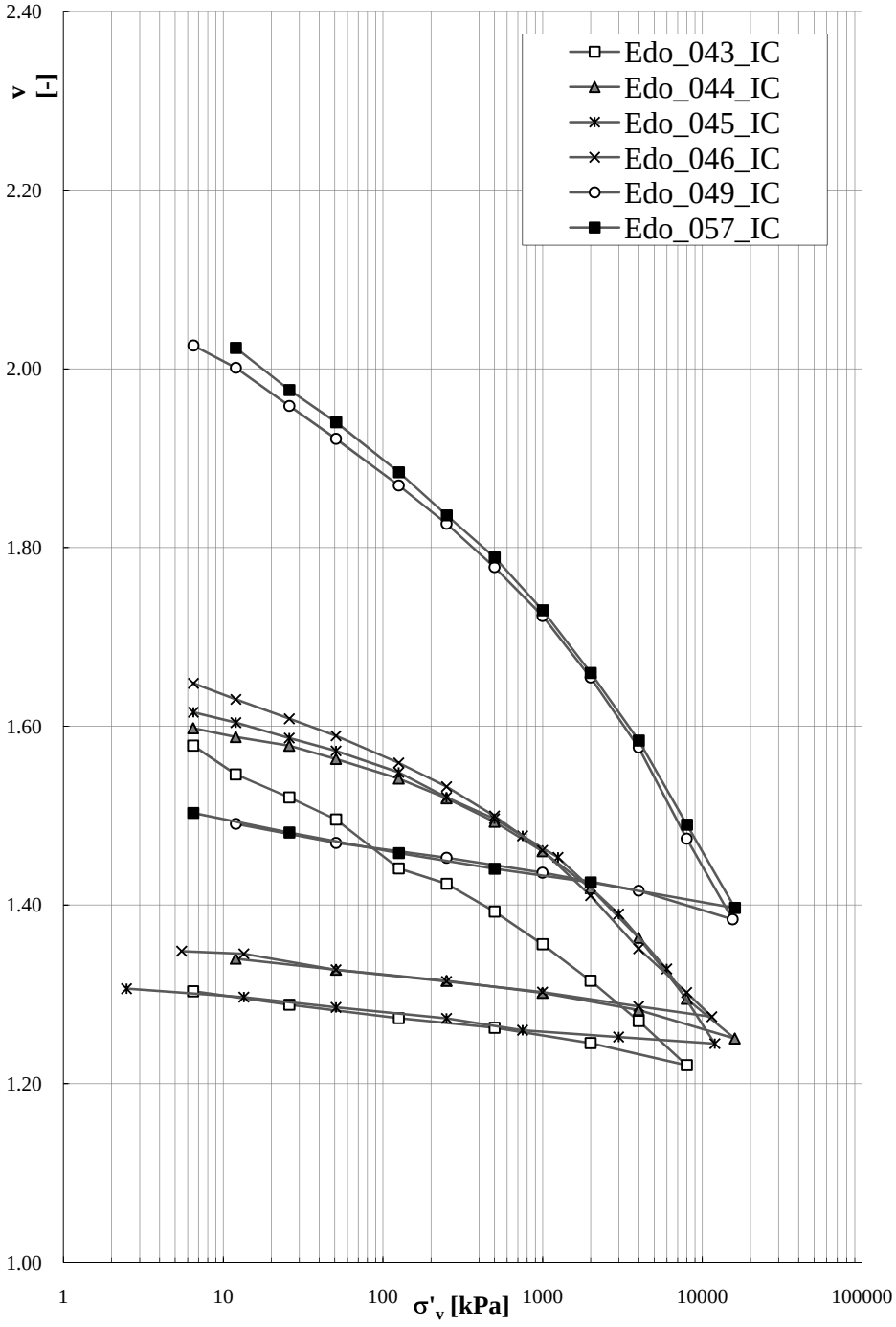

Figure 5. 10 : Compression curves from oedometer tests on 70% sand-30% fines samples.

Some of these samples were prepared as slurries and some were dry compacted with the aim of widening the range of initial void ratios. First it can be observed that these curves are more scattered than for the 100% sand samples. This could be related to the different sample preparation techniques. Moreover the slurry samples tend to be less compressibile than the dry compacted. Two groups of curves can be distinguished in the compression chart. The curves that refer to each group seem to maintain a parallelism even at around 10 to 20 MPa, with the exception of test Edo_046_IC. They might eventually result in a convergence only at stresses higher than those investigated.

The steepness of all the curves increases with increasing pressure, but this trend is not fast enough to allow a convergence to a unique normal compression line with void ratio that are still meaningful. For the dry compacted samples, it can be seen that the curves from test Edo_049 and test Edo_057 seem to almost be overlapping.

50%Sand-50%Fines

In Figure 5.16 the compression curves of the soil composed of 50% sand and 50% fines are shown. A higher number of tests was required in order to investigate the behaviour of this soil.

Firstly, it can be noted that, if compared to the samples previously shown that were mostly sandy, the 50%sand-50%fines oedometer curves were more scattered. Thus the existence of a unique 1D-NCL was harder to define.

Given the huge amount of data on 50-50 samples, the behaviour of slurry and dry compacted samples was initially analysed separately.

As for the 70-30 mixtures, the 50-50 specimens seem to be less compressible if prepared as slurry. However, as a general trend, it can be noticed that the majority of the curves lie parallel to each other even at high stresses, although a slight increase in their steepness with increasing stresses can be noticed.

As is shown in Figure 5.10, dry compacted samples from different initial specific volumes do not converge to a unique normal compression line and do not show a clear yielding point.

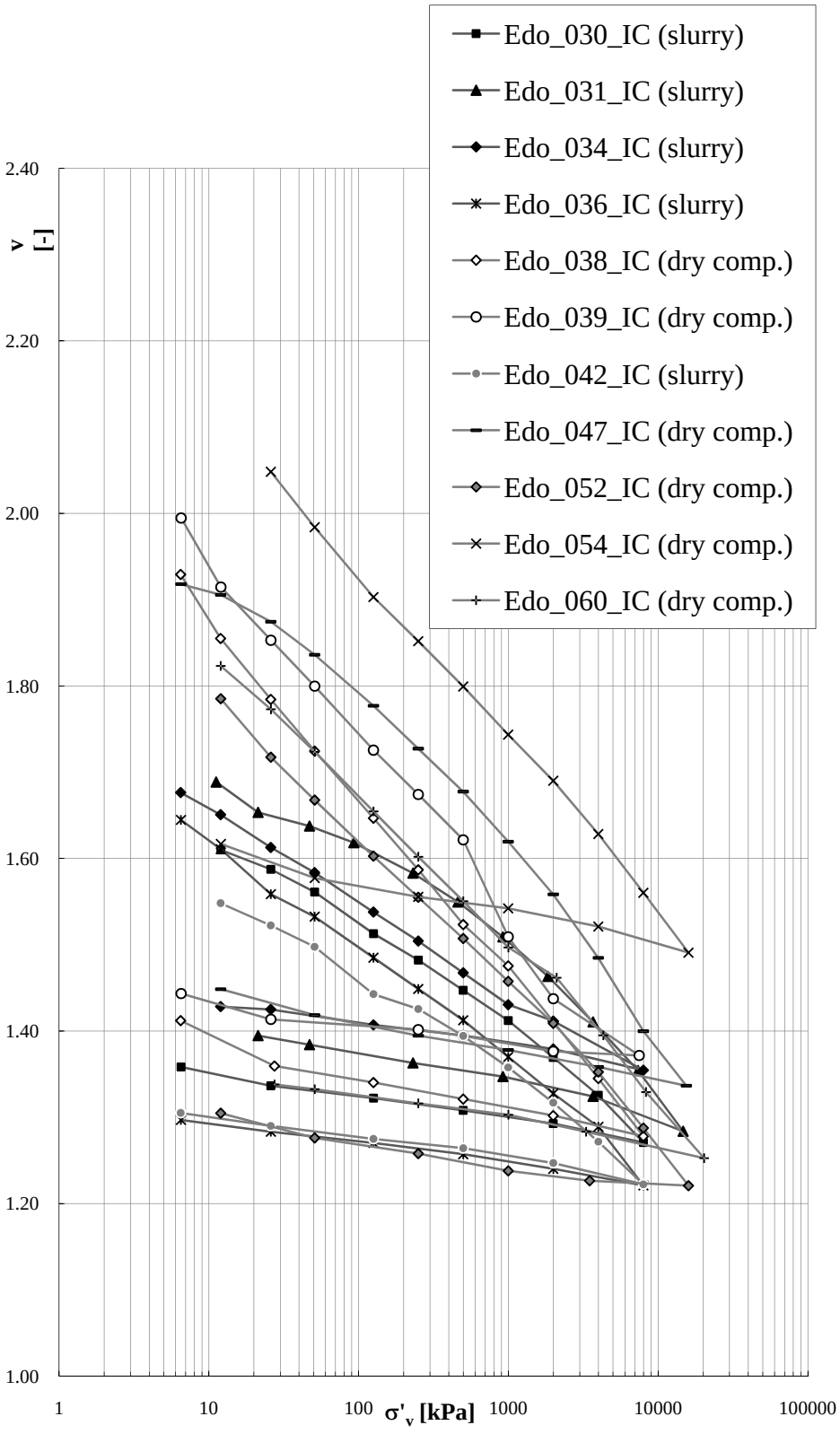

Figure 5. 11: Compression curves from oedometer tests on 50% sand-50% fines samples.

Only curves from Edo_038 e Edo_052 converge at around 2 MPa. This might be ascribed to some inaccuracies in the measurement of the initial specific volume. The

steepness of test Edo_039 is not understood, thus this test was not taken into account in the following analysis.

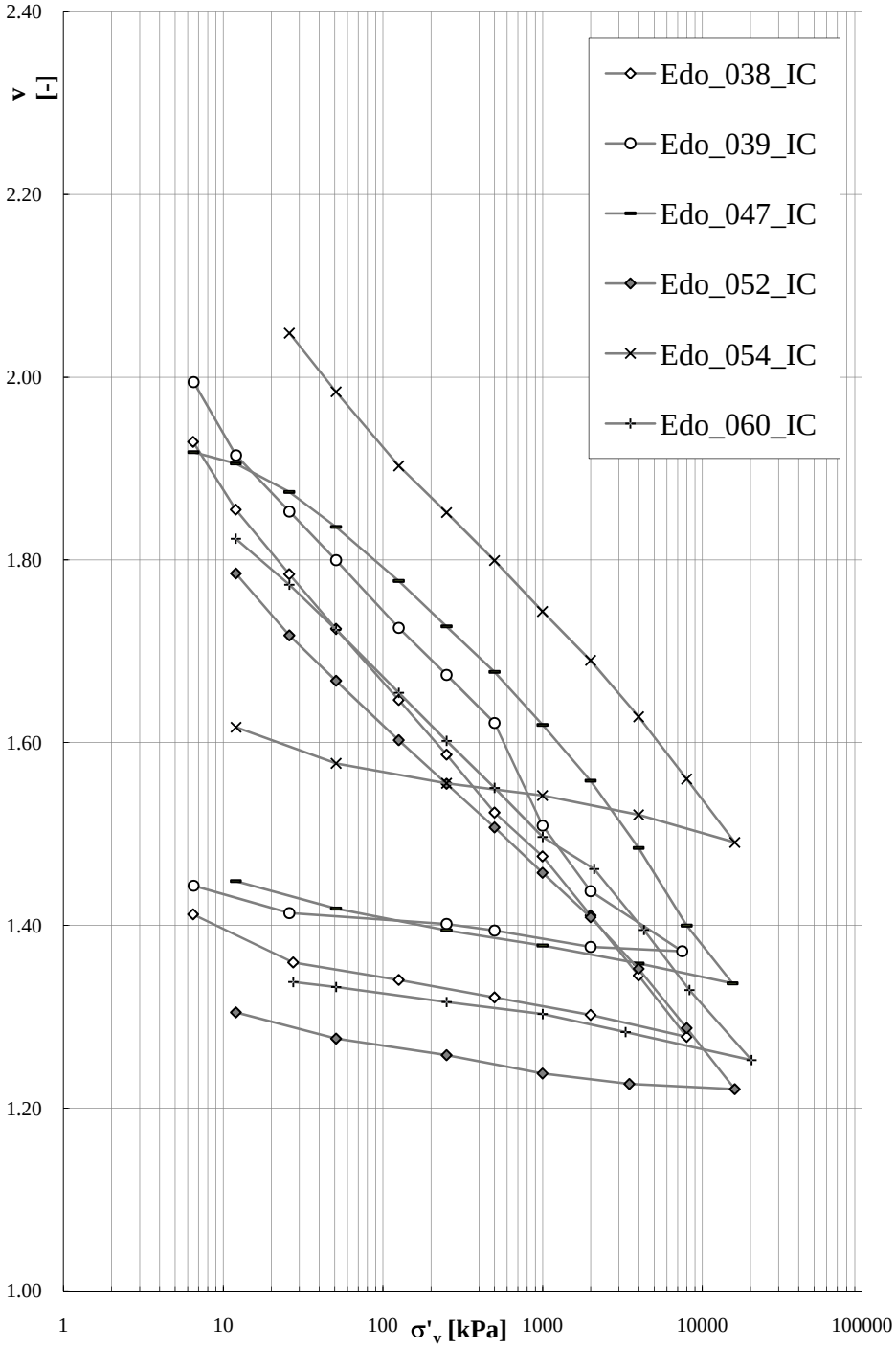

Figure 5. 12: compression curves from oedometer tests on 50% sand-50% fines samples obtained from dry compaction.

The slurry samples are generally less scattered than dry compacted ones. This is due to the limited water content range, according to the recommendations as Burland (1990).

The curves from Edo_036 e Edo_042 converge at around 2 MPa: this might be ascribed to some inaccuracies in the measurement of the initial specific volume. The last loading step of test Edo_034_IC is steeper, thus this test was not taken into account in further considerations.

As seen for dry compacted samples, the compression curves from different initial densities remain substantially parallel to each other and do not show a clear yielding point. This parallelism is maintained even to large pressures.

It has to be investigated whether the compression curves from slurry and dry compacted samples can be considered to remain parallel or if they tend to converge to a unique NCL. If so, it has to be studied if this curve can be reached at reasonable stress levels. Further considerations on the mechanical behaviour and on the compressibility parameters of the curves can be found in section 5.3.1.

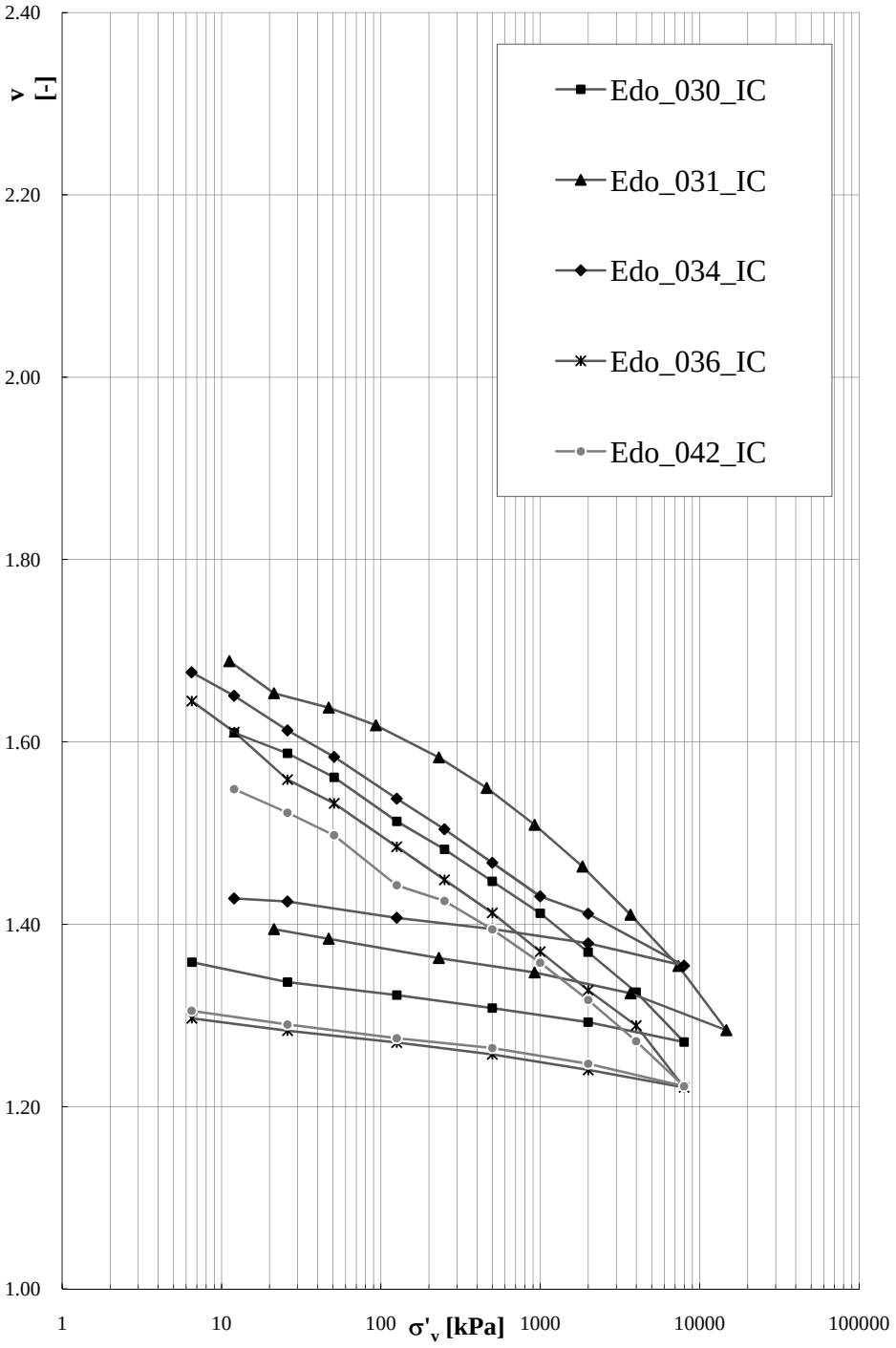

Figure 5. 13: Compression curves from oedometer tests on 50% sand-50% fines samples obtained from slurry.

100% fines

In Figure 5.12, the normal compression curves for 100%fines samples are shown. All the samples, except test Edo_033_IC, were prepared as slurries.The data are quite scattered. Several samples were compressed from very similar initial densities.

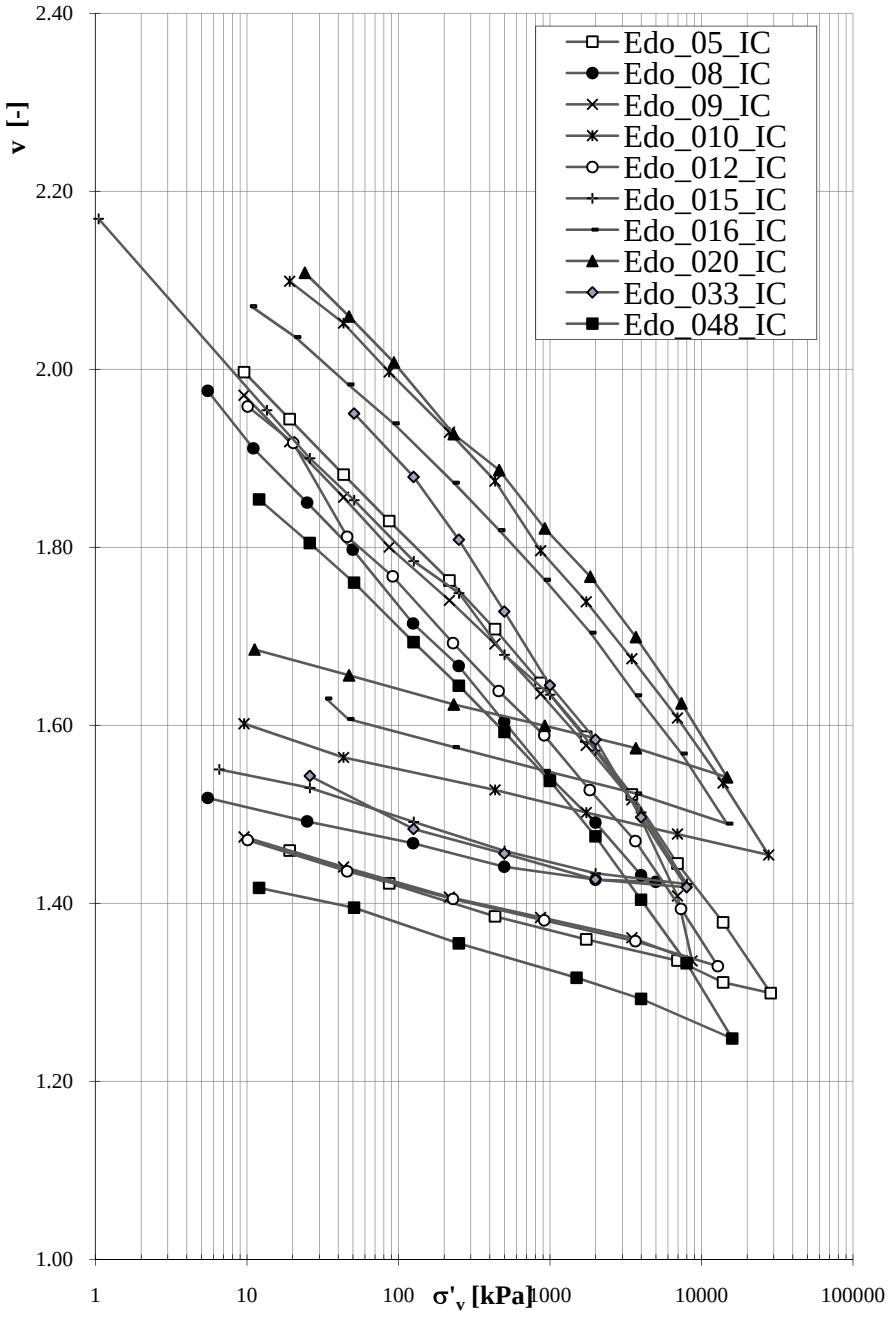

Figure 5. 14: Compression curves from oedometer tests on 100% fines samples.

Thus, in order to investigate if they converge or not to a unique NCL, it is convenient to analyse the behaviour of samples with quite different initial specific volumes (see Section 5.3.1). Test Edo_012_IC was not considered in further considerations because its steepness highlights some inaccuracies.

5.3.1. Results of the oedometer tests: mechanical behaviour

According to the results of the oedometer tests a unique NCL could be identified only for the 100% sand. As is shown in the chart below, sandy samples from different initial densities reach a unique 1D-NCL. When the soils reach this line, a yielding point can be identified and the main mechanism involved in the plastic volumetric strain for a sand is particle breakage (Coop and Lee, 1993). Loose and dense samples both eventually arrive at a unique NCL, the denser sample yielding at higher stresses. The grains of a sand in a loose state will have a reduced number of interparticle contacts, thus each contact will have to sustain higher interparticle stresses, resulting in a yielding at lower stresses than dense samples. The convergence of the normal compression lines from the 100% sand agrees with what found by Carrera (2008) for the Stava soils.

For the other soil compositions containing increasing fines content, the results of the oedometer tests seem to determine a transitional mode of behavior, although some peculiar features can be described for all the mixtures.

In the chart below, the loading paths of two oedometer tests carried out on 70%sand-30%fines soil composition are reported. They represent the widest range of initial densities investigated for this mixture within the oedometer tests programme.

No unique 1D-NCL exists for 70%-30% samples at the investigated stresses. Nevertheless, a slight trend of convergence of the two NCLs can be hypothesized at stresses beyond those applied. However, this is unlikely to happen at densities

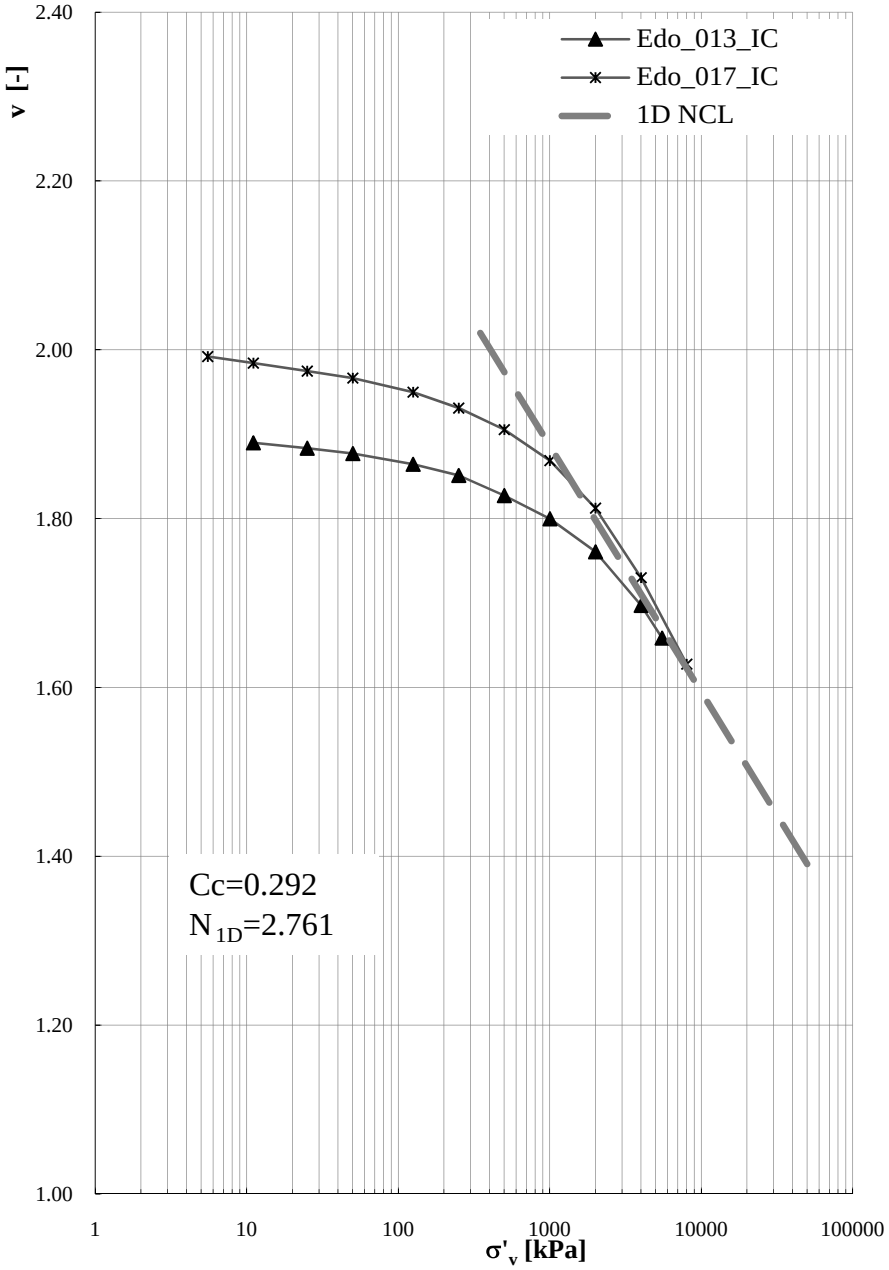

Figure 5. 15: One-dimensional NCL and oedometer curves (loading curve) for 100% sand samples.

higher than $v = 1$. Particle breakage is likely to be the main mode of behaviour involved, given that Venice soils are mainly non-plastic. This contrasts with what found by Carrera (2008) studying mixtures of Stava soils. In that case, soils composed by 70% sandy fraction and 30% fines converged to a unique 1D-NCL. This might suggest that the Venice soils show a higher tendency towards transitional behavior than the Stava soils, although no unique normal compression line is reached.

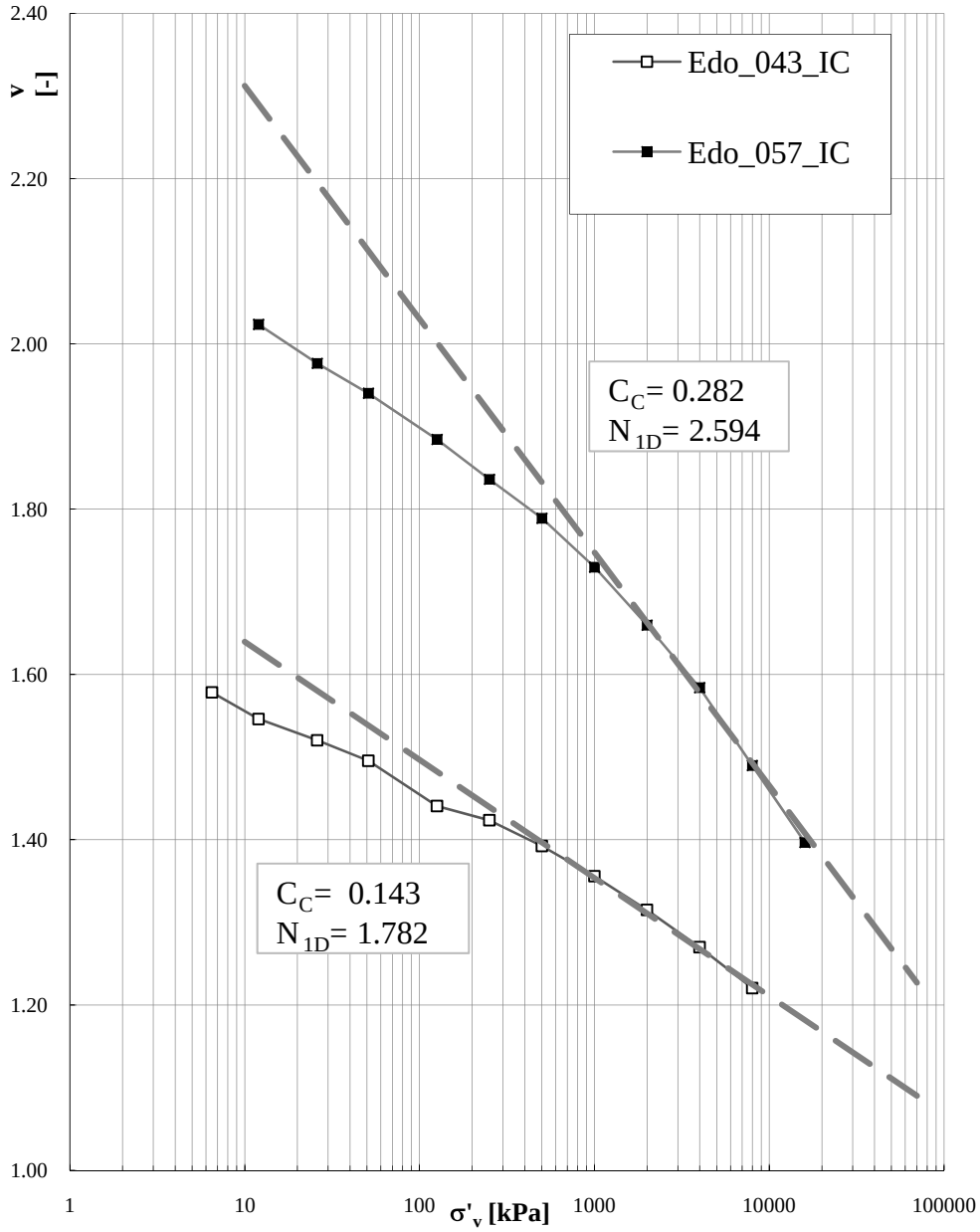

Figure 5. 16: One-dimensional NCLs and loading curves for oedometer tests on 70% sand-30%fines.

In Figure 5.15, three loading curves from oedometer tests performed on dry compacted samples composed of 50% sand and 50% fines are reported.

No unique 1D-NCL exists for these samples for the stresses investigated. Nevertheless, a slight trend of convergence of the two NCLs can be hypothesized at stresses beyond those applied. Tests Edo_054 and Edo_052 represents the widest range of initial specific volume obtained for this mixture prepared by the dry compaction method, whereas Test Edo_047 has an intermediate value. No unique

1D-NCL seems to exist for 50%-50% samples at the investigated stresses. The three loading paths are parallel, only Test Edo_047 seems to be slightly steeper than the others. Nevertheless, no convergence of the NCLs can be identified for 50-50 dry compacted samples. Carrera (2008) found that for Stava mixtures composed by 50% sand and 50% fines a unique normal compression line could be found.

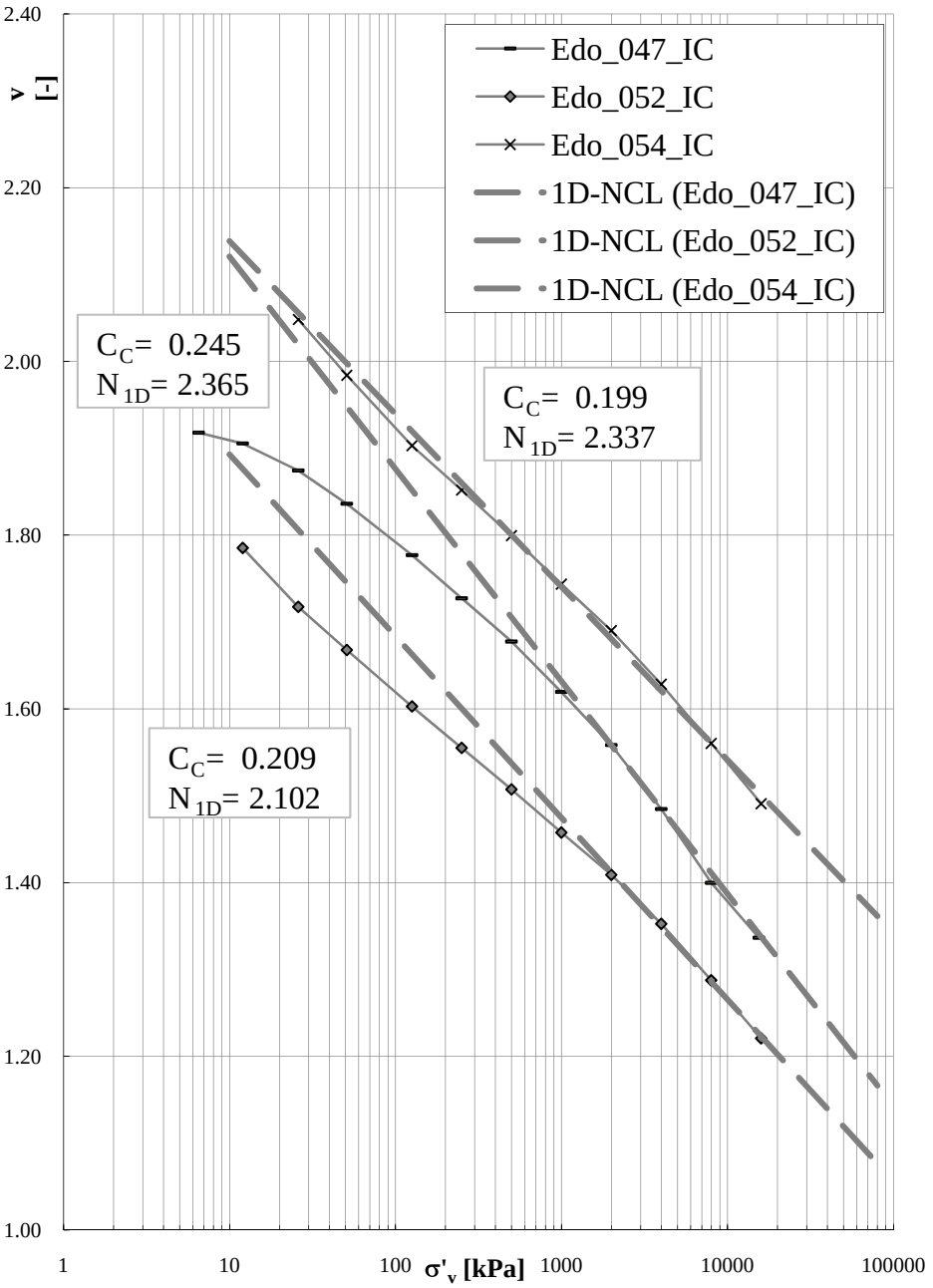

Figure 5. 17: One-dimensional NCLs and loading curves for oedometer tests on 50% sand-50%fines obtained from dry compaction.

In Figure 5.16 the loading curves from oedometer tests on 50-50 slurry samples are reported. They remain parallel even at stresses up to around 15 MPa. No unique 1D-NCL exists for these samples at the investigated stresses, although the initial specific volume range is narrower than that obtained for the dry compacted samples.

However, the steepnesses of the NCLs determined for the loading curves for the two sample preparation techniques needs to be compared (for further considerations on the compressibility parameters, see section 5.3.2).

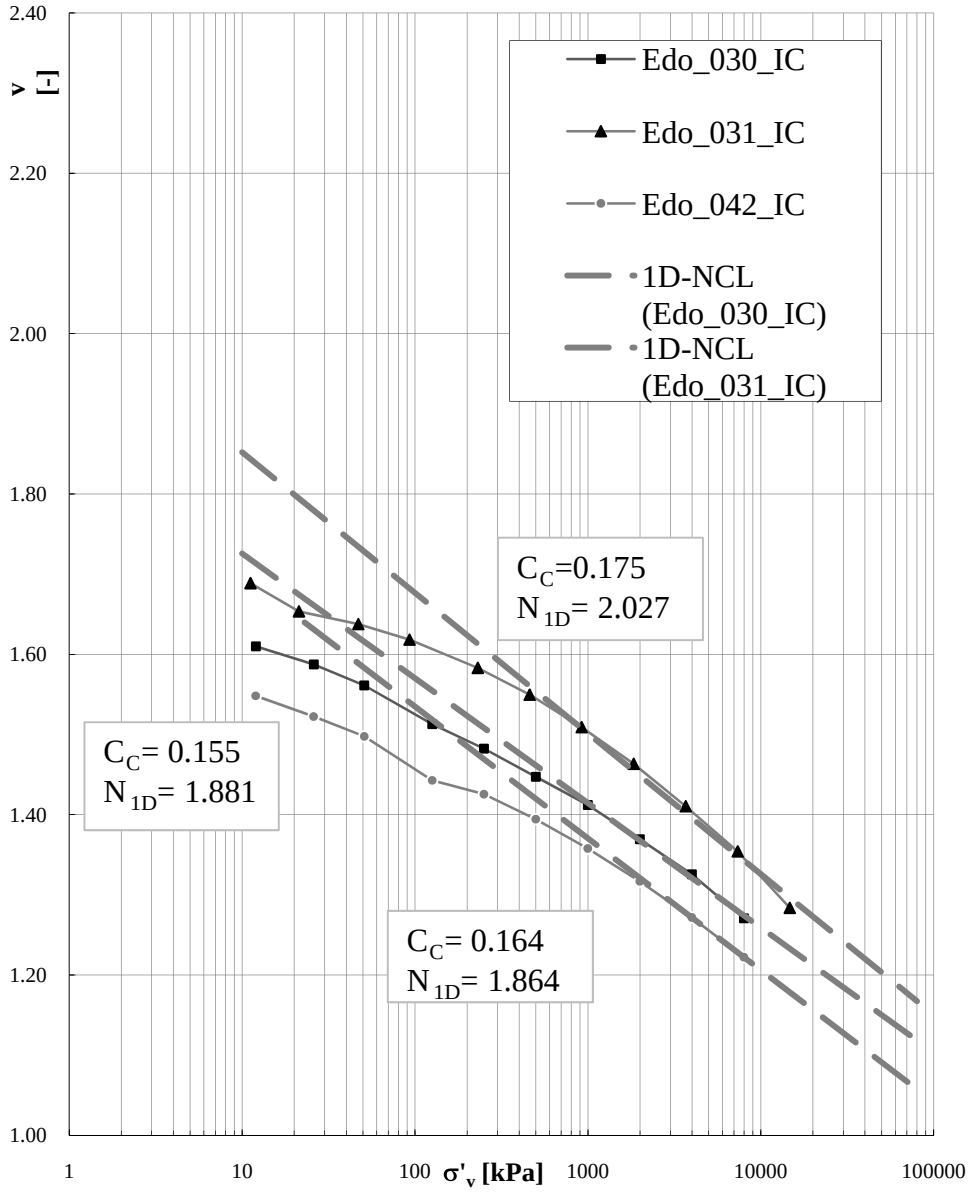

Figure 5. 18: One-dimensional NCLs and loading curves for oedometer tests on 50% sand-50%fines obtained from slurry.

In figure 5.17, all the trend lines with respect to the oedometer tests on the soils composed of 50% sand and 50% fines fraction are reported.

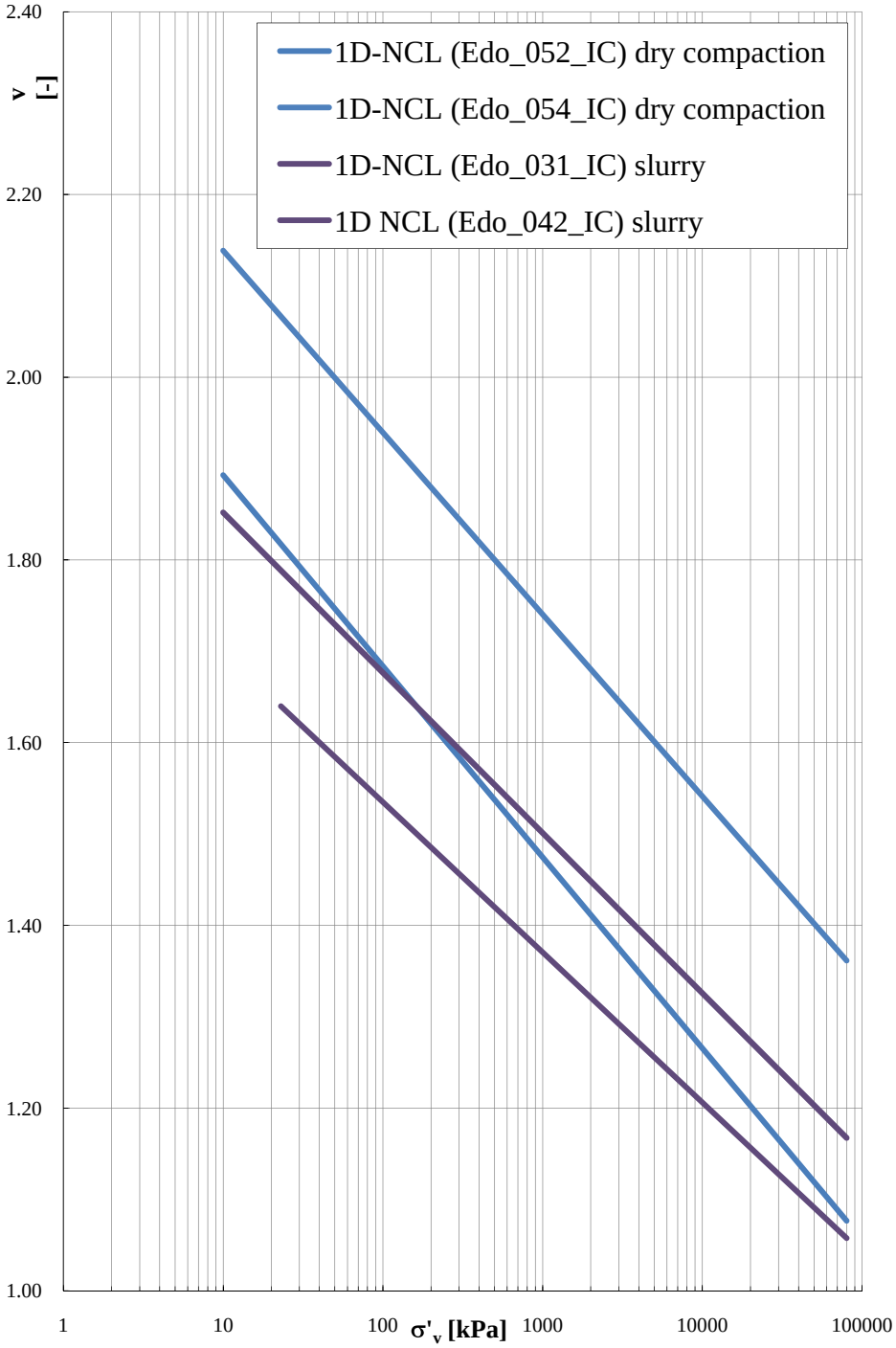

Figure 5. 19: One-dimensional NCLs for chosen oedometer tests on 50%sand-50%fines samples.

The overall view of the normal compression lines shows that dry compacted samples are slightly more compressible than slurry ones. If only the two tests with the highest and the lowest densities are considered, again the trend lines remain parallel and do not converge, even at 100 MPa. Thus it can be stated that soils composed of 50%sand and 50% fines have a transitional behavior. Again, as seen for the 70%sand-30%fines mixtures, given the presence of fines it can only be hypothesized that the main mechanism involved is particle breakage.

In Figure 5.18 two loading curves from oedometer tests on 100% fines samples are shown. As seen for the mixtures 70-30 and 50-50, the two tests were chosen in order to cover the widest range of initial specific volumes for soils composed by 100% of fines fraction. Also for these soils a transitional behaviour seems to be identified. This contrasts with the results found by Carrera (2008) for Stava soils, who identified a convergence to a unique NCL.

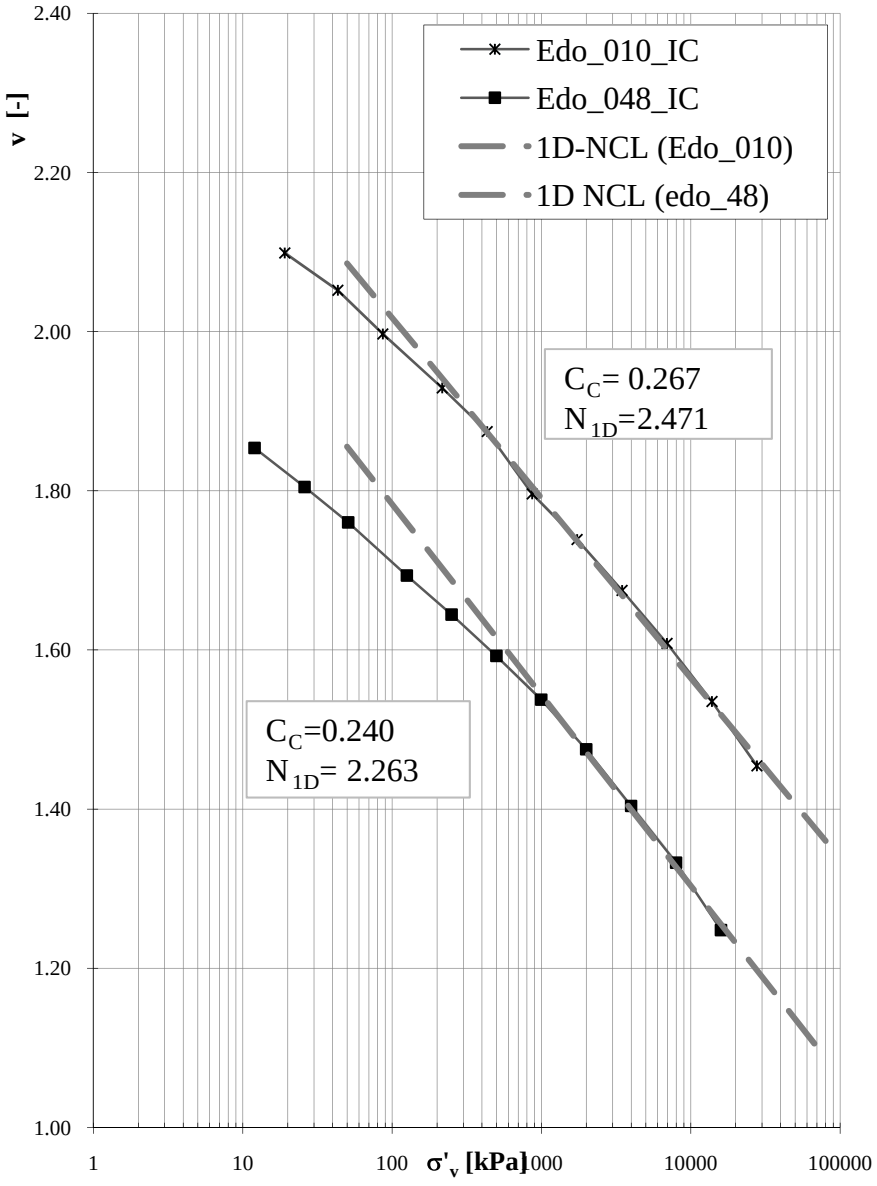

Figure 5. 20: One-dimensional NCLs and oedometer loading curves for tests on 100% fines.

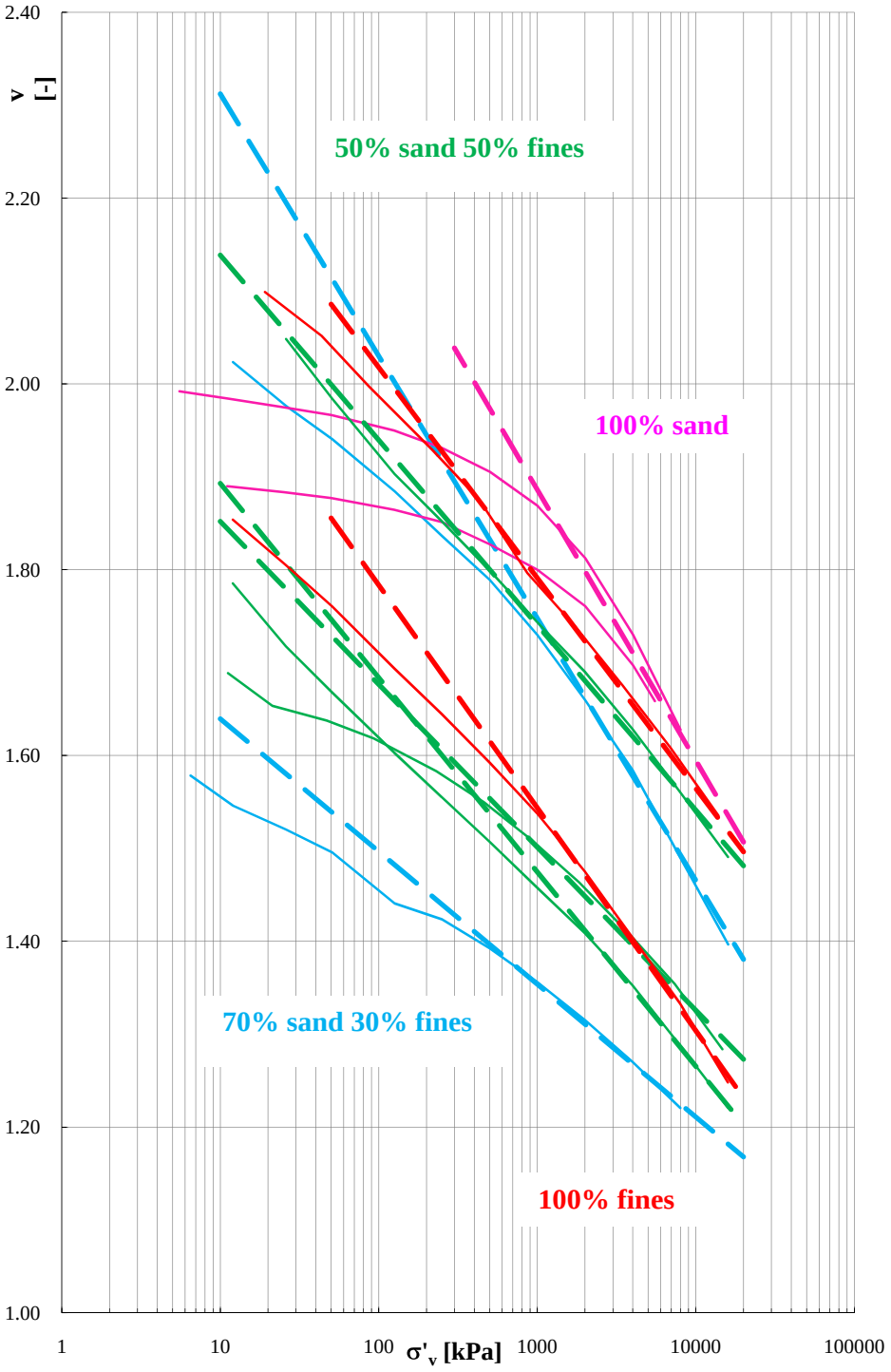

Figure 5. 21: choice of 1D-NCL and loading curves for oedometer tests representative of all the soil compositions

In the graph below, the NCLs referring to the chosen oedometer tests are reported in order to obtain an overall view of their steepness. It can be observed that as the

fines content increases, the NCLs flatten until a minimum is reached and for higher f_c the normal compression lines become steeper again: the 100% fines NCLs, however, remain flatter than the 100% sand curves.

It could be stated that to f_c between 50%-70% correspond the most compacted states, at which the fines fill the soil voids the most. This behavior totally agrees with the results found by Carrera on Stava soils.

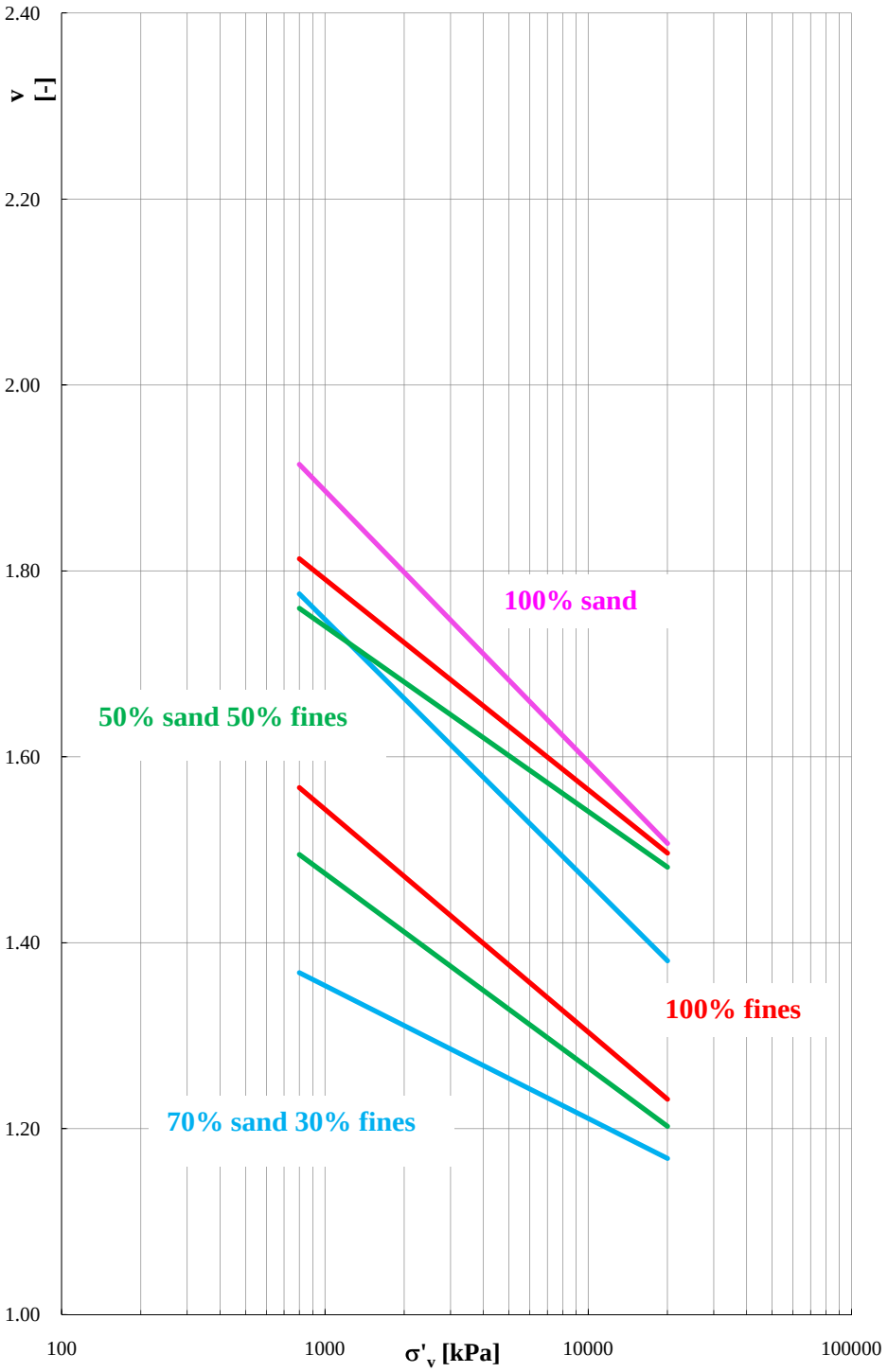

Figure 5. 22: 1D-NCLs for some tests representative of all the soil mixtures.

5.3.2. Results of the oedometer tests: compressibility

For each mixture of soils, the compression index, C_C, the intercept at 1 kPa, N_{1D}, and the swelling index, C_S, were calculated. When a unique normal compression line was found, those parameters were calculated for this line, whereas in case of transitional behaviour they were determined for several curves. Moreover, only the stress-strain data referring to the last three loading steps were considered for the calculation of C_C and N_{1D}. This is where the compression paths usually become linear on the semi-logarithmic chart $v - \log \sigma_v^{'}$.

Some values for these compressibility parameters were shown also in the previous paragraph. The following tables presents a comprehensive summary of the results.

Test	C_c	C_s	N_{1D}
Edo_02_IC	0.41	0.02	2.45
Edo_04_IC	0.41	0.03	2.28
Edo_013_IC	0.23	0.03	1.52
Edo_014_IC	0.24	0.02	1.61
Edo_017_IC	0.31	0.02	1.83
Edo_041_IC (floating ring oedometer)	0.42	0.02	2.37
Edo_051_IC (floating ring oedometer)	0.47	0.04	2.74
Edo_056_IC (floating ring oedometer)	0.47	0.03	2.33
Average value (STD oedometer only tests)	0.32	0.02	1.94
Average value	0.45	0.03	2.48

(floating ring oedometer tests)			
Average value (all tests)	0.37	0.03	2.14

Table 5. 7: Compressibility parameters for the oedometer tests performed on 100% sand samples

Test	C_c	C_s	N_{1D}
Edo_043_IC (slurry)	0.14	0.03	0.78
Edo_044_IC (slurry)	0.21	0.02	1.15
Edo_045_IC (slurry)	0.24	0.02	1.2
Edo_046_IC (slurry)	0.2	0.02	1.08
Edo_049_IC (dry compaction)	0.31		1.68
Edo_055_IC (dry compaction)	0.44	0.02	2
Edo_057_IC (dry compaction)	0.28	0.02	1.59
Edo_058_IC (dry compaction)	0.26	0.01	1.42
Average value	0.26	0.02	1.36

Table 5. 8: Compressibility parameters for the oedometer tests performed on 70% sand-30%fines samples

Test	C_c	C_s	N_{1D}
Edo_030_IC (slurry)	0.16	0.03	0.88

Edo_031_IC (slurry)	0.18	0.03	1.03
Edo_034_IC (slurry)	0.11	0.03	0.77
Edo_036_IC (slurry)	0.13	0.02	0.77
Edo_042_IC (slurry)	0.16	0.03	0.86
Edo_059_IC (slurry)	0.21	0.06	1.21
Edo_038_IC (dry compaction)	0.2	0.03	1.08
Edo_039_IC (dry compaction)	0.18	0.02	1.11
Edo_040_IC (dry compaction)	0.23	0.04	1.26
Edo_047_IC (dry compaction)	0.24	0.01	1.37
Edo_052_IC (dry compaction)	0.21	0	1.1
Edo_054_IC (dry compaction)	0.2	0.01	1.34
Edo_060_IC (dry compaction)	0.17	0.03	1.02
Average value	0.18	0.03	1.06

Table 5. 9: Compressibility parameters for the oedometer tests performed on 50%sand-50%fines samples

Test	C_c	C_s	N_{1D}
Edo_05_IC (slurry)	0.23	0.04	1.33
Edo_010_IC (slurry)	0.23	0.04	1.32
Edo_012_IC (slurry)	0.26	0.02	1.4
Edo_015_IC (slurry)	0.24	0.05	1.34

Edo_016_IC (slurry)	0.23	0.05	1.45
Edo_020_IC (slurry)	0.25	0.05	1.57
Edo_033_IC (dry compaction)	0.26	0.06	1.42
Edo_048_IC (slurry)	0.24	0.06	1.26
Average	0.24	0.05	1.39

Table 5. 10: Compressibility parameters for the oedometer tests performed on 100% fines samples

In the graph below the trend of the Compression Index C_c with increasing fines content is presented: the values decrease for fines content of around 30-50%, but for 100% fines content samples increase again. The two values for 100% sand samples refer to the average calculated for tests from standard oedometer and tests from floating ring oedometer. It can be noted that C_c, N_{1D} and C_s all show on average higher values for the samples tested in floating ring oedometers.

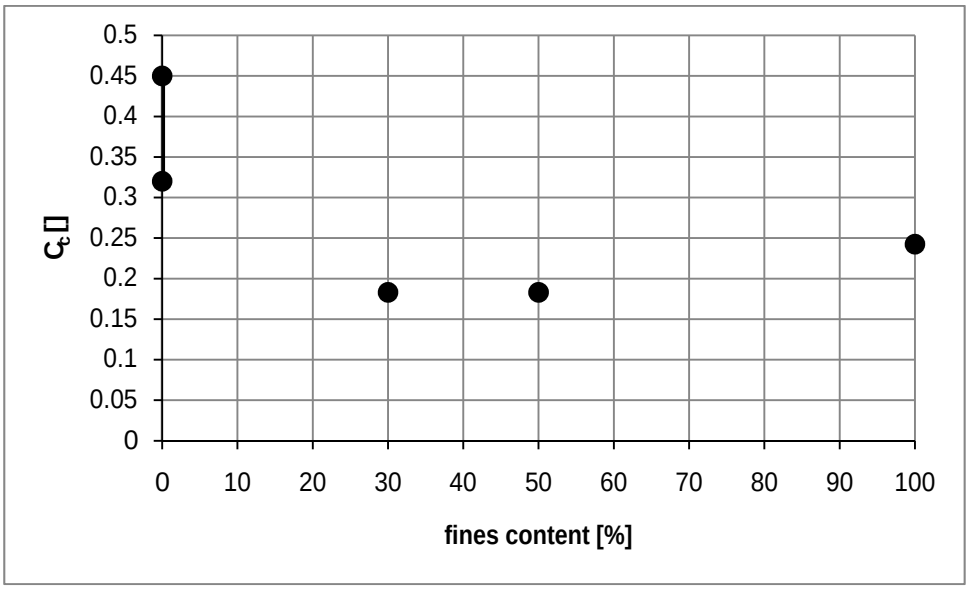

Figure 5. 23: Compression index Cc with varying fines percentages

With increasing fines content also the intercept at 1 kPa N_{1D} and the swelling index C_s follow a similar path. Between 30 and 50% of fines content the parameters are stable whereas they increase again for 100% fines samples.

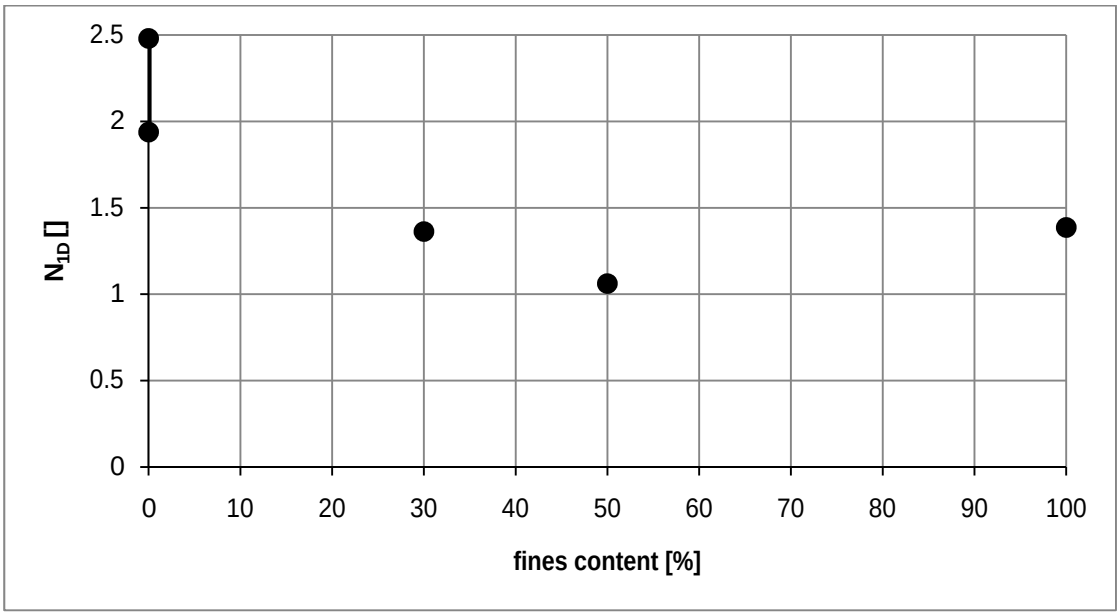

Figure 5. 24: intercept at 1 kPa N_{1D} with increasing fines content

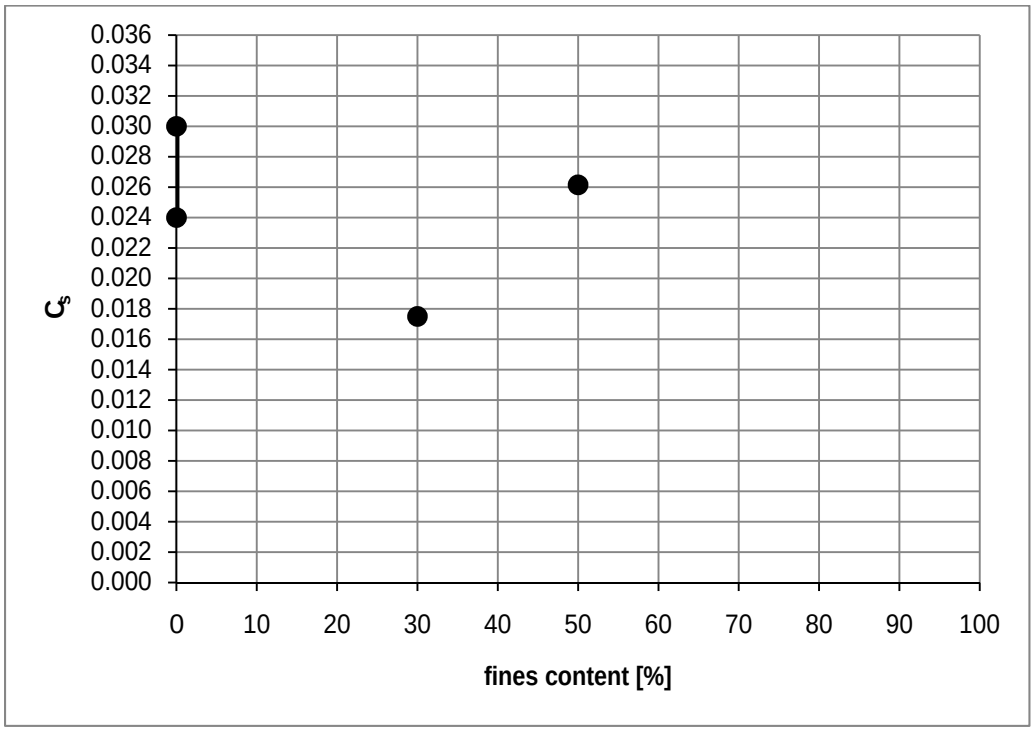

Figure 5. 25: swelling index Cs with increasing fines content

It is interesting to compare these results with data previously found for Venice soils. Simonini *et al.*, 2002, studied natural samples of soils coming from the Venice lagoon within a wide research project with the aim of obtaining a better understanding of their mechanical characteristics. The samples were divided into three groups, with respect to the grain size distribution, medium to fine sand, silt and silty clay. These groups were defined as:

- Medium to fine sand (SP-SM);

- Silt (ML);
- Very silty clay (CL).

All the different kind of natural samples were tested at stresses not exceeding 6 MPa. The compression index of the curves showed a great range of variation even in the same class of material. However, no observations were made with respect to a transitional behaviour analysis: it has to be pointed out that only SP-SM and ML samples seemed to converge, while CL samples somehow were more scattered.

This contrasts with the behaviour of the mixtures tested within this research, whose compression curves remained parallel, with the exception of sandy samples (convergence at around 10 MPa).

Simonini *et al.* found quite wide ranges of compressibility index C_c: 0.12-0.20 for fine sand samples, 0.17-0.30 for silt samples, 0.20-0.36 for silty clay samples. These values as well as the swelling index C_s and the intercept at 1 kPa N_{1D} can be compared to the values found for the different mixtures, although some preliminary considerations have to be made.

Each group, defined as fine sand, silt and silty clay, can be compared to the samples composed by different soil mixtures analysed within this research.

In the following table, a resume of the results presented by the Simonini *et al.* is summarised.

Comparison of C_c values		
SOILS MIXTURES		NATURAL SAMPLES (Simonini et al. (2002))
100% sand	0.23-0.47 (overall) 0.23-0.30 (std. oedometers) 0.42-0.47 (only floating ring oedo.)	SP-SM samples: 0.12-0.20 ML samples: 0.17-0.30

70% sand-30% fines	0.14-0.30 (overall) 0.26-0.30 (dry compacted samples) 0.14-0.21 (slurry)	CL samples: 0.20-0.36
50% sand-50% fines	0.11-0.24 (overall) 0.18-0.24 (dry compacted) 0.11-0.21 (slurry)	
100% fines	0.25-0.45	

Table 5. 11: Comparisons of the compression index values with previous results found in literature on Venice soils.

SOILS MIXTURES	
100% sand	1.52-2.74 (overall) 1.52-2.45 (std. oedometers) 2.33-2.74 (only floating ring oedo.)
70% sand-30% fines	0.78-2 (overall) 1.36-2 (dry compacted samples) 0.78-1.2 (slurry)

50% sand-50% fines	0.77-1.37 (overall) 1.02-1.37 (dry compacted) 0.77-1.21 (slurry)
100% fines	1.26-1.57 (overall)

Table 5. 12: Summary of the intercept at 1 kPa N_{1D} values

SOILS MIXTURES	
100% sand	0.02-0.04 (overall) 0.02-0.03 (std. oedometers) 0.02-0.04 (only floating ring oedo.)
70% sand-30% fines	0.01-0.03- (overall) 0.01-0.02 (dry compacted samples) 0.02-0.03(slurry)
50% sand-50% fines	0. 01-0.06(overall) 0.01-0.03 (dry compacted) 0.03-0.06 (slurry)
100% fines	0.02-0.06 (overall)

Table 5. 13: Summary of the swelling index C_S values

100% Sand samples

The compressibility index varies within the range 0.23-0.47, but for samples loaded to high pressures the parameter varies within the range 0.42- 0.47, whereas for the other samples it varies within 0.23- 0.30. Therefore it can be said that standard oedometer samples have the same compressibility range (0.20-0.30) as the fine sandy samples studied by Simonini et al., loaded up to 6 MPa. Moreover, it can be observed that high pressure oedometer curves seem to be more parallel than the normal compression curves coming from standard tests, although even the latter do not seem to converge to a unique normal compression line, not considering test Edo_017.

The intercept at 1 kPa N_{1D} values for the samples constituted by 100% sand follow a similar path to the one of the compression index. The swelling index Cs also have a very similar pattern as Cc.

70%Sand-30%fines

The compressibility index of 70-30 samples prepared with dry compaction technique varies within the range of 0.26-0.30, while for the samples prepared as slurry the values varies within 0.14-0.21. Again there is quite a good agreement with the results found in previous studies (range 0.12-0.20 for fine sandy samples and 0.17-0.30 for the silts). Therefore it can be observed that the compressibility of 70-30 samples coming from dry compaction seem to be more similar to the silty samples studied by Simonini et al., whereas the compressibility values of 70-30 slurry samples are closer to the fine sandy samples.

50%Sand-50%Fines

The compressibility index values vary within the range 0.11-0.24, particularly 0.11-0.21 for slurry samples and 0.18-0.24 for dry compacted samples. These values were compared to the data found by Simonini *et al*. Those values cover a wide range, 0.12-0.20 for fine sands, 0.17-0.30 for the silts, 0.20-0.36 for silty clays. Both 50-50 slurry and dry compacted samples have compressibility values that are closer to the fine sands range, as well as the 70-30 slurry samples.

100% fines

The compressibility index for the 100% fines mixtures which consists of clayey silt vary within the range 0.25-0.45. If compared to the data from Simonini *et al*., the values are closer to the Cc values found for the samples defined as silty clay.

CHAPTER 6

The microstructural properties of soils

6.1. Introduction

In this chapter the results are shown of a study performed by means of Scanning Electron Microscopy on samples coming from the compression tests. The main objective of the analysis was to identify, if possible, some patterns or mode of orientation that could explain at a micro-scale level the reason for transitional behaviour. In other terms, an investigation of microstructure, particularly microfabric and particle orientations, was undertaken. In order to create a reference framework for the experimental evidence, a review of some important studies in this field is presented.

6.2. Soil structure and fabric

Structure is the combination of fabric, which is the arrangement of particles in space, and inter-particle bonding (non-frictional inter-particle forces such as cementation) (Foster and De, 1971; Mitchell and Soga, 2005). Fabric consists of quite different features and these vary a great deal when considering a natural or reconstituted soil sample. For example, with respect to a mudrock considered in its in-situ conditions, fabric can include all the features developed during its geological history: discontinuities such as bedding, joints and faults, particle orientation and aggregations, the presence of fossils, sedimentary structures (varves, cross-bedding, ripple marks, flame structures, desiccation cracks) and variations in particle grading/ sorting (Wilkinson and Fenton, 2010). When considering a sand, fabric is determined by the number, orientation and size of contacts between the soil particles (Oda and Nakayama, 1989; Oda *et al*., 1982).

The effects of structure on a macroscopic scale can be seen in the standard laboratory tests, such as oedometer and triaxial tests, whereas, in order to study the microstructure of soils, different techniques have to be used because fabric and inter-particle bonding are on a microscopic scale. Moreover, the combination of particle arrangement and bonds is at the origin of the different mechanical behaviour of remoulded and undisturbed specimens of the same material (Baudet and Stallebrass, 2004). The effects of microstructure on the behaviour of coarser grained soils, such as sands, has been the object of computer modelling at the particle level, particularly of stress propagations through materials with different initial fabrics (Chang *et al*., 2003).

The methods available nowadays that allow to investigate soil microstructure, if modelling is not taken into account, are essentially visual analysis techniques. They have been developed

especially with respect to mudrock and clays studies, but in recent years they have been applied also to study the microstructure of soils with non-uniform gradings. Scanning Electron Microscopy is one of the most used techniques aimed at investigating soil microstructure and to relate it to the mechanical response in compression and shearing. For example, a normally compressed reconstituted sample at a certain initial specific volume, before the oedometer test is performed, has a certain particle arrangement and there is a unique single compression line corresponding to this feature, whereas, on the contrary, a given compression line may be produced by different samples having different initial densities (Wilkinson and Fenton, 2010).

6.3. Literature review of SEM applied in soils microstructure studies

Scanning Electron Microscopy (SEM) is a visual analysis technique, which is quite widespread because of its several applications. In the geotechnical field, it has been applied particularly to the study of mudrock microstructure, fabric together with bonding (Cotecchia, 1996; Gasparre, 2007; Sivakumar *et al*., 2002; Tovey and Hounslow, 1995; Zhang *et al*., 2004). Scanning electron micrographs of thin sections allows to highlight the presence of cement between sand particles (Cuccovillo and Coop, 1999).

6.2.1. Undisturbed samples

Over the last few decades much research has been carried out with the aim of investigating the correlation between macroscopic engineering properties of clays, in order to develop more reliable design parameters for a variety of geotechnical problems. Microstructure becomes particularly relevant when considering swelling phenomena, therefore it was tried to gain a better understanding of microstructural properties.

Tovey *et al*. (1973) studied the swelling properties of Lud clay from Israel with a scanning electron microscope, comparing undisturbed and equivalent laboratory compacted slurry samples. Stereomicrographs allowed to draw pore size distribution curves for undisturbed and reconstituted samples, so that a comparison could be performed in order to investigate the swelling mechanisms of clay.

Cotecchia (1996) investigated the microstructure of reconstituted and natural samples of Pappadai clay. Clay particle arrangements and inter-particle contacts could be identified and analysed using SEM, particularly by means of large magnifications. Moreover, the main differences in microstructure between natural and reconstituted clays could be detected, this being the presence of bonding features. Samples features before and after the tests were also compared through SEM. Within the Venice soils and transitional soils framework in general, in this chapter the main focus will be given to remoulded samples (Section 6.2.2).

Cola (1994) presented electron microscope images taken on undisturbed Venice silty clay samples collected from the Fusina site. From this study several microstructural features were described. The upper sample grains collected at a depth of 4.4 showed a spatial disposition in particle packets connected in a relatively continuous and regular assemblage with an alveolar structure, probably due to a low energy lagoon environment.

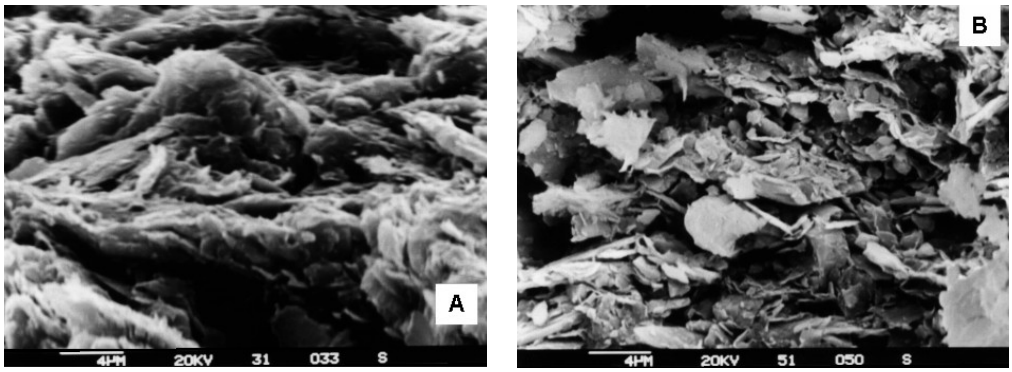

Figure 6. 1: Scanning Electron Microscope images of undisturbed silty clay samples from Fusina (Cola, 1994): (a) sample from 4.4 m; (b) sample from 12.3 m of depth.

As can be seen in the figure, in the lower sample, collected from a depth of 12.3 m, the particles seem to be aggregated with an irregular structure in small, well-defined packets and arranged with edge-to-face or edge-to-edge contacts, characteristic of a higher energy depositional environment (Simonini *et al.*, 2006). This visual analysis allowed to confirm previous observations by Bonatti (1968), who reported chaotic structures and micro-cross stratification in samples coming from the Motte di Volpego site. Sediments deposited from turbulent water flow, e.g. that of rivers, are frequently characterised by these microstructural features.

Through a microscopic investigation Jommi and Sciotti (2004) observed the soil fabrics of undisturbed samples and laboratory compacted samples of a well graded clayey soil collected from a river embankment (70% silt, 27% clay and 3% sand). The field compacted and the laboratory compacted sample microstructural were compared and the main conclusion was that the natural microstructure features are difficult to erase.

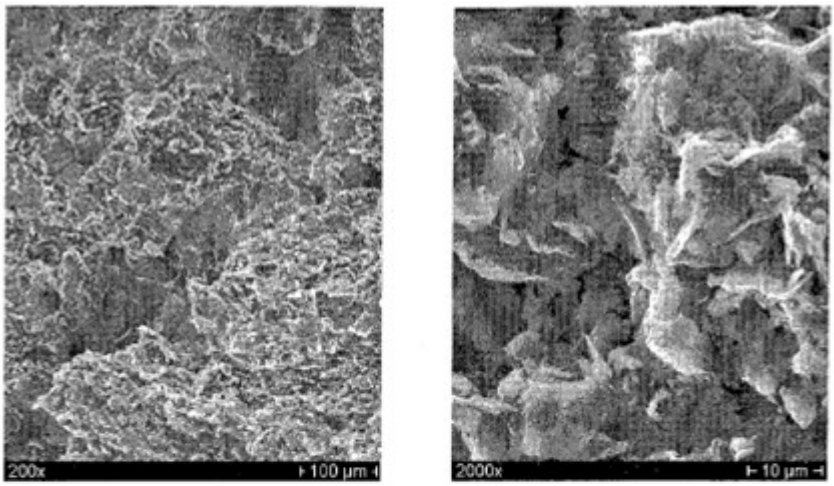

(a)

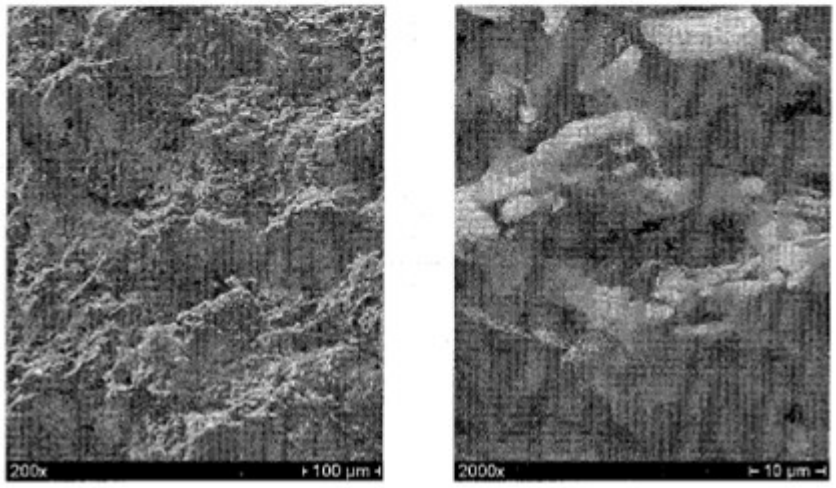

(b)

Figure 6. 2 a and b: comparison between microstructure of SEM samples of field compacted (a) and laboratory compacted (b) soils of a river embankment at two different magnifications (modified from Jommi and Sciotti, 2005).

Gasparre (2005) presented the results of an SEM analysis, aimed at investigating the microstructure of undisturbed samples of London clay, with particular attention to bonding characteristics. The structure and the nature of the clay from different strata were investigated in order to correlate them with large and small strain mechanical response. A more open structure was found in shallower units which corresponded also to higher clay content than the deeper units. These differences affected the mechanical behaviour of the different units. As a common practice, sketches were drawn of the particular features of each samples (Cotecchia, 1996; Gasparre, 2005), as reported in the figures below.

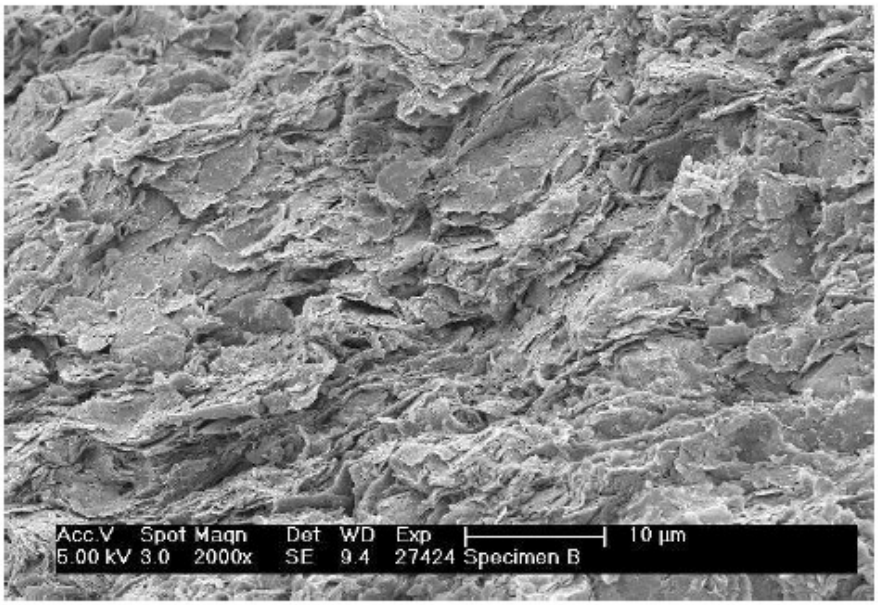

Figure 6. 3: London clay sample SEM image (from Gasparre, 2005).

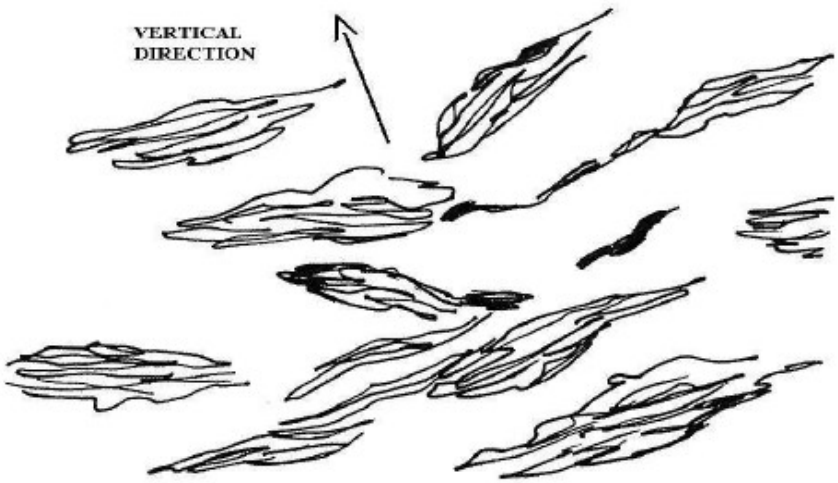

Figure 6. 4: Sketches representing orientated domains of London clay particles referring to the SEM image reported in Figure 6.3 (from Gasparre, 2005).

Wilkinson and Fenton (2010) studied the microstructure of mudrocks, particularly Oxford clay and Gault clay, by means of Scanning Electron Microscopy in order to perform a quantitative analysis able to link micro-scale features with the material geological history. In the figure below, SEM images of a vertical surface of an undisturbed specimen of Oxford clay are shown.

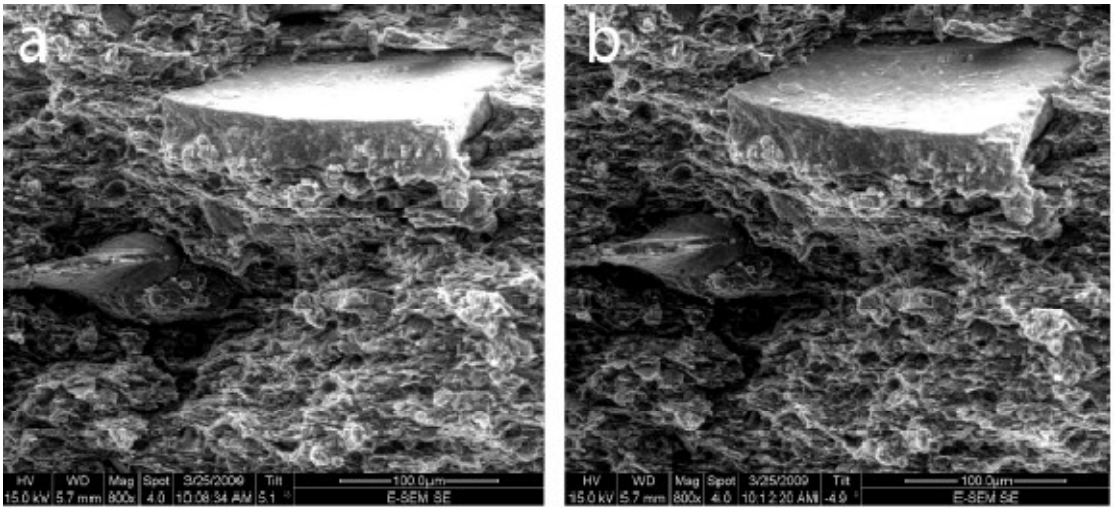

Figure 6. 5: Scanning Electron Microscope images of the same area of an Oxford clay sample, only with a 10° angular difference between the view directions (from Wilkinson and Fenton, 2010).

The innovative approach presented in this study, following work by Carl Zeiss (2008), allows to create a three dimensional elevation model of the soil surface by means of the two images shown in Figure 6.5, given that they refer to the same area, but they only differ of the 10° angular difference between the view direction.

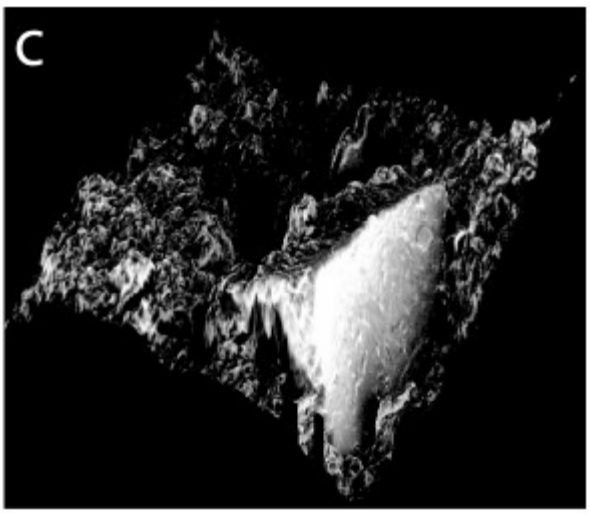

Figure 6. 6: 3D elevation model of the surface of the Oxford clay sample shown in Figure 6.5 (from Wilkinson and Fenton, 2010)

6.2.2. Reconstituted samples

Nocilla *et al*. (2006) tried to link the lack of convergence of the compression paths of reconstituted samples of well-graded soils from the Po river embankment to initial differences in their fabrics, via SEM study. Broken surfaces from selected samples, having different initial specific volumes were studied. However, unfortunately the images showed a very complex fabric, as can be seen in the figure below, and it was not possible to identify visually features that could distinguish the samples, either created with different methods or at different initial specific volumes. Moreover, no clay peds could be identified, therefore the initial hypothesis of the role of ped breakage as a fundamental mode of plastic strain mechanisms did not find any experimental evidence. It was also concluded that a similar analysis should be carried out on soils with a transitional behaviour but having simpler mineralogy and grading.

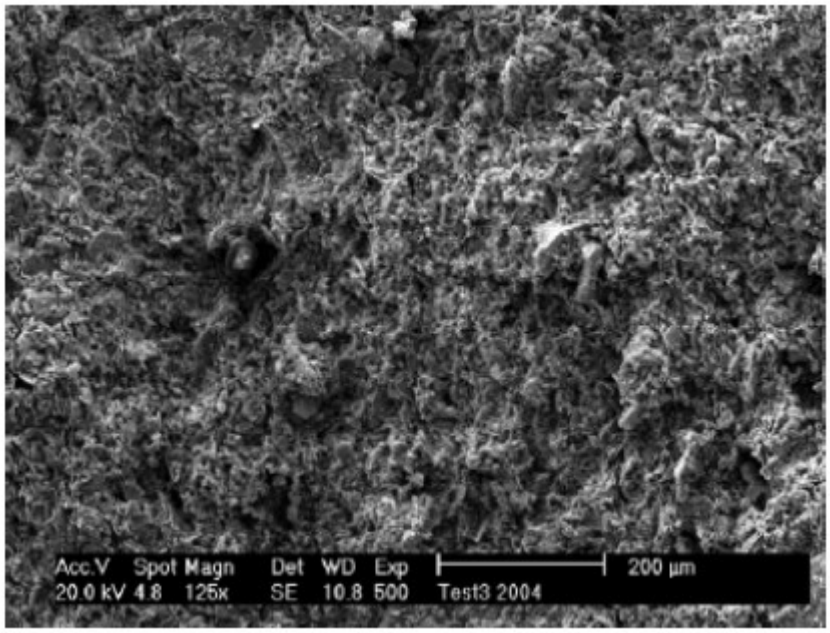

Figure 6. 7: Scanning Electron Micrograph of a slurry sample with an 8% clay content, compressed to a vertical effective stress of 14.31 MPa and with an initial specific volume of $v_0 = 2.604$ (from Nocilla *et al*., 2006).

Through SEM analysis Chang (2008) studied the fabrics of reconstituted samples obtained with mixture of gold mine tailings. The moist tamped samples showed an aggregated fabric, whereas in the slurry specimens the particles were placed in a more homogeneous disposition, more similar to their in-situ conditions.

However, for most studies which applied these techniques to soil microstructure investigation, they were mainly applied only for qualitative purposes. Although researchers have long recognised the influence of microfabric and of the associated porosity on the macroscopic behaviour of soils, very few attempts have been made to quantify the

fabrics, Smart and Tovey (1982), among the notable cases. Characterising soil properties using a quantitative approach via SEM is still challenging (see Section 6.5 for details).

Bisdom & Schoonderbeek (1983), among others, studied the large scale porosity in soils, sediments and rocks by means of low magnification optical microscopy and scanning electron microscopy using the back scattered electron mode (see Section 6.3.2 for details). Not only porosity, but also particle orientation can be investigated with imaging techniques.

Tovey & Smart studied orientation patterns in fine-grained sediments (e.g. Tovey 1980; Smart & Tovey 1988; Tovey *et al*. 1989, 1992b), using high magnification electron micrographs. More objective microfabric analysis can be obtained with SEM in comparison with optical microscopies. The main difficulty in these studies lies in the determination of a grey level threshold able to distinguish between voids and soil grains. Tovey and Hounslow (1995) showed a quantitative method able to study microporosity and particle orientation in the analysis of soils and sediments.

Hattab and Flereau (2010) studied kaolinite particle orientations in laboratory prepared samples, through SEM observations, after different triaxial loading phases with the aim of finding, if possible, a coupling between macroscopic behaviour and changes in particle spatial disposition.

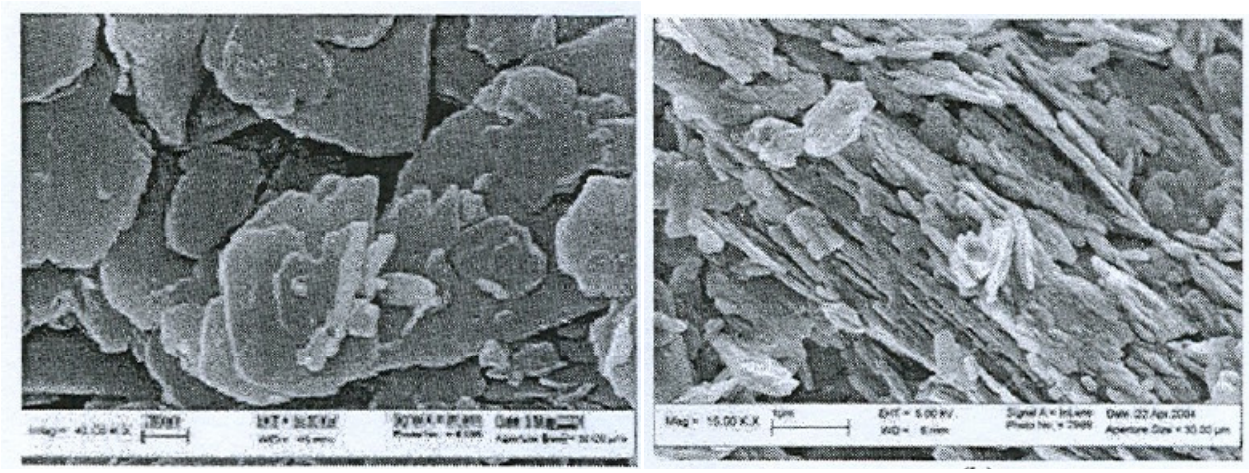

Figure 6. 8: SEM observations of kaolinite particles front view (a) and side view (b) (Hattab and Flereau, 2010)

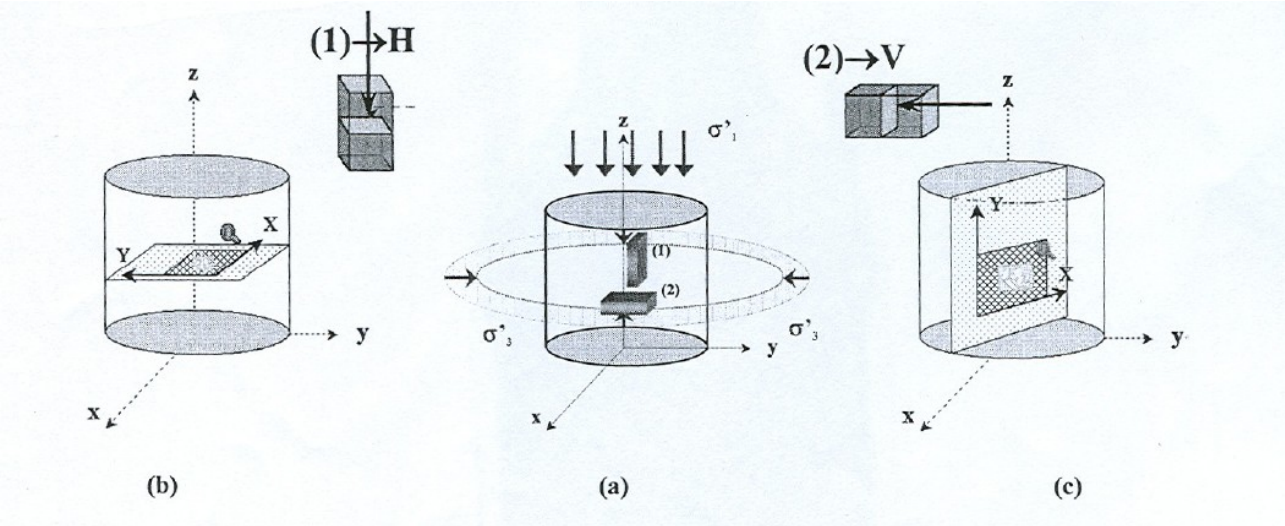

Figure 6. 9: Locations for the vertical and horizontal planes of observation with respect to the overall sample (from Hattab and Flereau, 2010).

6.4. Introduction to scanning electron microscopy

The use of the scanning electron microscope is widely spread out in many research applications. Particularly, it is the most used microscale imaging device. The apparatus provides a very large depth of field and, as a consequence, two-dimensional taken images appear 3D. However, the three-dimensional measurements deriving from one single picture are not reliable enough.

Images obtained from scanning electron microscope allows to measure surface morphology, identified in light and dark areas. The interparticle contacts between clays platy grains are not easily measurable only from imaged surfaces. Moreover, their orientations would not necessary provide a link to the macro-scale behaviour. This might not be the case for samples characterised by different gradings.

6.3.1. Imaging soils microstructure

Several factors need to be taken into consideration when imaging structure and fabric of clayey soils, particularly mudrock. The best available technique is chosen with respect to the experimental evidence about the material structure to focus on.

Firstly, two dimensional data require less effort than techniques able to provide three dimensional information. Moreover, the sample preparation itself, required to get the soil in a reasonable state for imaging, causes a certain degree of disturbance, which is more apparent at higher magnifications. The maximum reachable magnification depends on each technique and the image quality is not necessarily perfect. Sometimes the pictures turn out to be fuzzy and distorted.

A soil sample for imaging with Scanning Electron Microscope can be prepared using different methodologies and the procedure itself might need to occur at varying conditions of pressure and temperature. However, in general high vacuum conditions are required. The main difficulty related to this factor is that vacuum sucks the moisture out of the samples causing pore pressure to collapse.

In order to overcome this problem of preserving the moisture content of specimens, several solutions have been implemented.

	Features	**Notes**
Freeze drying	The sample is frozen then the pressure is lowered such that sublimation of the water occurs	Ice-whiskers grow and force the fabric apart
Critical point drying	The sample is dried at the critical pressure and temperature conditions, in order to pursue absence of surface tension between liquid and vapour phases of water.	This kind of drying should cause less damage to the sample, but it is difficult to locate the critical point and very high temperature and pressure is required.
Embedding	The sample is impregnated with a resin in order to preserve its structure. It becomes harder and easy to handle.	If speed is needed, the resin can be forced in the sample under vacuum conditions
Environmental SEM	The samples are examined in a chamber filled with water vapour. Pressure and temperature are controlled in order to reduce evaporation of the moisture from the sample. However, a large amount of water vapour is required. High quality SEM images can be obtained.	A compromise between maintaining the moisture content and reaching the wanted image resolution needs to be found. In order to maintain a constant temperature of the sample, its dimensions need to be thought in relation with its thermal conductivity
Cryo-SEM	A method to avoid water loss completely is to shock freeze the sample in slushy liquid nitrogen (at 210 °C) this will form amorphous/ non crystalline ice which does not change	The sample dimensions need to be controlled in order to avoid crystal formation in the centre of the specimen during

	volume on freezing.	freezing.

Table 6. 1: Summary of the most important types of Scanning Electron Microscopy techniques (modified from Wilkinson, 2010).

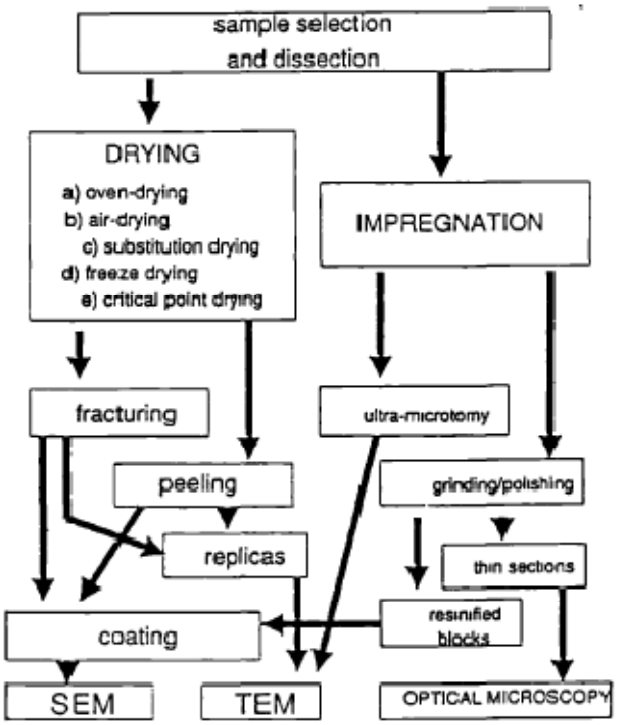

Figure 6. 10: Flow chart of the most important sample preparation phases that lead to either SEM or to other techniques, such as Optical Microscopy (from Cotecchia, 1996).

In order to choose the technique able to highlight the soil features with the best accuracy, the soil features need to be taken into account. The most challenging case occurs when clays and mudrocks are analysed. A three dimensional study of the soils fabric can be essentially based on:

1. surface topography;
2. structure visualisation.

6.3.2. The scanning electron microscope apparatus

Scanning electron microscopy is a very widely used imaging technique that allows to analyse microscale properties of materials. It can reach resolution up to 10-50 nm. As can be seen from the scheme in figure 6.11, the equipment consists of a gun which shoots a narrow beam of high energy electrons against the sample surface and magnetic lenses direct them onto the target in order to reduce the size of the scanned area. The electrons sourced from the gun are called primary (high energy electrons). When they impact with the sample surface, secondary electrons (low energy electrons) are released from the material in a way that depends on the topography of the sample constituents. Both primary and secondary

electrons allow to acquire images. A detector receive the back scattered electrons and send the produced message to the PC which converts the signal into magnified images of the area being scanned. In order to perform this analysis, the samples must be placed in a vacuum environment . The vacuum has a tendency to dehydrate the materials.

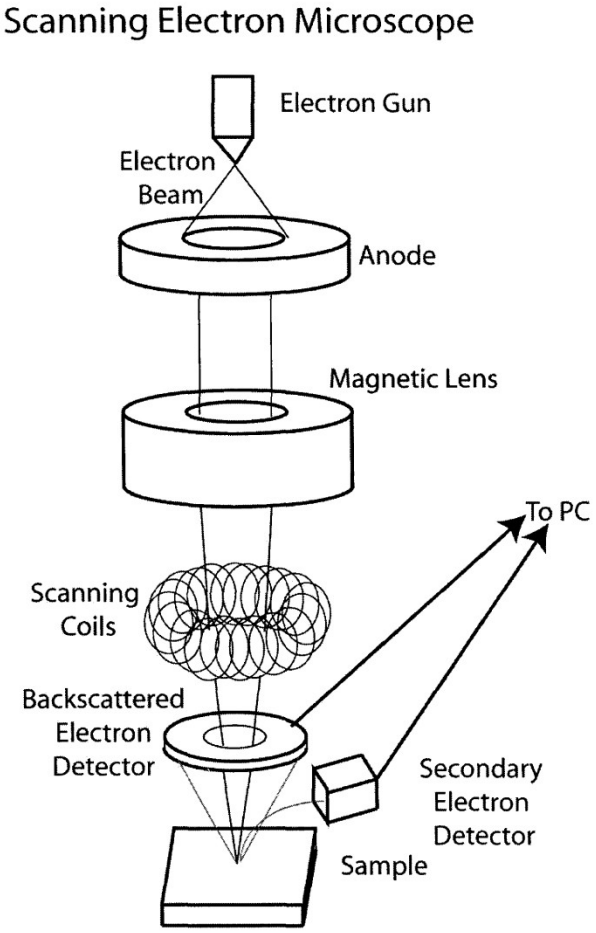

Figure 6. 11: General Lay-out of a Scanning electron microscope device (from Wilkinson, 2010).

In the figure below a detail of the back scattered electrons spatial resolution is shown with particular attention to the depth reached within the sample, which is around 2 □m. In Figure 6.13 another flow chart representing the Scanning Electron Microscope technique is shown.

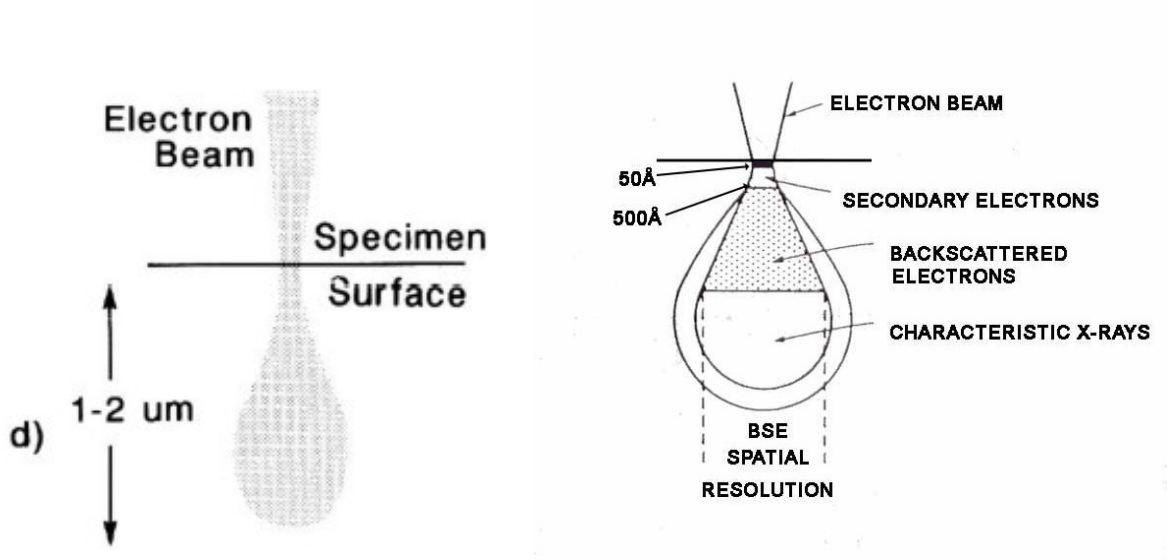

Figure 6. 12: Particular of the back scattered electrons spatial resolution (image courtesy of Dr. Huggett).

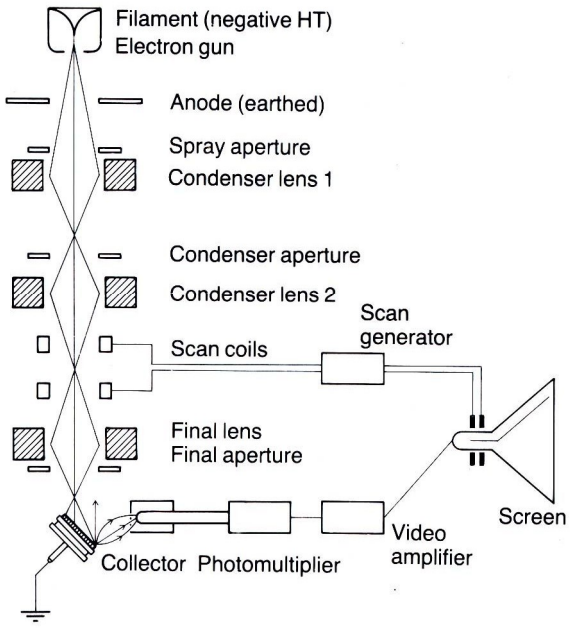

Figure 6. 13: Detail of the passages involved in SEM analysis from the creation of the electron beam to the PC signal acquisition (image courtesy of Dr. Huggett).

6.5. Microstructure study of the Venice silts: laboratory procedure and scanning electron microscopy

6.4.1. Sample preparation

At the end of the oedometer tests the samples were collected and one vertical and one horizontal surface for each sample were broken, the sample being still humid. The samples were left to air-dry for three days in a temperature controlled environment. Given the material features, air drying was adopted, because it does not affect dramatically the soil structure. The samples were then sent to Dr. Jenny Huggett who prepared them in order to be analysed in the variable pressure Scanning Electron Microscope (LEO 1455 VP manufactured by Oxford instruments) at the National History Museum, London. The basic principle of the apparatus and the techniques used were similar to those documented in the literature (e.g. Smart & Tovey, 1982).

A freshly fractured vertical and horizontal fragment of each sample was mounted on an aluminium stub, gold-coated and examined in a LEO SEM, with digital imaging. All the samples were analysed at high vacuum pressures. As suggested in previous studies, reference marks were placed on the samples in order to ensure that the correct orientation of the surfaces was observed.

6.4.2. Imaging

The aim of Scanning electron microscope imaging is trying to identify differences in fabric between samples with different initial specific volumes. In the table below the details of the analysed samples are summarised. The samples were prepared using two different techniques. Although the initial void ratios are quite different, the final void ratios are quite close. The samples were both loaded to the same maximum vertical effective stress.

Nocilla *et al*. (2005) carried out an extensive study of the microstructure of the soils from the Po river embankment through scanning electron microscopy on vertically broken surfaces coming from one-dimensionally compressed samples. Due to the complexity of fabric, in that case it was not possible to identify important visual differences between samples with different initial void ratios e_0, one-dimensionally compressed to the same pre-consolidation pressure σ'_p, having similar final void ratios e_f. A similar visual analysis study on oedometer tests samples consisting of 50% fines-50% sandy mixture is being carried out in order to identify some differences in fabric that might allow to quantify at a microscale the transitional behaviour found in laboratory tests.

Processing SEM images

Thresholding a grey-level image provides the necessary binary image for the analysis and the choice of the appropriate grey level threshold is vital in order to remove degradation inherent in all imaging systems. A clear explanation of this requirement is provided by Tovey and Hounslow (1995). They state that in an ideal digital image for microstructure measurements, e.g. porosity, there will be essentially two phases, one bright and one dark. In Scanning Electron Microscopy the solids are relatively brighter than the voids, whereas in fluorescence microscopy and transmission electron microscopy the reverse is true. An adequate binary image should correctly segment the original picture into two components: the voids corresponding to the zero value and the solids to the value of unity. In order to represent this feature, histograms of intensity are usually drawn.

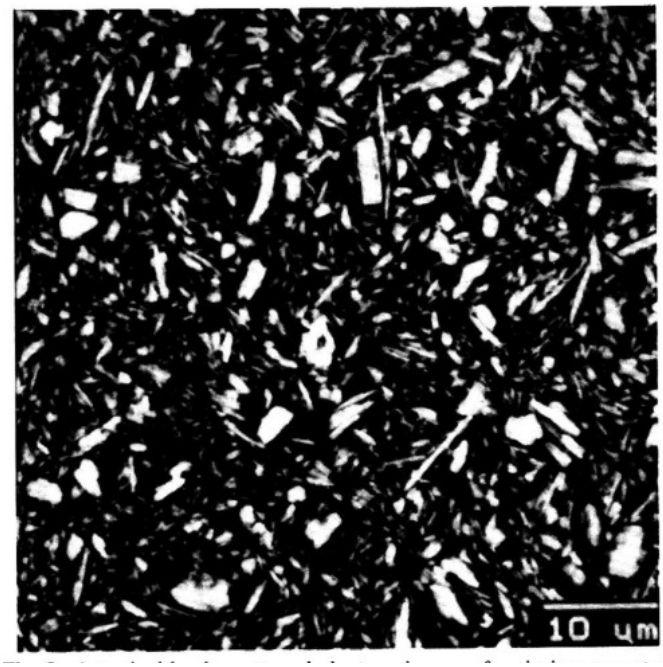

Figure 6. 14: SEM picture of a slurry sample constituted by a resin impregnated with kaolin, normally consolidated up to 700 kPa (from Tovey and Hounslow, 1995).

Very few original SEM images show a bimodal histogram of intensity, where one peak is associated to the voids and the other to the soil grains. A certain degree of noise is present. In these cases, an objective threshold can be set at the minimum between the two peaks or at the mid-point between them, if they are located far apart. For the majority of the samples, however, images will not show such well conformed histograms where the correct separation in voids and solids will lie close to the most popular intensity class. Therefore it appears clear that the determination of an objective threshold becomes difficult. As can be observed in Figure 6.15, showing the single unimodal distribution for the SEM image in Figure 6.14, some fine features are lost in the neighbourhood of larger features, highlighting the difficulty of thresholding this image. Particles close to the resolution limit of the equipment may also create further difficulties.

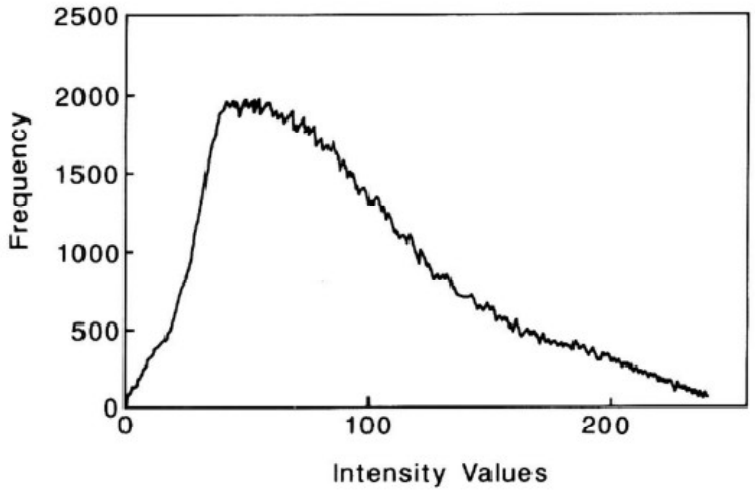

Figure 6. 15: Histograms of grey scale value determined for the surface in Figure 6.14 (from Tovey and Hounslow, 1995).

The interactions between the specimen and the electron beam in SEM, to a certain extent, degrade the output image, because of the spreading of the beam.

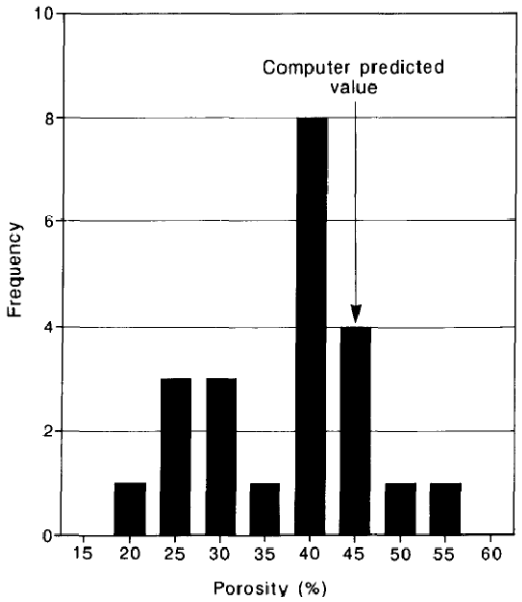

Figure 6. 16: Example of subjectivity effects in processing quantitatively SEM images. Histograms showing porosities obtained only via subjective methods (Tovey and Hounslow, 1995).

6.4.3. The laboratory programme

Oedometer tests were carried out on 50% sand-5% fines specimens, prepared with different sample preparation techniques and trying to reach two quite different initial specific volumes.

The investigation was limited to the observation of microfabric of the soil deriving from the definite stress-strain state at the end of the mono-dimensional compression test. The main aim of this SEM analysis was to analyze the particle orientation in samples consisting of 50% sand and 50% fines prepared with different techniques, with respect to both horizontal and vertical fractured surfaces.

FIRST SESSION

Two oedometer tests samples were chosen, because the samples had different specific volume but quite similar final void ratio and they both were compressed up to 8 MPa. In the table below some details can be found regarding the oedometer test parameters.

Test number	**Sample prep. technique**	$\sigma'_{v\max}$	v_0	v_f	**Accuracy in the void ratio measurements**
Edo_038_IC	Dry compaction with undercompaction	8 MPa	1,93	1,41	0,02
Edo_042_IC	Slurry	8 MPa	1,58	1,30	0,05

Table 6. 2: Details regarding some experimental variables during oedometer tests on the 50% sand-50%fines samples chosen for the first SEM analysis session.

SECOND SESSION

The same approach was implemented in order to choose the samples to be analused in the second session. Also in this case one dry compacted and a slurry specimen were selected, with very close initial densities, but similar final void ratios. However, the applied stresses were different, although close and quite high, due to some laboratory occurrences.

Sample	Preparation method	$\sigma'_{v\max}$ MPa	v_0	v_f
Edo_059_IC	slurry	13	1.85	1.36
Edo_060_IC	dry compaction	20	1.84	1.25

Table 6. 3: Details regarding some experimental variables during oedometer tests on the 50% sand-50% fines samples chosen for the second SEM analysis session.

6.6. Analysis of the results

In this paragraph a summary of the methodology applied in the images processing is described. In further sections the SEM images collected will be presented together with a first qualitative appreciation of the main distinguishable features of the samples. Moreover, the samples characteristics will be compared and a quantitative approach involving particle orientation micrographs will be introduced.

6.5.1. Imaging

For each sample (4 in total: 2 vertical surfaces and 2 horizontal surfaces) five different values of magnification were used:

- 40 X (this magnification were used to take a picture of each sample in order to be able to recognise which surface was being analysed);
- 200 X;
- 600 X;
- 1500 X;
- 3500 X.

The picture below shows the microscope chamber at the beginning of the imaging session. The information bar shows some parameters such as the pressure inside the camera and the magnification related to the image.

Figure 6. 17: Samples at the beginning of the first imaging session in the microscope chamber.

The choice of the magnifications at which observing the specimens surfaces, as pointed out by Tovey and Houslow (1995) should be consistent with the purpose of the study and consistent with the resolving power of the instrument.

6.5.2. Image processing

All the images were processed using Image J (Rasband, 2009), a public domain Java image processing. The information bar were removed and saved apart. Then the new images were converted to grey scale and the contrast was enhanced, procedure also known as equalisation. In the figures below, the original image and the one without information bar and with enhanced contrast referring to picture jh0267 are reported.

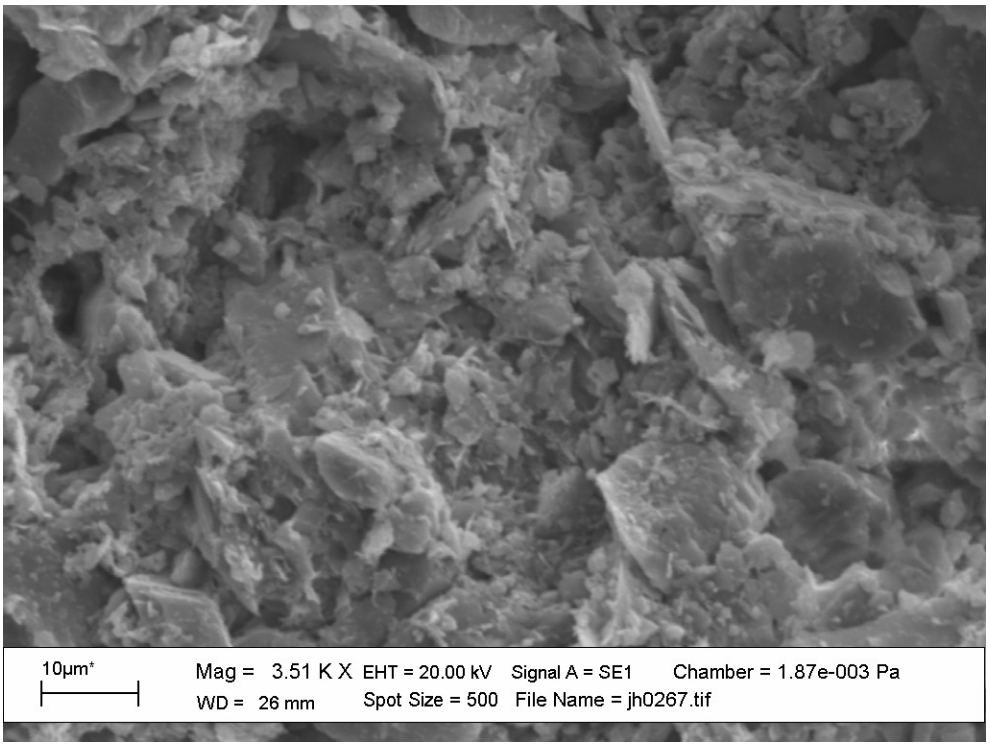

Figure 6. 18: Image of 3.5 K X magnificated specimen Edo_042_IC (vertical surface).

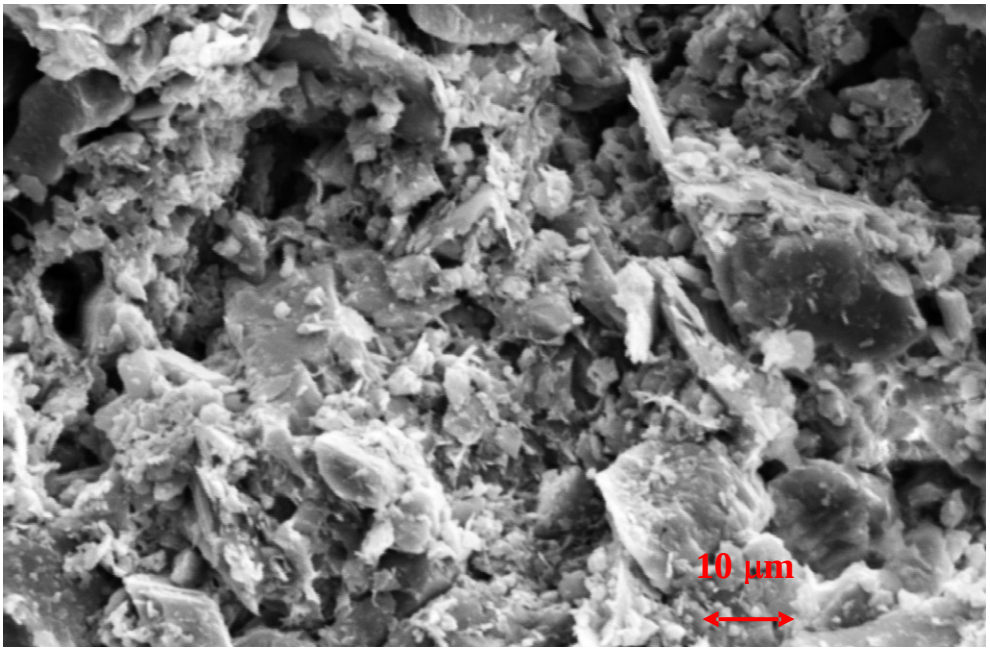

Figure 6. 19: Enhanced contrast image of 3.5 K X magnificated specimen Edo_042_IC (vertical surface).

The program allows to adjust the image to different grey level istograms. As previously introduced with respect to the work by Tovey and Hounslow (1995), there is a need to reduce subjectivity effect when thresholding images. The structure of the soil in the images is determined by peaks and throughs and the grey level is related to the topography of the surface, which allows to determine porosity and particle orientation within the sample's

image. Therefore, different grey level thresholds produce different orientation measurements (Wilkinson, 2010). Tovey and Hounslow highlighted a great dependence of particle orientation diagrams on the grey level threshold used in the processing.

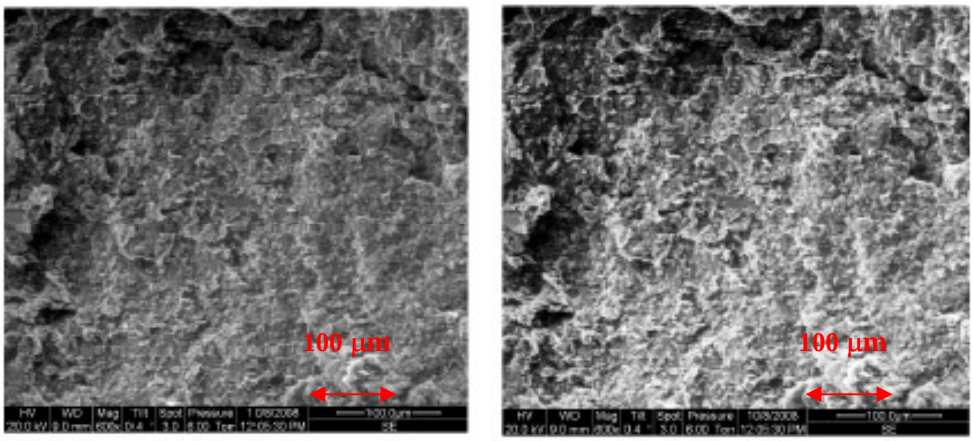

Figure 6. 20: Original SEM image of Gault clay sample and the respective stretched contrast image (from Wilkinson and Fenton, 2010).

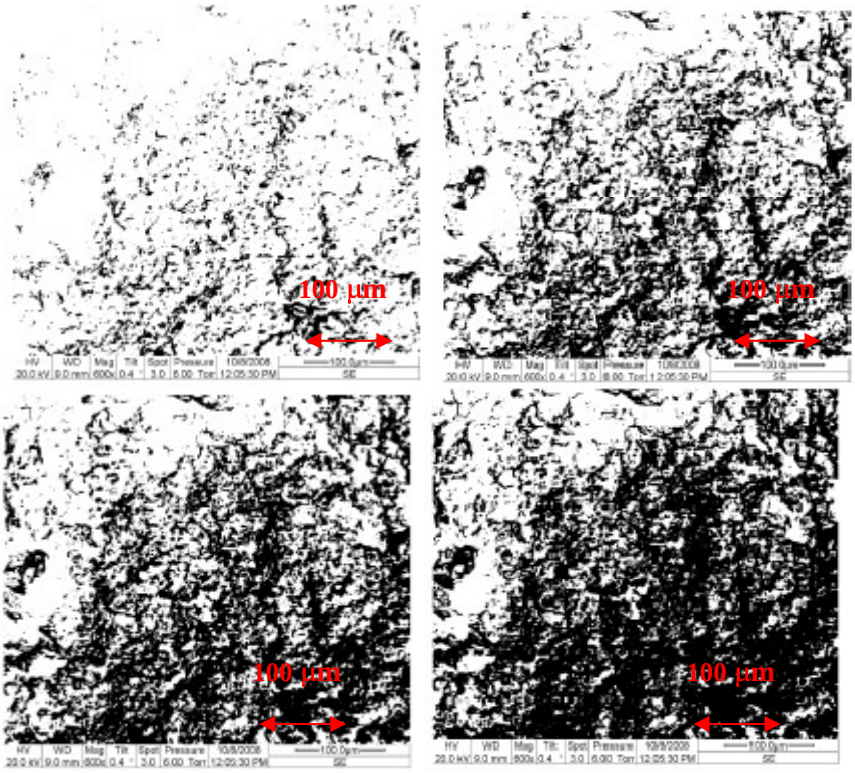

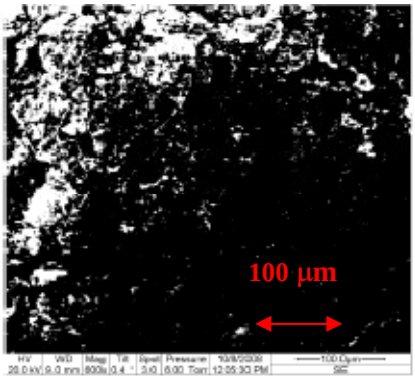

Figure 6. 21: Influence of different grey level thresholds (from 20 to 80%) on the binary images obtained from SEM picture of a broken surface of a Gault clay sample (modified from Wilkinson and Fenton, 2010).

The upper 25% and lower 25% of grey levels can usually be considered separately, because they give semi-indipendent measurements of the structure (Wilkinson, 2010). In the figure below, upper 25% and lower 25 % grey level thresholds referring to Figure 6.19 (sample Edo_042_IC vertical at a magnification of 3.5 K X) are shown.

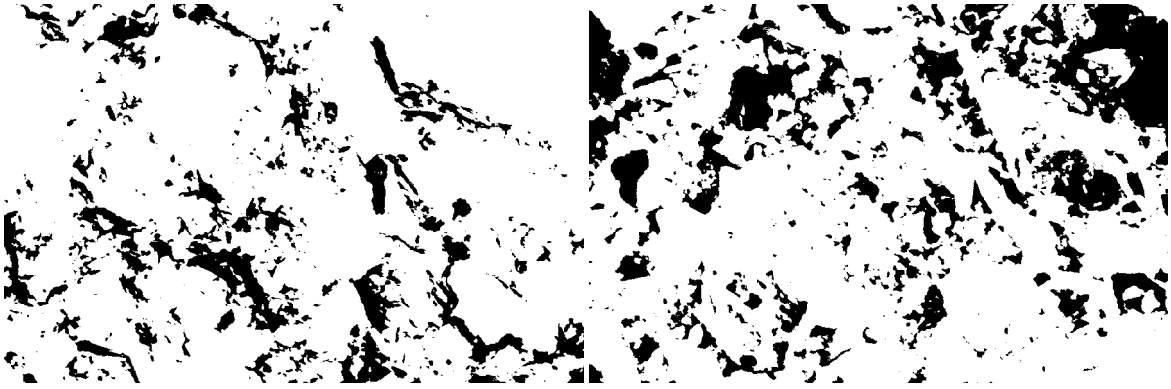

a b

Figure 6. 22: Example of different grey level scale in thresholding an SEM image in order to obtain binary images: upper 25% grey level threshold (a), Lower 25% grey level threshold (b) for the sample in Figure 6.19.

The grey levels threshold images were converted to binary files via ImageJ (Rasband, 2009) and the corresponding data were analysed through the ImageJ function Analyse. Information is obtained on particles area, diameters, perimeter, circularity and other shape factors and orientations, such as Aspect Ratio. In the figure below, an image created through ImageJ is reported which refer to the lower 25% grey level threshold of the sample previously described. The particles are replaced by best-fitting ellipses having the same moment of inertia.

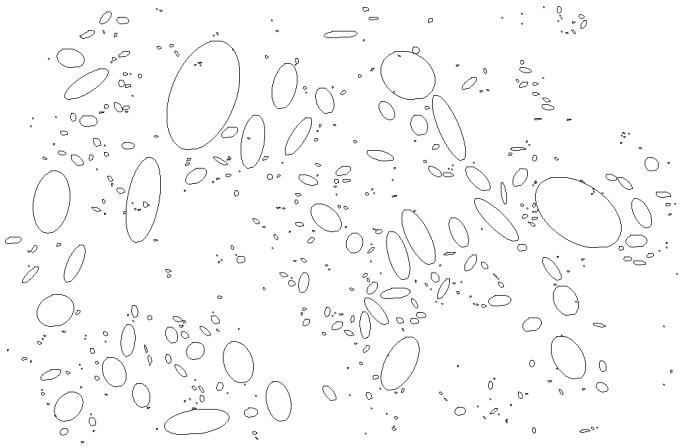

Figure 6. 23: Ellipses having the same moment of inertia of the particles identified through lower 25% grey level threshold in relation to Figure 6.22 (b).

Once obtained these ellipses, corresponding to an approssimation of the soil particles, determined from the procedure described above, it was possible to perform a study of the particles orientation. The orientation is defined as based on the inclination towards the horizontal axis of the image of the ellipse primary axis, ellipse angle directly measured from the analyse particle function in Image J. All the angle values that resulted from Image J processing were measured in pixel, a pixel being 10 μm . Therefore, all the data too small to give a meaningful angle value (between 1 and 4 pixels) were not considered in the following analysis. Diagrams summarising the particles orientation, the so-called rose diagrams, were plotted. In the figure below, the rose diagram referring to Figure 6.23 is reported.

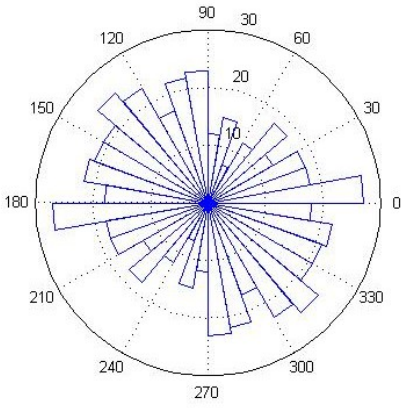

Figure 6. 24: Rose diagram of the particle orientations derived from figure 6.23.

A rose diagram is a powerful means that shows graphically the high or low level of alignment of the soil particles. In the Figure below, the rose diagrams referring to an Oxford and a Gault clay sample are reported with the aim of showing the difference between a material that has a great level of aligned particles and a soil with much less alignment.

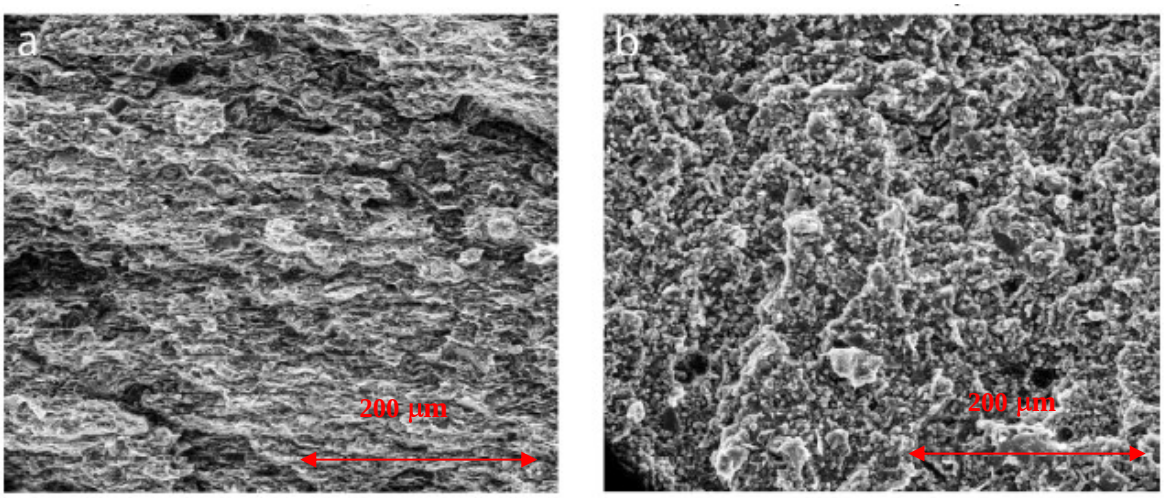

Figure 6. 25: SEM image of Oxford clay sample (a) and of Gault clay sample (b) (modified from Wilkinson and Fenton, 2010).

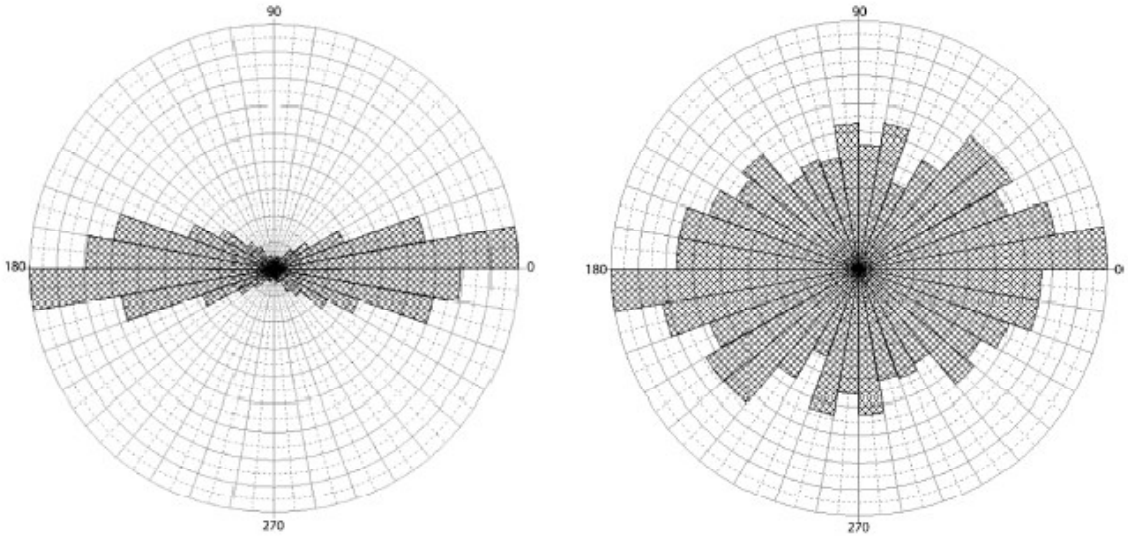

Figure 6. 26: Rose diagrams referring to the images in Figure 6.25 (modified from Wilkinson and Fenton, 2010).

6.7. Presentation of the results

In the following sections, the main features of the surfaces of the different samples will be described, trying to identify the main similarities and differences between them. The images are illustrated in Figures 6.27 to 6.53. The pictures refer to either fractured plane orientated in the vertical direction or a horizontal plane. In the tables below, a summary of the taken pictures during both imaging sessions is presented.

SAMPLE 42 VERTICAL (slurry)		SAMPLE 42 HORIZONTAL (slurry)	
MAGNIFICATION	Image name	MAGNIFICATION	Image name
40 X	jh0256.tif	40 X	jh0268.tif
200 X	jh0257.tif	200 X	jh0269.tif
200 X	jh0258.tif	600 X	jh0270.tif
601 X	jh0259.tif	600 X	jh0271.tif
601 X	jh0260.tif	600 X	jh0272.tif
601 X	jh0261.tif	600 X	jh0273.tif
601 X	jh0262.tif	600 X	jh0274.tif
601 X	jh0263.tif	1.50 K X (charging effect)	jh0275.tif
1.50 K X	jh0264.tif	1.50 K X	jh0276.tif
1.50 K X	jh0265.tif	1.50 K X	jh0277.tif
	jh0266.tif	1.50 K X	jh0278.tif
3.51 K X	jh0267.tif	3.56 K X	jh0279.tif
		3.50 K X	jh0280.tif

Table 6. 4: Summary of the images acquired during the first session referring to the sample Edo_042_IC.

SAMPLE 38 VERTICAL (dry compaction)		SAMPLE 38 HORIZONTAL (dry compaction) (more charging effect)	
MAGNIFICATION	Image name	MAGNIFICATION	Image name
40 X	jh0281.tif	40 X	jh0292.tif
200 X	jh0282.tif	607 X	jh0293.tif
601 X	jh0283.tif	607 X	jh0295.tif
1.5 K X	jh0284.tif	1.5 K X	jh0296.tif

3.5 K X	jh0285.tif	3.5 K X	jh0297.tif
601 X	jh0286.tif	600 X	jh0298.tif
1.5 K X	jh0287.tif	1.50 K X	jh0299.tif
3.50 K X	jh0288.tif	1.50 K X	jh0300.tif
600 X	jh0289.tif	1.50 K X	jh0301.tif
1.5 K X	jh0290.tif	3.50 K X	jh0302.tif
1.5 K X	jh0291.tif	3.5 K X	jh0303.tif

Table 6. 5: Summary of the images acquired during the first session referring to the sample Edo_038_IC.

SAMPLE 60 VERTICAL (dry compaction)		**SAMPLE 60 HORIZONTAL (dry compaction)**	
MAGNIFICATION	Image name	**MAGNIFICATION**	Image name
52 X	jh0455.tif	52 X	jh0485.tif
200 X	jh0456.tif	200 X	jh0486.tif
600 X	jh0457.tif	600 X	jh0487.tif
600 X	jh0458.tif	600 X	jh0488.tif
600 X	jh0459.tif	4.04 K X	jh0490.tif
1.5 K X	jh0460.tif	601 X (?)	jh0491.tif
1.5 K X	jh0461.tif	600 X (?)	jh0492.tif
3.5 K X	jh0462.tif		
200 X	jh0463.tif		

Table 6. 6: Summary of the images acquired during the second session referring to the sample Edo_060_IC.

SAMPLE 59 VERTICAL (slurry)	**SAMPLE 59 HORIZONTAL (slurry)**

MAGNIFICATION	Image name	MAGNIFICATION	Image name
50 X	jh0464.tif	55 X	jh0493.tif
200 X	jh0465.tif	200 X	jh0494.tif
200 X	jh0466.tif		
600 X	jh0467.tif		
600 X	jh0468.tif		
600 X	jh0469.tif		
1.5 K X	jh0470.tif		
1.50 K X	jh0471.tif		
3.50 K X	jh0472.tif		
1.50 K X	jh0473.tif		

Table 6. 7: Summary of the images acquired during the second session referring to the sample Edo_059_IC.

6.6.1. Sample Edo_042_IC (slurry)

In this paragraph a summary of the SEM images obtained with reference to the slurry sample called Edo_042_IC are showed. The first two pictures represent the specimen itself, photographed at low magnification at the beginning of the session.

200 X MAGNIFICATION

As can be appreciated in both images referring to the 200X vertical an horizontal surface, there does not seem to be a preferential particle orientation The overall microstructure is quite homogeneous. At this magnification clay particles aggregates around minerals or bigger grains cannot be seen.

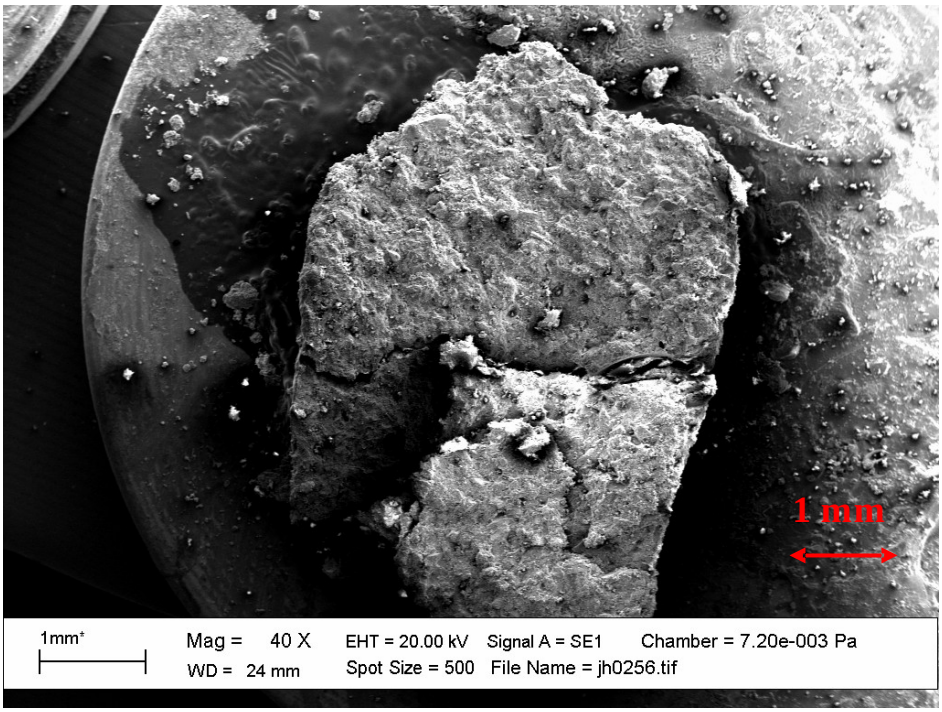

Figure 6. 27: vertical surface of sample Edo_042_IC (image jh0256.tif).

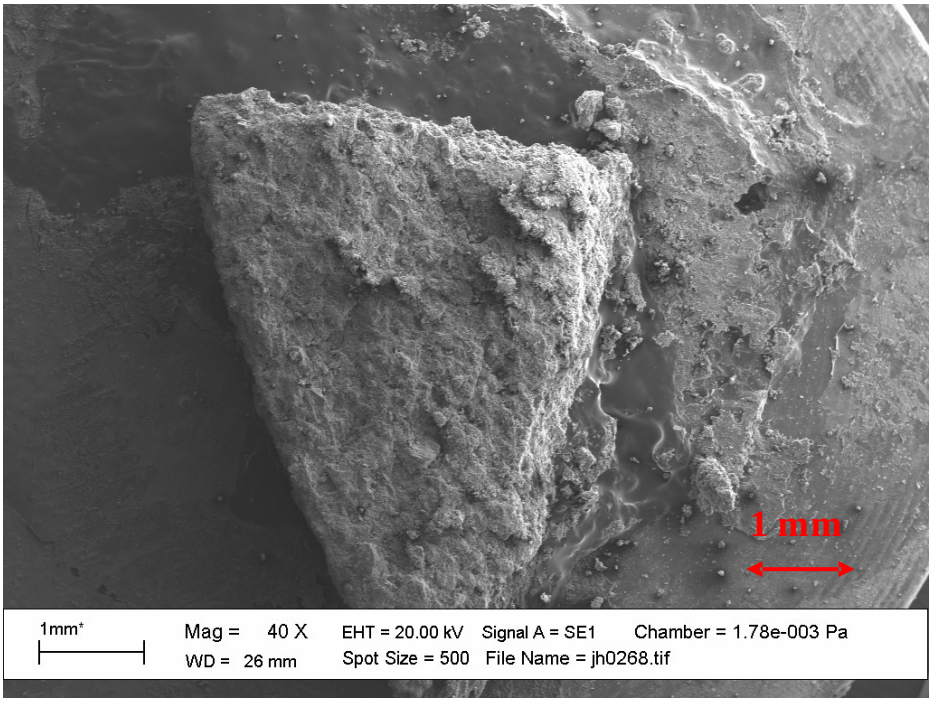

Figure 6. 28: horizontal surface of sample Edo_042_IC (image jh0268.tif).

.

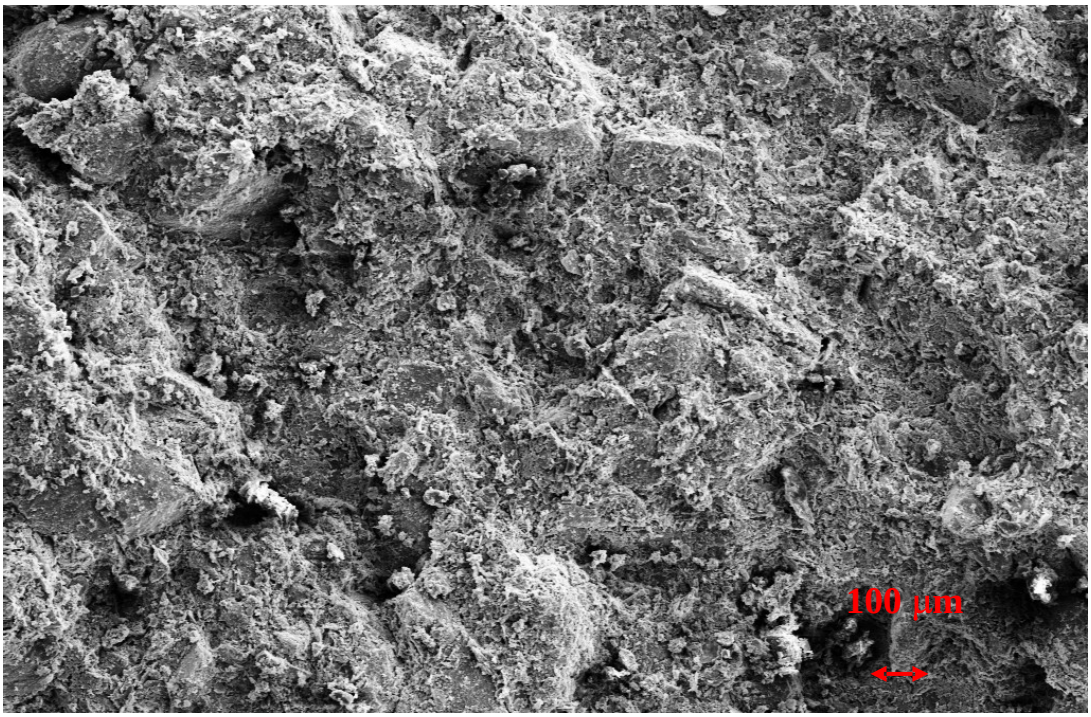

Figure 6. 29: Magnification at 200X of the surface shown in figure 6.27, picture with enhanced contrast effect (image jh0257.tif).

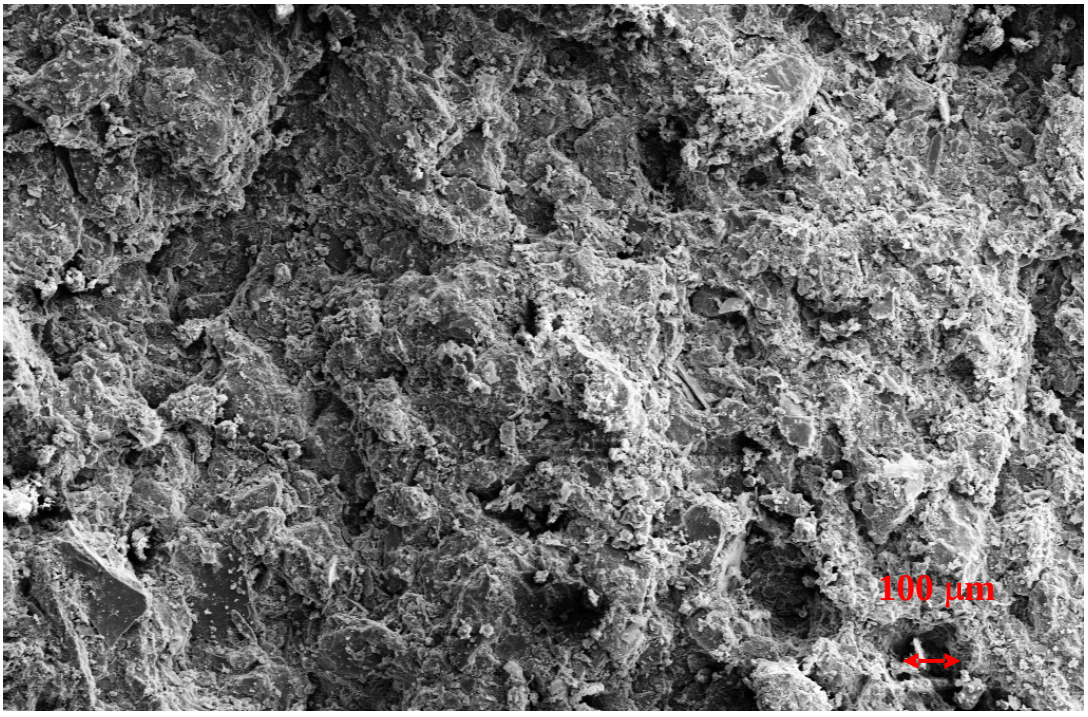

Figure 6. 30: Magnification at 200X of the surface shown in Figure 6.28, picture with enhanced contrast effect (image jh0269.tif).

600 X MAGNIFICATION

In Figures 6.31 and 6.32 the 600 X magnificated pictures with enhanced contrast are shown. In the figure below a fracture through the sample in the vertical direction can be observed. Again peaks and throughs do not show a preferential orientation.

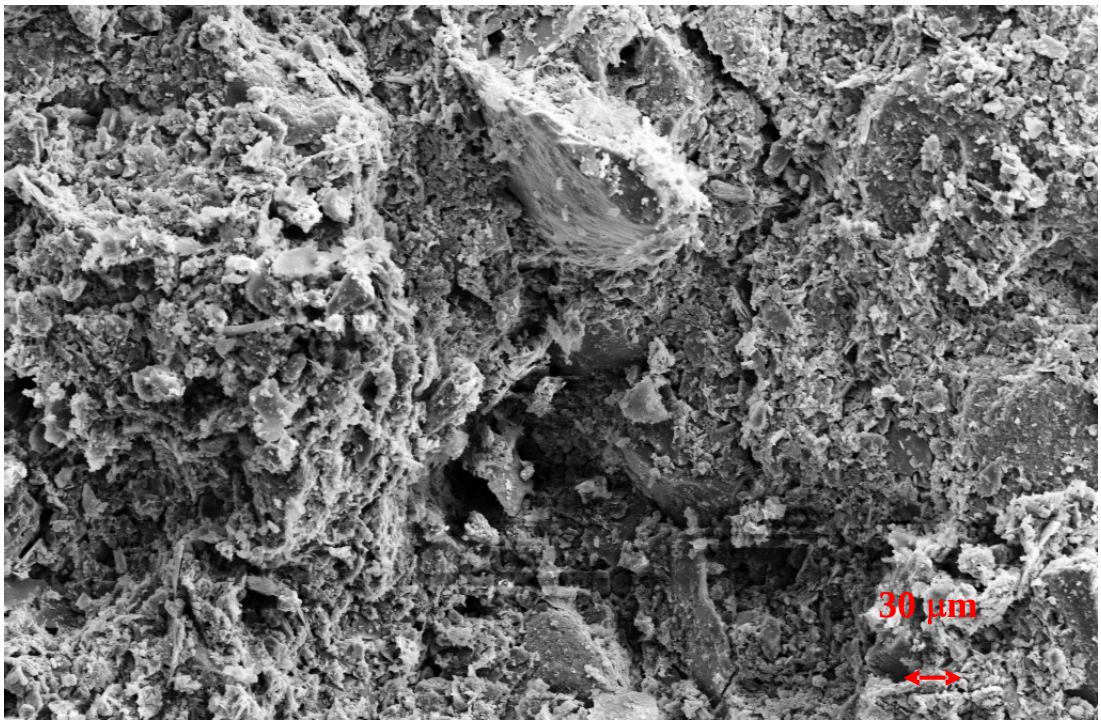

Figure 6. 31: Magnification at 600X of the surface shown in Figure 6.27, picture with enhanced contrast effect (image jh262.tif).

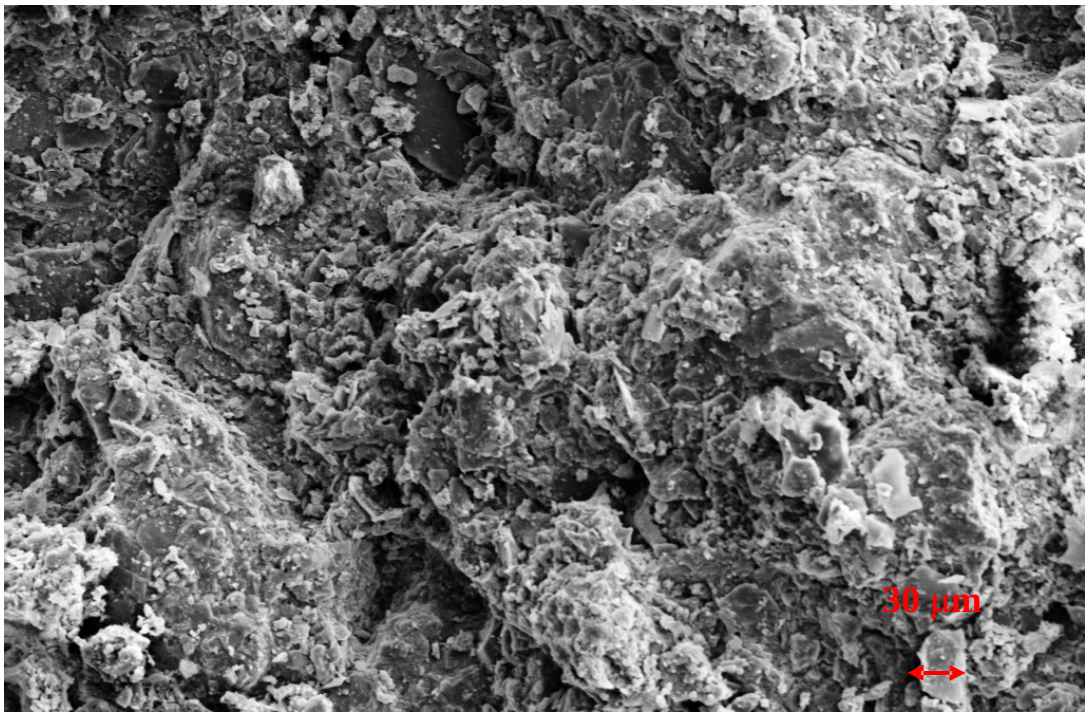

Figure 6. 32: Magnification at 600X of the surface shown in figure 6.28, picture with enhanced contrast effect (image jh0272.tif).

This might be in agreement with the fact that the sample was originally a slurry. A silt grain with clay particles aggregated around its surface can be seen, however, this is affected by some charging effect.

1500 X and 3500 X MAGNIFICATION

In the following pictures high (1500 X) and very high (3500 X) magnification images are reported with respect to both vertical and horizontal surface of sample Edo_042_IC. At this scale quite rough particle edges can be appreciated, however, still a random particle orientation can be seen. The void presence is not irrelevant.

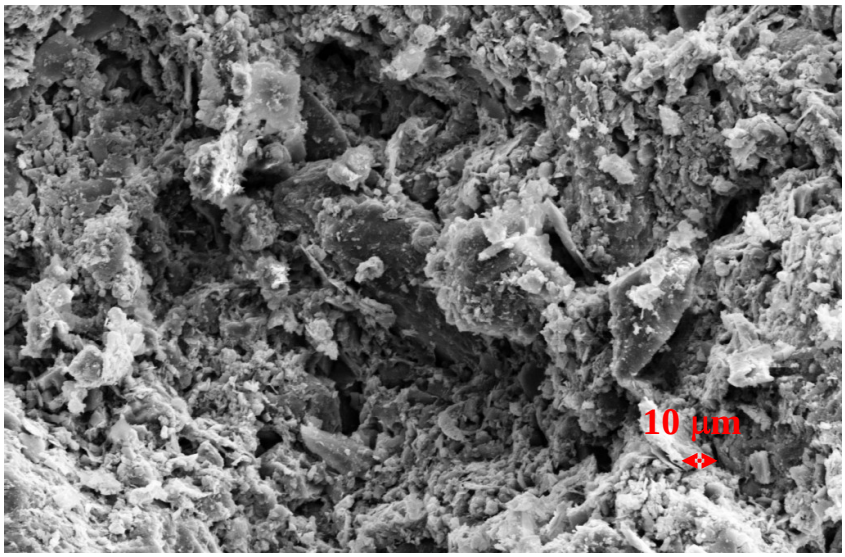

Figure 6. 33: 1500 X magnification of a detail referring to the vertical surface shown in Figure 6.27 (image jh0264.tif).

In Figure 6.34, some particle aggregates seem to form two orientated planes which form an angle of around 90°. However, this statement might be misleading, given the magnification and therefore the small surface considered in the image. This angle is a feature that can probably be ascribed to an angular sandy grain.

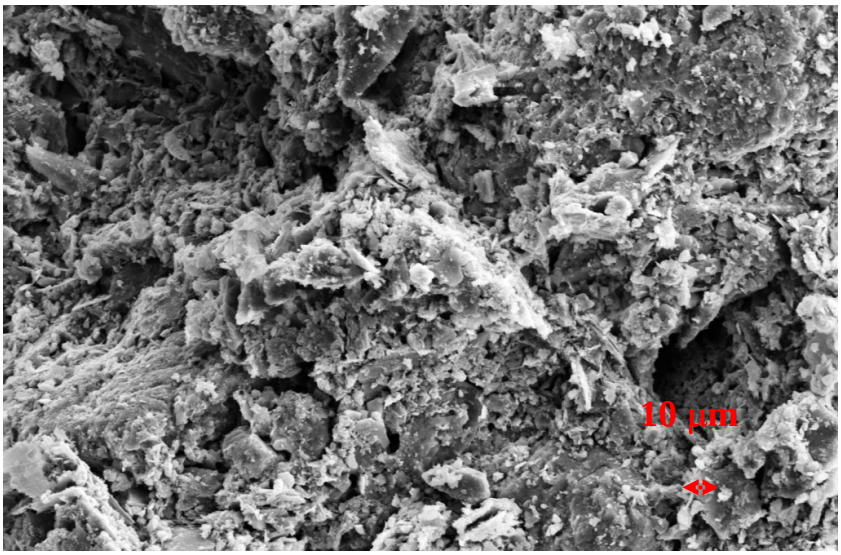

Figure 6. 34: 1500 X magnification of a small area referring to the horizontal surface shown in Figure 6.28 (image jh0265.tif).

In the figure below, the erratic spatial distribution of clayey particles, achieved with the slurry technique can be appreciated. Moreover, a more attentive view of the particles shape is allowed. Clays tend to distribute on bigger particles surfaces or around minerals. Some calcite mineral can also be seen in the picture. Given their right angled shape, some planes might be identified, but these coincide with the single particle sides inclinations, not with preferential orientation planes.

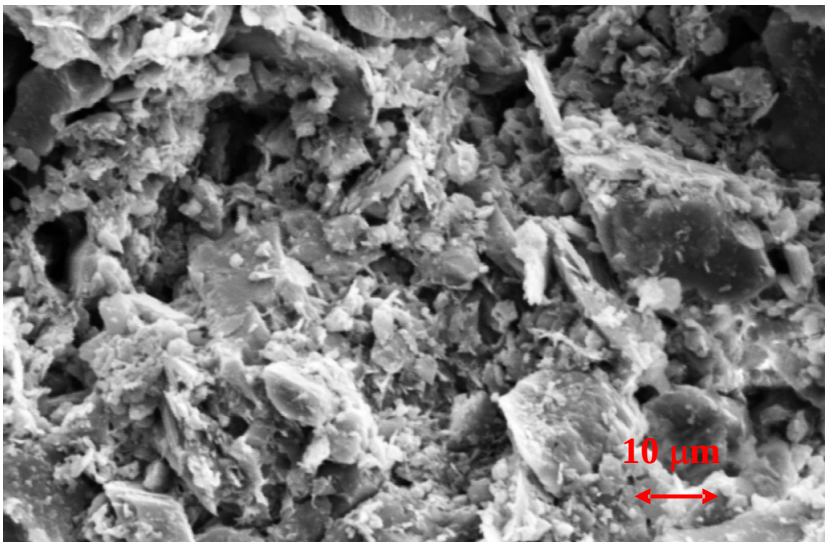

Figure 6. 35: 3500 X magnification of a small area referring to the vertical surface shown in Figure 6.27 (image jh0269.tif).

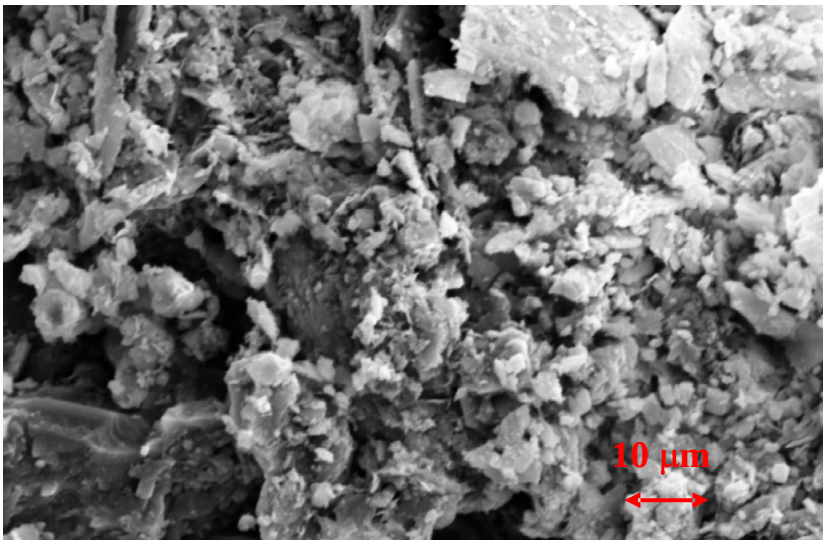

Figure 6. 36: 3500 X magnification of a small area referring to the horizontal surface shown in Figure 6.28 (image jh0279.tif).

No great differences can be seen between Figure 6.35 and Figure 6.36. Therefore at these orders of magnification, particle shapes and contacts predominate with respect to fabric. However, from the horizontal surface presented in Figure 6.30 pores in the sample fabric seem to be more evident than from the point of view shown in Figure 6.29. It becomes more difficult to identify minerals, but also from this side smaller particles tend to form aggregates on bigger grains surfaces. The light colour of small grains might also be due to some charging effect, given the high magnification.

6.6.2. Sample Edo_038_IC (dry compaction)

In the Figure below, the image of the vertically broken surface of the dry compacted sample Edo_038_IC is reported. The layered structure due to the sample preparation technique can already be seen and a quite steep sliding surface on the right side of the sample is identified, see the charging effect.

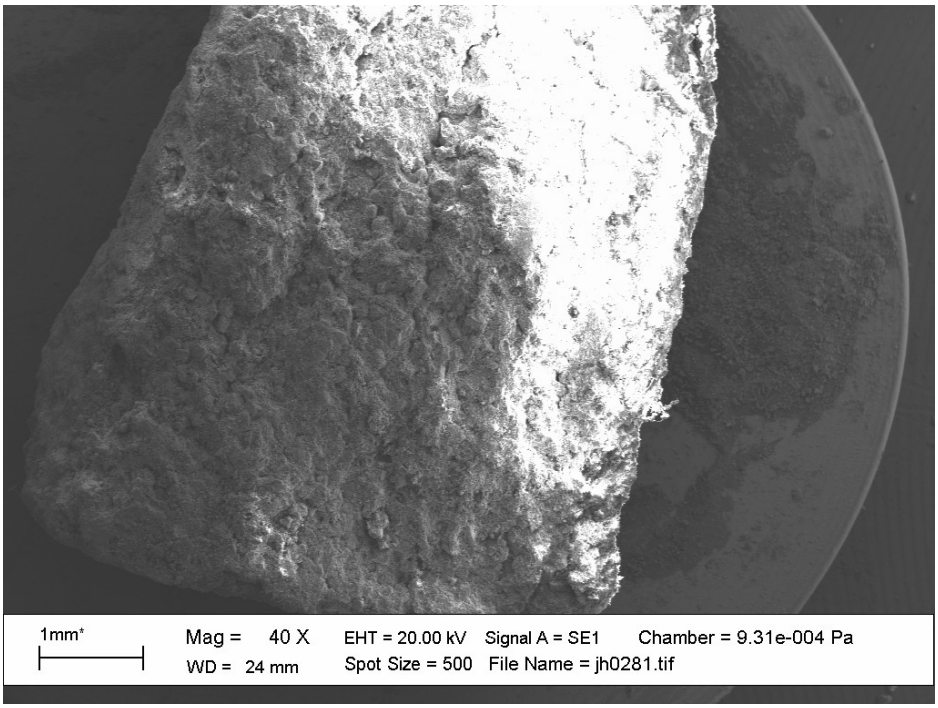

Figure 6. 37: vertical surface of sample Edo_038_IC, obtained from primary electrons imaging (image jh0281.tif).

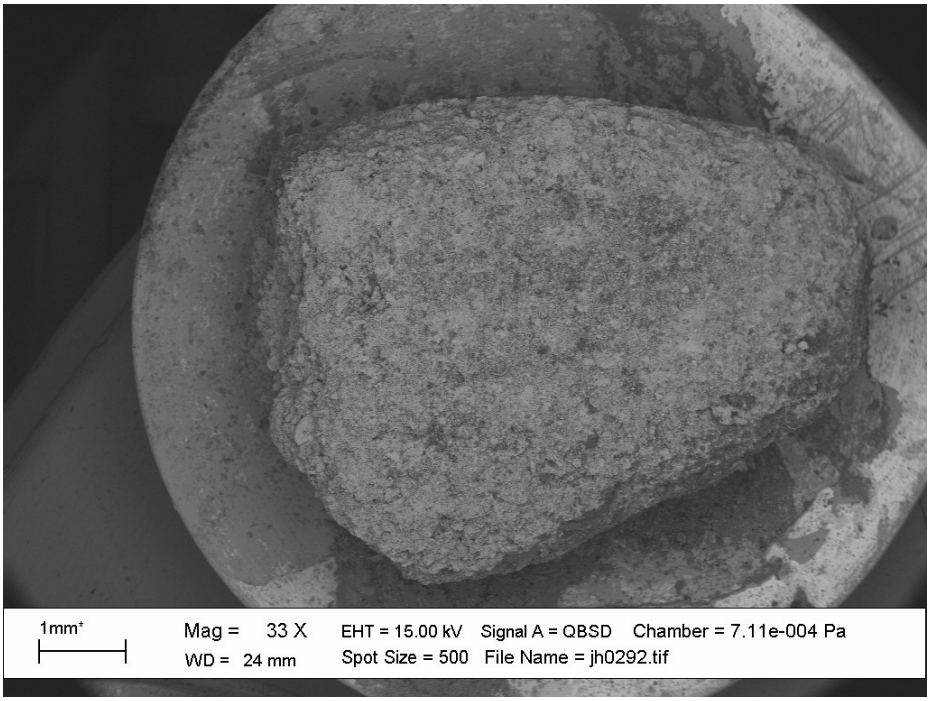

Figure 6. 38: horizontal surface of sample Edo_038_IC, obtained from back scattered electrons imaging (image jh0292.tif).

Unfortunately, in this case a comparison of the 200 X magnificated vertical and horizontal samples cannot be performed.

600 X MAGNIFICATION

In Figure 6.39 to 6.41, 600 X magnificated specimens are shown.

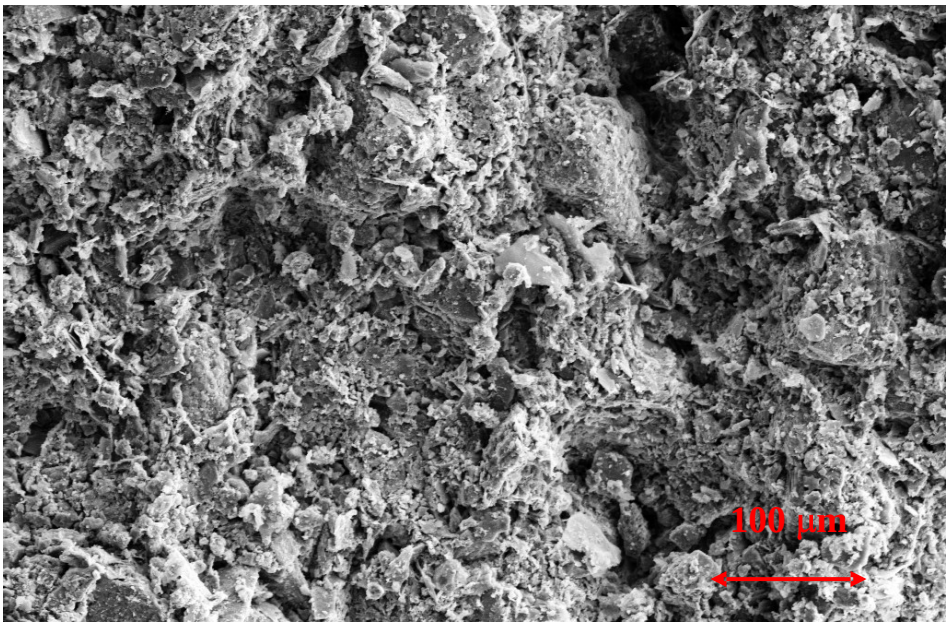

Figure 6. 39: Magnification at 600X of the vertical surface shown in figure 6.37, picture with enhanced contrast effect (image jh0289.tif).

As observed for the previous sample, no particular orientated fabric can be identified. The structure is quite uniform. In Figure 6.4o and 6.41, two images referring to the horizontal surface of the specimen, obtained from the same magnification are reported. As can be noted, in the latter some electrons charging effect occurred, whereas in Figure 6.34, back scattered electrons option was used, in order to avoid this disturbance. Some honey-comb structure due to dry compaction can be observed in Figure 6.40, particularly it is shown that finer particles tend to occupy inter-particle voids.

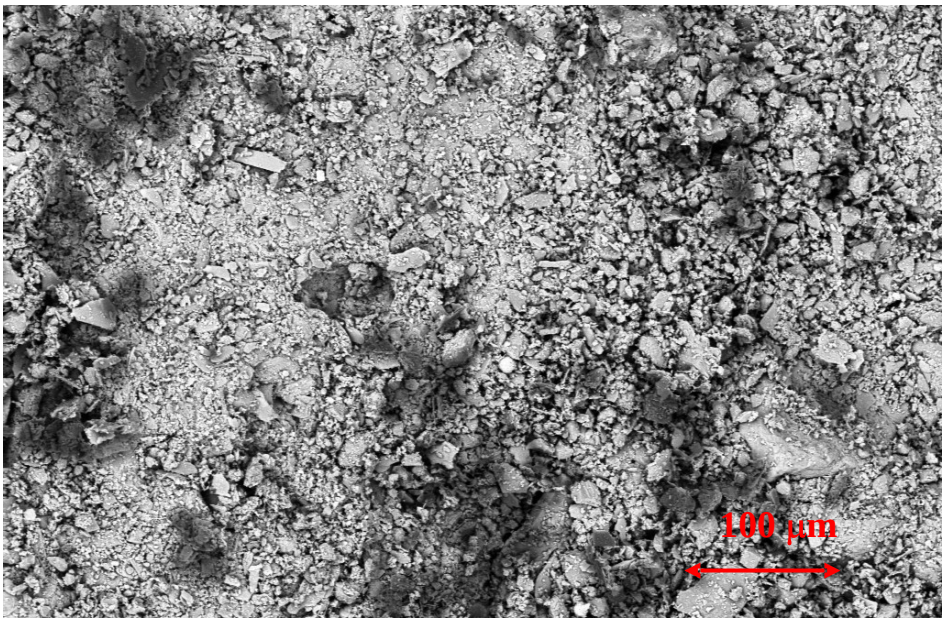

Figure 6. 40: Magnification at 600X of the horizontal surface shown in figure 6.38, image obtained from back scattered electrons mode, picture with enhanced contrast effect (image jh0293.tif).

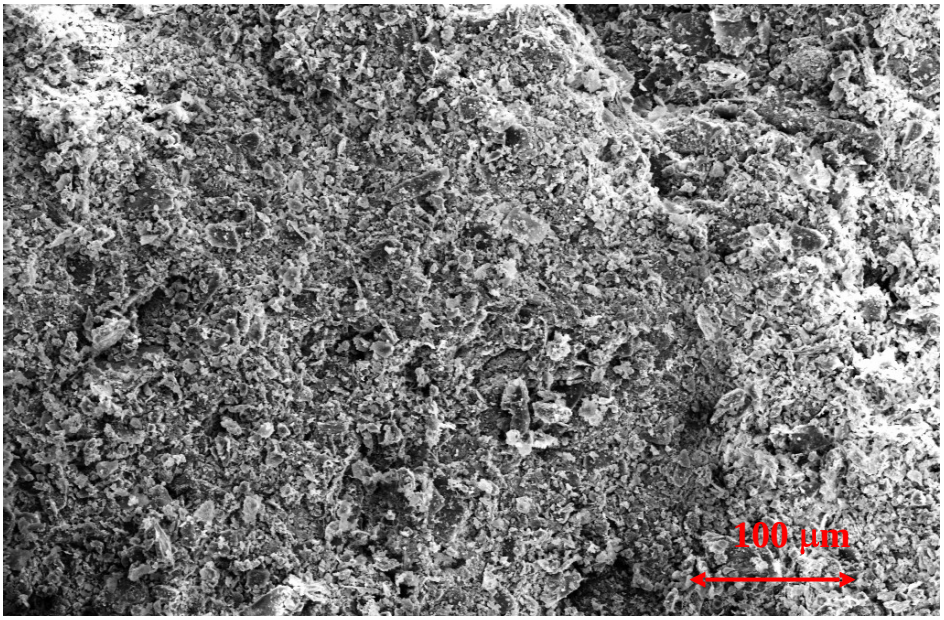

Figure 6. 41: Magnification at 600X of the horizontal surface shown in figure 6.38, image obtained from primary electrons mode, picture with enhanced contrast effect (image jh0298.tif). See the comparison between Figures 6.40 and 6.41 for the results obtained from primary or backscattered electrons (Image jh0298.tif).

Much more flattened particle spatial distribution is shown from the view in the images taken on the horizontal surface, see Figure 6.41. If compared to similar pictures (Figure 6.31) obtained from the previous sample, much less evidence of the clay particles tendency to form clusters or to aggregate on bigger grains surfaces can be found. This might be probably linked to the fact that the sample Edo_038_IC was dry compacted, therefore finer particles, during the compaction itself in layers, were slightly forced into the soil voids.

1500 X MAGNIFICATION

Highly magnificated sample (1500 X) images are reported below. Given the larger number of pictures taken at this magnification, a comparison between different areas of the surface can be made. From this analysis it can be appreciated that the structure has a larger number of voids in comparison with the slurry sample. The darker area on the upper side of the picture might be related either to a large pore or to the surface boundary steep boundary due to the fracturing, aimed at providing the sample for the SEM study. The same can be said for the left side of Figure 6.42.

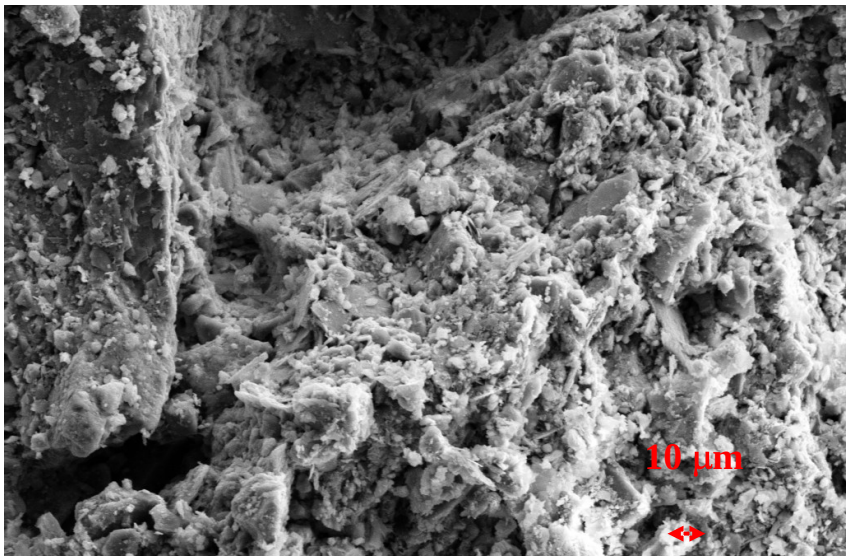

Figure 6. 42: 1500 X magnification of a small area referring to the vertical surface shown in Figure 6.37 (image jh0284.tif).

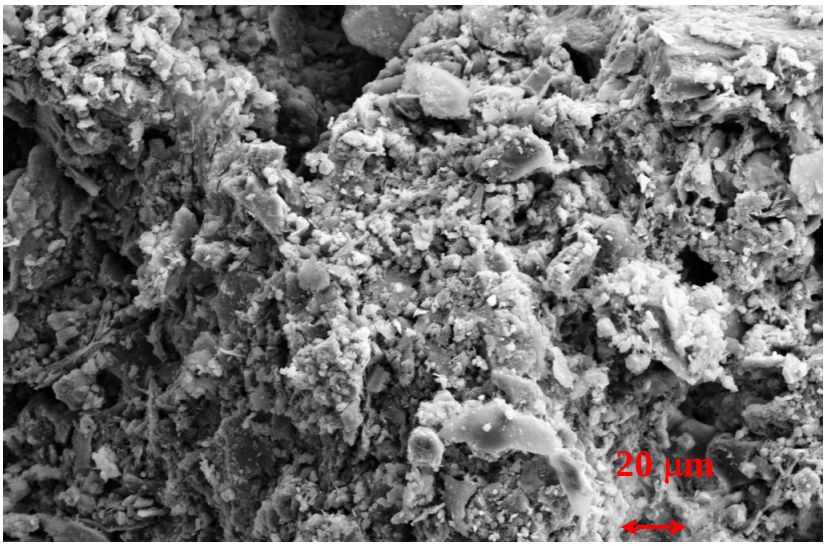

Figure 6. 43: 1500 X magnification of a small area referring to the vertical surface shown in Figure 6. 37 (image jh0287.tif).

In Figure 6.44 an example of finer particles probably aggregating on the surface of a carbonate crystal is shown. However, the peaks and throughs distribution on the lower right side of the picture might suggest that a non-perfectly uniform fabric was prepared by means of dry compaction. As an overall impression, on top of the image there seems to be a group of horizontally orientated particles just above randomly orientated grains. This could be related to the layered structure of the specimen that could only be highlighted during the normal compression itself.

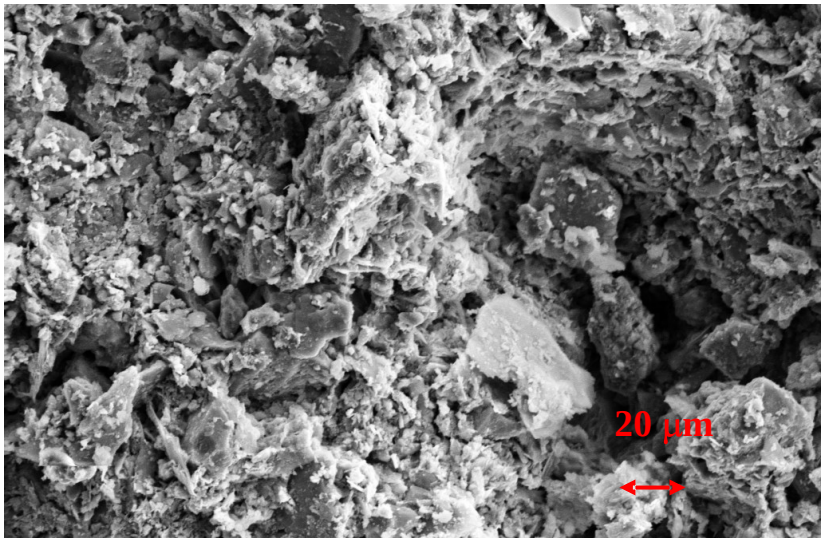

Figure 6. 44: 1500 X magnification of a small area referring to the vertical surface shown in Figure 6. 37 (image jh0290.tif).

In Figure 6.45, another example of carbonate crystal is shown, surrounded by the fines particles and the direction of its upper side, which is close to the horizontal direction might suggest a preferential orientated domain, induced again by the sample preparation mode and by the oedometer test itself. There seems to be an almost vertical division line that somehow separates the surface in two areas.

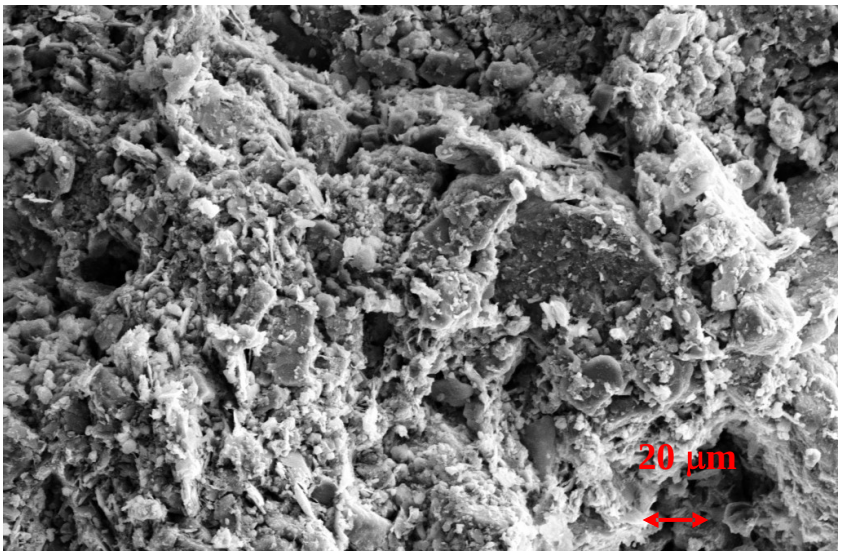

Figure 6. 45: 1500 X magnification of a small area referring to the vertical surface shown in Figure 6. 37 (image jh0291.tif).

It is now interesting to compare these observation, valid for the vertical surface, to the experimental evidences for the horizontal specimen. The view of the horizontal surface of the sample, shown in Figure 6.46, depicts a quite scattered fabric. The majority of the particles that can be seen and that are therefore located on top of the surface are quite fine, given that the charging effect is more evident with decreasing grain diameter.

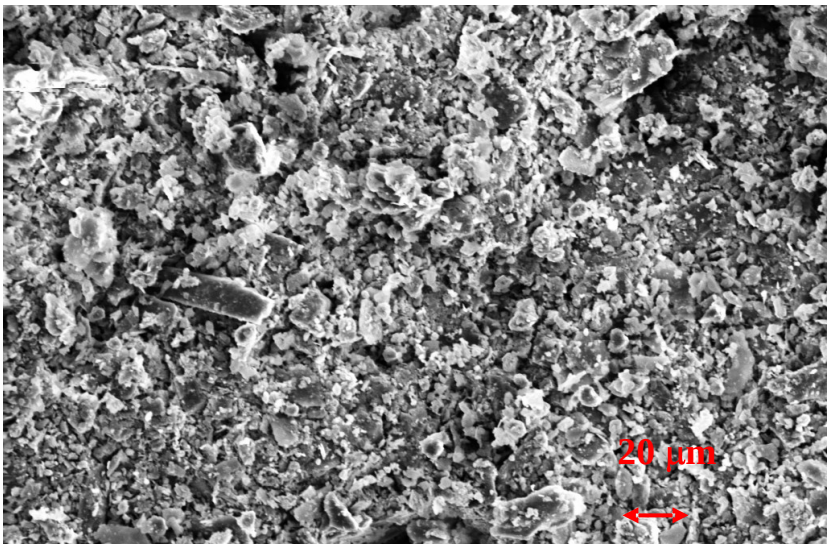

Figure 6. 46: 1500 X magnification of a small area referring to the horizontal surface shown in Figure 6. 38 (image jh0296.tif).

In Figure 6.47, a quite clear example of sharp edge-to-edge and edge-to-side inter- particle contacts can be seen. The darker areas on the upper side and on the lower right side of the picture are probably a sign of the honey-comb structure deriving from dry-compaction (see Figure 6.40 for the 600X magnification). As an overall impression there seems to be a diagonal consisting of the sharp edges of some platy particles and a more orientated domain is probably located on the bottom left side of the picture. Figures 6.48 and 6.49 show similar scattered microfabrics views.

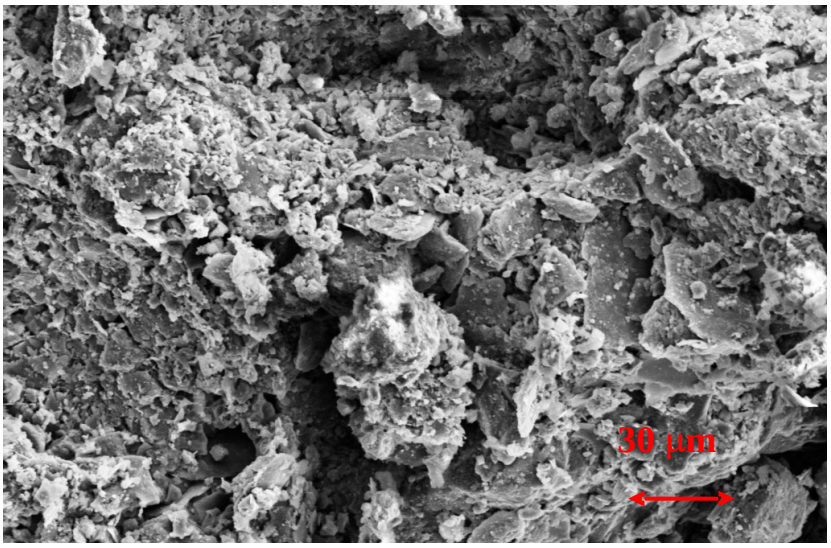

Figure 6. 47: 1500 X magnification of a small area referring to the horizontal surface shown in Figure 6. 38 (image jh0299.tif).

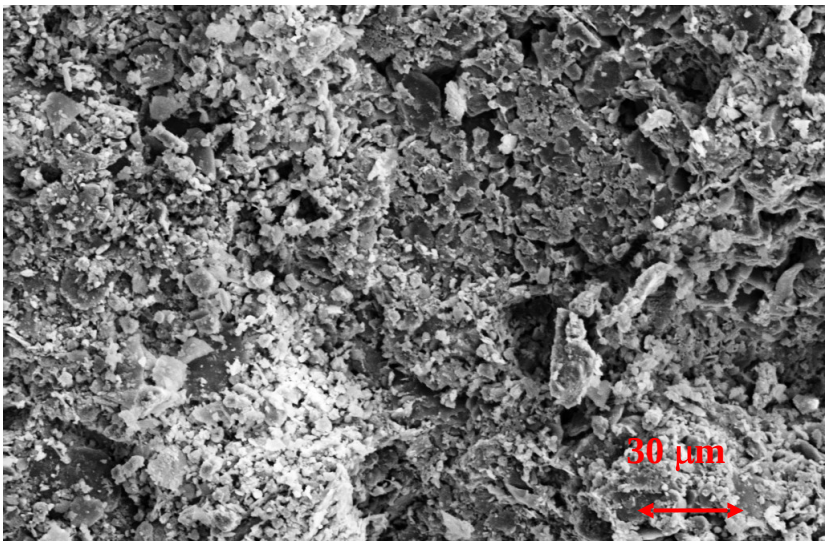

Figure 6. 48: 1500 X magnification of a small area referring to the horizontal surface shown in Figure 6. 38 (image jh0300.tif).

As seen for the images in Figures from 6.36 to 6.39, also in Figures from 6.40 to 6.42 some darker areas occur representing voids or non homogeneous fabric due to the compaction or a non perfectly uniform addition of distilled water for apparent cohesion within the dry mixture. In figure 6.43 it is possible to identify a particle with quite right sides close to a rhomboid and it can be hypothesized the presence of a carbonate crystal.

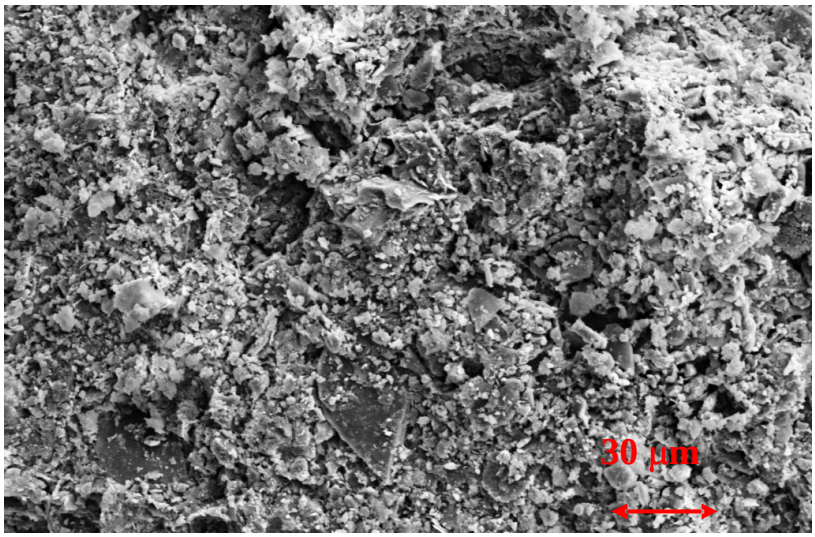

Figure 6. 49: 1500 X magnification of a small area referring to the horizontal surface shown in Figure 6. 38 (image jh0301.tif).

3500 X MAGNIFICATION

In the following images very high magnification pictures of the samples microstructure are reported. The platy shape of clayey particles that tend to aggregate is a constant feature. Particularly, in Figure 6.50 there seems to be a slight trend for fines angular particles to assume a low angle of inclination with respect to the horizontal of the image, either clockwise or anticlockwise.

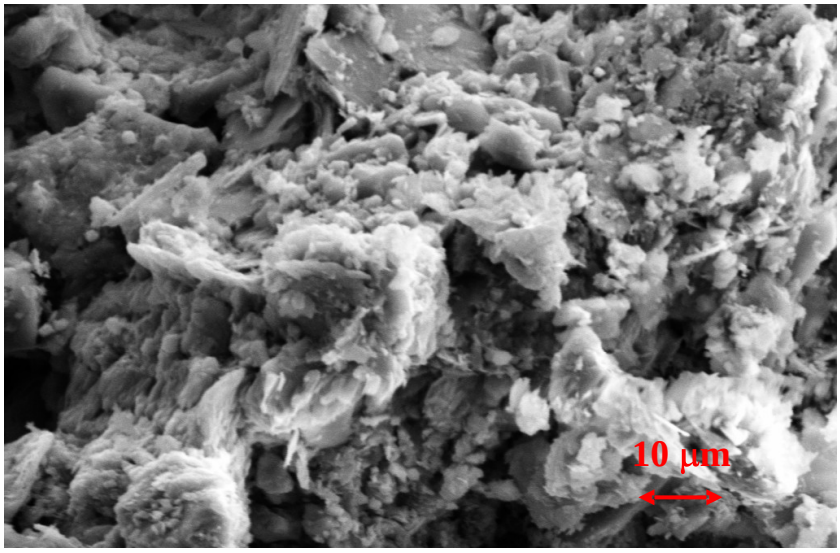

Figure 6. 50: 3500 X magnification of a small area referring to the vertical surface shown in Figure 6. 31 (image jh0285.tif).

In the Figure 6.51 no such feature seems to occur, but the presence of a carbonate crystal surrounded by voids and finer particles is shown. Two groups of particles seem to indicate that a diagonal orientation of around 110° anticlockwise toward the horizontal axis of the image is predominant, this coinciding with one side of the carbonate crystal. However, given the very high magnification of the image this feature is probably more related to local phenomena than to a microfabric property throughout the whole sample.

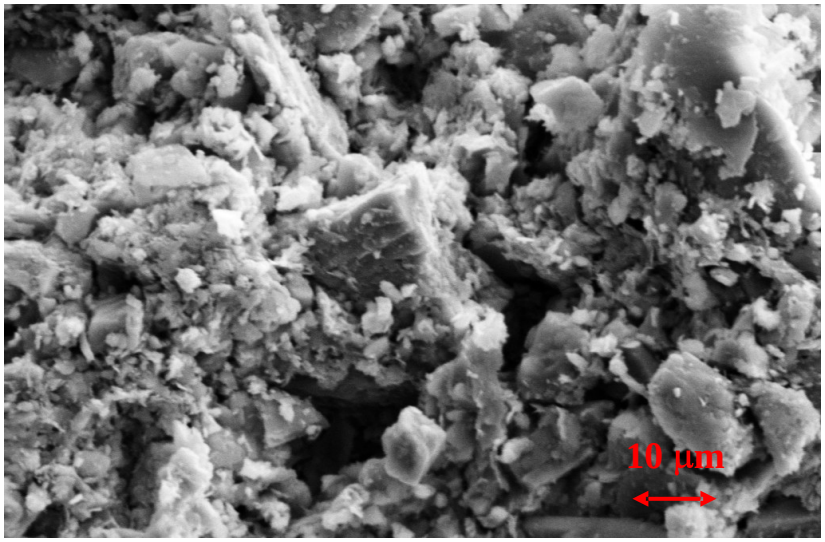

Figure 6. 51: 3500 X magnification of a small area referring to the vertical surface shown in Figure 6. 51 (image jh0288.tif).

An analysis of the particles distribution from the horizontal surface, showed in Figures from 6.52 to 6.53, can be performed.

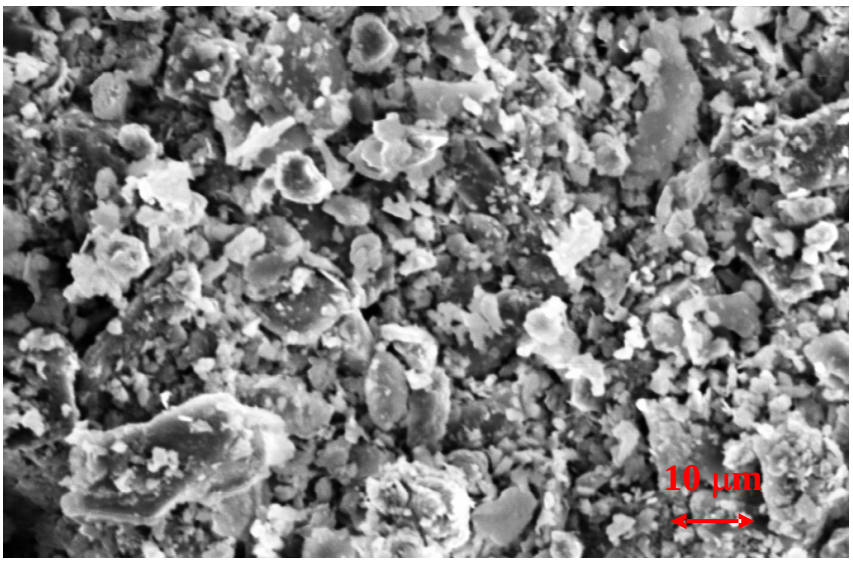

Figure 6. 52: 3500 X magnification of a small area referring to the horizontal surface shown in Figure 6. 38 (image jh0297.tif).

This point of view depicts particles of different dimensions and shape that tend to form clusters, with finer grains located on the bigger grains surfaces. An orientated domain in the vertical direction might be identified in the lower right part of the image. This might be ascribed to clayey platy particles. However, given that the Venice soils are mainly non plastic, this feature is probably more easily related to random local particle distribution.

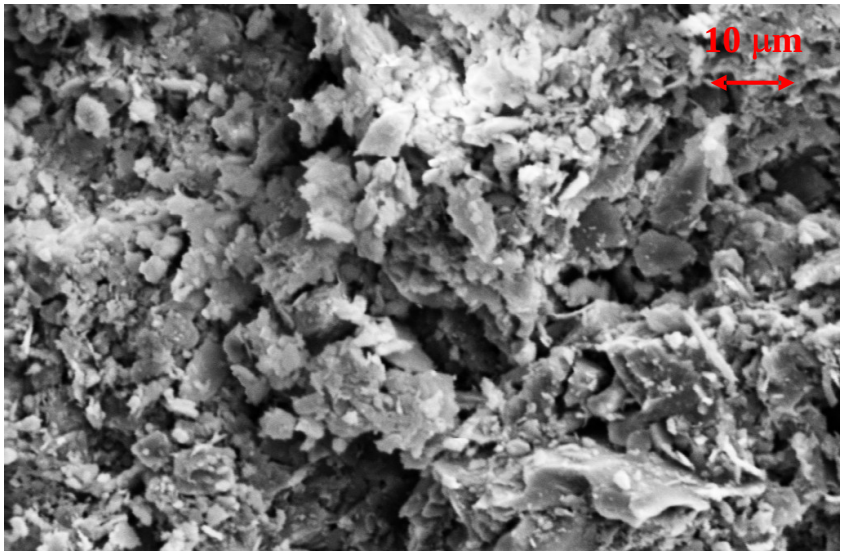

Figure 6. 53: 3500 X magnification of a small area referring to the horizontal surface shown in Figure 6. 38 (image jh0302.tif).

6.8. Interpretation of the results: orientation graphs

In order to perform a study of the particles orientation, according to the procedure described in section 6.5.2., a selected number of images was chosen for each sample. In particular, one image for each magnification was selected, referring to both vertical and horizontal surfaces of the same sample.

Note on the use of the grey level threshold

In the Figures below, some examples of the differences in the particle orientation diagrams obtained from the 25% upper or 25% lower grey levels threshold are reported.

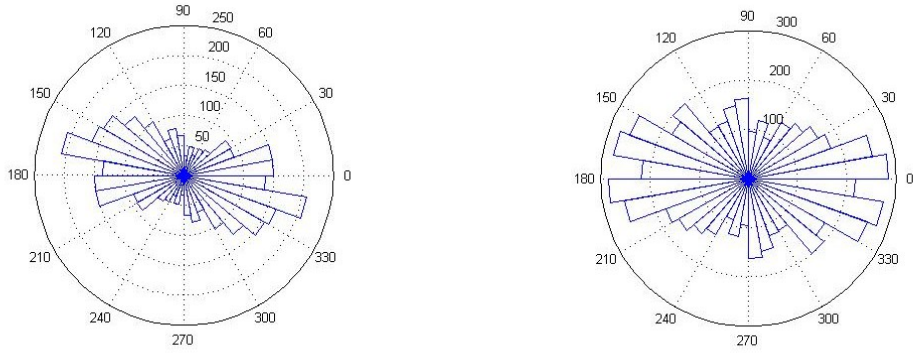

Figure 6. 54: Upper and lower grey levels threshold (200X) referring to image 0257.tif .

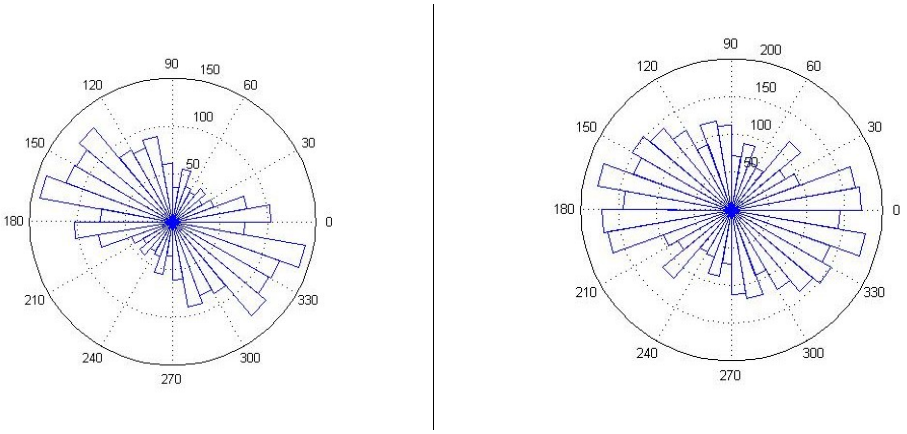

Figure 6. 55: Upper and lower grey level threshold (200X) referring to image 0269.tif .

In the following paragraphs the upper 25% of grey levels was sat as the threshold to study the samples microstructure with reference to particle orientation. The rose diagrams, as already introduced in 6.5.2, represent the orientation of the long axis of the ellipses with the same moment of inertia of the particles, as calculated during equalisation.

Sample Edo_042_IC

In Figures from 6.56 to 6.59, the rose diagrams corresponding to both the vertical and horizontal analysed surfaces of the 50%-50% slurry sample are shown. Unfortunately, no preferential direction can be detected with the exception of Figure 6.58 (b) which refers to the horizontal 600 X magnificated image reported in Figure 6.40.

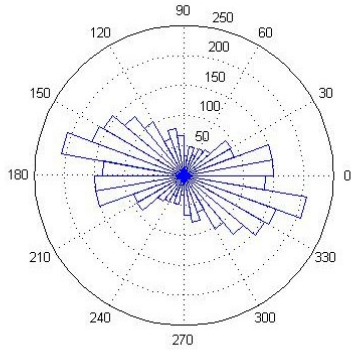

VERTICAL (a)

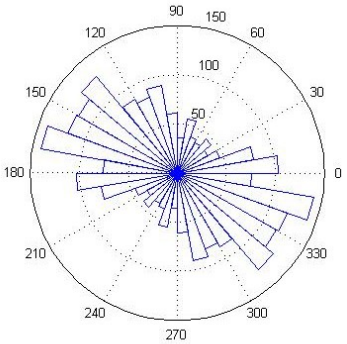

HORIZONTAL (b)

Figure 6. 56: Rose diagrams referring to 200 X magnificated images: (a) vertical surface (image jh0257.tif) and (b) horizontal surface (image jh0269.tif).

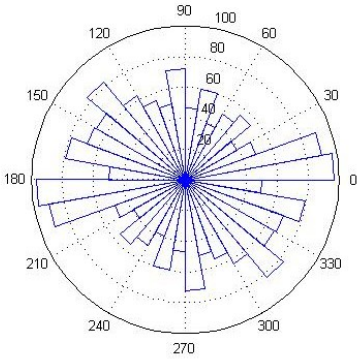

VERTICAL (a)

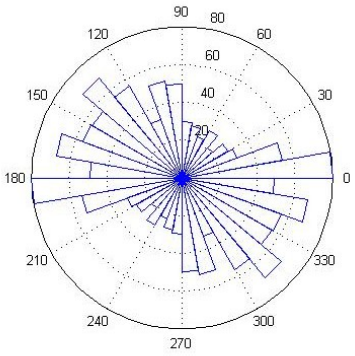

HORIZONTAL (b)

Figure 6. 57: Rose diagrams referring to 600 X magnificated images: (a) vertical surface (image jh0262.tif) and (b) horizontal surface(image jh0272.tif).

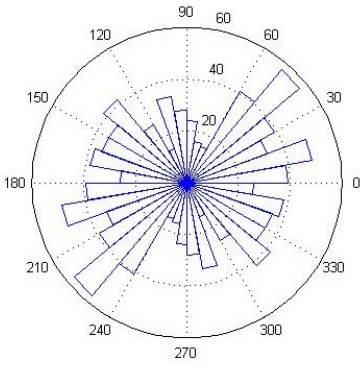

VERTICAL (a)

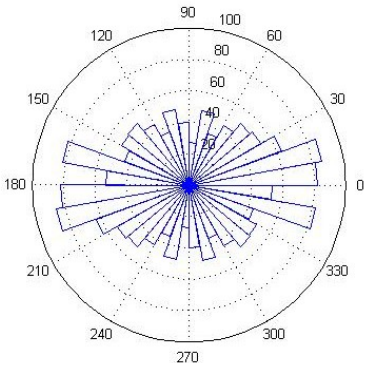

HORIZONTAL (b)

Figure 6. 58: Rose diagrams referring to 1500 X magnificated images: (a) vertical surface (image jh0264.tif) and (b) horizontal surface(image jh0265.tif).

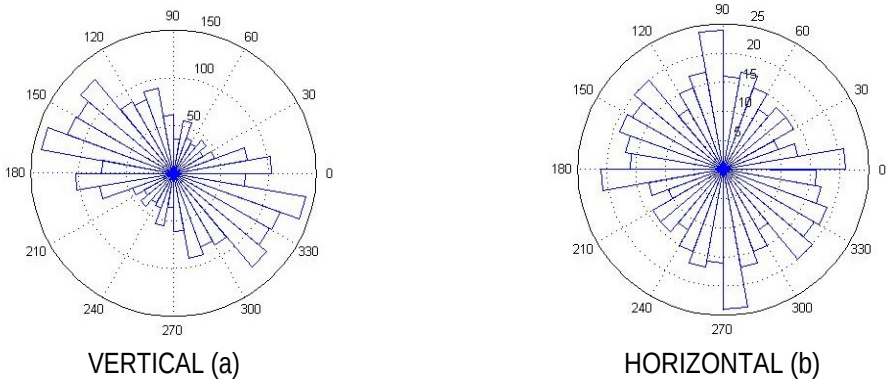

Figure 6. 59: Rose diagrams referring to 3500 X magnificated images: (a) vertical surface (image jh0269.tif) and (b) horizontal surface(image jh0279.tif).

Sample Edo_038_IC

In this paragraph, the rose diagrams corresponding to both the vertical and horizontal analysed surfaces of the 50%-50% dry compacted sample are reported. Figures from 6.60 to 6.63 present a summary of the performed particle orientation analysis.

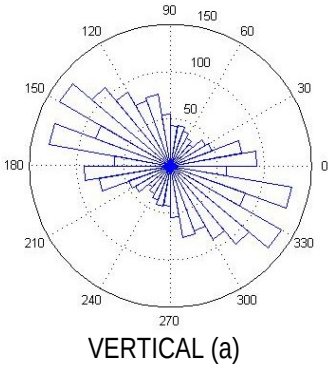

Figure 6. 60: Rose diagrams referring to 200 X magnificated images: (a) vertical surface (image jh0282.tif).

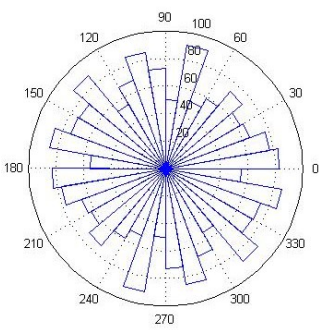

VERTICAL (a)

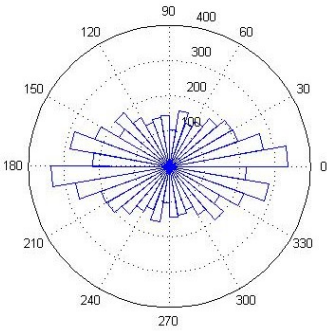

HORIZONTAL (b)

Figure 6. 61: Rose diagrams referring to 600 X magnificated images: (a) vertical surface (image jh0289.tif) and (b) horizontal surface (image jh0293.tif).

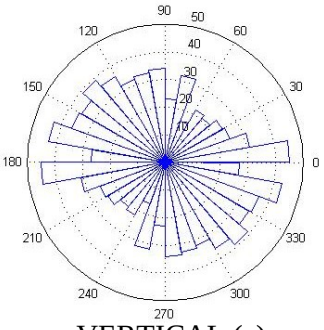

VERTICAL (a)

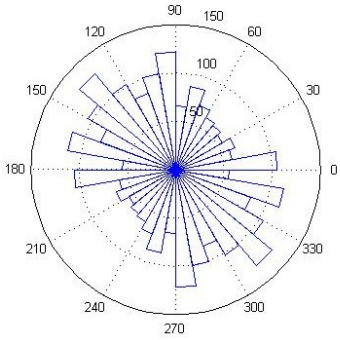

HORIZONTAL (b)

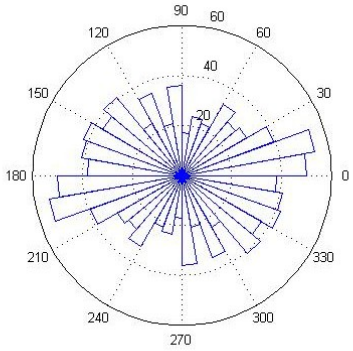

VERTICAL (c)

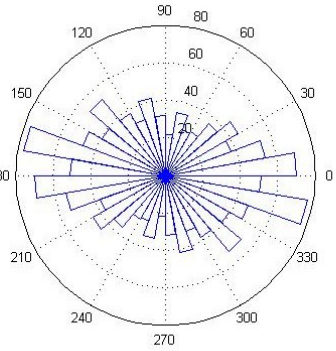

HORIZONTAL (d)

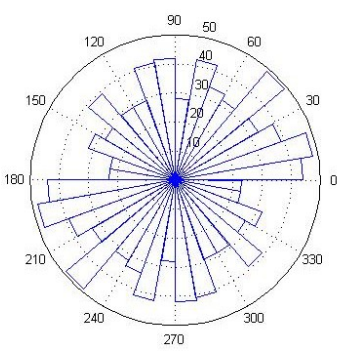

VERTICAL (e)

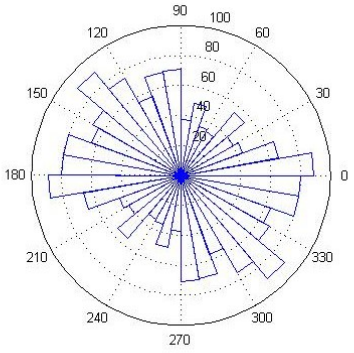

HORIZONTAL (f)

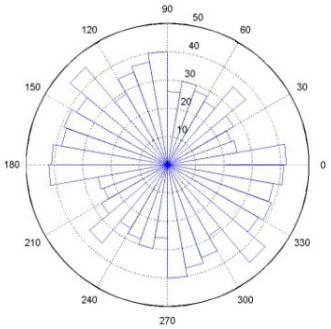

VERTICAL (f)

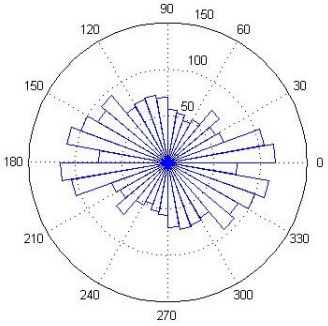

HORIZONTAL (g)

Figure 6. 62: Rose diagrams referring to 1500 X magnificated images: (a) vertical surface (image jh0284.tif), (c) vertical surface (image jh0287.tif), (e) vertical surface (image jh0290.tif) (f) (jh0291.tif) and (b) horizontal surface(image jh0296.tif), (d) horizontal surface (image jh0299.tif), (f) image jh0300.tif and (g) image jh0301.tif.

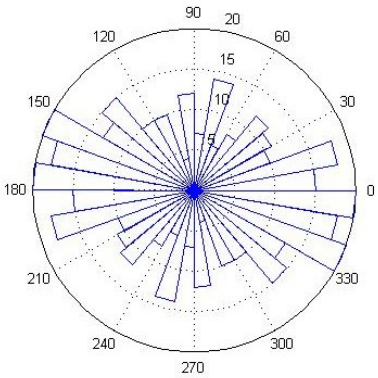

VERTICAL (a)

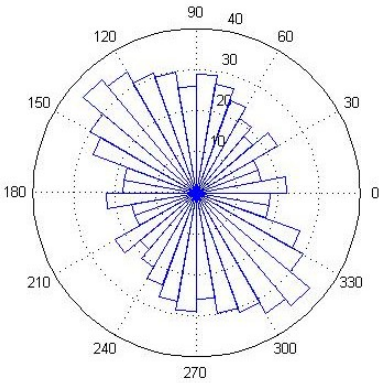

HORIZONTAL (b)

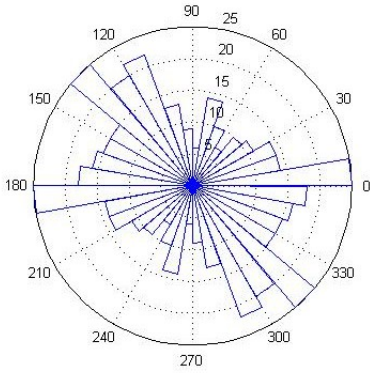

VERTICAL (c)

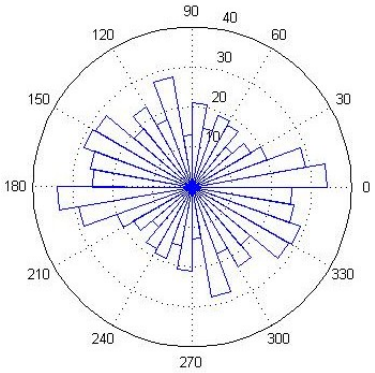

HORIZONTAL (d)

Figure 6. 63: Rose diagrams referring to 3500 X magnificated images: (a) vertical surface (image jh0285.tif), (c) vertical surface (image jh0288.tif) and (b) horizontal surface (image jh0297.tif) and (d) horizontal surface (image jh0302.tif).

CONCLUSIONS AND FINAL REMARKS

The silty soils from the Venice lagoon naturally consist of a highly chaotic inter-bedding of layers of sand, silts and clay. Within the transitional soils framework the mechanical behaviour of different mixtures of Venice sands and fines were analysed by means of oedometer and triaxial tests. Subsequently, a study of the microstructure of soil samples was performed with the aim to identify a possible link between features at this scale and the experimental results obtained from the laboratory tests. With respect to the oedometer tests, the main features that can be summarised are:

- 100% sand samples, when normally compressed even at very high stresses, reached a unique 1D-NCL;
- 70%sand-30%fines specimens did not reach a unique 1D-NCL, although with increasing stresses, the steepnesses of the curves decreased;
- 50%sand-50%fines specimens normally compressed at very high stresses remained parallel and did not reach a unique 1D-NCL;
- 100% fines specimens showed parallel normal compression curves even at high stresses.

When considering the influence on the compressibility parameters of different percentages of fines in the granular mixtures, the results showed that at fines content between 30% and 50% the compressibility index, the intercept at 1 kPa and the swelling index had a minimum value, whereas with higher contents the values increased again.

Selected oedometer test samples consisting 50% sand and 50% fines, loaded in one-dimensional compression at similar stress values and with different initial specific volumes, were analysed by means of Scanning Electron Microscopy. Freshly broken vertical and horizontal surfaces were observed at different magnifications with the aim of studying particle orientations. At all magnifications no preferential angles, occurring both in vertical and horizontal surfaces, could be identified. At very high magnification, some preferential orientations were observed, but unfortunately they coincided with some particle sides forming angles with the horizontal axis of the picture.

Suggestions for future work might be to perform another pair of oedometer tests on 50-50 specimens with different initial specific volume in order to obtain another comparison between vertical and horizontal surfaces and see if the absence of pattern in particle orientation is confirmed.

REFERENCES

- ASTM, (1973). Evaluation of Relative Density and its role in Geotechnical Projects Involving Cohesionless Soils, ASTM ST P 523
- ASTM, (1976). Soil specimen preparation for laboratory testing. ASTM Special Technical Publication 599
- Altuhafi, F. N. and Coop, M.R.(2009). On the Compression of Sands. Submitted to Géotechnique
- Altuhafi, F.N., Baudet, B.A. and Sammonds, P. (2010). The mechanics of subglacial sediment: an example of new "transitional" behaviour. Canadian Geotechnical Journal. Vol. 47, pp. 775-790 (16)
- Atkinson J., Geotecnica meccanica delle terre e fondazioni, McGraw-Hill
- Arab, A (2009). Comportement monotone et cyclique d'un sable limoneux – On monotonic and cyclic behavior of silty sand. Comptes Rendus de l'Academie des Sciences Serie II b/Mecanique, 337 (8), 621-631.
- Bardet J.P., Esperimental Soil Mechanics, Prentice Hall
- Belloni, L.G., Rizzo, A., Caielli, A. and Mayerle G. Influenza sedimentologica sulle caratteristiche geotecniche dei terreni della laguna veneta
- Burland, J.B. (1990). On the compressibility and shear strength of natural clays. Géotechnique Vol. 40, No. 3, pp. 329-378.
- L. G. Belloni, A. Rizzo, A. Caielli, G. Mayerle. (2007).Influenza sedimentologica sulle caratteristiche geotecniche dei terreni della laguna veneta. Atti del XXIII Convegno Nazionale di geotecnica, Padova-Abano Terme, 16-18 Maggio 2007,pp. 147-159.
- Been K., Jefferies M. G. and Hackey J. E. (1991). The critical state of sands. Géotechnique, Vol. 41, No. 3, pp 365-381.
- Biscontin, G., Cola, S., Pestana, J.M. and Simonini, P., (2007). Unified compression model for Venice Lagoon Natural silts. Journal of Geotechnical and Geoenvironmental Engineering, Vol. 133, No. 8 August 1, 2007.
- Cannarile, A., (2004), .Tesi di laurea in geotecnica. Università di Bologna.
- Carrera A., (2008). Mechanical Behaviour of Stava tailings, Ph. D. Thesis, Politecnico di Torino.

- Cola S., Simonini P.(2002). Mechanical behavior of silty soils of the Venice lagoon as a function of their grading characteristics. Canadian Geotechnical Journal.

- Colombo-Colleselli. Elementi di Geotecnica (3°ed.). Zanichelli.

- Cubrinovski Misko, Rees Sean (2008). Effects of fines on undrained behaviour of sands Geotechnical Special Publication, 181, Proceedings of the Geotechnical Earthquake Engineering and Soil Dynamics IV Congress 2008.

- Cola, S. and Simonini, P. (2002). "Mechanical behaviour of silty soils of the Venice lagoon as a function of their grading characteristics." Canadian Geotechnical Journal 39: 879-893.

- Colombo, P., 1987. Aspetti geotecnici ed idraulici nella laguna di Venezia. Intervento al VI Congresso nazionale dell'ordine dei geologi, Venezia, Fondazione Cini, 25-27 Settembre 1987

- Colombo, P. and Matteotti, G. 1963. Contributo allo studio delle caratteristiche geotecniche dei terreni della laguna di Venezia e zone limitrofe. Atti dell'Istituto Veneto di scienze, lettere ed arti. Anno accademico CXXI – Classe di scienze matematiche e naturali

- G. Cortellazzo, G. Ricceri, P. Simonini. (2007). Analisi retrospettiva del comportamento del terreno di fondazione di un rilevato sperimentale ubicato nella laguna di Venezia. Atti del XXIII Convegno Nazionale di geotecnica, Padova-Abano Terme, 16-18 Maggio 2007,pp. 515-522.

- Coop,M.R., The Mechanics of Uncemented Carbonate Sands, Geotechnique, 1990, Vol: 40, Pages: 607 - 626

- Coop, M. R. & Atkinson, J. H. (1993). 'The mechanics of cemented carbonate sands', Géotechnique 43, No. 1, 53-67

- Coop M.R., Cotecchia F., (1995). The compression of sediments at the Archaelogical site of Sibari. In 'The interplay between geotechnical Engineering and Engineering geology', Proceedings of XI European Conference on Soil Mechanics and Foundation Engineering, Copenaghen, Danish Geotechnical Society, 8, 19 - 8,26.

- Coop M.R. and Lee I.K., (1993). The behaviour of Granular Soils at Elevated Stresses. Predictive Soil Mechanics, Houlsby, G.T. % Schofield, A.N. editors. (Thomas Telford, London), pp. 186-198 (Proc. C.P. Wroth Memorial Symposium, 1992)

- Ferreira, P.M.V. and Bica, A.V.D., (2006). Problems in identifying the effects of structure and critical state in a soil with a transitional behaviour. Géotechnique 56, No. 7, 445-454
- Gasparre, A., Coop, M.R. & Cotecchia, F. (2003). ‘An experimental investigation of creep processes in a crushable sand, Deformation Characteristics of Geomaterials, Di Benedetto et al. (eds), 2003 Swets & Zeitlinger, Lisse, ISBN 90 5809 604 1
- Gemelli S. (2008). Indagine di laboratorio sul comportamento non drenato di una sabbia ad elevato contenuto di feldspati, mediante l’impiego di tecniche sperimentali innovative. Tesi di laurea in geotecnica. Università di Bologna
- Gottardi G. e Tonni L., Use of piezocone tests to characterise the silty soils of the Venetian lagoon (Treporti test site). Proceedings ISC-2 on Geotechnical and Geophysical Site Characterisation (Porto, 19-22 September 2004), Viana da Fonseca & Mayne (eds), 2004 Millpress, Rotterdam, ISBN 90 5966 009 9
- Jardine, R.J., Symes, M.J. and Burland, J.B., (1984). The measurement of soil stiffness in the triaxial apparatus. Géotechnique, Vol. 35, No. 3, pp. 378-382.
- Juárez-Badillo E.(2008). Undrained monotonic response of clean and silty sands.Geotechnique, 58, (6), 536-538.
- Klotz, E.U.; Coop, M.R (2002). On the identification of critical state lines for sands. Geotechnical Testing Journal, 25, (3), 289-302.
- Hattab, M. & Fleureau, J., (2010). Experimental analysis of kaolinite particle orientation during triaxial path. International Journal for Numerical and Analytical Methods in Geomechanics. Volume 35, Issue 8, pages 947–968, 10 June 2011
- Head, K. M. (1986). Manual of soil laboratory testing. Vol.2-3. (2°ed.).
- Huang, A.-B., Hsu, H.-H., and Chang, J.-W. (1999). The behaviour of a compressible silty fine sand. Canadian Geotechnical Journal 36, 88-101.
- Ladd R.S (1978). Preparing test specimens using undercompaction. Geotechnical Testing Journal 1, (1), 16-23
- Lancellotta R. Geotecnica (3°ed.) Zanichelli.
- Lee, I.K., Coop, M.R., The Intrinsic Behaviour of Decomposed Granite Soil, Geotechnique, 1995, Vol: 45, Pages: 117 - 130
- Long, M., Gudjonsson, G., Donohue, S. and Hagberg, K., (2010). Engineering characterisation of Norwegian glaciomarine silt. Journal of Engineering Geology Volume 110, Pages 51–65

- Martins F.B., Bressani L.A., Coop M.R., Bica, V.D., (2001). Some aspects of the compressibility behaviour of a clayey sand. Canadian Geotechnical Journal, Vol. 38, No. 6, pp. 1177-1186.
- Mitchell, J.K., 1976, Fundamentals of soil behaviour. New York, John Wiley & sons
- Nocilla, A., (2005).The mechanics of silty soils from the Po river embankment. PhD thesis, Universita′ degli studi di Brescia
- Nocilla, A., Coop M.R. and Colleselli F., (2005). Indagine al microscopio elettronico sulla microstruttura del limo argilloso degli argini del Po. Internal Technical Report, n° 3.University of Brescia. In italian.
- Nocilla A., Coop, M.R. and Colleselli F., (2006). The mechanics of an Italian silt: an example of transitional behaviour. Géotechnique 56, No. 4, 261-271
- Nocilla A. and Coop M.R., (2008).The behaviour of sub-soils from the Po river embankments: an example of transitional behaviour in natural soils. Rivista italiana di geotecnica 1/2008
- Nova, R. (2002). Fondamenti di meccanica delle terre. Mc Graw-Hill.
- Pitman, T. D., Robertson, P. K., and Sego, D. C. (1994). Influence of fines on the collapse of loose sands. Canadian Geotechnical Journal 31, (5), 728-739.
- Rasband, W., 2009, ImageJ v1.431, National Institute of Health, USA.
- Ricceri, G., 1976. Problemi geotecnici del sottosuolo veneziano. Estratto degli Atti e memorie dell′Accademia Patavina di Scienze, Lettere ed Arti. Volume LXXXVIII (1975-1976) – Parte II: Classe di Scienze Matematiche e Naturali
- Ricceri, G. and Previatello, P., 1976. Caratteristiche geotecniche del sottosuolo della Laguna Veneta. Estratto degli Atti e memorie dell′Accademia Patavina di Scienze, Lettere ed Arti. Volume LXXXVIII (1975-1976) – Parte II: Classe di Scienze Matematiche e Naturali
- Ricceri, G., Simonini, P. and Cola, S. (2002). "Applicability of piezocone and dilatometer to characterize the soils of the Venice lagoon." Geotechnical and Geological Engineering, 20:89-121.
- Saccenti A., (2005). Sul comportamento meccanico dei terreni della Laguna di Venezia. Tesi di Dottorato, Università degli Studi di Ferrara.
- Salgado R.,Bandini P., Karim A (2000). Shear strength and stiffness of silty sand. Journal of Geotechnical and Geoenvironmental Engineering, 126, (5), 451-462.

- Sanzeni A., (2006). A study on the compression behavior of the Venetian Lagoon silty sand. PhD thesis, Consorzio delle Università di Parma, Brescia, Ferrara e Bologna.
- Savioli V., Indagine sperimentale sul comportamento transizionale di miscele granulari. Tesi di laurea in geotecnica. Università di Bologna.
- Shipton, B.J.I. and Coop, M.R., Nocilla A., (2006). Particle breakage in transitional soils. Proceedings of Geomechanics and Geotechnics of Particulate Media – Hyodo, Murata & Nakata (eds). Pp. 143-147
- Simonini, P. and Cola, S. (2000). "Use of piezocone to predict maximum stiffness of Venetian soils." Journal of Geotechnical and Geoenvironmental Engineering, ASCE, 126(4):378-382.
- Thevanayagam S., Shenthan T., Mohan S., Liang J.(2002). Undrained fragility of clean sands, silty sands and sandy silts. Journal of Geotechnical and Geoenvironmental Engineering, 128, (10), 849-859.
- Thevanayagam, S. (1998). Effect of fines and confining stress on undrained shear strength of silty sands. Journal of Geotechnical and Geoenvironmental Engineering 124, (6).
- Thevanayagam, S. and Mohan, S. (2000). Intergranular state variables and stress-strain behaviour of silty sands. Géotechnique 50, (1), 1-23.
- Tonni L. and Gottardi G., Analysis and interpretation of piezocone data on the silty soils of the Venetian lagoon (Treporti test site). Can. Geotech. J. 48: 616–633 (2011).
- Tovey, N.K., and Hounslow, M.W.,1995, Quantitative micro-porosity and orientation analysis in soils and sediments. Journal of the Geological Society, London, v.152, p.119-129
- Tovey, N.K., Frydman S. and Wong K.Y., A study of swelling clay in the scanning electron microscope. Proc. 3rd International Conference on Expansive Soils. Vol. 2. (Haifa), pp 45-54
- Verdugo, R., Ishihara, K. (1996) 'The steady state of sandy soils', Soils and foundations Vol. 36, No. 2, 81-91, June 1996, Japanese Geotechnical Society
-
- Vilhar, G., (2009). Odnos med napetosmi in deformacijami za meljine peske… deformacija. PhD thesis, University of Lubjana
- Wan, R. G. and Guo, P.J. (2001). Effect of microstructure on undrained behaviour of sands. *Canadian Geotechnical Journal* 38, 16-28.

- Wang Gonghui, Sassa Kyoji, Fukuoka, Hiroshi; Tada, Takahiro (2007). Experimental study on the shearing behavior of saturated silty soils based on ring-shear tests. Journal of Geotechnical and Geoenvironmental Engineering, 133, (3), 319-333.
- Wilkinson, S., (2010) Ph.d Thesis submitted, Imperial College of Science Technology and medicine.
- Wilkinson, S. and Fenton, C., (2010). The application of stereo E-SEM in understanding 3Dmudrock structure. (--)
- Yamamuro Jerry A., Lade Poul V.(1998). Steady-state concepts and static liquefaction of silty sands. Journal of Geotechnical and Geoenvironmental Engineering, 124, (9), 868-877.
- Yang S.L., Sandven R., Grande L.(2006). Steady-state lines of sand-silt mixtures.

  Canadian Geotechnical Journal, 43, (11), 1213-1219.
- Yao, Y.P, Sun D.A.; Luo T.(2004). A critical state model for sands dependent on stress and density. International Journal for Numerical and Analytical Methods in Geomechanics, 28, (4), 323-337.